Modeling of Powder Spreading in Laser Powder Bed Fusion and Roller Rotational Strategies

Modeling of Powder Spreading in Laser Powder Bed Fusion and Roller Rotational Strategies

By

Mohamed Awad Salim, B.Sc., M.Sc.

A Thesis

Submitted to the School of Graduate Studies in Partial Fulfillment of the Requirements for the Degree Doctor of Philosophy

McMaster University

DOCTOR OF PHILOSOPHY (2025) McMaster University

(Mechanical Engineering) Hamilton, Ontario, Canada

TITLE:	Modeling of Powder Spreading in Laser Powder Bed Fusion and Roller Rotational Strategies
AUTHOR:	Mohamed Awad Salim B.Sc. in Mechanical Engineering (Cairo University) M.Sc. in Mechanical Engineering (Cairo University)
SUPERVISOR:	Dr. M. A. Elbestawi
CO-SUPERVISOR	Dr. Stephen Tullis
NUMBER OF PAGES:	xxi/196

Abstract

Powder spreading is critical in Laser Powder Bed Fusion (PBF-LP), directly influencing the powder bed's uniformity, packing density, and overall quality. This work focuses on optimizing spreading speed, roller configurations, and rotational speed strategies through Discrete Element Method (DEM) simulations to enhance the performance of additive manufacturing processes. The research is structured around three key objectives.

First, the influence of varying spreading speeds on powder bed characteristics is analyzed. Results indicate that increasing spreading speed reduces packing density and layer thickness for non-rotating, counter-rotating, and sub-rolling configurations due to powder dragging. In contrast, the super-rolling configuration effectively balances momentum transfer, enhancing packing density and layer thickness while maintaining uniformity, albeit with a slight increase in surface roughness.

Second, the study evaluates the impact of circumferential speed on powder spreading. It reveals that forward-rotating rollers significantly improve packing density, layer thickness, and mass fraction as rotational speed increases, while counter-rotating rollers show a decline in these metrics. Despite improving productivity, larger roller sizes lead to greater powder bursts, non-uniformity, and surface roughness, highlighting the need for optimized operational parameters.

Lastly, adaptive rotational speed strategies (Profiles A–F) are introduced to address challenges in high-speed spreading. Profile F stands out as the optimal configuration, achieving maximum packing density, minimal variation coefficients, and superior mass fraction. Its high initial clockwise rotational speed, gradually reduced to zero, ensures uniform powder deposition, minimal surface roughness, and stability under high spreading speeds.

This work offers a comprehensive framework for optimizing PBF-LP powder spreading processes, emphasizing the interplay between spreading speed, roller size, and rotational strategies. These findings provide valuable insights for enhancing efficiency, reliability, and quality in roller-spreading in additive manufacturing.

Acknowledgment

I would like to express my deepest gratitude to my supervisor, **Dr. Mo Elbestawi**, for his invaluable guidance, continuous support, and encouragement throughout my PhD journey. His insightful advice and constructive feedback have been instrumental in shaping my research and academic growth.

I am also sincerely grateful to my co-supervisor, **Dr. Stephen Tullis**, for his mentorship, technical expertise, and thoughtful discussions, which have significantly contributed to the progress and depth of this work. His patience and keen insights have been invaluable in refining my research.

Finally, I am deeply thankful to my parents for their unwavering love and encouragement, which have been my source of strength throughout my life.

Table of Contents

List of Figures

List of Tables

1 Introduction

1.1. Additive Manufacturing

Additive Manufacturing (AM), commonly referred to as 3D printing, has revolutionized the manufacturing industry by enabling the production of complex and customized parts with high precision. Unlike traditional subtractive manufacturing methods, which remove material to create a part, AM builds parts layer by layer from digital models. This technology has applications in various industries, including aerospace, biomedical, automotive, and consumer goods, due to its ability to produce intricate geometries and reduce material waste [1]. Among the various AM techniques, Laser Powder Bed Fusion (PBF-LP) has emerged as one of the most prominent methods for producing high-quality metal parts.

1.2. Laser Powder Bed Fusion (PBF-LP)

Laser Powder Bed Fusion (PBF-LP) is a powder-based additive manufacturing process that uses a high-intensity laser to melt layers of metal powder to create a solid part. The process begins with the deposition of a thin layer of powder by blade or roller onto the building plate, followed by the melting of the powder using a laser, as described in Figure 1-1. This sequence is repeated layer by layer until the final part is completed. PBF-LP offers several advantages, including producing parts with complex geometries, high dimensional accuracy, and excellent mechanical properties [2,3]. However, the quality of the final part is highly dependent on the quality of the powder bed, which is influenced by the powder spreading process.

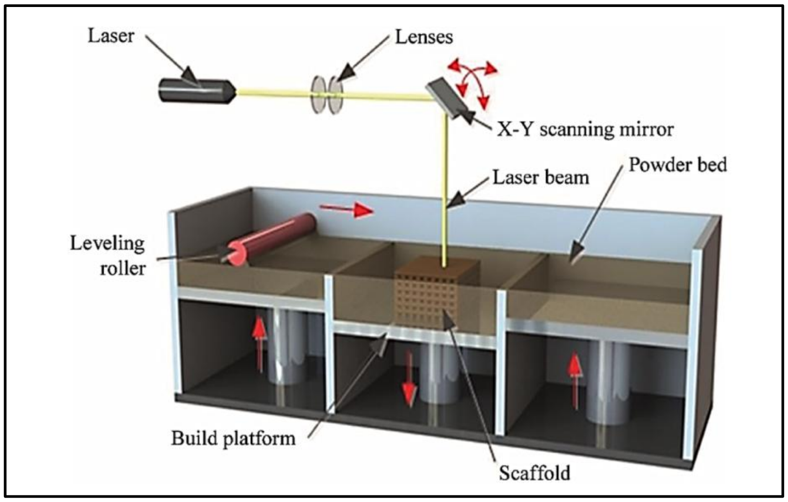

Figure 1-1: PBF-LP system schematic with roller-spreading mechanism [4,5]

1.3. Spreading Mechanisms in PBF-LP

The powder spreading process in PBF-LP is a critical step that directly affects the quality of the powder bed and, consequently, the final part. Two primary spreading mechanisms are used in PBF-LP: roller spreading and blade spreading. The roller-spreading technique uses a roller to distribute the powder across the building plate [6–8], as presented in Figure 1-2b. The roller can be configured in different ways, such as non-rotating, counter-rotating, or forward-rotating, each affecting the powder distribution differently. Roller spreading is known to achieve higher packing density due to the normal force exerted by the roller, which compacts the powder more effectively. [7]. The blade-spreading technique uses a blade to distribute the powder across the building plate [9,10], as illustrated in Figure 1-2a. While blade spreading is simpler in design, it often results in lower packing density compared to roller spreading, as it does not provide the same level of compaction [11]. The choice of spreading mechanism and its parameters, such as spreading speed, rotational speed, and roller configuration, significantly impact the quality of the powder bed. Poor powder spreading can lead to defects such as uneven layer thickness, low packing density, and surface roughness, adversely affecting the final part's mechanical properties and dimensional accuracy.

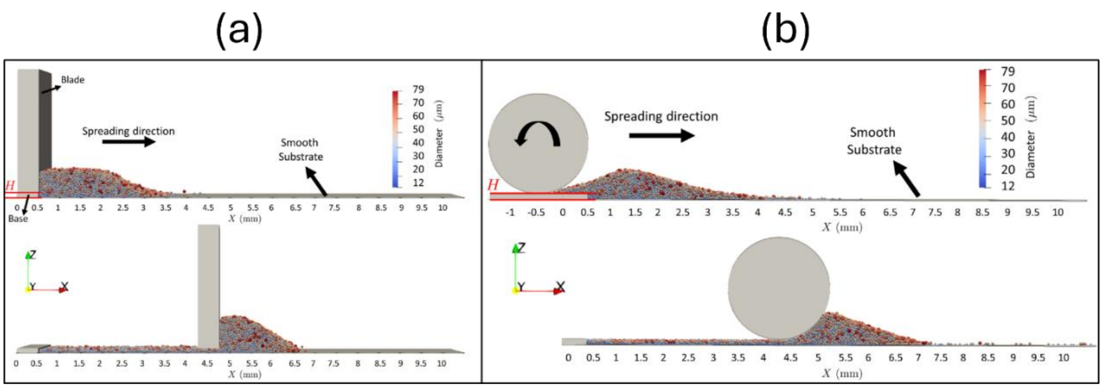

Figure 1-2. Simulation setup of the spreading process using both the blade and the roller [12]. (a) blade and (b) Roller

1.4. Literature Review

1.4.1. Roller Spreading vs. Blade Spreading

The choice between roller spreading and blade spreading has been a topic of extensive research in PBF-LP. Roller spreading is generally preferred over blade spreading due to its ability to achieve higher packing density. The normal force exerted by the roller compacts the powder more effectively, leading to a more uniform and dense powder bed [6]. In contrast, blade spreading tends to produce lower packing density, as it does not provide the same level of compaction. However, blade spreading is simpler in design and more suitable for specific applications where high packing density is not critical [9]. Several studies have compared the performance of roller spreading and blade spreading. For instance, Zhang et al. [7] conducted a Discrete Element Method (DEM) simulation to compare the two spreading methods. They found that roller spreading achieved higher packing density due to the normal force exerted by the roller. Similarly, Haeri et al. [11] demonstrated through experimental and simulation studies that roller spreading resulted in more uniform powder distribution compared to blade spreading.

1.4.2. Roller-spreading Configurations

The roller configuration plays a significant role in determining the quality of the powder bed. There are three primary roller configurations used in PBF-LP:

- **Non-Rotating Roller**: In this configuration, the roller does not rotate as it moves across the powder bed. This configuration is less common but useful in specific scenarios where minimal disturbance to the powder bed is desired [10].
- **Counter-Rotating Roller**: In this configuration, the roller rotates in the same direction as its movement, as shown in Figure 1-3. This counter-rotation helps to break up powder agglomerates and promotes more uniform powder distribution. However, it can also decrease packing density at higher rotational speeds due to the increased momentum transfer in the spreading direction to the powder particles [13].
- **Forward-Rotating Roller**: In this configuration, the roller rotates in the opposite direction as its movement, as shown in Figure 1-3. This forward rotation helps to grip and drag the powder into the bed, increasing the packing density. However, it can also lead to uneven surfaces and inaccurate layer thickness due to the release of stored elastic energy in the powder bed [14].

The choice of roller configuration depends on the specific requirements of the PBF-LP process. For example, forward-rotating rollers are often used when high packing density is desired, while counter-rotating rollers are preferred for applications requiring uniform powder distribution.

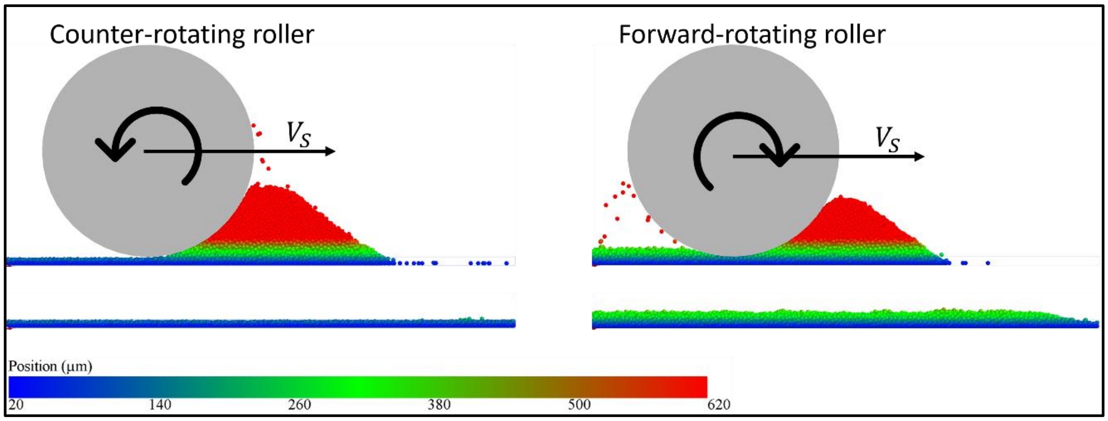

Figure 1-3. Sketches of counter-rotating and forward-rotating rollers during spreading of powder, which is coloured by powder position in Z-direction (i.e., layer thickness).

1.4.3. Effect of spreader's dynamics on different rolling-spreading configurations

The key parameters influencing blade and roller dynamics can be summarized as spreading and circumferential speeds. The circumferential speed, in turn, is determined by the roller's rotational speed and radius. Therefore, examining the effects of spreading speed, rotational speed, and roller radius provides a comprehensive understanding of how spreader dynamics impact the powder spreading process.

The spreading speed is a critical parameter that influences the quality of the powder bed. Higher spreading speeds can lead to reduced packing density and increased surface roughness due to the limited time for powder particles to settle and reorganize. Conversely, lower spreading speeds allow for more time for particle rearrangement, resulting in higher packing density [9,10,12,16–22]. The effect of spreading speed varies depending on the roller configuration. For example, in counter-rotating rollers, higher spreading speeds can amplify the reduction in packing density [6,8,11,12,23–25]. Meanwhile, the forward-rotating roller can grip and drag powder into the bed, increasing the packing density [14,26]. However, this approach can also lead to uneven surfaces and inaccurate layer thickness as the powder bed may spring back after the roller passes due to the release of stored elastic energy [27]. Several studies have investigated the impact of spreading speed on powder bed quality. Yao et al. [10] found that a spreading speed of ≤0.1 m/s yielded favourable results for stainless steel 316L powder, while higher speeds led to reduced packing density and increased surface roughness. Similarly, Meier et al. [17] observed that higher spreading speeds resulted in more turbulent particle trajectories, leading to non-uniform packing density and increased surface roughness.

The rotational speed of the roller also significantly impacts the powder bed quality. In counter-rotating rollers, higher rotational speeds can decrease packing density due to the increased circulation of particles in the powder heap, which prevents them from settling into the bed [13]. In forward-rotating rollers, the effect of rotational speed is more nuanced, as it can either increase or decrease packing density depending on the relationship between the rotational speed and the spreading speed [8]. Experimental and simulation studies have provided insights into the effects of rotational speed on powder bed quality. For instance, Seluga [28] observed that increasing the rotational speed of a counter-rotating roller led to a marginal increase in powder bed density at low speeds, but this effect diminished at higher speeds. Similarly, Zhang et al.[8] found that the rotational speed of a counter-rotating roller significantly impacted powder bed density, with higher speeds leading to reduced density due to increased particle circulation. Limited studies have explored the impact of roller radius on powder bed quality. For example, Zhang et al. [8] conducted

DEM simulations to investigate the effect of roller diameter of a counter-rotating roller on powder bed density. They found that larger rollers resulted in higher packing density due to increased particles in the compression zone.

Vibration is an essential dynamic parameter that has emerged to improve uniformity for both blade and roller spreaders. Introducing vibrations into the spreading process can enhance powder compaction and improve layer uniformity. Vibration has been explored as a potential method to improve powder spreading in PBF-LP. Vibrating spreaders can help to compact the powder bed and reduce the formation of cavities and voids [29]. However, the use of vibration in powder spreading also has some drawbacks. For example, excessive vibration can lead to particle segregation and uneven powder distribution, which can negatively impact the quality of the powder bed. Therefore, the vibration frequency and amplitude must be carefully controlled to achieve the desired compaction without introducing additional defects.

1.4.4. Effect of Powder Characteristics on Spreading Performance

The characteristics of the feedstock powder, such as particle size, particle size distribution, and particle shape, also play a crucial role in determining the quality of the powder bed. Fine powders, for example, tend to have poor flowability due to interparticle cohesion, which can lead to uneven spreading and low packing density [17]. Coarser powders, on the other hand, generally exhibit better flowability but may result in lower packing density if the particle size is too large [10]. The particle size distribution of the powder can also affect the packing density. Multimodal powders, which consist of particles of different sizes, can achieve higher packing density than monomodal powders, as the smaller particles can fill the voids between the larger particles. However, the use of multimodal powders can also lead to particle segregation, which can negatively impact the uniformity of the powder bed [30]. Particle shape is another important factor that influences powder spreading. Spherical particles generally exhibit better flowability and can achieve higher packing density compared to non-spherical particles [11]. However, certain non-spherical particles, such as ellipsoidal particles, can achieve high packing density if well-aligned during the spreading process.

1.4.5. Effect of powder bed characteristics on part quality

The density of the powder bed directly impacts the quality of the final printed part. Higher powder bed density generally results in better part quality, reducing the likelihood of defects such as porosity, lack of fusion, and keyholing [31]. Conversely, low powder bed density can lead to poor part quality, increasing the likelihood of defects and reducing the part's mechanical properties [32]. Several studies have investigated the relationship between powder bed density and part quality. For example, Gong et al. [31] found that higher powder bed density resulted in better mechanical properties, such as tensile strength and fatigue resistance, in Ti-6Al-4V parts produced by PBF-LP. Similarly, Yang et al. [32] observed that low powder bed density increased porosity and reduced mechanical properties in stainless steel parts.

Cavities and voids in the powder bed can significantly impact the quality of the final printed part. These defects can lead to uneven melting and density variations, acting as stress concentrators and reducing the part's mechanical properties [7]. Additionally, cavities and voids can lead to poor interlayer bonding, compromising the part's structural integrity [11]. Several strategies have been proposed to reduce the formation of cavities and voids in the powder bed, including optimizing spreading parameters, such as spreading speed and roller configuration and using vibration to promote particle rearrangement [10]. However, these strategies must be carefully controlled to avoid introducing additional defects, such as particle segregation and uneven powder distribution [33].

Layer thickness is another critical parameter affecting the powder bed's quality. Thicker layers generally result in higher packing density, providing more space for particle rearrangement [17]. However, excessively thick layers can lead to uneven melting and defects such as lack of fusion, particularly in regions where the powder is not fully compacted [32]. Conversely, thinner layers can result in lower packing density due to the increased static and dynamic wall effects, which hinder particle rearrangement [16]. However, thinner layers are often preferred for high-precision applications, as they allow for finer control over the part geometry [34]. Surface roughness is another important factor that influences the quality of the final printed part. High surface roughness can lead to poor part quality, increasing the likelihood of defects such as cracks and stress concentrations [35]. Conversely, low surface roughness generally results in better part quality, reducing the likelihood of defects and improving the part's mechanical properties [24].

Optimizing the powder spreading process by carefully selecting the spreading mechanism, spreading speed, and roller configuration is essential to mitigate these defects. This thesis aims to address these challenges by investigating the effects of different spreading parameters on powder bed quality and proposing strategies to improve the spreading process in PBF-LP.

1.5. Research Gap and Motivation

Despite the extensive research on powder spreading in PBF-LP, several gaps remain in understanding how different roller-spreading parameters, such as spreading speed, rotational speed, and roller configuration, affect the powder bed quality. Most studies have focused on blade-spreading and counter-rotating roller configurations, but there is a lack of comprehensive research on forward-rotating roller configurations. Furthermore, challenges associated with high spreading speed should be investigated to find innovative ways to avoid these challenges, such as cavity formation. This research addresses these gaps by conducting a comprehensive numerical study using DEM to investigate the effects of different spreading parameters on powder bed quality. By understanding the complex interactions between these parameters, this research aims to develop strategies to optimize the powder spreading process in PBF-LP, leading to improved part quality and reduced production costs.

1.6. Research Objectives

The primary objectives of this research are as follows:

1. To develop a numerical model using the Discrete Element Method (DEM) to simulate the powder spreading process and validate the model against experimental data.
2. To investigate the effects of spreading speed on powder bed quality in PBF-LP for different roller-spreading configurations, especially forward-rotating
3. To investigate the effects of circumferential speed on powder bed quality in PBF-LP for different roller-spreading configurations.

4. To investigate the interaction effects between spreading and circumferential speeds and their combined impact on powder bed quality.
5. To propose strategies for adaptive rotational speed to avoid the drawbacks of high spreading speed.

1.7. Methodology

The Discrete Element Method (DEM) is a numerical technique used to simulate the behaviour of granular materials, such as metal powders, at the particle level. In DEM, each particle is treated as an individual entity, and the interactions between particles are modelled using contact mechanics. This method allows for the detailed analysis of particle motion, packing density, and force distribution during the powder spreading process [36]. The translational and rotational motions of each particle are governed by Newton's Second Law of Linear and Rotational Motion [37,38]. The DEM first computes all acting forces and then determines accelerations. Through time integration, the velocity and position of each particle are accurately calculated [36].

A mathematical model based on contact mechanics describes particle interactions, incorporating normal and tangential forces, cohesion, and rolling resistance. The Hertz–Mindlin contact [39] model with Johnson-Kendall-Roberts (JKR) [40] cohesion is used to account for particle adhesion and energy dissipation. The static and dynamic angles of repose of stainless steel 316L powder are experimentally measured and compared with simulation results to validate the model. The material properties, including friction coefficients and surface energy, are calibrated to represent powder behaviour accurately.

The simulations were performed using Altair EDEM software [41], employing a carefully selected time step that does not exceed 20% of the Rayleigh time to maintain numerical stability and accuracy. Besides, the mesh size was defined as three times the smallest particle's radius to ensure precise particle contact detection. Key performance metrics such as packing density, layer thickness, and mass fraction are computed at various points along the building plate to assess powder bed uniformity. Additionally, surface roughness is evaluated using the centerline average method to quantify variations in powder layer topography.

1.8. Thesis Outline

This thesis is systematically organized to investigate the influence of roller dynamics on powder bed quality in Laser Powder Bed Fusion (PBF-LB/M), with a particular focus on the powder spreading process. The structure of the thesis reflects a logical progression from comprehensive analysis of roller dynamics to advanced strategy development, as outlined below:

- **Chapter 1** introduces Laser Powder Bed Fusion and emphasizes the significance of powder spreading in achieving high-quality layers. It introduces the concept of roller dynamics, outlines the motivation and research objectives, and describes the methodological framework adopted throughout the thesis.
- **Chapter 2** investigates the effect of **spreading speed** on powder bed quality using roller-based spreading configurations, particularly forward-rotating rollers. This chapter establishes the baseline impact of translational dynamics on the powder layer's uniformity and density and the adverse effects of high spreading speed.

- **Chapter 3** extends the investigation by analyzing the effect of **circumferential speed**, which is governed by roller rotational speed and roller size (i.e., roller's radius). This chapter explores how rotational dynamics influence spreading performance and examines the interaction between circumferential and translational speeds to develop a more comprehensive understanding of roller dynamics.
- **Chapter 4** builds on the insights gained from Chapters 2 and 3 to propose **adaptive rotational speed strategies**. These strategies mitigate the negative effects of high spreading speeds identified earlier by dynamically adjusting circumferential speed to maintain powder bed quality under various operating conditions.
- **Chapter 5** concludes the thesis by summarizing the key findings from the previous chapters, emphasizing how each contributes to a holistic understanding of roller dynamics in PBF-LB. It also highlights the practical implications of the proposed strategies and outlines potential avenues for future research.

References

[1] I. Gibson, D.W. Rosen, B. Stucker, Additive Manufacturing Technologies: 3D Printing, Rapid Prototyping, and Direct Digital Manufacturing, 2010. https://doi.org/10.1007/978-1-4419-1120-9.

[2] S.A. Khairallah, A.T. Anderson, A. Rubenchik, W.E. King, Laser powder-bed fusion additive manufacturing: Physics of complex melt flow and formation mechanisms of pores, spatter, and denudation zones, Acta Mater 108 (2016) 36–45. https://doi.org/10.1016/j.actamat.2016.02.014.

[3] M. Yakout, M.A. Elbestawi, S.C. Veldhuis, Density and mechanical properties in selective laser melting of Invar 36 and stainless steel 316L, J Mater Process Technol 266 (2019) 397–420. https://doi.org/10.1016/j.jmatprotec.2018.11.006.

[4] C. Vyas, G. Poologasundarampillai, J. Hoyland, P. Bartolo, 3D printing of biocomposites for osteochondral tissue engineering, in: 2017: pp. 261–302. https://doi.org/10.1016/B978-0-08-100752-5.00013-5.

[5] M. Taghian, M.H. Mosallanejad, E. Lannunziata, G. Del Greco, L. Iuliano, A. Saboori, Laser powder bed fusion of metallic components: Latest progress in productivity, quality, and cost perspectives, Journal of Materials Research and Technology 27 (2023) 6484–6500. https://doi.org/10.1016/j.jmrt.2023.11.049.

[6] H. Chen, Y. Chen, Y. Liu, Q. Wei, Y. Shi, W. Yan, Packing quality of powder layer during counter-rolling-type powder spreading process in additive manufacturing, Int J Mach Tools Manuf 153 (2020) 103553. https://doi.org/10.1016/j.ijmachtools.2020.103553.

[7] J. Zhang, Y. Tan, X. Xiao, S. Jiang, Comparison of roller-spreading and blade-spreading processes in powder-bed additive manufacturing by DEM simulations, Particuology 66 (2022) 48–58. https://doi.org/10.1016/j.partic.2021.07.005.

[8] J. Zhang, Y. Tan, T. Bao, Y. Xu, X. Xiao, S. Jiang, Discrete element simulation of the effect of roller-spreading parameters on powder-bed density in additive manufacturing, Materials 13 (2020). https://doi.org/10.3390/ma13102285.

[9] Y. Lee, A.K. Gurnon, D. Bodner, S. Simunovic, Effect of Particle Spreading Dynamics on Powder Bed Quality in Metal Additive Manufacturing, Integr Mater Manuf Innov 9 (2020) 410–422. https://doi.org/10.1007/s40192-020-00193-1.

[10] D. Yao, X. An, H. Fu, H. Zhang, X. Yang, Q. Zou, K. Dong, Dynamic investigation on the powder spreading during selective laser melting additive manufacturing, Addit Manuf 37 (2021). https://doi.org/10.1016/j.addma.2020.101707.

[11] S. Haeri, Y. Wang, O. Ghita, J. Sun, Discrete element simulation and experimental study of powder spreading process in additive manufacturing, Powder Technol 306 (2016) 45–54. https://doi.org/10.1016/j.powtec.2016.11.002.

[12] M.Y. Shaheen, A.R. Thornton, S. Luding, T. Weinhart, The influence of material and process parameters on powder spreading in additive manufacturing, Powder Technol 383 (2021) 564–583. https://doi.org/10.1016/j.powtec.2021.01.058.

[13] W. Nan, M. Pasha, M. Ghadiri, Numerical simulation of particle flow and segregation during roller spreading process in additive manufacturing, Powder Technol 364 (2020) 811–821. https://doi.org/10.1016/j.powtec.2019.12.023.

[14] M. Tang, Y. Guo, W. Zhang, H. Ma, L. Yang, W. Wei, L. Wang, S. Fan, Q. Zhang, On recoated powder quality with a forward rotating flexible roller in laser powder bed fusion of 30 wt% 5 μm SiCp/AlSi10Mg composites, Mater Des 225 (2023). https://doi.org/10.1016/j.matdes.2022.111489.

[15] B. Cheng, X. Li, C. Tuffile, A. Ilin, H. Willeck, U. Hartel, Multi-Physics Modeling of Single Track Scanning in Selective Laser Melting: Powder Compaction Effect, (2018) 1887–1902. https://www.researchgate.net/publication/330383209.

[16] Y.M. Fouda, A.E. Bayly, A DEM study of powder spreading in additive layer manufacturing, Granul Matter 22 (2020) 1–18. https://doi.org/10.1007/s10035-019-0971-x.

[17] C. Meier, R. Weissbach, J. Weinberg, W.A. Wall, A.J. Hart, Critical influences of particle size and adhesion on the powder layer uniformity in metal additive manufacturing, J Mater Process Technol 266 (2019) 484–501. https://doi.org/10.1016/j.jmatprotec.2018.10.037.

[18] L. Si, T. Zhang, M. Zhou, M. Li, Y. Zhang, H. Zhou, Numerical simulation of the flow behavior and powder spreading mechanism in powder bed-based additive manufacturing, Powder Technol 394 (2021) 1004–1016. https://doi.org/10.1016/j.powtec.2021.09.010.

[19] D. Yao, X. Liu, J. Wang, W. Fan, M. Li, H. Fu, H. Zhang, X. Yang, Q. Zou, X. An, Numerical insights on the spreading of practical 316 L stainless steel powder in SLM additive manufacturing, Powder Technol 390 (2021) 197–208. https://doi.org/10.1016/j.powtec.2021.05.082.

[20] V. Lampitella, M. Trofa, A. Astarita, G. D'Avino, Discrete Element Method Analysis of the Spreading Mechanism and Its Influence on Powder Bed Characteristics in Additive Manufacturing, Micromachines (Basel) 12 (2021) 392. https://doi.org/10.3390/mi12040392.

[21] Z. Xiang, M. Zhang, R. Yan, Q. Yin, K. Zhang, Powder-spreading dynamics and packing quality improvement for laser powder bed fusion additive manufacturing, Powder Technol 389 (2021) 278–291. https://doi.org/10.1016/j.powtec.2021.05.036.

[22] D. Yao, J. Wang, M. Li, T. Zhao, Y. Cai, X. An, R. Zou, H. Zhang, H. Fu, X. Yang, Q. Zou, Segregation of 316L stainless steel powder during spreading in selective laser melting based additive manufacturing, Powder Technol 397 (2022) 117096. https://doi.org/10.1016/j.powtec.2021.117096.

[23] L. Wang, Z. Zhou, E. Li, H. Shen, A. Yu, Powder deposition mechanism during powder spreading with different spreader geometries in powder bed fusion additive manufacturing, Powder Technol 395 (2022) 802–810. https://doi.org/10.1016/j.powtec.2021.10.017.

[24] E.J.R. Parteli, T. Pöschel, Particle-based simulation of powder application in additive manufacturing, Powder Technol 288 (2016) 96–102. https://doi.org/10.1016/j.powtec.2015.10.035.

[25] S. Haeri, Optimisation of blade type spreaders for powder bed preparation in Additive Manufacturing using DEM simulations, Powder Technol 321 (2017) 94–104. https://doi.org/10.1016/j.powtec.2017.08.011.

[26] T. Niino, K. Sato, Effect of Powder Compaction in Plastic Laser Sintering Fabrication, n.d.

[27] M. Ziaee, R. Hershman, A. Mahmood, N.B. Crane, Fabrication of demineralized bone matrix/polycaprolactone composites using large area projection sintering (LAPS), Journal of Manufacturing and Materials Processing 3 (2019). https://doi.org/10.3390/jmmp3020030.

[28] K.J. Seluga, Three Dimensional Printing by Vector Printing of Fine Metal Powders, 2001.

[29] R. Rothfelder, L. Lanzl, J. Selzam, D. Drummer, M. Schmidt, Vibrational Microfeeding of Polymer and Metal Powders for Locally Graded Properties in Powder-Based Additive Manufacturing, J Mater Eng Perform 30 (2021) 8798–8809. https://doi.org/10.1007/s11665-021-06271-5.

[30] M. Li, X. Wei, Z. Pei, C. Ma, Binder jetting additive manufacturing: observations of compaction-induced powder bed surface defects, Manuf Lett 28 (2021) 50–53. https://doi.org/10.1016/j.mfglet.2021.04.003.

[31] H. Gong, K. Rafi, H. Gu, G.D. Janaki Ram, T. Starr, B. Stucker, Influence of defects on mechanical properties of Ti-6Al-4V components produced by selective laser melting and electron beam melting, Mater Des 86 (2015) 545–554. https://doi.org/10.1016/j.matdes.2015.07.147.

[32] G. Yang, Y. Xie, S. Zhao, L. Qin, X. Wang, B. Wu, Quality Control: Internal Defects Formation Mechanism of Selective Laser Melting Based on Laser-powder-melt Pool Interaction: A Review, Chinese Journal of Mechanical Engineering: Additive Manufacturing Frontiers 1 (2022) 100037. https://doi.org/10.1016/j.cjmeam.2022.100037.

[33] W. Nan, M. Ghadiri, Numerical simulation of powder flow during spreading in additive manufacturing, Powder Technol 342 (2019) 801–807. https://doi.org/10.1016/j.powtec.2018.10.056.

[34] M. Yakout, M.A. Elbestawi, S.C. Veldhuis, On the characterization of stainless steel 316L parts produced by selective laser melting, International Journal of Advanced Manufacturing Technology 95 (2018) 1953–1974. https://doi.org/10.1007/s00170-017-1303-0.

[35] J.C. Snyder, K.A. Thole, Understanding laser powder bed fusion surface roughness, Journal of Manufacturing Science and Engineering, Transactions of the ASME 142 (2020). https://doi.org/10.1115/1.4046504.

[36] B.C. Burman, P.A. Cundall, O.D.L. Strack, A discrete numerical model for granular assemblies, Geotechnique 30 (1980) 331–336. https://doi.org/10.1680/geot.1980.30.3.331.

[37] J.Q. Gan, A.B. Yu, Z.Y. Zhou, DEM simulation on the packing of fine ellipsoids, Chem Eng Sci 156 (2016) 64–76. https://doi.org/https://doi.org/10.1016/j.ces.2016.09.017.

[38] H.P. Zhu, Z.Y. Zhou, R.Y. Yang, A.B. Yu, Discrete particle simulation of particulate systems: A review of major applications and findings, Chem Eng Sci 63 (2008) 5728–5770. https://doi.org/https://doi.org/10.1016/j.ces.2008.08.006.

[39] R.D. Mindlin, H. Deresiewicz, Elastic Spheres in Contact Under Varying Oblique Forces, J Appl Mech 20 (2021) 327–344. https://doi.org/10.1115/1.4010702.

[40] K.L. Johnson, K. Kendall, A.D. Roberts, Surface energy and the contact of elastic solids, Proceedings of the Royal Society of London. A. Mathematical and Physical Sciences 324 (1971) 301–313. https://doi.org/10.1098/rspa.1971.0141.

[41] Altair EDEM 2021.1, (n.d.). https://www.altair.com/edem/.

2 Accelerating laser powder bed fusion: the influence of roller-spreading speed on powder spreading performance

Citation

M.A. Salim, S. Tullis, M. Elbestawi, Accelerating Laser Powder Bed Fusion: The Influence of Roller-Spreading Speed on Powder Spreading Performance, Metals (Basel) 14 (2024) 1137. https://doi.org/10.3390/met14101137.

- Received: 14 August 2024
- Accepted: 3 October 2024
- Published: 5 October 2024

Author Contributions:

- **Mohamed Awad Salim:** Conceptualization, methodology, software, validation, formal analysis, investigation, resources, data curation, writing—original draft preparation and visualization
- **Dr. M. A. Elbestawi:** Conceptualization, supervision, methodology, resources and writing—review and editing
- **Dr. Stephen Tullis:** Conceptualization, supervision, methodology, formal analysis, investigation, resources and writing—review and editing.

2.1. Abstract

The powder spreading process is a fundamental element within the laser powder bed fusion (PBF-LP) framework, given its pivotal role in configuring the powder bed. This configuration significantly influences subsequent processing steps and ultimately determines the quality of the final manufactured part. This research paper presents a comprehensive analysis of the impact of varying spreading speeds, enabled by different roller configurations, on the powder distribution in PBF-LP. Utilizing extensive Discrete Element Method (DEM) modelling, we systematically examine how spreading speed affects vital parameters within the spreading process, including packing density, mass fraction, and actual layer thickness. Our exploration of various roller configurations has revealed that increasing spreading speed generally decreases packing density and layer thickness for non-rotating, counter-rotating and forward-rotating rollers with low clockwise rotational speed (sub-rolling) due to powder dragging. However, a forward-rotating roller with high clockwise rotational speed (super-rolling) balances momentum transfer, enhancing packing density and layer thickness despite increasing surface roughness This configuration significantly improves the uniformity and density of the powder bed, providing a technique to accelerate the spreading process while keeping packing density without reduction. Furthermore, it offers crucial insights for optimizing additive manufacturing processes by considering the complex relationship between spreading speed, roller configurations, and powder spreading quality.

2.2. Introduction

Laser powder bed fusion (PBF-LP) has emerged as a leading additive manufacturing technique that can produce complex and high-precision components, and it has diverse applications ranging from aerospace to biomedical engineering. At the heart of PBF-LP lies the controlled deposition of successive layers of fine powder, which is followed by laser scanning to selectively fuse and solidify the material [1–3]. The initial spreading of the powder material significantly influences the efficiency and quality of this layer-by-layer deposition process. In the domain of powder dispersion techniques in additive manufacturing, roller-spreading and blade-spreading represent two separate approaches. Roller-spreading [4–6] involves using a roller mechanism to distribute powder, while blade-spreading [7,8] utilizes a blade to push and distribute the powder material across the printing surface. Roller-spreading and blade-spreading techniques have significant differences in powder distribution efficiency. Roller-spreading typically achieves higher packing density due to the normal force exerted by the roller, which compacts the powder more effectively and promotes tighter particle packing through uniformly distributed force chains [5].

Reducing production time is of utmost importance in additive manufacturing, specifically concerning the duration of powder spreading [9,10]. By decreasing the duration of powder spreading, manufacturers can achieve accelerated production cycles, shorter lead times, and heightened productivity. This reduction in production time allows for swift responses to market demands, expedites product development, and enables rapid delivery of customized or on-demand parts. Moreover, shorter production times yield cost savings and improved resource utilization. However, it is crucial to strike a delicate balance between reducing production time and upholding the integrity and quality of the final parts. Employing adequate control and optimization of the powder spreading process becomes imperative to maintain uniformity, minimize defects, and meet the required specifications.

Effective management of powder spreading time unlocks substantial benefits in terms of speed, agility, and cost-effectiveness, thereby bolstering competitiveness across various industries. The augmentation of spreading speed in spreader operations demonstrates a positive correlation with expedited processes, thereby reducing the temporal outlay for spreading activities and enhancing the overall temporal efficiency within the production workflow.

The spreading speed of the spreader is a critical factor influencing the powder layer's quality. This speed determines the powder distribution rate and uniformity on the building plate. A shearing force is generated as the spreader moves across the powder bed at a spreading speed. This force causes powder particles to slide and deform against each other, promoting their redistribution and breaking up agglomerates [11]. An escalation in the speed at which the blade spreads contribute to a reduction in the packing density [7,8,11–18]. This is due to the limited time for powder particles to settle and reorganize into a more tightly compacted configuration. In contrast, a slower spreading speed allows for increased settling and rearrangement of the powder particles, leading to a higher packing density. This behaviour is observed consistently across various blade shapes [19–23]. Yao et al. [8]reveal an optimal operating parameter for spreading SS316L, which suggests that a spreading velocity of $\leq$0.1 m/s yields favourable results. However, the identified gap in the literature review underscores the necessity for additional experiments encompassing a more comprehensive range of traverse speeds to corroborate this finding. The spreading speed significantly influences the generation of shear force, a factor influenced by the counter-rotating roller's motion, which, in turn, leads to the breakup of powder agglomerates. However, the same spreading speed also results in a dragging effect on the powder, causing a decrease in the overall packing density [4,6,13,19,22–24]. Hence, the spreading speed governs roller-spreading's essential shearing and dragging mechanisms. The circumferential speed of a counter-rotating roller pushes the powder forward in line with the spreading speed, ensuring consistent behaviour at different rotational speeds. Conversely, in Seluga's experimental work[25], it was observed that there was a marginal increase in powder bed density alongside an increase in traverse speed within the low-speed regime (below 12 mm/s). This observation suggests that increasing the speed does not impact packing density at extremely low spreading speeds. The rationale behind this behaviour is attributed to the fact that at low spreading speeds, powder necessitates time to propagate and settle within the building plate. This disparity underscores the intricate nature of the spreading process and implies that distinct mechanisms may come into play across varying speed regimes.

Numerous experimental and computational investigations have consistently demonstrated that augmenting the spreading speed of blade and counter-rotating roller processes precipitates a reduction in layer thickness [12,16,20]. This phenomenon is attributed to the heightened dragging force that propels powders away from the substrate. The escalation in spreading speed induces a more turbulent trajectory of particles, resulting in heightened non-uniformity in packing density [8,15,21]and augmented surface roughness of the powder layer [4,17,22,23]. Particularly at heightened traverse speeds, particles deposited onto the powder bed retain substantial momentum, continuing to flow over a considerable distance. Consequently, this post-flow behaviour results in an uneven surface and, in some instances, may give rise to the formation of a discontinuous layer.

Limited studies suggest that a forward-rotating roller improves powder bed density more than a counter-rotating roller or blade. The forward-rotating roller can grip and drag powder into the bed, increasing the density [26,27]. However, this approach can also lead to uneven surfaces and inaccurate layer thickness as the powder bed may spring back after the roller passes due to the release of stored elastic energy [28]. The circumferential speed of a forward-rotating roller drags the powder backward, opposing the spreading speed. Therefore, the effect of increasing the spreading speed with a forward-rotating roller depends on the relationship between the spreading speed and the circumferential speed, which will be examined in our current study.

This research paper thoroughly and comprehensively analyzes the roller's spreading speed effect on powder distribution in PBF-LP. The study aims to understand the complex relationships associated with the roller's spreading speed under various rotation speed conditions, focusing on the forward-rotating configuration identified in the literature review. The investigation encompasses an in-depth exploration of the connections between the roller's spreading speed and the characteristics of the powder layer. Through extensive Discrete Element Method (DEM) modelling, the study examines the influence of the spreading speed of the roller and its connection to both the layer thickness and packing density of the powder layers. By addressing critical gaps identified in the literature and proposing practical solutions for enhancing process efficiency, this research contributes to advancing understanding and optimizing roller-based powder distribution in PBF-LP.

2.3. Methodology

The PBF-LP process encompasses a powder-spreading system comprising three fundamental components: powder delivery, spreading and collection, as depicted in Figure

2-1d. A simplified computational domain focuses on the powder spread process. The domain is shown in Figure 2-1a and includes the powder supply and collector chambers as well as the building plate and roller of radius 2.5mm (R_r). The dimensions of the domain and its components are normalized using the desired layer thickness (δ). Specifically, the domain length L_x is 60δ and the width L_y is 25δ. Periodic conditions are applied in the y-direction. The roller is swept down the length of the domain with a uniform speed (V_s) while simultaneously rotating at a specified angular speed (ω).

Roller-spreading cases can be classified into non-rotating, counter-rotating, and forward-rotating rollers based on the direction of the roller's rotational speed relative to its translational spreading speed. In the non-rotating case, the roller moves at a constant spreading speed (Figure 2-1b, V_s= 0.15 m/s) without any rotational motion, allowing the powder to be spread purely by translational movement. In the counter-rotating case, the roller rotates counterclockwise while advancing with spreading speed (Figure 2-1c, V_s = 0.15 m/s and ω = 60 rad/sec), introducing a circumferential speed velocity component in the same direction as the spreading at the roller bottom (i.e., surface velocity equals V_s+ωR_r). For the forward-rotating case, the roller rotates clockwise while advancing with spreading speed (Figure 1d, V_s= 0.15 m/s and ω = 60 rad/sec), introducing a circumferential speed velocity opposite to the direction of spreading at the roller bottom (i.e., surface velocity equals V_s – ωR_r).

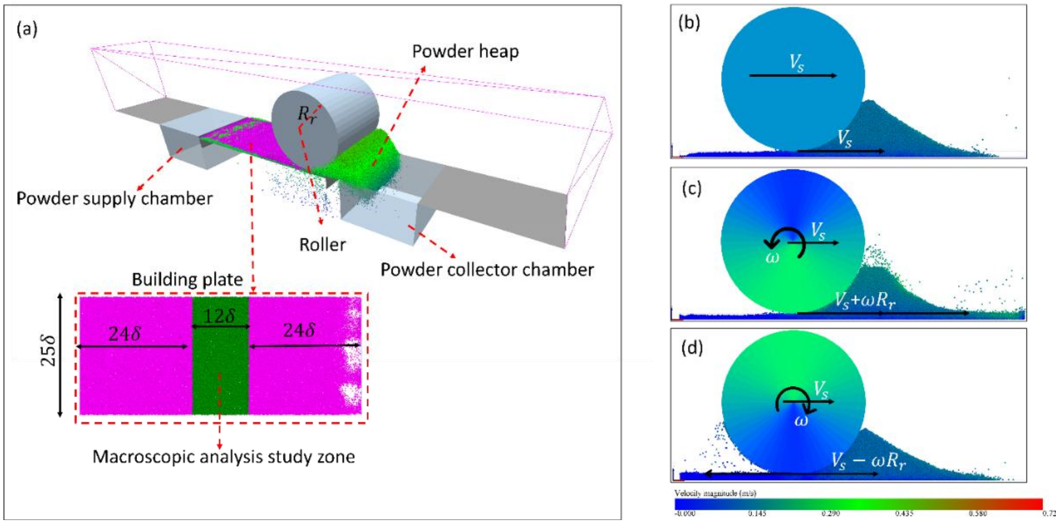

Figure 2-1. (a) Schematic of DEM model of powder spreading process in PBF-LP using a rolling-spreading technique. (b) Non-rotating roller with a spreading speed of 0.15 m/sec. (c) Counter-rotating roller with spreading speed of 0.15 m/sec and counterclockwise rotational speed of 60 rad/sec. (d) Forward-rotating roller with a spreading speed of 0.15 m/sec and clockwise rotational speed of 60 rad/sec . In (b), (c), and (d), both the powder and roller are colored according to velocity magnitude.

2.3.1. Mathematical model

In bed particles, the translational motion and rotational motion of each particle [29,30] are governed by the following expressions:

$$m_i \frac{dv_i}{dt} = m_i g + \sum_{j=1}^{p} \left(F_{ij,n} + F_{ij,s}\right) \mathrm{c} \tag{1}$$

$$I_i \frac{d\omega_i}{dt} = \sum_{j=1}^{p} \left(\tau_{ij,s} + \tau_{ij,r}\right) \tag{2}$$

where m_i, v_i, ω_i, and I_i are the mass, velocity, angular velocity, and moment of inertia of particle i, respectively; $F_{ij,n}$ and $F_{ij,s}$ are the normal and tangential interaction forces on particle i due to other particles j, and $\tau_{ij,s}$ and $\tau_{ij,r}$ are the torques generated by tangential force and rolling friction. The kinematics of all particles are updated by the time integration of the previous equations [31] .

Normal and tangential forces represent contributions of the contact forces between particles and the damping forces, which are added artificially to resolve the dissipation of kinetic energy. The normal and tangential forces have contact and damping force contributions:

$$F_{ij,n} = F^{n}_{c,ij} + F^{n}_{d,ij} \tag{3}$$

$$F_{ij,s} = F^{s}_{c,ij} + F^{s}_{d,ij} \tag{4}$$

Hertz-Mindlin contact model[32]with Johnson-Kendall-Roberts (JKR)[33] cohesion formulates the contact forces between particles (the same used for particles and walls with different coefficients), accounting for the influences of Van der Waals forces within the contact zone:

$$F^{n}_{c,ij} = \left[\frac{4E^*}{3R^*} r^3 - 4\sqrt{\pi r^3 \gamma E^*}\right] \tag{5}$$

$$F^{s}_{c,ij} = min\begin{cases} \mu_s \left|F^{n}_{c,ij}\right| \\ \left|8G^* \sqrt{R^* \alpha^n} \alpha^s\right| \end{cases} \tag{6}$$

$$F^{n}_{d,ij} = \left[-\sqrt{\frac{20}{3}}\left[\frac{-\ln e}{\sqrt{\ln^2 e + \pi^2}}\right]\left[E^* m^* (R^* \alpha^n)^{0.5}\right]^{0.5} u^{n}_{ij}\right] \tag{7}$$

$$F^{s}_{d,ij} = \left[-\sqrt{\frac{80}{3}}\left[\frac{-\ln e}{\sqrt{\ln^2 e + \pi^2}}\right]\left[G^* m^* (R^* \alpha^n)^{0.5}\right]^{0.5} u^{s}_{ij}\right] \tag{8}$$

where R^*, m^*, E^*, and G^* are the equivalent radius, mass, Young's modulus, and shear modulus:

$$R^* = R_i R_j / (R_i + R_j) \tag{9}$$

$$m^* = m_i m_j/(m_i + m_j) \tag{10}$$

$$E^* = E_i E_j/(E_i(1-\nu_j^2) + E_j(1-\nu_i^2)) \tag{11}$$

$$G^* = G_i G_j/(G_i(1-\nu_j) + G_j(1-\nu_i)) \tag{12}$$

where R_i, m_i, E_i, G_i, and ν_i are the radius, mass, Young's modulus, shear modulus, and Poisson's ratio, respectively; e, γ, μ_s, and μ_r are the coefficient of restitution, the surface energy, and the sliding and rolling friction coefficients; u_{ij}^n and u_{ij}^s are the normal and tangential relative velocities between particles i and j when a collision occurs; and α^n and α^s are the normal and tangential overlaps between particles i and j when a collision occurs. Friction torque is generated due to the moment of the tangential contact force. The rolling friction torque is created by applying a torque to the contact surfaces:

$$\tau_{ij,s} = R_i \times F_{c,ij}^s \tag{13}$$

$$\tau_{ij,r} = -\mu_r R_i F_{c,ij}^n \left[\frac{\omega_i}{|\omega_i|}\right] \tag{14}$$

2.3.2. Numerical model

The powder particle interactions are simulated by applying contact, friction, and cohesion forces as described in the previous mathematical model section. Altair EDEM software (2021.1) is used [34]. Selecting an appropriate time step is critical for achieving convergence and numerical stability. The time step used in these simulations is 1.62949e-7 seconds, equivalent to 20% of the Rayleigh Time, ensuring that the simulations accurately capture the dynamic processes and high-frequency phenomena while preventing instability and numerical errors. The mesh size was selected to be three times the radius of the smallest particle to ensure accurate detection of particle contacts, resulting in 4,018,008 cells within the computational domain.

2.3.3. Performance Parameters of the Spreading Process

Packing density, layer thickness, and mass fraction are defined to characterize the powder bed layer and help examine how roller-spreading parameters impact the efficacy of powder packing. The packing density (ρ_P) is defined as the ratio of the volume that is actually occupied by particles (V_p) to the volume of the spatial configuration being encompassed (V_{cuboid}), with the latter being determined based on the desired layer thickness. Local packing densities are determined by dividing the building plate into *N* regions in the *x*-direction. The normalized variance of the packing density ($\rho_{P,VC}$) over the bed gives a measure of the bed structure uniformity.

The local powder layer thickness ($\delta(x)$) is the average of the maximum elevation of the particles resting on the building plate within each local (*x*-location) region. The global average or actual thickness (δ_{act}) is simply the average of the local thickness and surface roughness (R_a) calculated using the centerline average method. The layer thickness and roughness can also be normalized with the desired layer thickness.

$$R_a = \frac{1}{N}\sum_{N} |\delta_i(x) - \delta_{act}| \tag{15}$$

The mass fraction (MF) of the powder layer is the ratio of the mass of powder particles deposited on the building plate to the total mass of the powder layer that is supposed to fill the desired layer thickness. A global average mass fraction MF_{avg} and its normalized variance MF_{vc} are obtained from the local *MF* values in the *x*-direction. The packing density is equivalent to the mass fraction when the layer thickness is equal to or less than the desired thickness. However, if the layer thickness exceeds the desired value, the mass fraction becomes greater than the packing density. The packing density and layer thickness combination measures how much powder material is effectively placed on the surface during the spreading process. Moreover, the mass fraction indicates the spreader's ability to distribute powder over the building plate.

In this study, we have taken a meticulous approach to address several simplifications and assumptions, especially regarding the use of an empty build plate for powder spreading. The choice of an empty build plate is not arbitrary; it is a careful decision that allows for better control of variables and isolates the effects of the roller on powder distribution. Simulating a loose powder layer introduces additional complex interactions beyond the primary focus of this investigation, including the dynamics of the roller and its impact on powder spread. By focusing on an empty build plate, we can concentrate on understanding the fundamental mechanisms of roller behavior without introducing the confounding variables that a loose powder layer may bring, thereby improving the clarity and precision of the findings.

2.3.4. Material calibration and model verification

The calibration of the Discrete Element Method (DEM) poses a well-known challenge in the literature [35,36]. As a preliminary evaluation of the model's performance, we compare the static angle of repose (AOR) formed by SS316 powder samples in both experimental and simulation settings. The simulation parameters of the material, including surface energy and sliding/rolling friction coefficients, are adjusted to match the experimental and numerical predictions of the AOR. Table 2-1 [8,37] presents the simulation parameters range for SS316L, which are used in the process of material calibration. A reduced Young's modulus was chosen to optimize the numerical stability of the model. This lower modulus helps achieve faster convergence during simulations by reducing the time step and ensuring efficient computation[18]. According to existing references, the AOR of SS316 is reported to be 21.3°[15,18]. By conducting an analysis of the effects of surface energy on the AOR, an optimal value of 0.001 J/m^2 is identified, leading to an AOR of 21.0°, as illustrated in Figure 2-2a.

Table 2-1.DEM parameters of Alloy SS 316L alloy.

Parameter	Value
Poisson's ratio,ν	0.3
bulk density,ρ	7800 kg/m3
Young's modulus, E	22 GPa
Coefficient of restitution, e	0.64
Coefficient of sliding friction,μ_s	0.6
Coefficient of rolling friction, μ_r	0.085
Surface energy,γ	0.0001-0.002 J/m^2

Further validation of the numerical model is done by comparing the dynamic repose angle (DRA) of SS316 powder during powder spreading. Measurements by Yao et al.[8] were done using a rectangular blade moving with a spreading speed of 0.05 m/sec for monomodal powder sizes of 34.8, 100, 123.2, and 166.4 µm. The current model's roller is replaced with a similar blade to match the experimental setup, and the dynamic repose angles of powders of different sizes show good agreement with the experimental measurements, as illustrated in Figure 2-2b-e and Table 2-2. The error in the comparison remains below 9.6% in all cases.

Table 2-2. Comparison of the calculated dynamic angle of repose with experimental and simulation values from Yao et al. [8]

Powder size(D),µm	The dynamic angle of Repose (deg)		
	Experimental value	Yao simulation	Current simulation
34.8	45.9°	44.0°	44°
100	30.4°	31.9°	33°
123.2	30.1°	32.2°	33°
169.4	32.3°	32.5°	33°

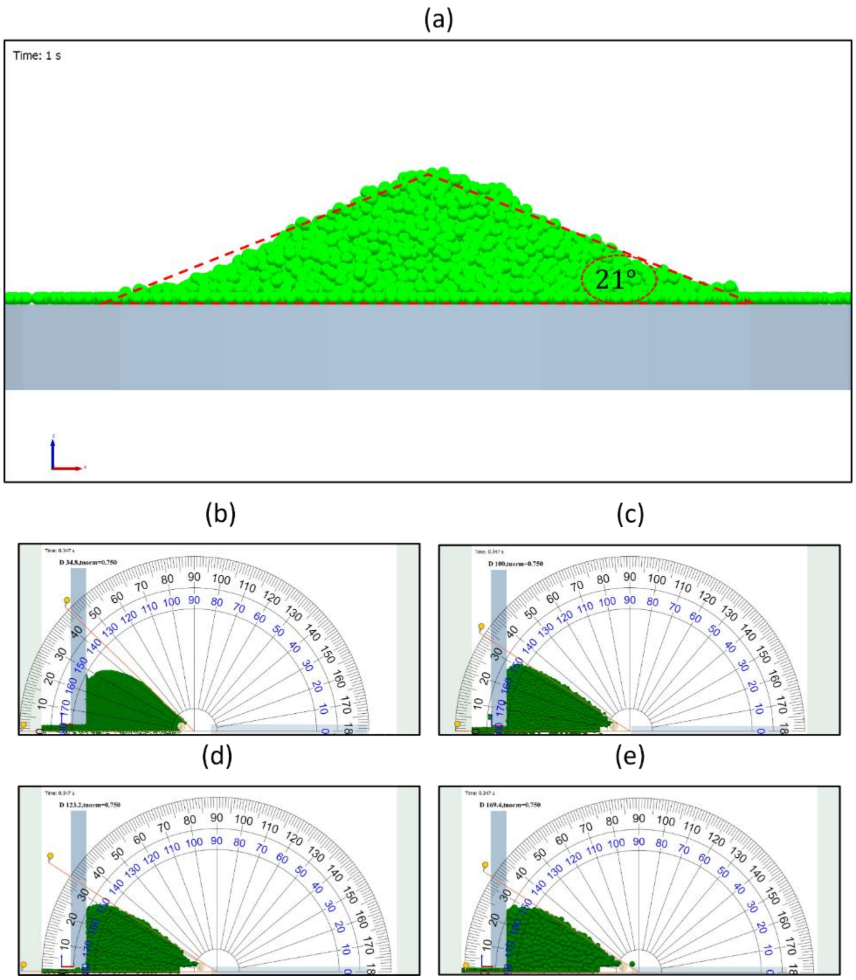

Figure 2-2.Simulated angle of repose of SS316, assuming γ = 0.001 J/m^2. (**a**) Static angle of repose; (**b**) Dynamic Repose Angle (DRA) for 34.8-µm-diameter powder. (**c**) DRA for 100 µm powder. (**d**) DRA for 123.2 µm powder. (**e**) DRA for 166.4 µm powder during blade spreading.

2.3.5. Simulation Conditions

This study focuses on the influence of spreading speed on powder flow dynamics within the context of the roller spreading process. Spreading speed varies from 0.025 m/s to 0.15 m/s. The use of spreading speeds between 0.05 and 0.15 m/s aligns with many studies [8] that explore the fundamental mechanics of the powder-spreading process under controlled conditions. The interplay between the spreading speed and the roller rotation speed is considered by using four different rotation speeds: a non-rotating roller ($\omega = 0$), a counter-rotating roller (ω = 60 rad/s), and two forward-rotating roller rotational speeds (10 and 60 rad/s). The two forward-rotating roller speeds are employed to simulate the effect of spreading speed when $V_s/R_r \geq \omega$ and when $V_s/R_r \leq \omega$, respectively.

SS316 powder with a single particle size of 50 μm is used, mitigating the complicating influence of powder size distribution, and the ratio of powder size to the desired layer thickness is maintained at 0.25. After carefully considering various factors, we have chosen a selection of mono-sized particles with a particle diameter-to-layer thickness ratio of 0.25. This choice simplifies the model, ensures numerical stability, and allows us to isolate the effects of powder size distribution, focusing on the impact of spreading speed. This controlled environment enables us to study the influences of roller speed and spreading conditions without introducing the added complexities of polydisperse powders. The 0.25 ratio closely reflects realistic powder sizes [38] , ensures sufficient powder packing, minimizes wall effects, and keeps our focus clear and unwavering.

2.4. Results and Discussion

As in the introduction, the effects of spreading speed have been previously investigated for non-rotating and counter-rotating rollers. Less attention has been paid to forward rolling, and little-to-no consideration has been given to the bed quality with the various regimes of forward rolling. There are cases that can be considered: pure rolling, sub-rolling, and super-rolling. Pure rolling occurs when the roller's circumferential speed (ωR_r) matches the spreading speed (V_s), sub-rolling occurs when the roller's circumferential speed is less than the spreading speed, and super-rolling occurs when the roller's circumferential speed is greater than the spreading speed. We start by presenting the results of the impacts of the spreading speed of non-rotating and counter-rotating rollers for our specific case of $D/\delta = 0.25$ and then examine and compare the effects of forward rolling. The results section is categorized into two types of analyses: microscopic and macroscopic. Microscopic analysis investigates the variations in local packing density, mass fraction, layer thickness over the building plates, and cavity formation. Conversely, macroscopic analysis examines the variations in average packing density, mass fraction, layer thickness, and powder distribution uniformity concerning spreading speed.

2.4.1. Microscopic Analysis

2.4.1.1. Effect of Spreading Speed on the Non-Rotating Roller

The non-rotating roller functions analogously to a blade and operates based on its spreading speed to distribute powder over the building plate. The packing density of the powder layer created by a non-rotating roller behaves similarly along the length of the building plate at different spreading speeds, which range from 0.025 to 0.15 m/s. Initially, the packing density increases to a certain level within the first 10% of the building plate length. Then, it fluctuates around this level, which is inversely proportional to the spreading speed, with more noticeable fluctuations at higher spreading speeds. Towards the final 20% of the building plate length, the packing density sharply rises to a maximum value before decreasing, as illustrated in Figure 2-3a. At a high spreading speed of 0.15 m/s, the roller displaces powder from the trailing edge (left side) to the leading edge (right side) of the building plate, resulting in the formation of a significant cavity on the trailing edge, as depicted in Figure 2-3c,d. The layer thickness distribution along the building plate mirrors the trend observed in packing density. The layer thickness fluctuates below the desired value throughout the majority of the building plate length, specifically to the last 20%. Notably, the peak in packing density corresponds to a peak in layer thickness, which frequently surpasses the desired layer thickness, as depicted in Figure 2-3b. This finding indicates a difference between this area's packing density and mass fraction. Additionally, the fluctuations in layer thickness increase with the spreading speed.

The behavior of powder spreading using a non-rotating roller can be explained by the dynamics of the roller and its interaction with the powder throughout the spreading process. At high spreading speeds, the roller pushes the powder away from the trailing edge due to the significant momentum transfer from the roller to the powder, creating a cavity. After the roller passes over the powder layer, the velocity of the powder decreases, and its direction changes to fill this cavity, as there is minimal resistance to flow. However, the amount of backflow is insufficient to fill the cavity, resulting in a large and continuous cavity at the trailing edge, as shown in Figure 2-4a–d. As the roller reaches the leading edge, the high-velocity powder collides with the solid boundary at the end of the building plate. This collision alters the powder's direction and interaction with the developing powder layer. The result is a powder buildup just before the leading edge and a significant reduction in packing density before the solid boundary (i.e., rebound zone), as illustrated in Figure 2-4f–i.

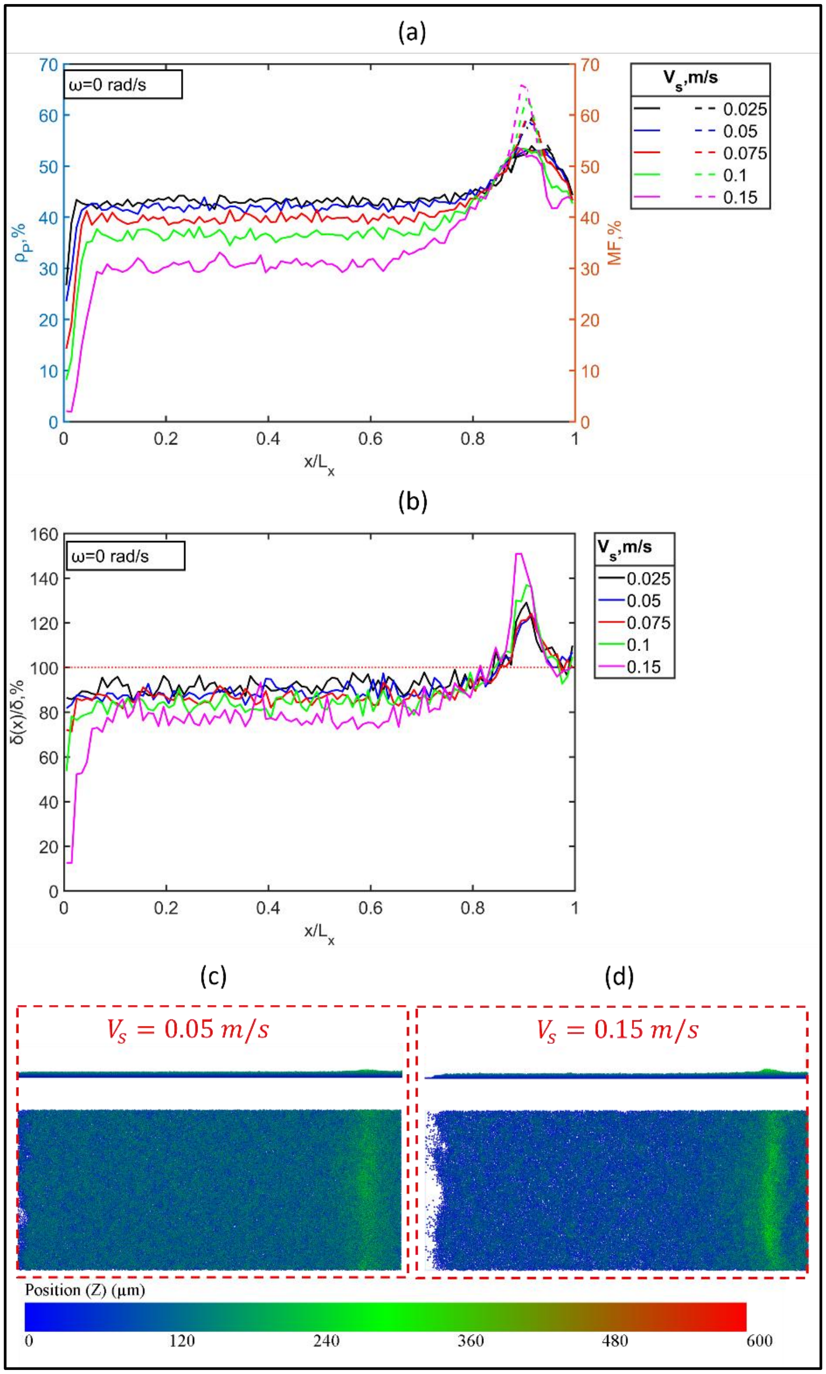

Figure 2-3.Powder layer characteristics of the non-rotating roller versus the building plate length; (**a**) packing density (solid lines) and a mass fraction (dashed lines); (**b**) layer thickness; (**c**) top view and front view of the powder bed after spreading with the speed of 0.05 m/s; and (**d**) top view and front view of the powder bed after spreading with the speed of 0.15 m/s, colored by powder position in Z-direction (i.e., layer thickness).

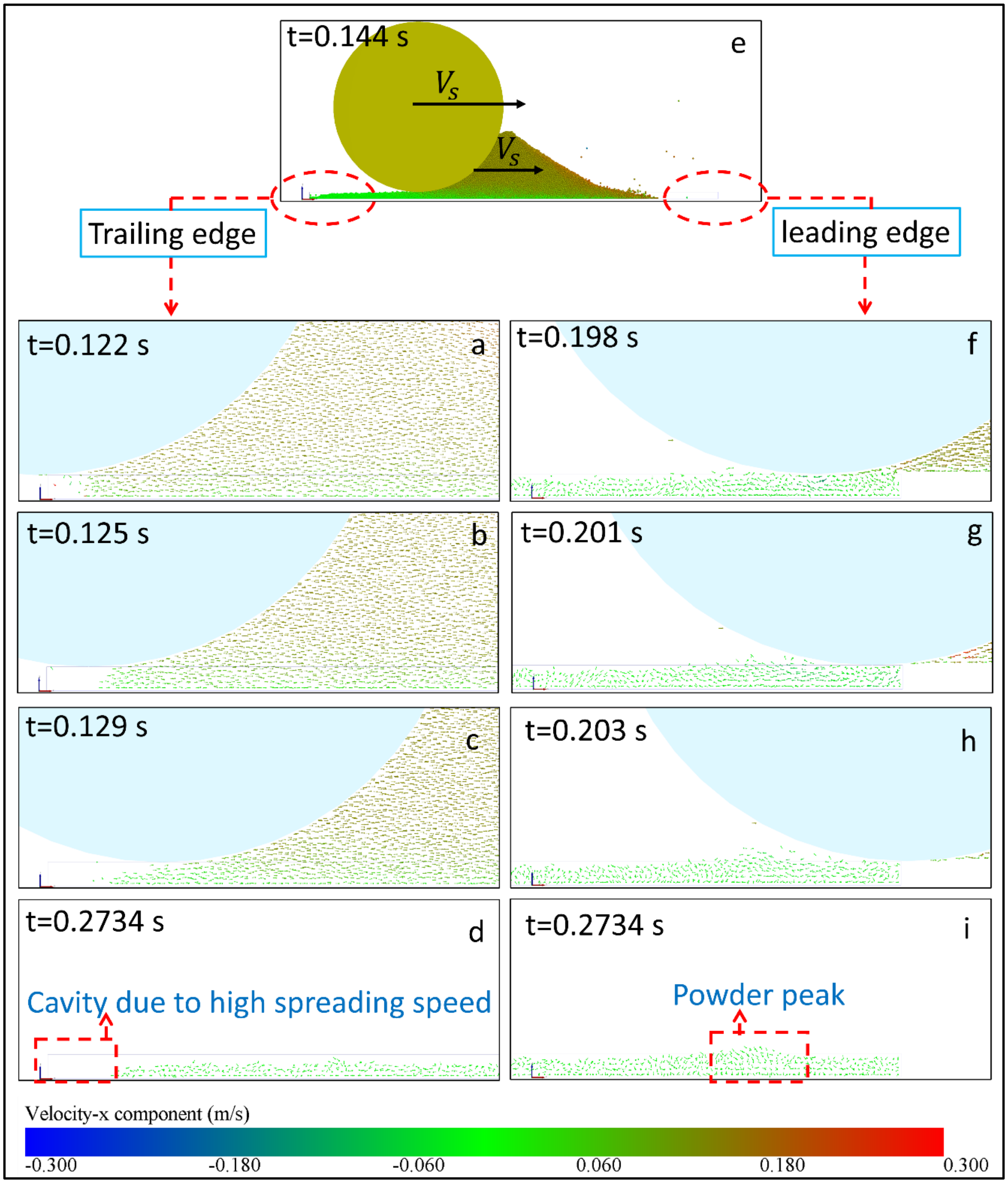

Figure 2-4.(**a**–**d**, **f**–**i**) Velocity vector fields illustrating powder distribution for a non-rotating roller moving at 0.15 m/s during spreading. Subfigures (**a**–**d**) show the development of powder dynamics on the trailing edge (left side) of the building plate over time, while subfigures (**f**–**i**) depict the development on the leading edge (right side) over the same time intervals. Subfigure (**e**) shows the powder heap during the spreading process, with velocity vectors colored by the x-component of velocity, highlighting the flow and heap formation.

2.4.1.2. Effect of the Spreading Speed on Counter-Rotating Roller

The counter-rotating roller, which operates at an angular speed of 60 rad/s, undergoes variations in spreading speed from 0.025 to 0.15 m/s. The trend of packing density along the building plate for the counter-rotating roller is similar to that of the non-rotating roller. At lower spreading speeds, the packing density remains relatively stable along the length of the building plate with only minor fluctuations. However, as the spreading speed increases, significant variations occur, particularly in the last 20% of the building plate. In this region, the packing density sharply rises to peak values before abruptly decreasing, as shown in Figure 2-5a. Similarly, the layer thickness shows more intense fluctuations at higher spreading speeds, especially in the final 20% of the plate. This thickness remains below the desired value for most of the build plate length, as illustrated in Figure 2-5b. These fluctuations correspond with the peaks in packing density observed in Figure 2-5a, where the layer thickness exceeds the desired value, indicating that the mass fraction is greater than the packing density at this location. At a spreading speed of 0.05 m/s, the powder layer appears uniform and compact with minimal disturbances. In contrast, at a spreading speed of 0.15 m/s, the powder layer exhibits significant non-uniformity, with more pronounced small voids and lower powder compaction, which is consistent with the fluctuations observed in the graphs, as presented in Figure 2-5a,d. Consequently, small vacancies (voids) form within the powder layer produced by the counter-rotating roller as the spreading velocity increases (see the difference between this figure and Figure 2-5c,d). This finding from our simulations aligns with the results obtained by Chen et al. from their experimental imaging [4].

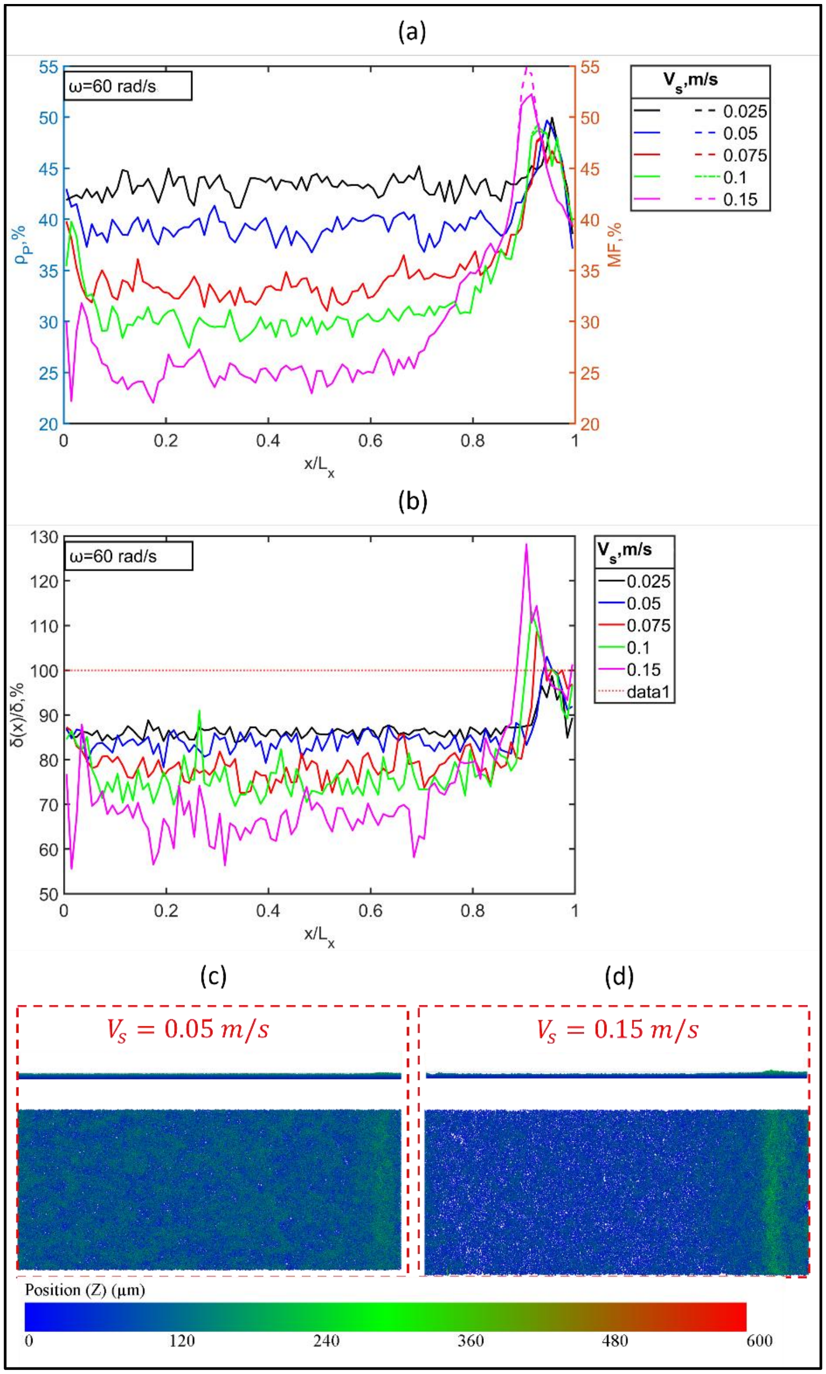

Figure 2-5.Powder layer characteristics of a counter-rotating roller rotating at 60 rad/s versus building plate length. (**a**) Packing density (solid lines) and mass fraction (dashed lines), (**b**) layer thickness, and (**c**) top view and front view of the powder bed after spreading with the speed of 0.05 m/s. (**d**) Top view and front view of the powder bed after spreading with the speed of 0.15 m/s, colored by powder position in Z-direction (i.e., layer thickness).

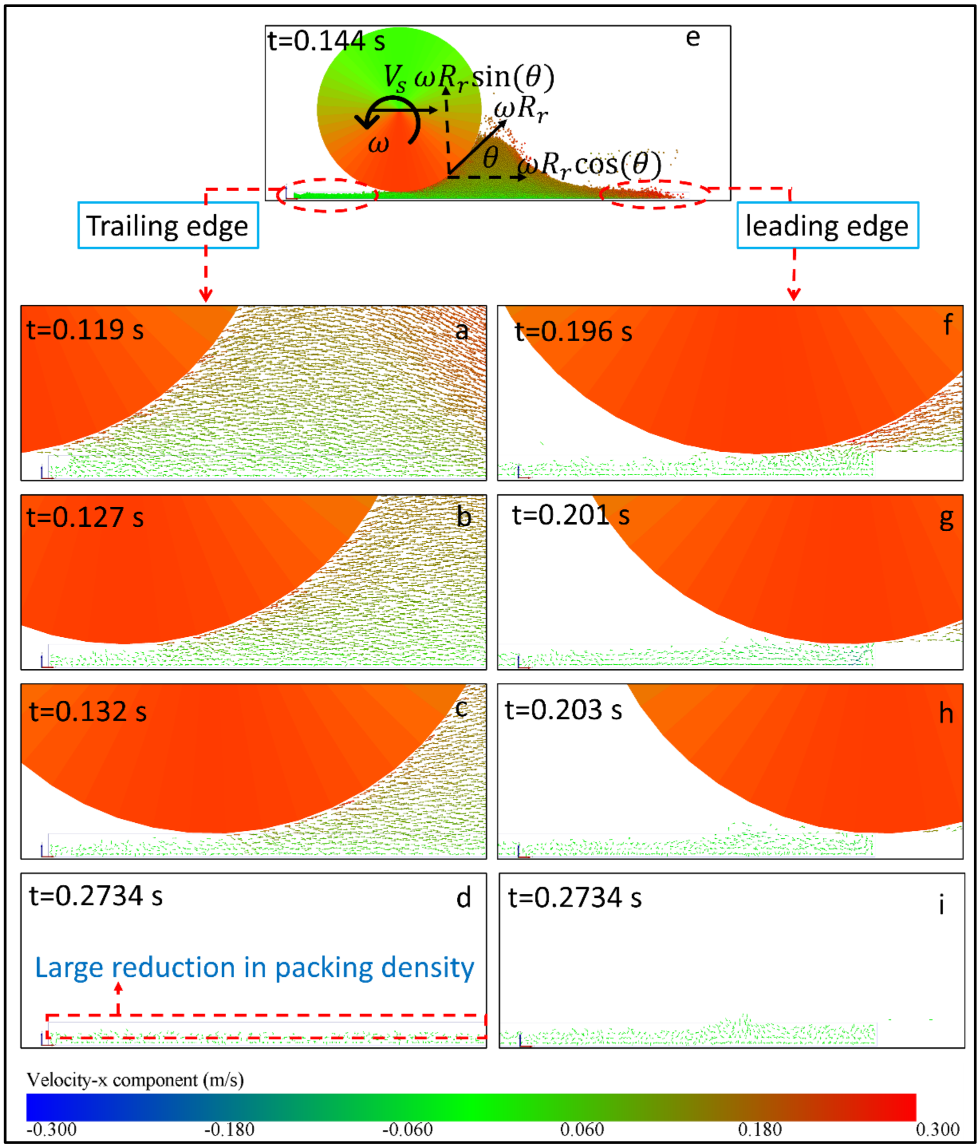

Figure 2-6. (**a**–**d**, **f**–**i**) Velocity vector fields illustrating powder distribution for a counter-rotating roller moving at 0.15 m/s and rotating at 60 rad/s during spreading. Subfigures (**a**–**d**) show the development of powder dynamics on the trailing edge (left side) of the building plate over time, while subfigures (**f**–**i**) depict the development on the leading edge (right side) over the same time intervals. Subfigure (**e**) shows the powder heap during the spreading process with velocity vectors colored by the x-component of velocity, highlighting the flow and heap formation.

The operation of a counter-rotating roller can be explained as the interplay between the linear spreading velocity in the x-direction and the circumferential velocity generated by the roller's counterclockwise rotation. The circumferential velocity introduces an additional x-velocity component to the roller surface, enhancing the transfer of x-momentum to the powder layer, as shown in Figure 2-6e. As the roller initiates the powder spreading process on the building plate, it is anticipated that the powder will be displaced from the trailing edge, resulting in a cavity similar to that observed with a non-rotating roller. However, observations show a notable decrease in the powder layer after the roller has passed instead of a clearly defined cavity, as illustrated in Figure 2-6a–d. This reduction is attributed to the heightened momentum transfer from the roller to the powder. The counterclockwise rotation of the roller also introduces a y-direction momentum component, dispersing and lifting the powder upwards, which prevents the formation of a distinct cavity at the trailing edge and promotes a reduction in powder density within the layer. Analogous to the behavior of a non-rotating roller, as the counter-rotating roller approaches the leading edge, the high-velocity powder collides with the solid boundary at the end of the build plate. This collision alters the powder's trajectory and interaction with the forming layer, leading to powder accumulation just before the leading edge and a significant decrease in packing density near the solid boundary, as shown in Figure 2-6f–i.

2.4.1.3. Effect of the Spreading Speed on Forward-Rotating Roller

The movement of a forward-rotating roller pertains to its horizontal displacement in the positive x-direction across a surface caused by its spreading speed. Concurrently, the roller's clockwise rotation generates additional velocity at its surface. The x-component of this velocity**,** being in the negative x-direction, contributes to the roller's surface speed by subtracting the spreading speed and the x-component of the tangential speed. This analysis allows us to divide the roller's movement into two distinct categories: sub-rolling and super-rolling. Sub-rolling occurs when the spreading speed is greater than or equal to the circumferential speed, while super-rolling occurs when the spreading speed is less than or equal to the circumferential speed.

Sub-Rolling

In this setup, a roller rotates forward at a speed ranging from 0.025 m/s to 0.15 m/s while rotating clockwise at 10 rad/s. In each simulation, the spreading speed is ensured to be greater than or equal to the circumferential speed. At a spreading speed of 0.025 m/s, the packing density remains stable along the entire length of the building plate, with only a slight reduction at the leading edge. As the spreading speed increases, the packing density at the trailing edge experiences an initial reduction, and it then increases to a specific value with fluctuations around it; it finally decreases again at the leading edge, as shown in Figure 2-7a. These fluctuations become more pronounced at higher spreading speeds. Notably, the packing density reductions at the trailing and leading edges intensify as the spreading speed increases. A small and discontinuous cavity formation in the powder at the trailing edge at 0.15 m/s supports this observation, as presented in Figure 2-7c,d. The mass fraction trends align with the packing density but are generally higher. As the spreading speed increases, the difference between the packing density and the mass fraction narrows. The layer thickness also fluctuates along the building plate, often exceeding the desired layer thickness at the leading edge, where the mass fraction is significantly higher than the packing density. The layer thickness exceeds the desired value at a spreading speed of 0.025 m/s, as illustrated in Figure 2-7b. Similar to non-rotating and counter-rotating rollers, the layer thickness and packing density decrease with increasing spreading speed.

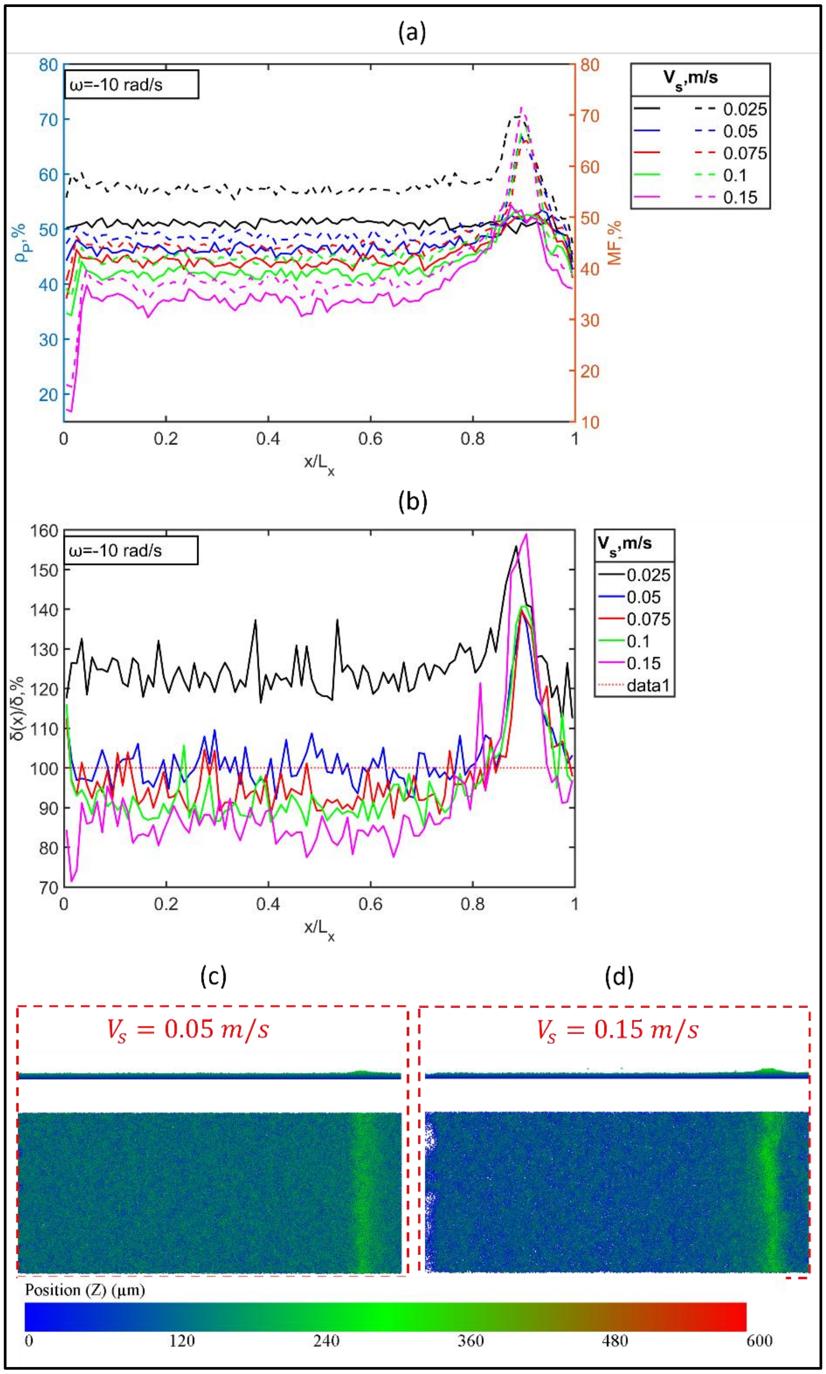

Figure 2-7. Powder layer characteristics of the forward-rotating roller rotating at 10 rad/s (i.e., sub-rolling case) versus the building plate length. (**a**) Packing density (solid lines) and mass fraction (dashed lines), (**b**) layer thickness, and (**c**) top view and front view of the powder bed after spreading with the speed of 0.05 m/s. (**d**) Top view and front view of the powder bed after spreading with the speed of 0.15 m/s, colored by powder position in Z-direction (i.e., layer thickness).

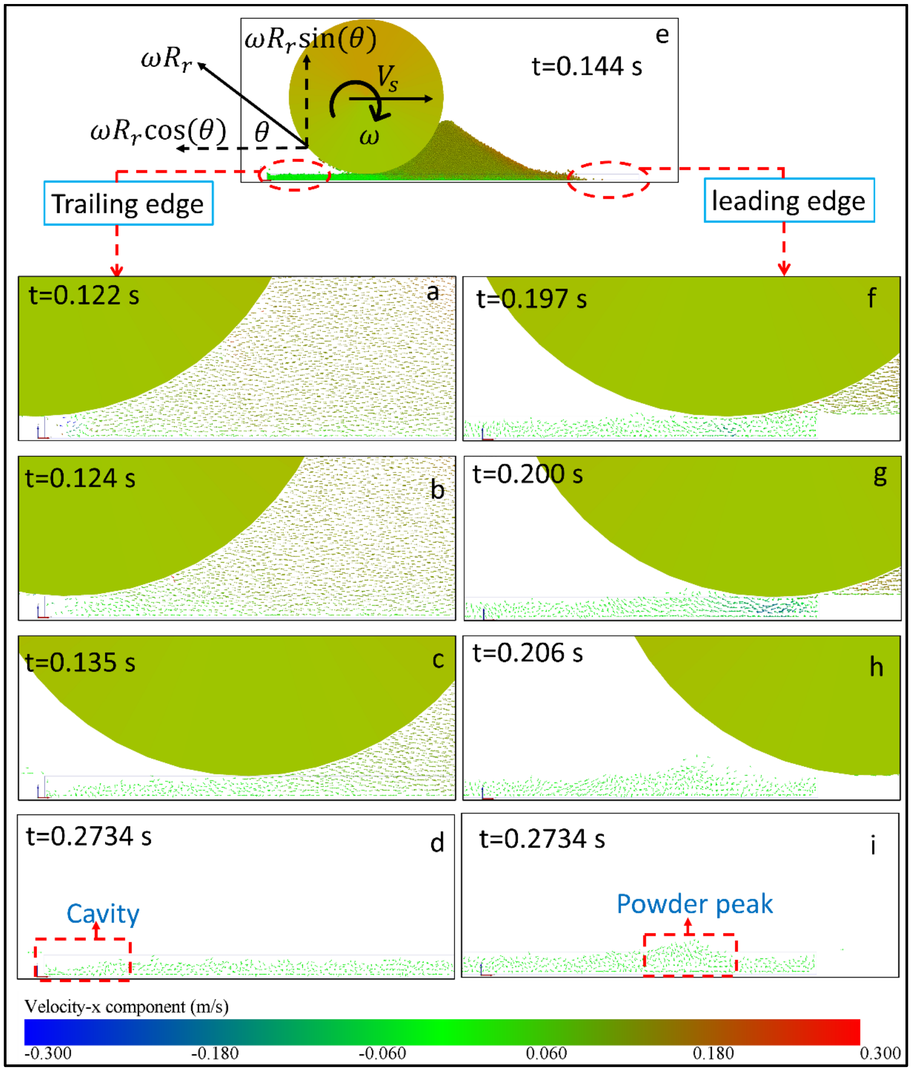

Figure 2-8. (**a**–**d**, **f**–**i**) Velocity vector fields illustrating powder distribution for a forward-rotating roller moving at 0.15 m/s and rotating at 10 rad/s during spreading. Subfigures (**a**–**d**) show the development of powder dynamics on the trailing edge (left side) of the building plate over time, while subfigures (**f**–**i**) depict the development on the leading edge (right side) over the same time intervals. Subfigure (**e**) shows the powder heap during the spreading process, with velocity vectors colored by the x-component of velocity, highlighting the flow and heap formation.

The roller generates significant force as it moves quickly across the powder, pushing it away from the edge behind it. This force, caused by the roller's speed, is counteracted by the negative x-component of the circumferential speed. As a result, less powder is pulled along by the roller, leading to smaller discontinuous cavities at the trailing edge compared to the scenario in which the roller is not rotating (the cavity is large and continuous), as shown in Figure 2-8a–d. As the roller approaches the leading edge, the high-speed powder collides with the solid boundary at the end of the build plate. This collision redirects the powder and influences how it interacts with the developing powder layer. Additionally, the circumferential speed pulls powder from the heap in front of the roller, causing it to spread in opposite directions. Consequently, there is a buildup of powder just before the leading edge, resulting in a noticeable decrease in packing density near the leading edge, as illustrated in Figure 2-8f–i. At low spreading speeds, the circumferential speed causes the powder to disperse backward along the building plate, countering the motion of the roller. In some cases, such as at 0.025 and 0.05 m/s, more powder accumulates above the desired layer thickness, causing the mass fraction to exceed the packing density.

Super-Rolling

In this experimental setup, a forward-rotating roller operates at a spreading speed ranging from 0.025 m/s to 0.15 m/s while rotating clockwise at 60 rad/s. Throughout the simulations, it is ensured that the spreading speed is either smaller than or equal to the circumferential speed of the roller. The packing density remains relatively stable, fluctuating around a consistent average value at different spreading speeds. However, a significant reduction in packing density is observed at the leading edge, with the extent of this reduction being inversely proportional to the spreading speed. It is observed that a continuous cavity is formed at a leading edge at a low spreading velocity (i.e.,$V_s = 0.025 \text{ and } 0.05 \text{ m/s}$) and become small and discontinuous cavities at a high spreading speed (i.e., $V_s = 0.15 \text{ m/s}$), as presented in Figure 2-9c,d. At a spreading speed of 0.025 m/s, the mass fraction peaks at the trailing edge and gradually decreases, culminating in a substantial reduction at the leading edge, as shown in Figure 2-9a. As the spreading speed increases, the mass fraction tends to fluctuate around values higher than the packing density, which is followed by a marked reduction at the leading edge. The variation in layer thickness along the building plate length mirrors the trend observed in packing density. It consistently remains higher than the desired layer thickness, except at the leading edge, where it falls below the desired value, as presented in Figure 2-9b. Both the mass fraction and layer thickness decrease as the spreading speed increases.

The main feature of a forward-rotating roller, particularly in the context of super-rolling, is its rapid clockwise rotation. This rotation produces a negative x-component and a positive y-component on the roller's rear surface. The negative x-component exerts a force that pushes the powder in the opposite direction of the spreading motion. In contrast, the positive y-component disperses the powder (powder burst) across the building plate once the roller has passed. This process increases powder accumulation on the building plate, causing the layer thickness to exceed the desired level along the entire plate length, except at the leading edge, as illustrated in Figure 2-10a–d.

Similar to other roller configurations, as the roller approaches the leading edge, the high-speed powder collides with the solid boundary at the end of the plate. This collision alters the powder's direction and affects its interaction with the developing powder layer. The roller's high circumferential speed also pulls additional powder from the heap in front with high momentum, dispersing it in opposite directions, as shown in Figure 2-10f–i. This activity leads to noticeable powder buildup just before the leading edge and creates a continuous cavity at the leading edge, as shown in Figure 2-9c. When the spreading speed increases to match the circumferential speed, an equilibrium is established between the momentum transfer from the spreading speed (positive x-component) and the circumferential speed (negative x-component). This balance reduces the size of the cavity at the leading edge, making it discontinuous, as presented in Figure 2-9d and Figure 2-11f–

i. Therefore, a high spreading speed and a clockwise rotational speed maintain a stable packing density across the building plate.

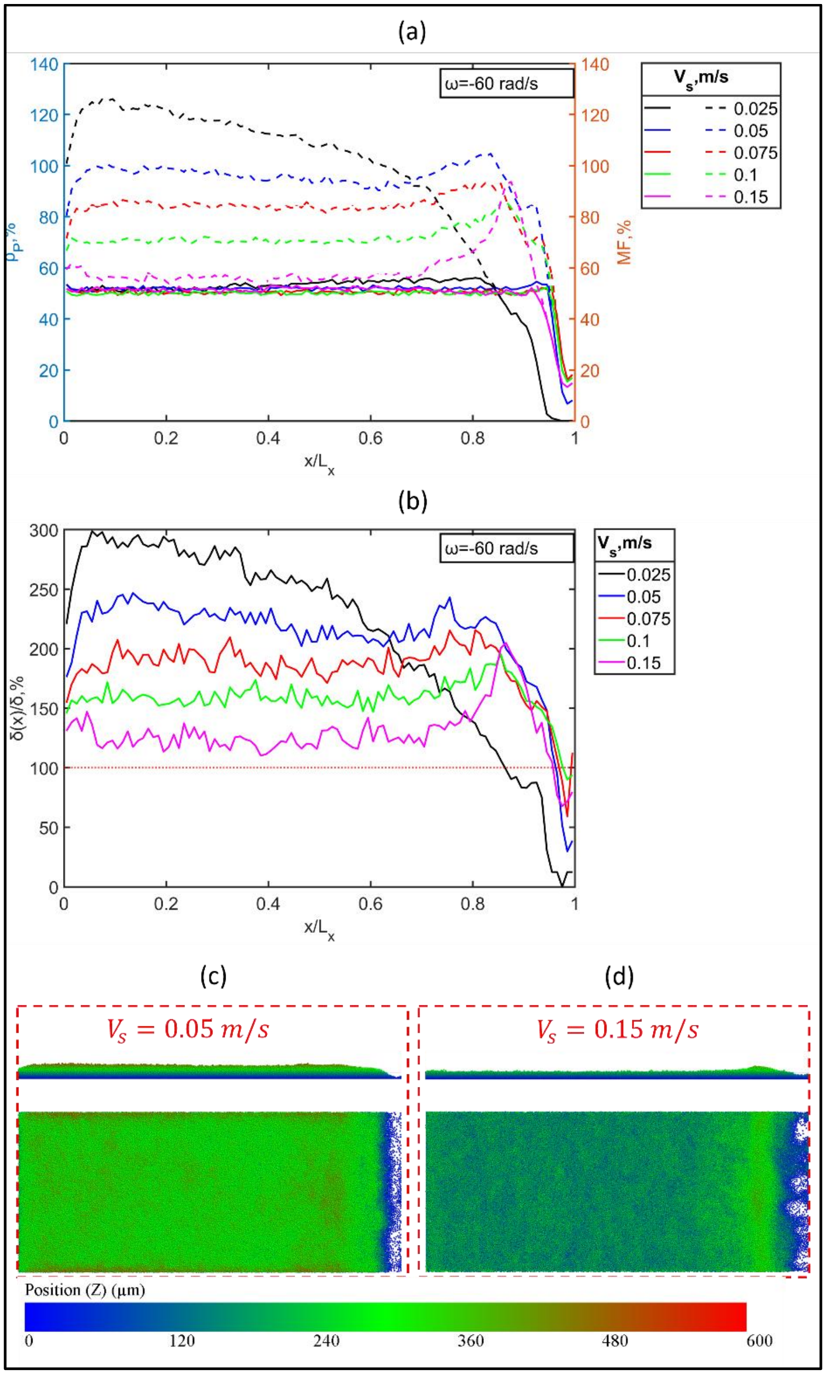

Figure 2-9.Powder layer characteristics of a forward-rotating roller rotating at 60 rad/s (i.e., super-rolling case) versus the building plate length. (**a**) Packing density (solid lines) and mass fraction (dashed lines), (**b**) layer thickness, and (**c**) top view and front view of the powder bed after the spreading process with the speed of 0.05 m/s. (**d**) Top view and front view of the powder bed after spreading with the speed of 0.15 m/s, colored by powder position in Z-direction (i.e., layer thickness).

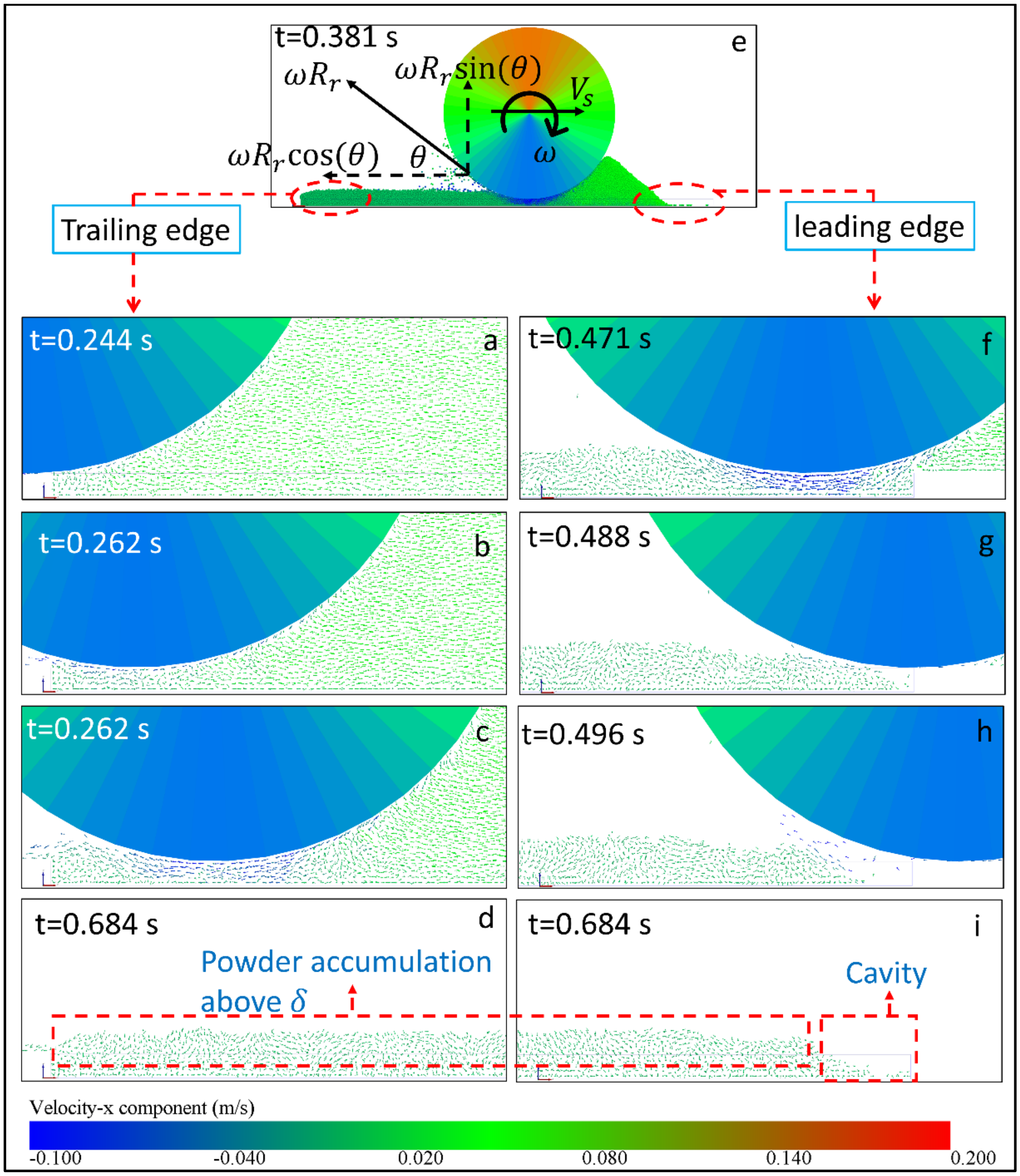

Figure 2-10. (**a**–**d**, **f**–**i**) Velocity vector fields illustrating powder distribution for a forward-rotating roller moving at 0.05 m/s and rotating at 60 rad/s during spreading. Subfigures (**a**–**d**) show the development of powder dynamics on the trailing edge (left side) of the building plate over time, while subfigures (**f**–**i**) depict the development on the leading edge (right side) over the same time intervals. Subfigure (**e**) shows the powder heap during the spreading process, with velocity vectors colored by the x-component of velocity, highlighting the flow and heap formation.

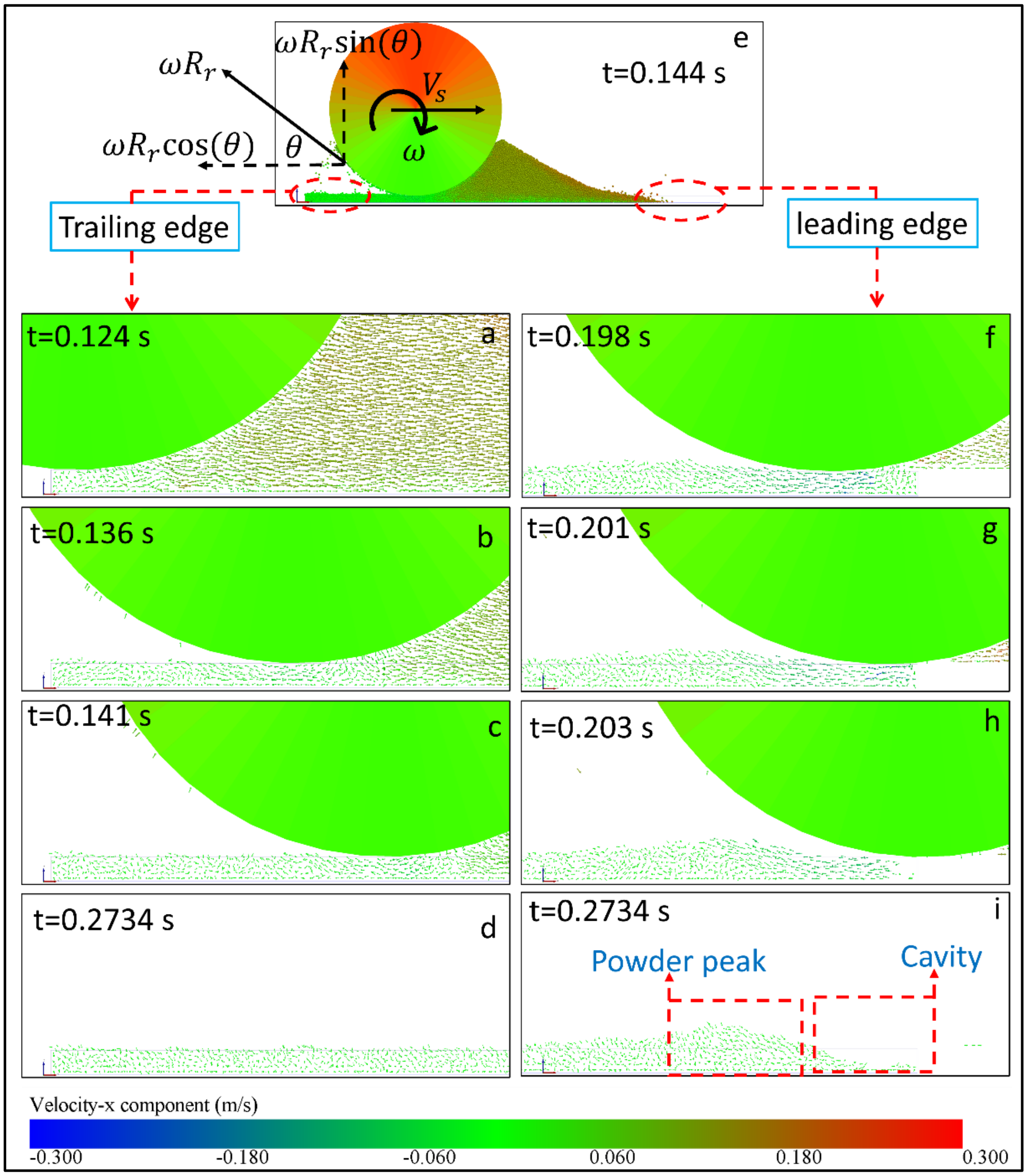

Figure 2-11. (**a**–**d**, **f**–**i**) Velocity vector fields illustrating powder distribution for a forward-rotating roller moving at 0.15 m/s and rotating at 60 rad/s during spreading. Subfigures (**a**–**d**) show the development of powder dynamics on the trailing edge (left side) of the building plate over time, while subfigures (**f**–**i**) depict the development on the leading edge (right side) over the same time intervals. Subfigure (**e**) shows the powder heap during the spreading process, with velocity vectors colored by the x-component of velocity, highlighting the flow and heap formation.

2.4.2. Macroscopic Analysis

2.4.2.1. Effects of the Spreading Speed on the Macroscopic Properties

The influence of the spreading speed on macroscopic properties, including packing density, mass fraction, layer thickness, and uniformity, is examined by evaluating these properties' average values and variations within the study area, highlighted in Figure 2-1d. The current study shows that the packing density of the powder layer developed by non-rotating and counter-rotating rollers experiences a reduction with increasing spreading speed, a trend that aligns with previous research [17–19]. Specifically, as the spreading speed of the non-rotating roller increases from 0.025 to 0.15 m/s, there is a notable reduction in average packing density of 28.7%, as shown in Figure 2-12. For the counter-rotating roller, rotating at 60 rad/s, the same increase in spreading speed results in a more significant reduction in packing density of 42.8%. Similarly, the sub-rolling roller, rotating at 10 rad/s, shows a 29% reduction in packing density under the same conditions. Conversely, the packing density of the powder layer developed by the super-rolling roller, which rotates at 60 rad/s, fluctuates with a maximum change of only 7%. This result indicates that the clockwise rotation, balanced with the spreading speed, compensates for the reduction in packing density due to the high spreading speed.

When considering mass fraction, it is essential to note that the layer thickness developed by non-rotating, counter-rotating, and sub-rolling rollers falls below the desired layer thickness. In contrast, the layer thickness developed by super-rolling and rolling rollers exceeds the desired layer thickness. Consequently, the mass fraction is identical to the packing density of non-rotating, counter-rotating, and sub-rolling rollers. At the same time, it exceeds the packing density in the case of rolling and super-rolling rollers. Notably, the mass fraction experiences a reduction of 48.2% when the spreading speed of the super-rolling roller, which rotates at 60 rad/s, increases from 0.025 to 0.15 m/s.

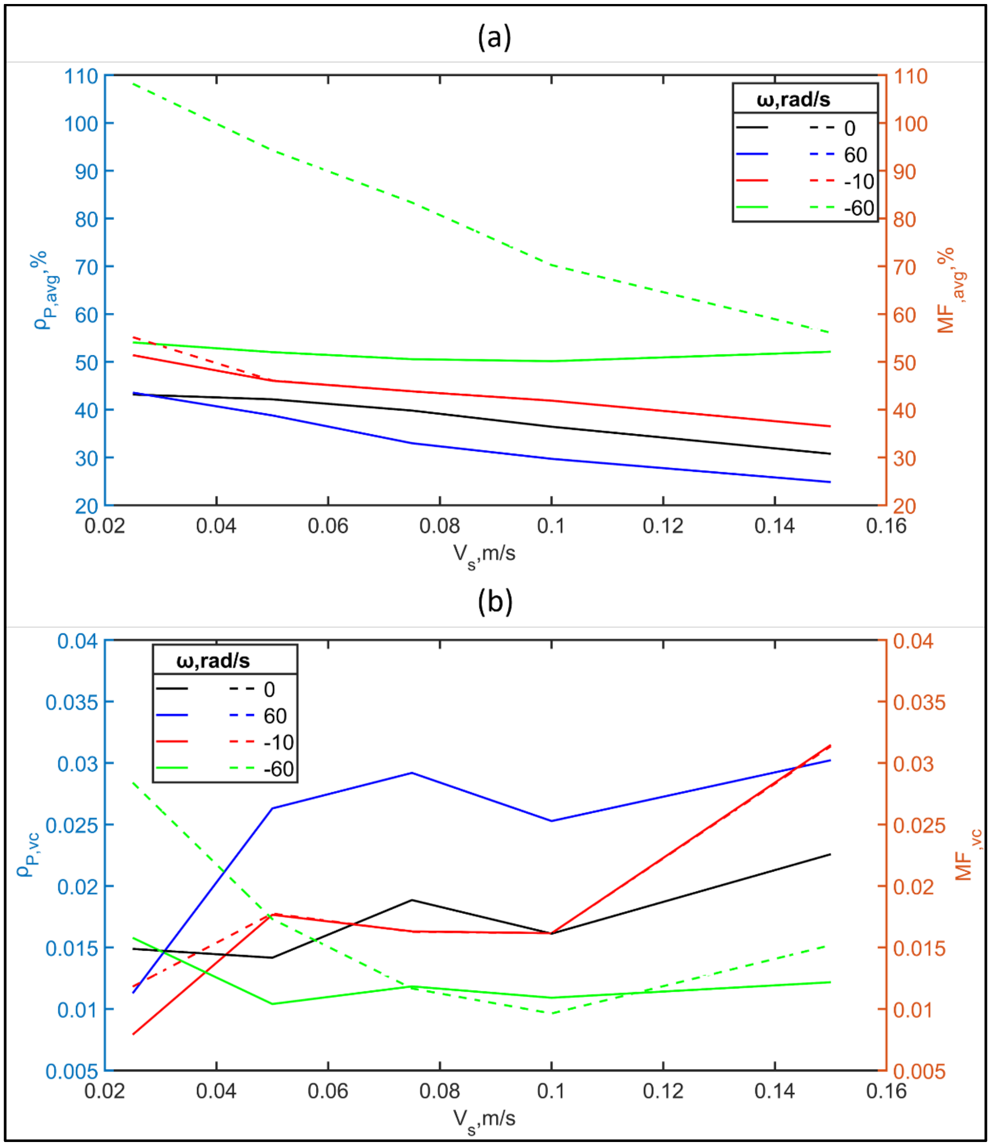

Figure 2-12. Packing density and mass fraction characteristics of study zone versus spreading speed for different roller configurations. (**a**) Average packing density (solid lines) and average mass fraction (dashed lines) and (**b**) variation coefficient of packing density (solid lines) and mass fraction (dashed lines).

As the spreading speed of the non-rotating roller increases from 0.025 to 0.15 m/s, the average layer thickness decreases by 17.2%, as shown in Figure 2-13. The counter-rotating roller, rotating at 60 rad/s, also shows a 22% decrease in average layer thickness with the same increase in spreading speed. Moreover, the sub-rolling roller, rotating at 10 rad/s, demonstrates an even more significant reduction in average layer thickness of 32.7%. The layer thicknesses produced by the non-rotating, counter-rotating, and sub-rolling rollers are lower than the desired layer thickness. Conversely, the layer thicknesses produced by the super-rolling and rolling rollers exceed the desired layer thickness. For the super-rolling roller, an increase in spreading speed from 0.025 to 0.15 m/s results in a 50% reduction in layer thickness.

Non-rotating and counter-rotating rollers maintain a constant level of surface roughness (approximately 2.9% of the desired layer thickness in this study). However, adding clockwise rotational speed to the roller dynamics increases surface roughness (3.7% in the case of sub-rolling and 10.4% in the case of super-rolling). Generally, regardless of the rotational speed and spreading speed, the roller-spreading process is random, maintaining a specific level of variation in the packing density distribution. However, counterclockwise rotation compared to clockwise rotation is better in terms of powder layer uniformity due to the turbulent motion of powder resulting from the clockwise rotational speed (i.e., powder burst).

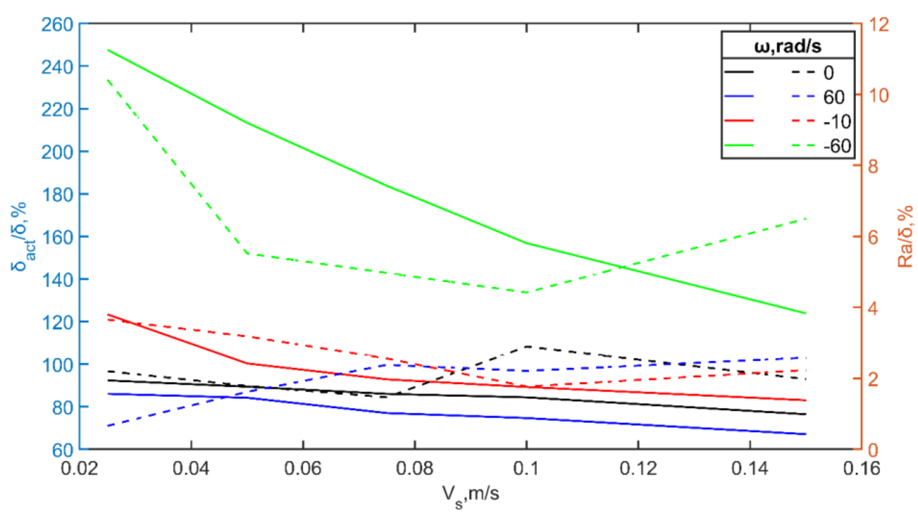

Figure 2-13. Average layer thickness and surface roughness of study zone developed by different roller configurations versus the spreading speed.

The enhanced spreading speed in the counter-rotating roller closely mirrors that of the non-rotating roller with more pronounced effects. Likewise, the enhanced spreading speed in the sub-rolling roller closely mirrors that of the non-rotating roller. The behaviors of non-rotating, counter-rotating, and sub-rolling rollers can be explained similarly by understanding momentum transfer from the roller to the particles. When the roller is not rotating (ω = 0) and moves solely with the spreading speed, the majority of the particles attain velocities approximately equal to the spreading speed ($V_{particles} = V_s$). In the case of the counter-rotating roller, the addition of circumferential speed increases the roller's surface speed, thereby enhancing the particle velocities ($V_{particles} = V_s + \omega R_r$). Conversely, with the sub-rolling roller, the circumferential speed acts in the opposite direction, reducing the roller surface speed and consequently lowering the particle velocities ($V_{particles} = V_s - \omega R_r$). Despite the reduction, the resultant particle speed remains effective in the direction of spreading. At a high spreading speed, the powder moves away from the left solid boundary of the building plate while being compressed toward the right solid boundary due to the dragging force, indicating the presence of fewer particles. When the spreading speed is high, the particles deposited on the powder bed continue flowing for a specific distance due to the excessive momentum exchanged with the roller. This excessive momentum exchange causes particles to be dragged out of the building plate, reducing the packing density. This considerable transferred momentum leads to more powder disturbance, causing an uneven surface and a reduction in layer thickness. Conversely, particles settle more quickly and uniformly onto the powder bed at low spreading speeds due to the reduced kinetic energy and momentum. This minimized momentum exchange leads to less disturbance of the powder bed, resulting in a more even distribution, higher packing density, smoother surface, more consistent layer thickness, and, unfortunately, longer total printing time. The increased rotational speed of the counter-rotating roller contributes to elevated particle momentum, leading to less densely packed particles, and it is aligned with literature reviews [4,6,13,19,22–24]. When a sub-rolling roller moves forward at a spreading speed, it behaves similarly to a non-rotating roller. The increased spreading speed causes the powder to shift from the left side due to its generated momentum. This behavior of a sub-rolling roller is consistent with non-rotating and counter-rotating configurations as long as the circumferential speed remains below the spreading speed. The momentum exchange resulting from the spreading speed plays a more significant role than the momentum induced by the circumferential speed.

Conversely, different behavior is observed when dealing with a super-rolling roller, where the circumferential speed equals or exceeds the spreading speed. The backward circumferential speed component pulls the powder in the opposite direction of spreading. This causes the powder to disperse over the building plate after the roller passes (i.e., powder burst), compensating for the reduction in powder due to the high spreading speed. This compensation helps sustain the packing density despite the high spreading speed, differing from the behaviors observed in non-rotating, counter-rotating, and sub-rolling rollers.

Adopting a high spreading speed for the roller offers advantages in reducing spreading and production times. However, it is essential to recognize that high spreading speeds can decrease packing density and layer thickness. To counteract these effects, considering the behavior of the super-rolling roller explained previously, a higher clockwise rotational speed can be employed to establish a balance between the forward and backward momentum transfers to particles. When a forward-rotating roller dispenses powder at a spreading speed of 0.15 m/s while gradually increasing its rotational speed from zero to the threshold value ($\omega = V_s/R_r$), a significant enhancement in packing density is observed. Specifically, the packing density increases by 69.4%, and the layer thickness increases by 62%, as illustrated in Figure 2-14. This observation supports the notion that the increase in powder quantity due to the occurrence of powder bursts, which are caused by backward momentum transfer to particles, compensates for the reduction in powder amount resulting from the drag effect associated with higher spreading speeds.

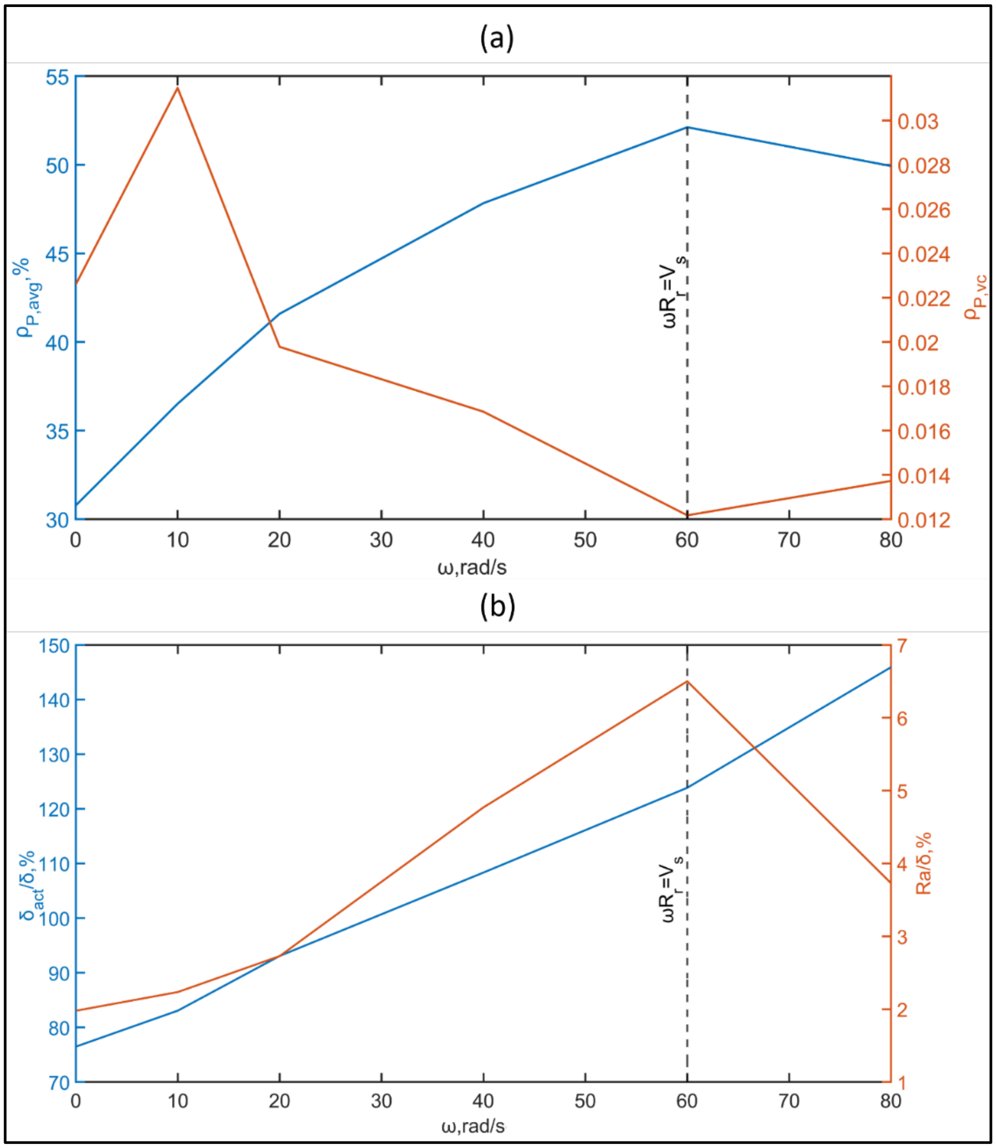

Figure 2-14. Macroscopic characteristics of powder layer formed by forward-rotating roller moves at 0.15 m/s versus rotational speed. (**a**) Packing density and its variation coefficient. (**b**) Layer thickness and surface roughness.

Furthermore, the increase in packing density is accompanied by a substantial reduction in the coefficient of variation, with a decrease of at least 46%. These findings demonstrate that implementing a higher clockwise rotational speed in conjunction with a high spreading speed can effectively enhance packing density and layer thickness while reducing variability, thus optimizing roller spreading.

2.4.2.2. Effect of the Resultant Speed

The combined effect of the roller's translational and rotational motions on the spreading process is examined by considering the resultant speed, which is the sum of the spreading and circumferential speeds. Analysis shows that the packing density remains relatively stable at higher values when the resultant speed is slightly negative or near zero (i.e., super-rolling roller). However, the mass fraction increases rapidly as the resultant speed moves further below zero, as shown in Figure 2-15. Conversely, as the resultant speed increases past zero, there are noticeable and identical declines in packing density and mass fraction. This trend suggests that higher positive resultant speeds, corresponding to higher spreading speeds or counter-rotating or sub-rolling rollers, adversely affect packing density and the spreader's ability to distribute powder uniformly over the building plate. The layer thickness decreases as the resultant speed shifts from negative to positive values, as presented in Figure 2-16. The thickness is the highest when the resultant speed is negative, indicating the effect of powder bursts due to clockwise rotation, and it gradually decreases as the resultant speed becomes positive. In contrast, the surface roughness is relatively high at negative values, and it decreases to almost zero as the resultant speed approaches positive values. This trend suggests that clockwise rotation (negative circumferential speed) results in a higher layer thickness and surface roughness. In contrast, counterclockwise rotation (positive circumferential speed) tends to smooth the surface and reduce the layer thickness. Therefore, achieving an optimal balance between spreading speed and roller rotation is crucial for maintaining a high-quality and efficient powder spreading process.

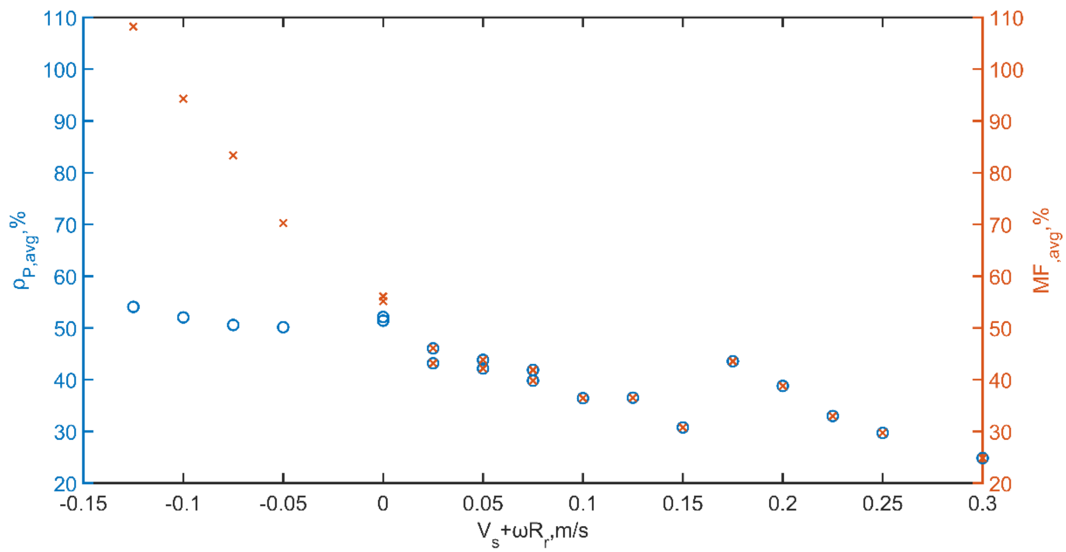

Figure 2-15. Average packing density and mass fraction versus the resultant speed.

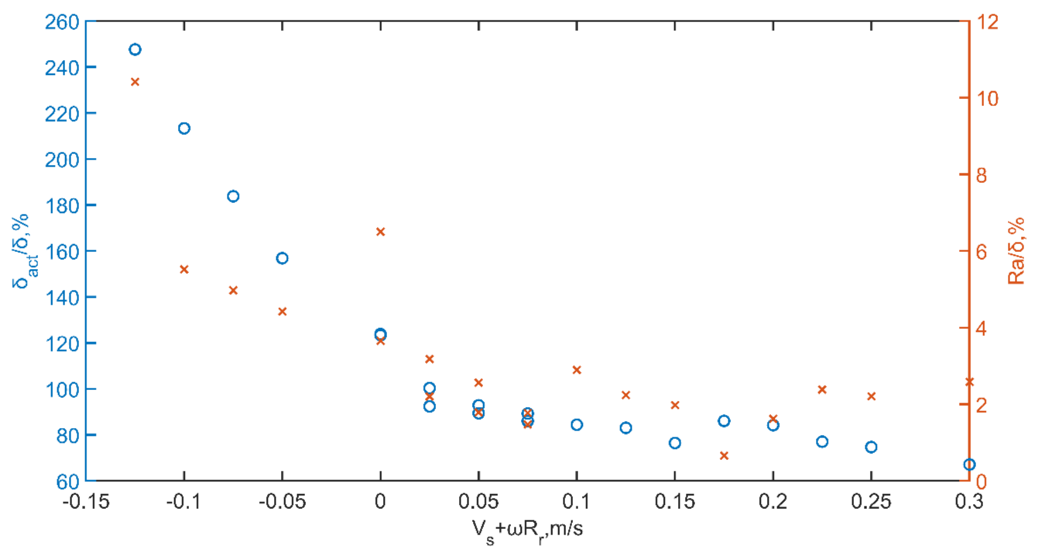

Figure 2-16. Average layer thickness and surface roughness versus the resultant speed.

2.5. Conclusions

Investigating the effects of escalating spreading speeds of various roller configurations on powder bed characteristics has provided valuable insights. The non-rotating and counter-rotating rollers, serving as baselines, exhibit similar trends. An increased spreading speed generally results in decreased packing density and layer thickness. This result occurs because the higher spreading speed transfers more momentum to the particles, dragging the powder off the building plate. With its additional rotational speed, the counter-rotating roller amplifies this effect, causing a more significant reduction in packing density and layer thickness compared to the non-rotating roller. Due to the dominance of spreading speed in the case of a forward-rotating roller at a low clockwise rotational (sub-rolling configuration), it follows a similar trend.

However, the forward-rolling roller at a high clockwise rotational speed (i.e., super-rolling configuration) presents a promising solution. A delicate balance is achieved in this configuration, where the circumferential speed equals or exceeds the spreading speed. This balance effectively manages forward and backward momentum transfers, leading to a powder burst phenomenon compensating for the powder reduction caused by high spreading speeds. This balance reassures us that the packing density and layer thickness can be maintained or even enhanced. The findings show that implementing a higher clockwise rotational speed in conjunction with high spreading speeds can significantly improve the packing density and uniformity of the powder bed. Specifically, a forward-rotating roller operating at a spreading speed of 0.15 m/s, with a gradually increasing rotational speed, enhances the packing density by 69.4% and the layer thickness by 62% while reducing the variation coefficient by 46%. Conversely, the surface roughness increases to 10.4% of the desired layer thickness, and the surface roughness values of other configurations increase to 3.7%.

The study emphasizes optimizing the roller's combined translational and rotational motions to achieve superior powder bed characteristics. The study lays the groundwork for further exploration into the complex dynamics of roller spreading processes and has immediate applications in enhancing the efficiency and quality of additive manufacturing techniques. Future work can expand on these findings by exploring different material properties, roller designs and dynamics to refine and enhance the powder-spreading process.

References

[1] M. Yakout, M.A. Elbestawi, S.C. Veldhuis, On the characterization of stainless steel 316L parts produced by selective laser melting, International Journal of Advanced Manufacturing Technology 95 (2018) 1953–1974. https://doi.org/10.1007/s00170-017-1303-0.

[2] M. Yakout, A. Cadamuro, M.A. Elbestawi, S.C. Veldhuis, The selection of process parameters in additive manufacturing for aerospace alloys, International Journal of Advanced Manufacturing Technology 92 (2017) 2081–2098. https://doi.org/10.1007/s00170-017-0280-7.

[3] E. Fereiduni, A. Ghasemi, M. Elbestawi, Unique opportunities for microstructure engineering via trace B4C addition to Ti-6Al-4V through laser powder bed fusion process: As-built and heat-treated scenarios, Addit Manuf 50 (2022) 102557. https://doi.org/10.1016/j.addma.2021.102557.

[4] H. Chen, Y. Chen, Y. Liu, Q. Wei, Y. Shi, W. Yan, Packing quality of powder layer during counter-rolling-type powder spreading process in additive manufacturing, Int J Mach Tools Manuf 153 (2020) 103553. https://doi.org/10.1016/j.ijmachtools.2020.103553.

[5] J. Zhang, Y. Tan, X. Xiao, S. Jiang, Comparison of roller-spreading and blade-spreading processes in powder-bed additive manufacturing by DEM simulations, Particuology 66 (2022) 48–58. https://doi.org/10.1016/j.partic.2021.07.005.

[6] J. Zhang, Y. Tan, T. Bao, Y. Xu, X. Xiao, S. Jiang, Discrete element simulation of the effect of roller-spreading parameters on powder-bed density in additive manufacturing, Materials 13 (2020). https://doi.org/10.3390/ma13102285.

[7] Y. Lee, A.K. Gurnon, D. Bodner, S. Simunovic, Effect of Particle Spreading Dynamics on Powder Bed Quality in Metal Additive Manufacturing, Integr Mater Manuf Innov 9 (2020) 410–422. https://doi.org/10.1007/s40192-020-00193-1.

[8] D. Yao, X. An, H. Fu, H. Zhang, X. Yang, Q. Zou, K. Dong, Dynamic investigation on the powder spreading during selective laser melting additive manufacturing, Addit Manuf 37 (2021). https://doi.org/10.1016/j.addma.2020.101707.

[9] I. Ribeiro, F. Matos, C. Jacinto, H. Salman, G. Cardeal, H. Carvalho, R. Godina, P. Peças, Framework for life cycle sustainability assessment of additive manufacturing, Sustainability (Switzerland) 12 (2020). https://doi.org/10.3390/su12030929.

[10] G. Taddese, S. Durieux, E. Duc, Sustainability performance indicators for additive manufacturing: a literature review based on product life cycle studies, International Journal of Advanced Manufacturing Technology 107 (2020) 3109–3134. https://doi.org/10.1007/s00170-020-05249-2.

[11] Y.M. Fouda, A.E. Bayly, A DEM study of powder spreading in additive layer manufacturing, Granul Matter 22 (2020) 1–18. https://doi.org/10.1007/s10035-019-0971-x.

[12] C. Meier, R. Weissbach, J. Weinberg, W.A. Wall, A.J. Hart, Critical influences of particle size and adhesion on the powder layer uniformity in metal additive manufacturing, J Mater Process Technol 266 (2019) 484–501. https://doi.org/10.1016/j.jmatprotec.2018.10.037.

[13] M.Y. Shaheen, A.R. Thornton, S. Luding, T. Weinhart, The influence of material and process parameters on powder spreading in additive manufacturing, Powder Technol 383 (2021) 564–583. https://doi.org/10.1016/j.powtec.2021.01.058.

[14] L. Si, T. Zhang, M. Zhou, M. Li, Y. Zhang, H. Zhou, Numerical simulation of the flow behavior and powder spreading mechanism in powder bed-based additive manufacturing, Powder Technol 394 (2021) 1004–1016. https://doi.org/10.1016/j.powtec.2021.09.010.

[15] D. Yao, X. Liu, J. Wang, W. Fan, M. Li, H. Fu, H. Zhang, X. Yang, Q. Zou, X. An, Numerical insights on the spreading of practical 316 L stainless steel powder in SLM additive manufacturing, Powder Technol 390 (2021) 197–208. https://doi.org/10.1016/j.powtec.2021.05.082.

[16] V. Lampitella, M. Trofa, A. Astarita, G. D’Avino, Discrete Element Method Analysis of the Spreading Mechanism and Its Influence on Powder Bed Characteristics in Additive Manufacturing, Micromachines (Basel) 12 (2021) 392. https://doi.org/10.3390/mi12040392.

[17] Z. Xiang, M. Zhang, R. Yan, Q. Yin, K. Zhang, Powder-spreading dynamics and packing quality improvement for laser powder bed fusion additive manufacturing, Powder Technol 389 (2021) 278–291. https://doi.org/10.1016/j.powtec.2021.05.036.

[18] D. Yao, J. Wang, M. Li, T. Zhao, Y. Cai, X. An, R. Zou, H. Zhang, H. Fu, X. Yang, Q. Zou, Segregation of 316L stainless steel powder during spreading in selective laser melting based additive manufacturing, Powder Technol 397 (2022) 117096. https://doi.org/10.1016/j.powtec.2021.117096.

[19] L. Wang, Z. Zhou, E. Li, H. Shen, A. Yu, Powder deposition mechanism during powder spreading with different spreader geometries in powder bed fusion additive manufacturing, Powder Technol 395 (2022) 802–810. https://doi.org/10.1016/j.powtec.2021.10.017.

[20] A. Phua, C. Doblin, P. Owen, C.H.J. Davies, G.W. Delaney, The effect of recoater geometry and speed on granular convection and size segregation in powder bed fusion, Powder Technol 394 (2021) 632–644. https://doi.org/10.1016/j.powtec.2021.08.058.

[21] Q. Wu, C. Qiao, J. Wang, D. Yao, Y. Wu, W. Fan, M. Li, X. An, Adaptability investigations on bottom modified blade in powder spreading process of additive manufacturing, Addit Manuf 49 (2022) 102477. https://doi.org/10.1016/j.addma.2021.102477.

[22] S. Haeri, Y. Wang, O. Ghita, J. Sun, Discrete element simulation and experimental study of powder spreading process in additive manufacturing, Powder Technol 306 (2016) 45–54. https://doi.org/10.1016/j.powtec.2016.11.002.

[23] S. Haeri, Optimisation of blade type spreaders for powder bed preparation in Additive Manufacturing using DEM simulations, Powder Technol 321 (2017) 94–104. https://doi.org/10.1016/j.powtec.2017.08.011.

[24] E.J.R. Parteli, T. Pöschel, Particle-based simulation of powder application in additive manufacturing, Powder Technol 288 (2016) 96–102. https://doi.org/10.1016/j.powtec.2015.10.035.

[25] K.J. Seluga, Three Dimensional Printing by Vector Printing of Fine Metal Powders, 2001.

[26] M. Tang, Y. Guo, W. Zhang, H. Ma, L. Yang, W. Wei, L. Wang, S. Fan, Q. Zhang, On recoated powder quality with a forward rotating flexible roller in laser powder bed fusion of 30 wt% 5 µm SiCp/AlSi10Mg composites, Mater Des 225 (2023). https://doi.org/10.1016/j.matdes.2022.111489.

[27] T. Niino, K. Sato, Effect of Powder Compaction in Plastic Laser Sintering Fabrication, n.d.

[28] M. Ziaee, R. Hershman, A. Mahmood, N.B. Crane, Fabrication of demineralized bone matrix/polycaprolactone composites using large area projection sintering (LAPS), Journal of Manufacturing and Materials Processing 3 (2019). https://doi.org/10.3390/jmmp3020030.

[29] J.Q. Gan, A.B. Yu, Z.Y. Zhou, DEM simulation on the packing of fine ellipsoids, Chem Eng Sci 156 (2016) 64–76. https://doi.org/https://doi.org/10.1016/j.ces.2016.09.017.

[30] H.P. Zhu, Z.Y. Zhou, R.Y. Yang, A.B. Yu, Discrete particle simulation of particulate systems: A review of major applications and findings, Chem Eng Sci 63 (2008) 5728–5770. https://doi.org/https://doi.org/10.1016/j.ces.2008.08.006.

[31] B.C. Burman, P.A. Cundall, O.D.L. Strack, A discrete numerical model for granular assemblies, Geotechnique 30 (1980) 331–336. https://doi.org/10.1680/geot.1980.30.3.331.

[32] R.D. Mindlin, H. Deresiewicz, Elastic Spheres in Contact Under Varying Oblique Forces, J Appl Mech 20 (2021) 327–344. https://doi.org/10.1115/1.4010702.

[33] K.L. Johnson, K. Kendall, A.D. Roberts, Surface energy and the contact of elastic solids, Proceedings of the Royal Society of London. A. Mathematical and Physical Sciences 324 (1971) 301–313. https://doi.org/10.1098/rspa.1971.0141.

[34] Altair EDEM 2021.1, (n.d.). https://www.altair.com/edem/.

[35] M. Alizadeh, M. Asachi, M. Ghadiri, A. Bayly, A. Hassanpour, A methodology for calibration of DEM input parameters in simulation of segregation of powder mixtures, a special focus on adhesion, Powder Technol 339 (2018) 789–800. https://doi.org/10.1016/j.powtec.2018.08.028.

[36] T. Roessler, A. Katterfeld, Scaling of the angle of repose test and its influence on the calibration of DEM parameters using upscaled particles, Powder Technol 330 (2018) 58–66. https://doi.org/10.1016/j.powtec.2018.01.044.

[37] H. Chen, Q. Wei, S. Wen, Z. Li, Y. Shi, Flow behavior of powder particles in layering process of selective laser melting: Numerical modeling and experimental verification based on discrete element method, Int J Mach Tools Manuf 123 (2017) 146–159. https://doi.org/10.1016/j.ijmachtools.2017.08.004.

[38] D. Gu, M. Xia, D. Dai, On the role of powder flow behavior in fluid thermodynamics and laser processability of Ni-based composites by selective laser melting, Int J Mach Tools Manuf 137 (2019) 67–78. https://doi.org/10.1016/j.ijmachtools.2018.10.006.

3 Optimizing Roller-Spreading Performance in laser powder bed fusion: Numerical Study of the circumferential speed's effect

Author Contributions:

- **Mohamed Awad Salim:** Conceptualization, methodology, software, validation, formal analysis, investigation, resources, data curation, writing—original draft preparation and visualization
- **Dr. M. A. Elbestawi:** Conceptualization, supervision, methodology, resources and writing—review and editing
- **Dr. Stephen Tullis:** Conceptualization, supervision, methodology, formal analysis, investigation, resources and writing—review and editing.

3.1. Abstract

Roller-spreading is a fundamental process in laser powder bed fusion (PBF-LP), helping to create a tightly packed and uniform powder layer for optimal printing quality. This control over packing density and thickness helps optimize the printing process for better accuracy and reliability. In the recent study, discrete element method (DEM) simulations of stainless steel 316 are used to investigate the impact of circumferential speed on roller-spreading. Three roller configurations—non-rotating, counter-rotating, and forward-rotating were analyzed to assess their impact on packing density, layer thickness, and mass fraction. The results demonstrate that roller circumferential speed significantly influences powder bed uniformity, with forward-rotating rollers exhibiting higher packing density at a rotational speed close to the rolling speed and improved mass fraction compared to counter-rotating and non-rotating configurations. However, high rotational speeds lead to fast backward motion of powder (powder burst), leading to surface roughness and variations in layer thickness. The study also explores the impact of roller size on powder distribution, revealing that smaller forward-rotating rollers enhance powder compaction, leading to a denser, more uniform layer with improved thickness and surface roughness. Maintaining steady spreading and circumferential speeds is also a key factor in maintaining consistency within the spreading process. Besides, It is practical to have a buffer zone between building plate boundaries and the printing area to avoid cavities and non-uniform areas. Careful optimization of roller-based operations is crucial for improving quality and productivity by controlling the interaction between rotational speed, roller size, and normalized powder size.

3.2. Introduction

Laser powder bed fusion (PBF-LP) is a highly effective additive manufacturing process for producing diverse parts and components [1,2]. This process involves using a high-intensity laser to selectively melt zones of powder materials layer by layer, utilizing the laser as an energy source. PBF-LP comprises two major processes within each fabrication phase: powder spreading and laser scanning [3,4]. Numerous factors, including laser power, laser scanning speed [5,6] laser scanning strategy, and powder composition [7], can impact the quality and performance of components manufactured by PBF-LP. Notably, the powder spreading process is a key factor in determining the structure of the powder bed, which, in turn, influences the subsequent processing steps and ultimately dictates the quality of the final products. Moreover, the characteristics of the feedstock materials, encompassing shape, size distribution, surface morphology, composition, and flowability of the powders [8], significantly influence the qualities of the additively manufactured parts. Comprehending and optimizing the underlying factors involved in powder spreading is crucial to improving the overall quality of components manufactured through PBF-LP.

Generally, the PBF-LP process requires highly dense powder layers with lower surface roughness to produce non-porous layers after the laser scanning step [9]. Studies [10] indicate that higher powder bed packing density simultaneously results in higher melt tracks but shallower and narrower melt pools. When a powder bed is loose or has cavities, they will cause powder melting issues, leading to worse melting defects like balling, pores, and denudation, which will cause worse macro-quality parts for PBF-LP. In other words, a powder bed with a dense, uniform state is desirable for PBF-LP. Besides these, the structure of a powder layer determines its properties by how the powder is spread across it. Powders with a dense structure favour a higher thermal conductivity [11] and absorb more laser power [12]. Tran et al. [12] investigated the impact of particle size distribution on laser scattering and absorptivity [12]. To sum up, PBF-LP research also showed that before the laser scans the powder layer, the final part's properties depend on how the powder spreads out [13].

Roller-spreading and blade-spreading are two distinct techniques employed in the spreading of powder. Roller-spreading [14–16] utilizes a roller to distribute the powder evenly, whereas blade-spreading [17–19] involves using a blade to push the powder. Roller-spreading generally results in a higher packing density because the roller applies a normal force that compresses the powder efficiently. This compression enhances particle arrangement by generating evenly distributed force chains, forming a more compact powder layer [20]. Roller-spreading is driven primarily by the interaction between the roller and powder material. The roller's circumferential and spreading speeds contribute to four main spreading mechanisms: rolling, compression, shearing, and dragging. The spreading speed governs roller-spreading's shearing and dragging mechanisms, while circumferential speed controls its rolling and compression mechanisms. Our past work [21] covered the effect of the spreading speed on roller-spreading performance in different scenarios: counter-rotating, forward-rotating and non-rotating. Interestingly, Meyer et al. [22] adopted a different approach by studying the effects of the total surface velocity, which considers both the traverse and rotation speed of a counter-rotating roller, through experimental investigations. They found that packing density decreases with resultant velocity (i.e., summation of the spreading and circumferential speeds).

The impact of rotational speed on the packing density has been extensively studied, especially in cases of counter-rotating rollers. Most studies have shown that powder bed density decreases with increased rotation speed [15,16,23–25]. Nan et al. [15] explained this decreasing trend through simulations, suggesting that at higher rotational speeds, the intensified circulation of particles in the powder heap in front of the roller hindered their deposition onto the powder bed. However, the simulation work conducted by Zhang et al.[16] revealed that rotation speed did not significantly affect powder bed density. The effects of gap height and roller rotational speed on the spreading process have been investigated [15], which showed that a reduction in gap height or rotational speed leads to a reduction in particle segregation and, finally, a reduction in packing density. Furthermore, rotation speed influences not only powder bed density but also the surface condition of the powder bed. Experimental work by Seluga [23] indicated that layer quality can break down if the rotation speed increases. Zhang et al. [16] conducted simulation work demonstrating that the diameter of the counter-rotating roller directly impacts powder bed density, with an increase in the roller diameter resulting in higher powder bed density. Besides, they found that an increase in counter-rotating roller size prompts an increase in the number of particles in the compression zone where the ordinary contact force becomes more grounded, thus improving the densification of the powder bed. However, the impact of roller size must be expanded with different rotational speed configurations to understand this impact ultimately.

Numerous experimental studies documented in the literature [26–29] have consistently highlighted that the forward-rotating roller significantly enhances powder bed density compared to a counter-rotating roller or wiper(i.e. blade). This improvement can be attributed to the gripping and dragging action of the forward-rotating roller, effectively pulling powder into the powder bed and increasing the overall density [28]. However, the extent of powder bed density improvement achieved by using a forward-rotating roller is associated with other parameters, such as powder flowability or attached mechanical mechanisms. Nevertheless, the use of a forward-rotating roller may have adverse effects on powder spreading. Firstly, after the roller passes over, the powder bed can spring back due to the release of elastic energy stored in the powder bed [27]. This phenomenon can lead to an uneven surface and inaccurate layer thickness [30]. Secondly, the sizeable shear force exerted by the forward-rotating roller may deteriorate the powder bed surface, causing the printed parts beneath the new layer to shift [28]. Thirdly, the substantial compaction force can cause some particles to adhere to the roller, resulting in craters on the powder bed surface [28].

A deeper understanding of how roller-spreading parameters affect powder bed characteristics and spreading performance is achieved in this study by examining the interaction between the roller's circumferential speed and powder behaviour through a comprehensive numerical analysis using the discrete element method (DEM). The work will comprehensively cover various flow regions due to the interaction between roller dynamics and the powder and the nonuniformity resulting from the circumferential speed. Furthermore, it will explore the impact of circumferential speed(i.e., roller's radius and rotational speed) on packing density, layer thickness, and mass fraction.

3.3. Methodology

3.3.1. Discrete element method model

The discrete element method (DEM) is one of the best mathematical methods that can estimate the layout of powder during spreading by solving Newton's second law of motion [31] in which equation (1) governs translational motion and equation (2) governs rotational motion. The speed and location of all particles are calculated by the time integration of Newton's equations [32].

$$m_i \frac{dv_i}{dt} = m_i g + F_i \tag{1}$$

$$I_i \frac{d\omega_i}{dt} = T_i \tag{2}$$

Where F_i and T_i are the total force and torque acting on the particle i, respectively. Besides, m_i, v_i, ω_i and I_i are the mass, velocity, angular velocity, and moment of inertia of particle i. The contact forces between particles, which account for the impact of Van der Waals forces within the contact zone, are formulated using Hertz-Mindlin with JKR (Johnson-Kendall-Roberts) Cohesion [33,34]. The cohesive force of the JKR model is formulated as follows:

$$F_{JKR} = \left[\frac{4E^*}{3R^*} r^3 - 4\sqrt{\pi r^3 \gamma E^*}\right] \tag{3}$$

where R^*, E^*, γ and r are the equivalent radius, equivalent Young's modulus, surface energy and radius of contact area. expressions for R^*, $E^*$and r and any details about the mathematical model used in this work have been discussed in our previous work [21]. EDEM software [35] estimates all forces and torques acting on powder particles and does the time-integration of the particle's acceleration. In EDEM simulations, a time step of 20% of the Rayleigh Time is selected to ensure solution stability and mesh size of three times the minimum radius of the particle to ensure accurate particle contact detection.

Figure 3-1a illustrates the computational domain of the DEM model, which is used to simulate powder spreading in laser powder bed fusion. Roller spreads 112.32 mg of SS316 powder over the building plate, creating a powder layer with a 200 μm thickness (δ). The study conducted by Yao et al. [36] suggests that a spreading velocity of ≤100 mm/s yields favourable results for SS316 spreading. So, the Roller moves forward at a set spreading speed of 50 mm/sec (V_S) while also swirling at an angular speed (ω) during spreading, ensuring even distribution of the powder layer over the building plate of area $12000\mu m \times 5000\mu m$.

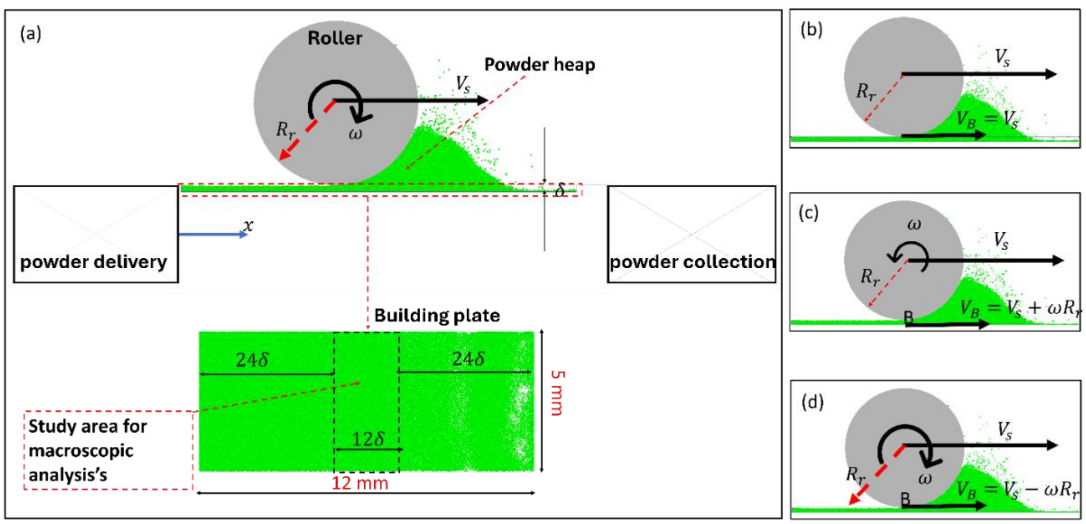

Figure 3-1. (a) Schematic of DEM model of powder spreading process in PBF-LP using a rolling-spreading technique. (b) Non-rotating roller (c) Counter-rotating roller (d) Forward-rotating roller.

Figure 3-1b-d illustrates three distinct roller-spreading configurations: non-rotating, counter-rotating, and forward-rotating rollers. In the **non-rotating configuration** (Figure 3-1b), the roller, modelled as a round blade, advances at a spreading speed of 50 mm/s without any rotational motion. As a result, the velocity at the roller's bottom point equals the spreading speed (i.e.,$V_B = V_s$). In the **counter-rotating configuration** (Figure 3-1c), the roller exhibits rotational and translational motion, with its circumferential speed aligned with the spreading velocity. In this study, the roller rotates counterclockwise, leading to a bottom point speed that is the sum of the spreading and circumferential speeds (i.e., $V_B = V_s + \omega R_r$) . In the **forward-rotating configuration** (Figure 3-1d), the roller also combines translational and rotational motion; however, unlike the counter-rotating case, the circumferential speed at the roller's bottom opposes the spreading velocity. Consequently, the bottom point velocity is determined by subtracting the circumferential speed from the spreading speed (i.e., $V_B = V_s - \omega R_r$) . In this study, the forward-rotating roller rotates in a clockwise direction. Based on the direction and magnitude of the bottom point velocity (V_B), the forward-rotating roller can be further classified into three sub-configurations:

I. **Sub-rolling:** V_B is positive and aligned with the spreading direction, indicating that the rotational speed is lower than the rolling rotational speed ($\omega_o = V_s/R_r$).

II. **Rolling:** V_B is zero, meaning the rotational speed matches the rolling rotational speed.

III. **Super-rolling:** V_B is negative, opposing the spreading direction, signifying that the rotational speed exceeds the rolling rotational speed.

Packing density (ρ_P) and layer thickness $\delta(x)$ are fundamental factors to consider when evaluating the packing of powder particles during the spreading process. The packing density, calculated as the ratio of the volume occupied by particles to the volume of the spatial configuration they encompass, quantifies how closely powder particles are packed in the deposited layer. Its variation coefficient ($\rho_{P,VC}$) and surface roughness of the powder layer (R_a) provide insights into the uniformity of the powder bed's structure over the building plate length. In addition, the mass fraction (MF) plays a crucial role in assessing the performance of forward-rotating rollers as spreaders. The mass fraction measures the ratio of the mass of deposited powder particles to the total mass of the powder layer intended for deposition. While packing density reflects particles' spatial arrangement, mass fraction measures the actual mass distribution within the powder layer. These metrics comprehensively understand the powder layer's quality and characteristics during powder spreading. The current study employs the same mathematical model described well in the past work [21].

This study used mono-sized stainless steel 316 powder, marked as SS316. The mono-sized powder choice is crucial for minimizing the complexities that can arise from variations in powder size distribution, making our analysis more efficient in studying the effect of roller dynamics. We have provided all the properties of SS316 in Table 3-1, which are used in DEM simulations. We have determined the surface energy of SS316 through precise material verification, which includes measuring the static and dynamic angles of repose, as elaborated in previous research [21].

Table 3-1: DEM parameters of Alloy SS 316L

Parameter	Value	ref
Poisson's ratio,ν	0.3	[36,37]
bulk density,ρ	7800 kg/m^3	
Young's modulus, E	22 GPa	
Coefficient of restitution, e	0.64	
Coefficient of sliding friction,μ_s	0.6	
Coefficient of rolling friction, μ_r	0.085	
Surface energy,γ	0.001 J/m^2	[21]

To ensure a comprehensive analysis, we have divided the powder into six groups, each with a range of particle sizes (particle diameter, D). These particle sizes are normalized relative to the layer thickness (normalized powder size, D⁄δ), with values set at 0.25, 0.35, 0.4, 0.5, 0.575, and 0.65. This normalization allows us to establish two distinct powder domains: those with particle sizes less than 0.5 and those exceeding 0.5. This categorization is crucial for understanding powder-spreading behaviour.

3.3.2. Simulation conditions

This study comprehensively analyzes how circumferential velocity impacts roller spreading. Hence, the study demonstrates the impact of rotational speed and size of the roller (i.e., roller radius, R_r) on the efficiency of the spreading process by performing a group of DEM simulations. The roller sizes are standardized concerning the thickness of the layer and are referred to as normalized roller sizes (R_r/δ). The first part of this work incorporates three distinct cases that meticulously investigate the combined effects of rotational speed's direction and magnitude on the roller-spreading process of powder, with its normalized size ranging from 0.25 to 0.65. The initial case features a round blade (i.e., non-rotating roller), while the subsequent two cases involve a counter-rotating and forward-rotating roller with a normalized roller size of 12.5. Both counter-rotating and forward-rotating rollers rotate at 10 to 90 rad/s. Additionally, The second part of this work tests the effect of roller size on the experiment's outcome using four different roller radius dimensions and three different roller configurations. The study uses a non-rotating roller, a counter-rotating roller that rotates at 40 rad/s, and a forward-rotating roller at 40 rad/s, each paired with four different normalized roller sizes: 7.5, 12.5, 17.5, and 22.5. This setup aims to uniformly distribute SS316 powder, characterized by a normalized powder size of 0.25.

3.4. Results and discussion

The results section thoroughly explores the influence of the roller's circumferential speed on the dynamics and overall performance of the powder-spreading process in laser powder bed fusion. Given that the circumferential speed is determined by the roller's rotational speed and size, the analysis begins by examining the effect of rotational speed variations, including its direction relative to the spreading speed. Subsequently, the role of roller size is investigated for three configurations: non-rotating, counter-rotating, and forward-rotating rollers. Notably, due to the limited research available on the forward-rotating configuration, we have dedicated particular attention to this area, especially the rolling and super-rolling cases. The results section is structured into two distinct analytical categories: microscopic and macroscopic. The microscopic analysis delves into powder behaviour during spreading, including powder distribution after spreading, packing density variations, mass fraction, layer thickness across the building plate, and cavity formation. Subsequently, the macroscopic analysis focuses on assessing and trending average packing density, mass fraction, layer thickness, and powder distribution uniformity concerning variations in rotational speed and roller size. This thorough analysis will provide you with a comprehensive understanding of the impact of the roller's circumferential speed.

3.4.1. Microscopic analysis

3.4.1.1. Powder particle flow regions for Roller-spreading.

During the spreading process, various powder flow zones develop in front of the roller, determined by particle speed and compressive forces. These zones include the avalanche, slow flow, quasi-static, and powder layer zones, common to both blade and roller spreading systems. As shown in Figure 3-2 and Figure 3-3, these zones span the entire width of the building plate, highlighting their uniform presence across the spreading area.

In the avalanche zone, the powder particles flow rapidly under gravity and compressive force on particles. The normal contact forces between particles are weak, but particle velocities are relatively higher in this zone. The particles fall faster under gravity and compressive force and spread to the slow-flow zone. The particles in the slow-flow zone move forward with roller movement to the Quasi-static zone at a relatively low speed. Since the particles in the quasi-static zone move at low velocity, literature calls this zone quasi-static. The particles are compressed and squeezed, forming a highly dense layer whose height is the same as the layer thickness. As the roller moves, the quasi-static zone particles spread and are finally deposited on the substrate, forming a stable powder layer zone. The powder layer zone is formed underneath the roller's surface within layer thickness, where the particles are settled and flattened by the translation motion of the roller.

The addition of rotational motion to the roller introduces new dynamics that affect the characteristics of the powder layer. When a roller rotates counterclockwise at high speeds, where the rotational speed exceeds the rolling speed ω_o, particles near the roller surface acquire higher velocities, approximately equal to $V_s + \omega R_r$. This increased velocity causes the particles to scatter away from the spreading area, creating a powder-splashing zone. As illustrated in Figure 3-2c, this splashing effect disrupts the uniform distribution of powder, reducing packing density and a thinner powder layer. In contrast, when the roller rotates clockwise with a high rotational speed that meets or exceeds the rolling speed (i.e., rolling and super-rolling configuration), particles beneath the roller surface are propelled with high velocity ($V_{particle}$=$V_s - \omega R_r$) backward after the roller passes over them. This phenomenon results in a powder burst zone, where particles are ejected and scattered behind the roller, as depicted in Figure 3-3c. The backward movement of particles relative to the spreading direction within the compact region causes the burst. Unlike non-rotating, counter-rotating, or blade configurations, which do not exhibit significant powder burst effects, this phenomenon is primarily induced by the forward-rotating roller dynamics of the roller rather than the applied compressive forces [36].

When powder bursts occur, they lead to a rougher surface and uneven packing density, which messes with the consistency of the layers. In a super-rolling setup, these bursts can cause the thickness of the layers to unexpectedly go beyond what we intended, as shown in Figure 3-4. Figure 3-4 highlights magenta-coloured particles within the desired layer and green-coloured ones above the target thickness. The magenta particles within the desired layer are stable and compact well, and their volume is used to calculate packing density. In cases involving forward-rotating, especially for super-rolling, it is essential to consider evaluating mass fraction, which considers the total mass of particles over the building plate not within the desired layer thickness. The mass fraction parameter gives us a clearer picture of a process's effectiveness. It goes beyond just looking at the surface and helps us understand the overall performance more meaningfully. By integrating these considerations, the effects of rotational and translational motions on the powder layer can be better understood and managed.

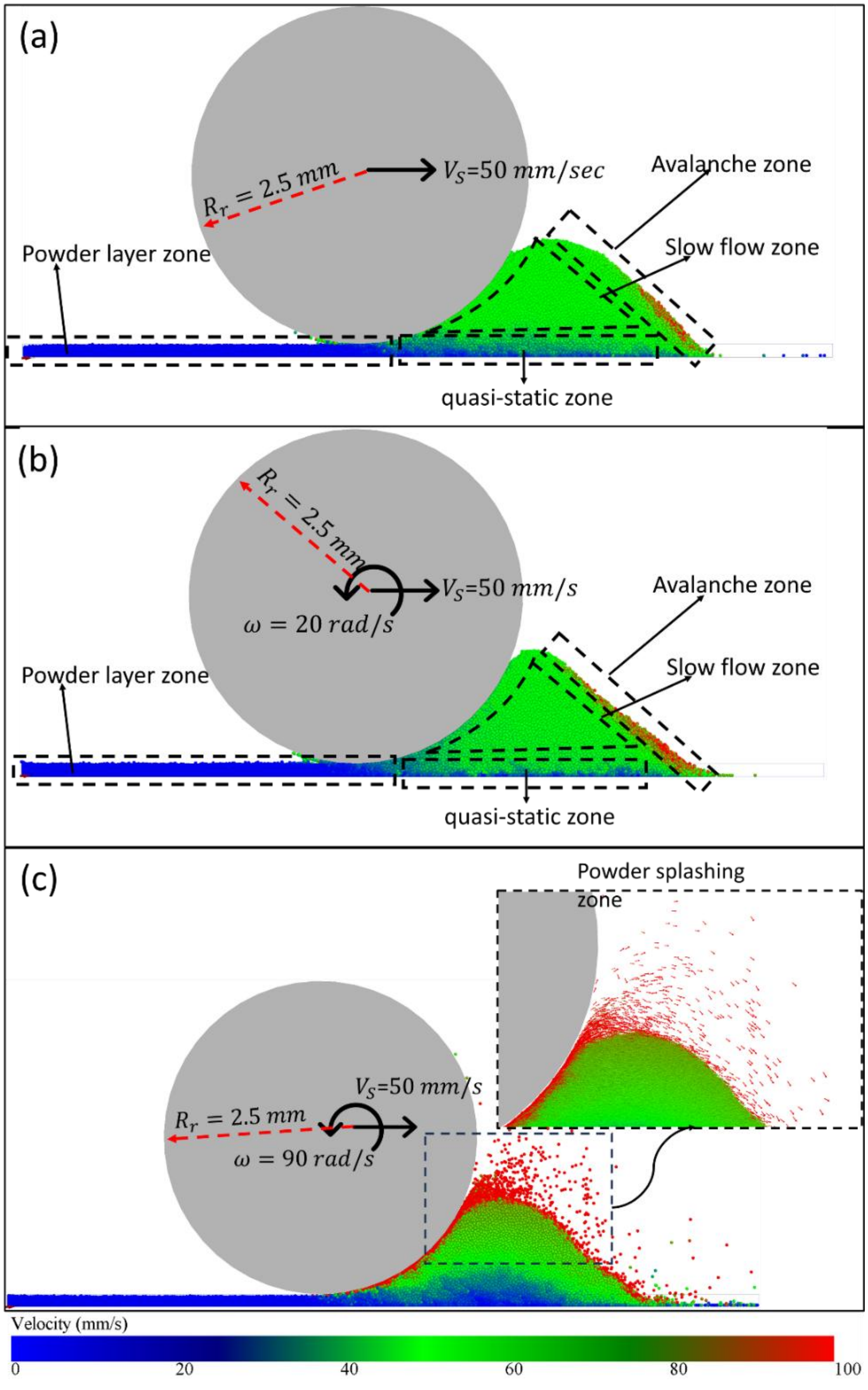

Figure 3-2. Powder flow zones during the spreading of powder with a normalized size of 25% at a spreading speed of 50 mm/s, visualized by powder speed magnitude under different roller configurations: (a) non-rotating roller, (b) counter-rotating roller at 20 rad/s(i.e., $\omega = \omega_o$), and (c) counter-rotating roller at 90 rad/s (i.e., $\omega > \omega_o$).

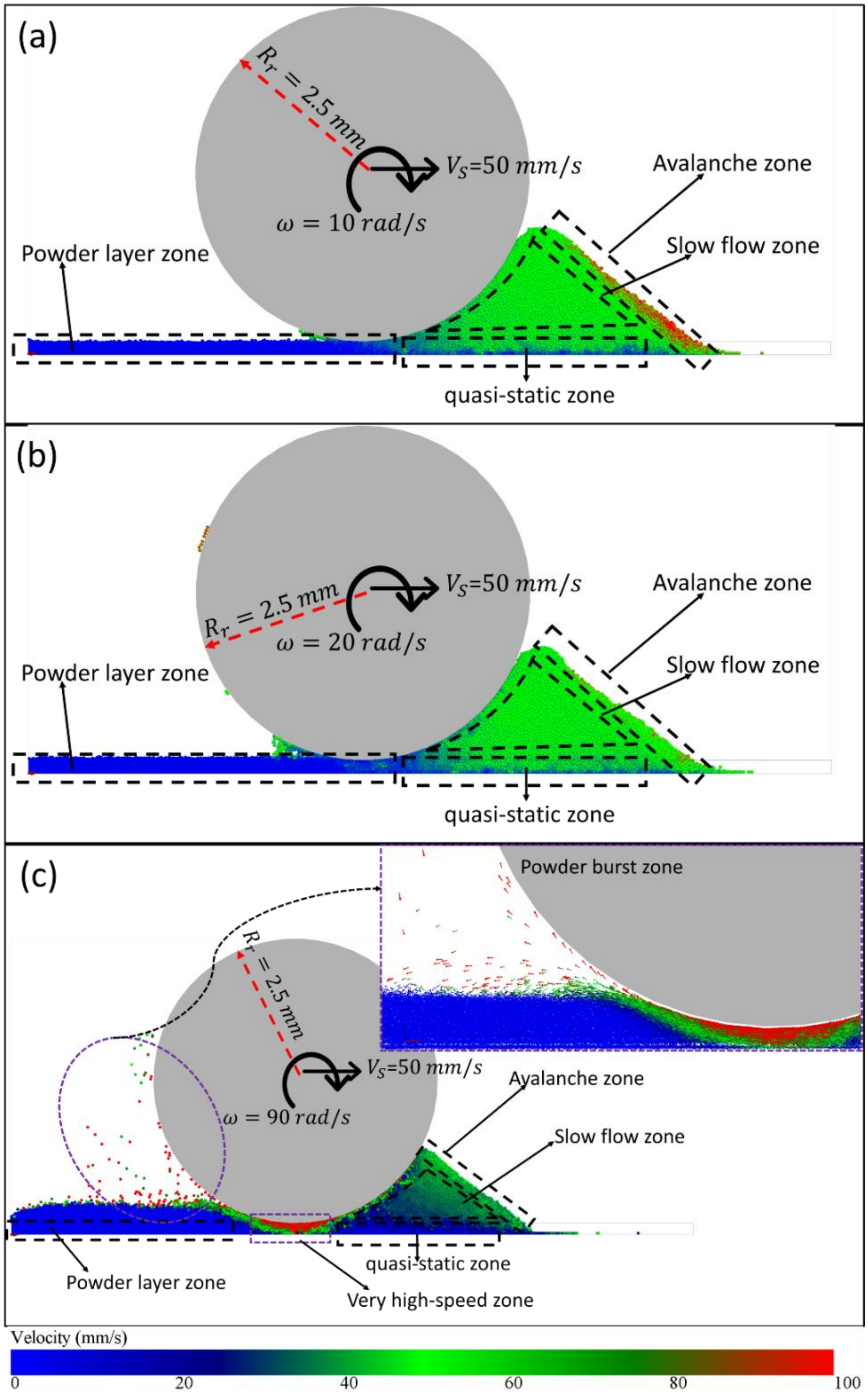

Figure 3-3. Powder flow zones of the forward-rotating roller during the spreading of powder with a size ratio of 25% at a spreading speed of 50 mm/s, visualized by powder speed magnitude under different roller configurations: (a) sub-rolling at 10 rad/s, (b) rolling at 20 rad/s, and (c) super-rolling at 90 rad/s

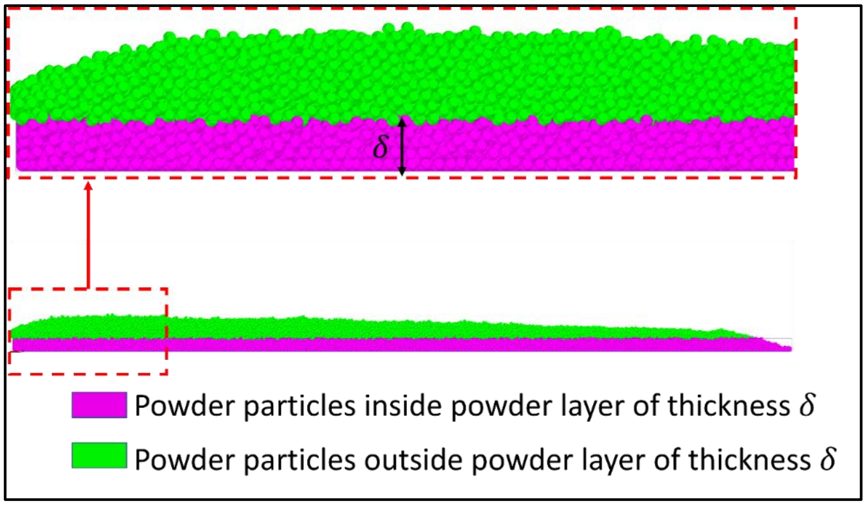

Figure 3-4. Side view of a powder layer with a size ratio of 25%, spread by a super-rolling roller moving at 50 mm/s and rotating at 90 rad/s (i.e., $\omega > \omega_o$).

3.4.1.2. The impact of the rotational speed on the distribution of powder along the building plate

3.4.1.2.1. Non-rotating roller

To understand the impact of rotational motion on the dynamics of a spreader and the resulting quality of the spreading process, it is essential first to examine the base case of a non-rotating roller. In this configuration, the roller is a round blade that pushes and spreads powder uniformly across the building plate without rotation. This non-rotating case is the foundation for understanding the variations in packing density, layer thickness, and mass fraction along the building plate, as outlined in the subsequent analysis.

The spreading process of a non-rotating roller with a radius of 2.5 mm moving at a speed of 50 mm/s reveals distinct spatial variations in packing density across the building plate. The variation can be categorized into three primary regions: the initial, stable, and impact regions. In the initial region, packing density increases from the left edge to an average value as the roller begins to spread the powder. The stable region, which extends approximately from $x/L_x = 0.1$ to $x/L_x = 0.8$, is characterized by relatively uniform packing density, as presented in Figure 3-5a. The packing density fluctuates slightly around a higher value for small powder sizes($D/\delta < 0.5$). However, for larger powder sizes ($D/\delta \geq 0.5$), the packing density undergoes significant fluctuations, beginning at the left edge and varying around a lower average value. In the impact region, starting from $x/L_x = 0.8$ to the right edge, packing density increases sharply due to the accumulation of powder particles redirected by their collision with the solid edge, forming a peak before suddenly decreasing. As illustrated in Figure 3-6a-b and supplementary Figure 6-1a-b and Figure 6-2a-b, a cavity initially forms at the right edge and becomes more pronounced as the normalized powder size reaches 0.5, indicating a progressive reduction in packing density with increasing powder size. Beyond this threshold, multiple cavities appear within the powder layer due to the drag effect on powder particles. Simultaneously, a cavity develops near the left side as a result of the moving roller's dragging effect, which intensifies at higher spreading speeds [21].

Layer thickness variation follows a trend similar to packing density, with three distinct regions along the building plate. The layer thickness increases in the initial region and stabilizes in the stable region. In the impact region, layer thickness increases sharply, reaching a peak above the desired layer thickness before suddenly decreasing, as shown in Figure 3-5b. For smaller particle sizes ($D/\delta \leq 0.5$), the layer thickness remains consistent and close to the desired thickness within this stable region. Larger particle sizes ($D/\delta > 0.5$) exhibit significant fluctuations in layer thickness, often remaining much lower than the desired thickness across most of the plate. However, near the right edge, substantial deviations occur, with layer thickness exceeding the desired value and becoming highly variable.

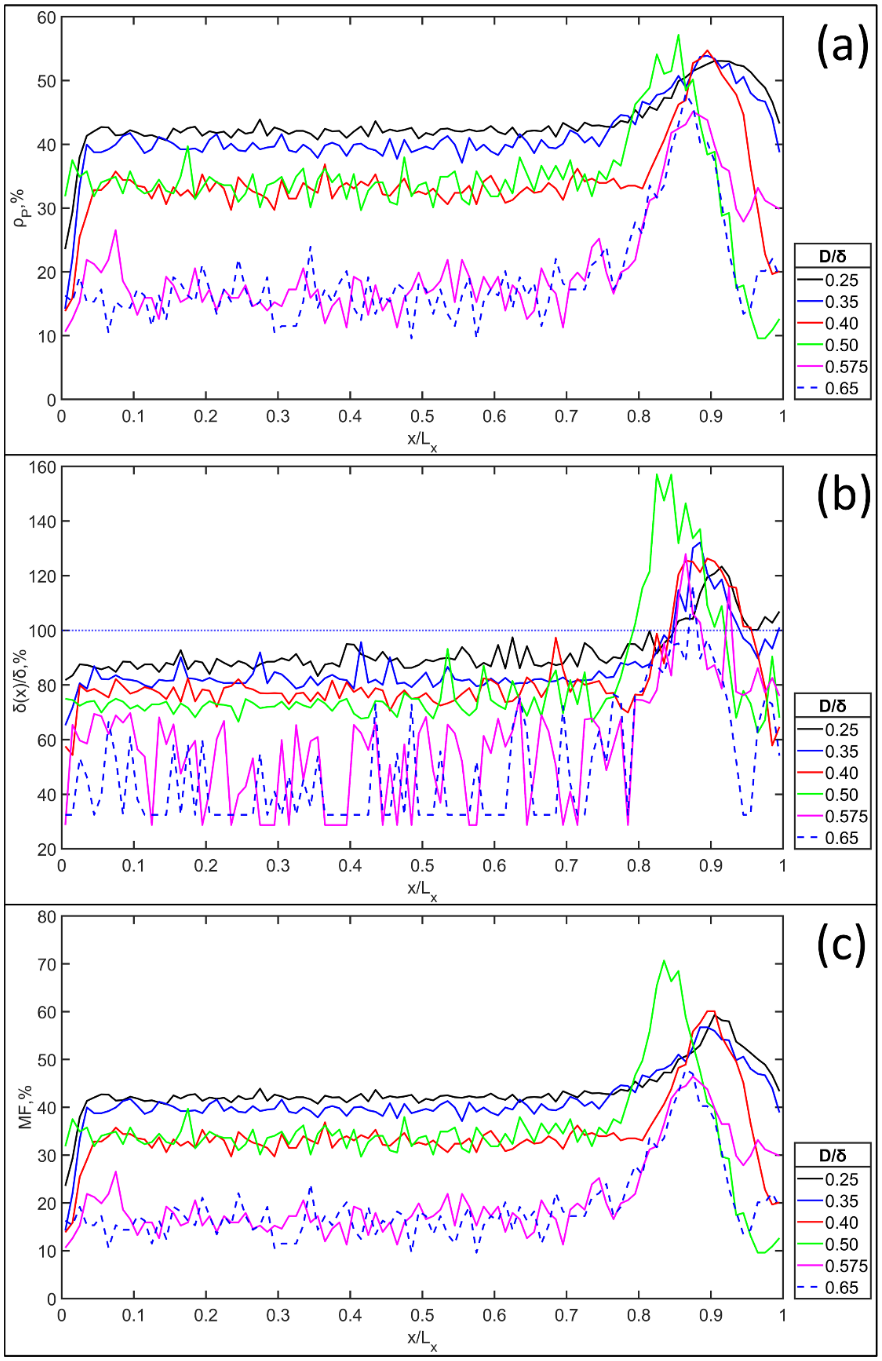

Figure 3-5. Powder layer characteristics for a non-rotating roller (radius = 2.5 mm) moving with a spreading speed of 50 mm/s along the building plate length with varying powder sizes: (a) Packing density (ρ_p, %); (b) Normalized layer thickness (δ(x)/δ,%); (c) Mass fraction (MF,%).

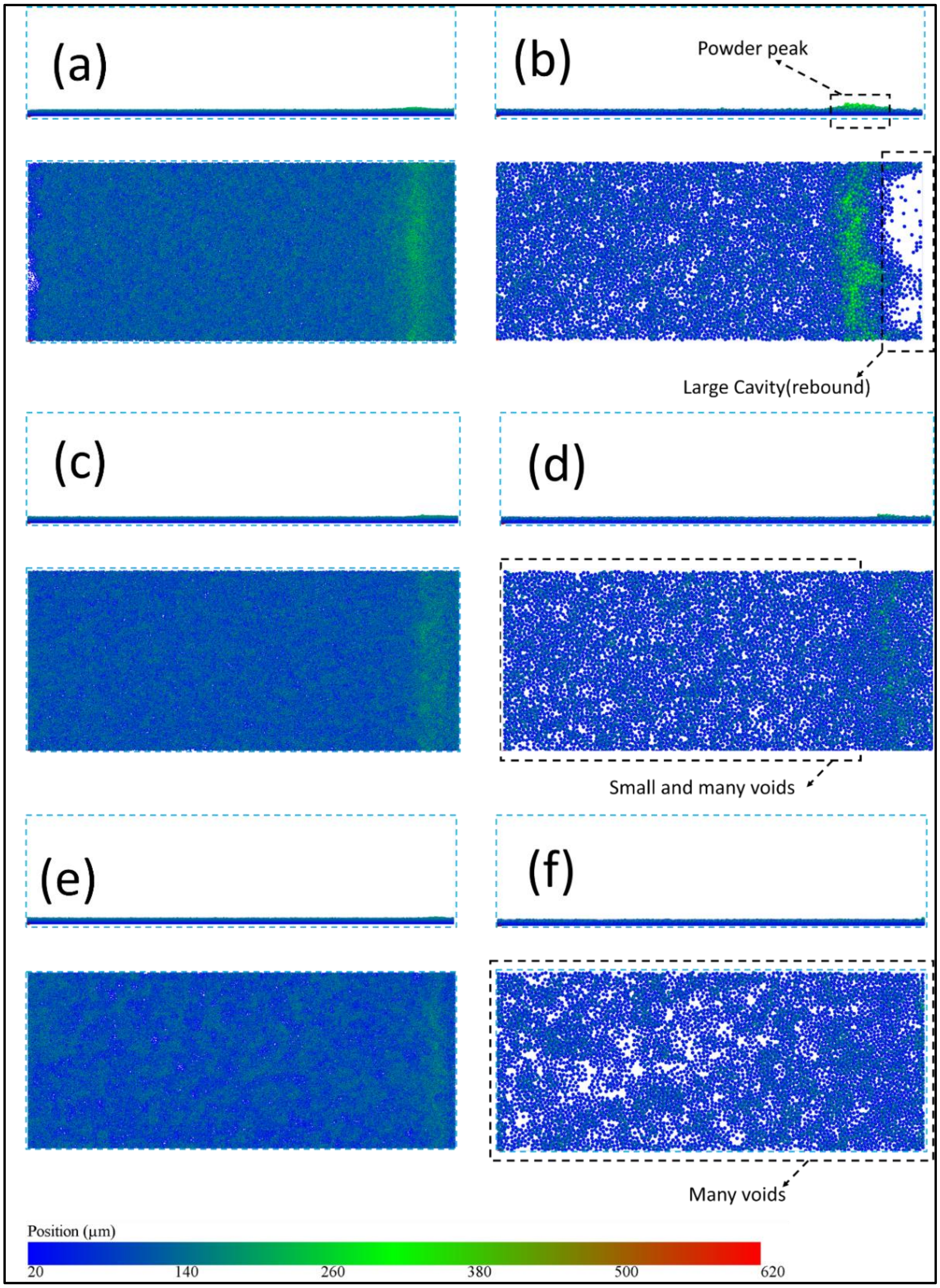

Figure 3-6.Top view and front view of the powder bed after spreading by roller (radius = 2.5 mm) with a spreading speed of 50 mm/s, coloured by powder position in Z-direction (i.e., layer thickness) at different rotational speeds and normalized powder sizes. (a)$\omega = 0\, rad/s\, \&\, D/\delta = 0.25$;(b)$\omega = 0\, rad/s\, \&\, D/\delta = 0.50$;(c)$\omega = 20\, rad/s\, \&\, D/\delta = 0.25$;(d)$\omega = 20\, rad/s\, \&\, D/\delta = 0.50$;(e)$\omega = 90\, rad/s\, \&\, D/\delta = 0.25$;and(f)$\omega = 90\, rad/s\, \&\, D/\delta = 0.50$.

The variation in mass fraction across the building plate is closely tied to the packing density and layer thickness behaviour. From the left edge to $x/L_x = 0.8$, where layer thickness remains below or equal to the desired value, the mass fraction follows the same trend as packing density, except it is greater in the impact region. In the impact region, the mass fraction exhibits a similar trend to the packing density but exceeds it due to powder accumulation near the right edge, as indicated in Figure 3-5c. This accumulation occurs when the packing density peaks and the layer thickness surpasses the desired value.

Hence, the spreading behaviour of the non-rotating roller is categorized into two non-uniform regions near solid edges and a uniform region between them, reflecting the influence of powder size and motion dynamics on the uniformity and stability of the powder layer. Notably, larger particle sizes ($D/\delta > 0.5$) exhibit higher fluctuations in packing density throughout the process.

3.4.1.2.2. Counter-rotating roller

Unlike the non-rotating roller, which primarily relies on translational motion to distribute powder, the counter-rotating roller (R_r=2.5mm) integrates a rotational speed varying from 10 rad/s to 90 rad/s with a translational speed of 50 mm/s.

The packing density distribution follows a pattern similar to the non-rotating roller, with three primary regions: initial, stable, and impact regions. For all normalized powder sizes ranging from 0.25 to 0.65 and at lower rotational speeds ($\omega < \omega_o$), packing density exhibits an initial increase from the left edge to an average value, which decreases with rotational speed, followed by fluctuations within the stable region, as illustrated in Figure 3-7a and supplementary Figure 6-3a through Figure 6-5a. However, as the rotational speed increases beyond ω_o, the initial development phase at the left edge disappears, and packing density begins fluctuating around the average value from the start of the spreading process until the impact region. The integration of counterclockwise rotational speed with a moving roller reduces the fluctuation range within the impact region, thereby improving uniformity near the right edge. However, when the powder sizes are larger ($D/\delta > 0.5$), the packing density distribution across the building plate remains relatively consistent, showing slight variation irrespective of the rotational speed employed, as illustrated in supplementary Figure 6-6 and Figure 6-7.

The spreading process of the counter-rotating roller reveals distinct improvements in powder distribution compared to the non-rotating case. The y-component of the circumferential speed generated by the rotation prevents powder from escaping the spreading area and compresses powder particles behind the roller, leading to a more uniform powder layer, as depicted in Figure 3-6c-f and supplementary Figure 6-1c-f. This effect minimizes cavity formation near the edges at moderate spreading speeds, a common issue in the non-rotating roller case. However, the circumferential speed effect diminishes at higher spreading speeds, leading to cavity development near the left edge [21]. Additionally, the integration of circumferential speed results in the formation of multiple small voids within the powder layer, reducing overall packing density. These voids grow and become more pronounced as the normalized powder size increases beyond 0.5, as shown in the supplementary Figure 6-2c-f.

Layer thickness variation in the counter-rotating roller case exhibits fluctuations around an average value across approximately 80% of the building plate length, as presented in Figure 3-7b and supplementary Figure 6-3b through Figure 6-5b. These fluctuations become more pronounced as the normalized powder size increases, particularly for $D/\delta > 0.5$, leading to a more non-uniform powder distribution, as shown in supplementary Figure 6-6b and Figure 6-7b.

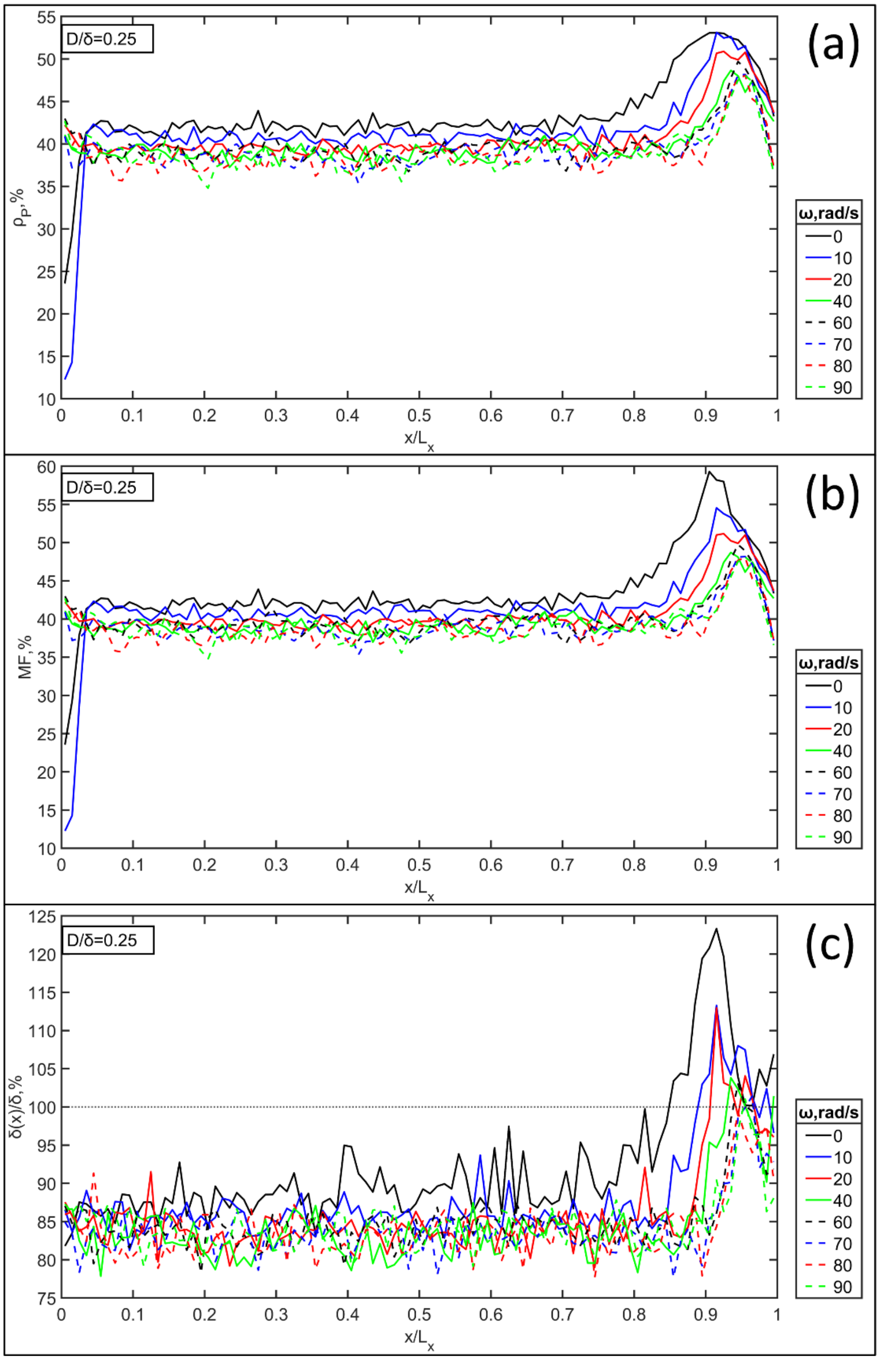

Figure 3-7. Characteristics of a powder layer with a normalized particle size of 0.25 spread using a counter-rotating roller (radius = 2.5 mm) at a spreading speed of 50 mm/s along the building plate length: (a) Packing density (ρ_p, %); (b) Normalized layer thickness (δ(x)/δ,%); (c) Mass fraction (MF,%).

Within the impact region, fluctuations exceed the desired layer thickness but tend to decrease as the counterclockwise rotational speed increases, improving uniformity in this region. The mass fraction distribution within the structure reveals a clear and intriguing pattern intricately linked to the packing density, primarily due to layer thickness along the majority of the building plate being below-desired layer thickness, as shown in Figure 3-7c and supplementary Figure 6-3 through Figure 6-7c.

The counter-rotating roller introduces a complex interplay between translational and rotational dynamics, leading to improvements and challenges in powder spreading. While it effectively reduces cavity formation near the edges for smaller powder sizes and enhances uniformity in the impact region, it also results in increased packing density and layer thickness fluctuations, particularly for larger powder sizes.

3.4.1.2.3. Forward-rotating roller

A forward-rotating roller is a spreading mechanism defined by its simultaneous translational and rotational motion. In this setup, the roller, with a radius of 2.5 mm, operates at a spreading speed of 50 mm/s while rotating clockwise at a rotational speed (ω) that varies from 10 rad/s to 90 rad/s. The rolling speed (ω_o) refers to the rotational speed at which the bottom of the roller maintains a velocity of zero, precisely at 20 rad/s. Based on the relationship between circumferential speed and translational speed, the forward-rotating roller operates in three distinct configurations: Sub-Rolling, Rolling, and Super-Rolling. The Sub-Rolling Configuration occurs when the roller rotates at a speed lower than the rolling speed, precisely at 10 rad/s. In contrast, the Rolling Configuration describes a scenario where the roller rotates precisely at the rolling speed. Lastly, in the Super-

Rolling Configuration, the roller rotates at a speed that exceeds the rolling speed, with rotational speed reaching up to 90 rad/s.

3.4.1.2.3.1. Sub-rolling

The packing density of the powder layer in the sub-rolling configuration closely resembles that of the non-rotating and counter-rotating rollers. This configuration exhibits higher fluctuated packing density throughout most of the building plate, excluding the impact region, compared to the non-rotating and counter-rotating rollers, as illustrated in Figure 3-8a and supplementary Figure 6-10a through Figure 6-14a. However, within the impact region, significant fluctuations in packing density occur, mirroring the behaviour observed in the non-rotating and counter-rotating rollers. Although the spreading speed in the positive x-direction exceeds the circumferential speed in the negative x-direction at the roller's bottom, the backward motion induced by the circumferential speed, besides the impact effect, pulls the powder behind the roller, leading finally to cavity formation at the right edge of the powder layer. These cavities become increasingly pronounced as the normalized powder size reaches or exceeds 0.5, particularly at higher values, as illustrated in Figure 3-9a–b and supplementary Figure 6-8a–b. Small voids develop within the powder layer for normalized powder sizes of 0.5 or greater, growing more distinct as the powder size increases, as shown in the supplementary Figure 6-9a–b.

The layer thickness profile along the building plate follows a fluctuating pattern similar to that observed in non-rotating and counter-rotating rollers. However, the sub-rolling configuration produces a thicker layer across most of the plate, as evidenced by Figure 3-8b and supplementary Figure 6-10b through Figure 6-14b. Due to the dominance of the spreading speed over the circumferential speed, the layer thickness remains below the desired value along the majority of the building plate length. However, in the impact region, fluctuations in layer thickness become more considerable, forming pronounced peaks which surpass the desired thickness. This suggests that within the impact region, powder accumulation is intensified due to the roller's combined translational (i.e., impact effect) and rotational motion (i.e., backward motion of powder). Therefore, the mass fraction distribution along the building plate mirrors the packing density behaviour until the impact region. However, mass fraction values in the impact region exceed packing density due to localized powder accumulation. These fluctuations become more pronounced as normalized powder size increases, and their onset occurs earlier for larger powder sizes. This behaviour is depicted in Figure 3-8c and supplementary Figure 6-10c through Figure 6-14c .

The sub-rolling configuration exhibits spreading behaviour that closely resembles the non-rotating and counter-rotating rollers but with generally higher values of packing density and layer thickness. Furthermore, the deviation between the sub-rolling configuration and the non-rotating diminishes as the normalized powder size increases, indicating that as normalized powder size increases, the effect of circumferential speed in the sub-rolling configuration diminishes.

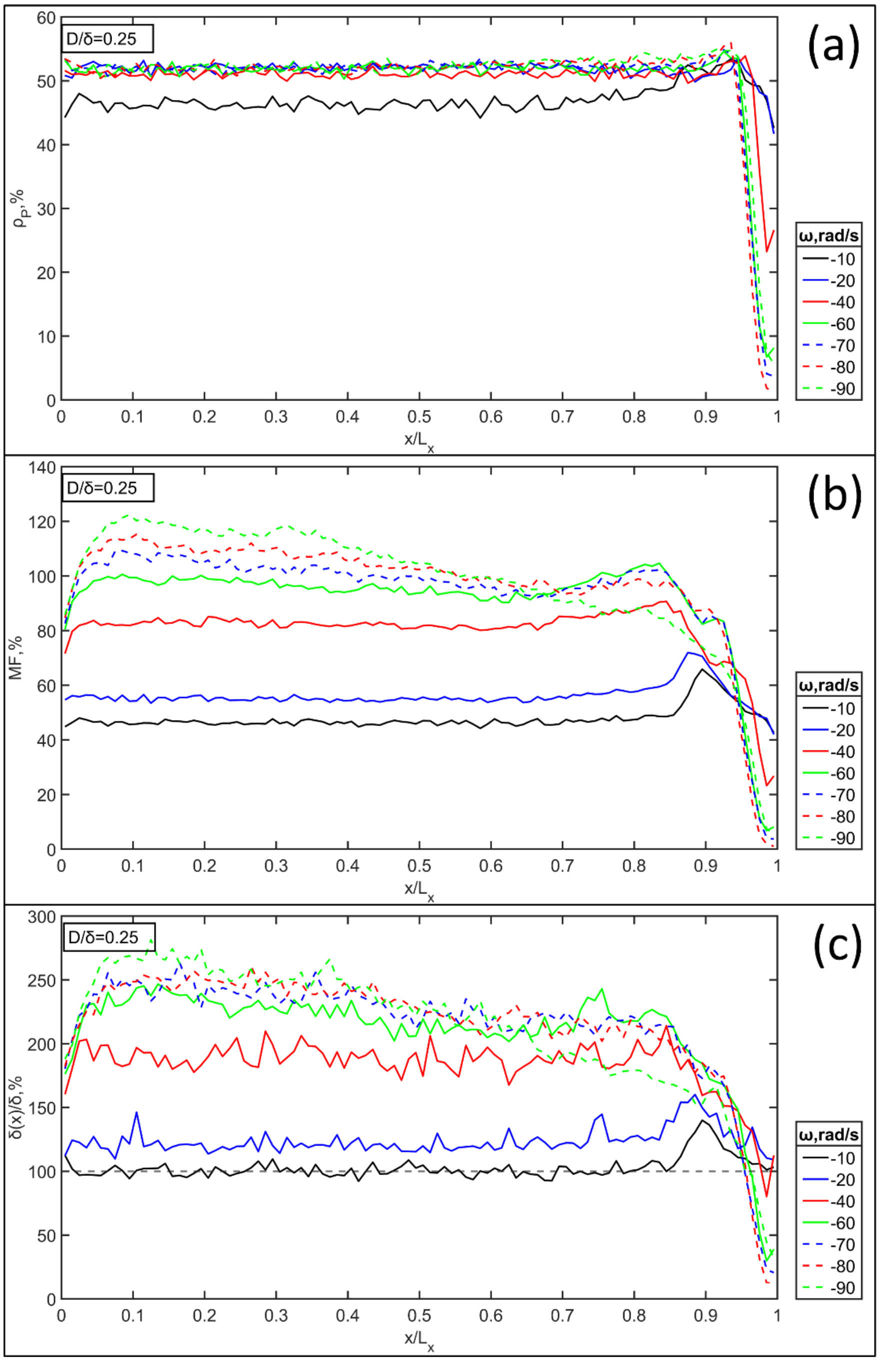

Figure 3-8. Characteristics of a powder layer with a normalized particle size of 0.25 spread using a forward-rotating roller (radius = 2.5 mm) at a spreading speed of 50 mm/s along the building plate length: (a) Packing density (ρ_p, %); (b) Normalized layer thickness (δ(x)/δ,%); (c) Mass fraction (MF,%).

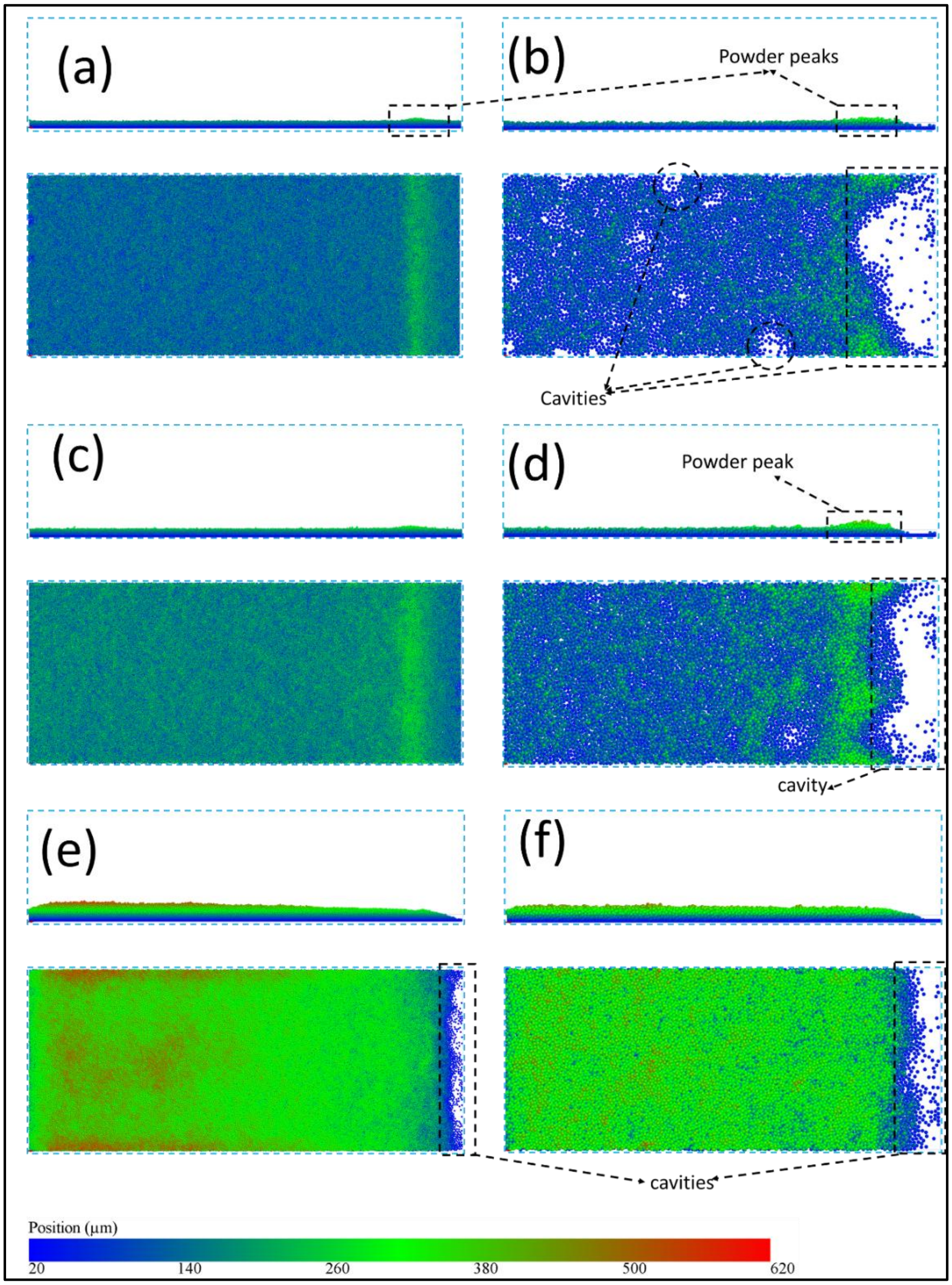

Figure 3-9.Top view and front view of the powder bed after spreading by forward-rotating roller (radius = 2.5 mm) with a spreading speed of 50 mm/s, coloured by powder position in Z-direction (i.e., layer thickness) at different rotational speed and normalized powder sizes ; (a)sub-rolling;$\omega = -10\,rad/s\,\&\,D/\delta = 0.25$;(b)sub-rolling ;$\omega = -10\,rad/s\,\&\,D/\delta = 0.50$;(c)Rolling ; $\omega = -20\,rad/s\,\&\,D/\delta = 0.25$;(d)rolling ; $\omega = -20\,rad/s\,\&\,D/\delta = 0.50$;(e)super-rolling; $\omega = -90\,rad/s\,\&\,D/\delta = 0.25$;and(f)super-rolling; $\omega = -90\,rad/s\,\&\,D/\delta = 0.50$.

3.4.1.2.3.2. Rolling

The Rolling Configuration represents a critical operational mode in powder spreading, characterized by the roller rotating at precisely the rolling speed ($\omega_o = 20\ rad/s$). In this configuration, the bottom of the roller maintains zero velocity relative to the building plate. For normalized powder sizes between 0.25 and 0.575, the packing density of the powder layer varies slightly around a relatively high level, beginning at the left edge and continuing to the impact region. Within the impact region, the packing density undergoes a notable drop, creating cavities at the right edge, an effect that intensifies as the normalized powder size increases, especially at 0.5, as shown in Figure 3-9c-d and supplementary Figure 6-8c-d. Similar to the behaviour observed in non-rotating and sub-rolling rollers, larger powder particles cause the impact region to shift upstream, leading to an earlier onset of density fluctuations. Nonetheless, the overall packing density remains more stable, with values closer to the peak density within the impact region. In contrast to the Sub-Rolling Configuration, which shows noticeable fluctuations, the variations in the Rolling Configuration are milder, leading to a more consistent and uniform distribution.

For higher normalized powder sizes exceeding 0.5, cavity formation becomes evident within the powder layer. These cavities grow in size with increasing powder dimensions due to the combined effects of powder drag and gravitational forces, as illustrated in the supplementary Figure 6-9c-d. At an extreme normalized powder size of 0.65, the packing density distribution closely resembles that of the non-rotating and sub-rolling rollers. This similarity suggests that the gravitational force acting on large powder particles dominates the spreading dynamics, reducing the influence of roller-induced motion on powder redistribution.

Layer thickness analysis further reinforces the high powder compaction effect of the Rolling Configuration. For normalized powder sizes between 0.25 and 0.575, layer thickness fluctuates around 100% to 120% of the desired thickness, demonstrating high powder compaction compared to previous configurations. However, the fluctuations become more pronounced for high normalized powder sizes (e.g., 0.65), with the average layer thickness dropping below the target value. As with the packing density, the impact region is characterized by significant oscillations between high peak values and minimal thickness levels, indicating localized powder displacement.

The mass fraction follows a pattern similar to the packing density but with more minor fluctuations. These fluctuations start from the left edge and extend toward the impact region. The mass fraction generally remains higher on average but gradually decreases as the normalized powder size increases. Mass fraction fluctuates significantly in the impact region, particularly for larger powder sizes. Mass fraction variation within the impact region is due to powder inertia and impact dynamics, which affects powder relocation, creating a powder peak followed by a significant reduction in mass fraction.

By operating at the critical rolling speed, this configuration reduces excessive powder displacement while maintaining a relatively stable layer thickness. Although challenges persist at larger normalized powder sizes due to gravity-induced effects and handling impact region fluctuations, the Rolling Configuration significantly improves sub-rolling, non-rotating and counter-rotating rollers.

3.4.1.2.3.3. Super-rolling

In the super-rolling configuration, the variation of packing density exhibits a distinct behaviour compared to sub-rolling and rolling configurations. For normalized powder sizes ranging from 0.25 to 0.65, once the clockwise rotational speed surpasses the rolling speed, packing density experiences a slight growth while maintaining a similar fluctuation pattern. This fluctuation extends across the building plate, but unlike sub-rolling and rolling, the impact region initiates at 90% of the building plate length rather than 80%. Consequently, this leads to a more uniform packing density distribution.

Within the impact region, there is a slight increase in packing density before a sudden drop, intensifying with increasing rotational speed. The reduction in packing density within this region results in cavity formation at the right edge, as shown in Figure 3-9e-f and supplementary Figure 6-8e-f, driven by the dominance of circumferential speed over the spreading speed, pulling powder backward. The severity of these cavities increases with normalized powder size and rotational speed. However, for lower normalized powder sizes, such as 0.25, the accumulated powder weight acts as a compressive force, redistributing powder into the cavity and reducing its size. Notably, for higher normalized powder sizes (0.575 and 0.65), packing density in the super-rolling configuration becomes more uniform than in sub-rolling and rolling configurations, as the accumulated powder prevents the development of internal cavities within the powder layer, as shown in the supplementary Figure 6-9e-f.

The layer thickness in the super-rolling configuration exhibits fluctuations at values higher than the desired thickness across most of the building plate length. For all normalized powder sizes, layer thickness fluctuates significantly from the left edge to approximately 80% of the building plate length, followed by a gradual reduction within the impact region. Near the right edge, a sharp decrease in layer thickness occurs due to cavity formation. As rotational speed increases, the overall layer thickness and the reduction near the right edge become more pronounced, particularly up to 60 rad/s ($3\omega_o$). Over most of the building plate, layer thickness exceeds the desired value by approximately 280%, a phenomenon attributed to the backward motion of powder caused by circumferential speed dominance. This results in powder accumulation behind the roller, forming layers up to three times the desired thickness. As the normalized powder size decreases, the accumulated powder distributes more evenly across the building plate, reducing surface roughness.

The mass fraction in the super-rolling configuration follows a trend similar to packing density but exhibits generally higher values. Across the building plate, mass fraction increases with rotational speed while experiencing fluctuations that are slightly more pronounced than those observed in packing density, particularly from the left edge to 80% of the building plate length, as illustrated in Figure 3-8c and supplementary Figure 6-10c through Figure 6-14c. These fluctuations become more significant as normalized powder size increases.

Within the impact region, mass fraction reaches a peak before undergoing a substantial decline, mirroring the behaviour observed in packing density and layer thickness. The extent of this reduction is amplified with increasing rotational speed. As the normalized powder size increases, the overall mass fraction decreases, with the reduction becoming more significant at larger powder sizes, particularly at 0.65. This reduction can be attributed to the large gravity force and the effect on the large powder size.

The super-rolling configuration improves packing density uniformity and reduces internal cavity formation, especially at higher normalized powder sizes. However, higher speeds and larger powder sizes cause noticeable fluctuations and cavity formation at the right edge. Layer thickness exhibits significant fluctuations, often exceeding the desired thickness due to powder accumulation behind the roller.

3.4.1.3. The impact of the roller size on the distribution of powder along the building plate

The influence of roller radius on packing density, layer thickness, and mass fraction differs notably among the three roller configurations—non-rotating, counter-rotating, and forward-rotating—as the roller radius varies from 7.5 to 22.5 times the desired layer thickness. In these cases, the roller spreads powder with a normalized powder size of 0.25 at a spreading speed of 50 mm/s.

In the non-rotating configuration, since the roller does not impart any additional circumferential motion, its radius has no direct influence on the spreading dynamics, as shown in supplementary Figure 6-15. However, the roller must be sufficiently large to ensure adequate powder deposition across the building plate. As a result, while the overall packing density and layer thickness remain primarily consistent, a minimal roller radius may lead to incomplete spreading and uneven layer formation.

In the counter-rotating setup, with the roller moving at 50 mm/s and spinning at 40 rad/s, the roller radius has a noticeable impact. A larger radius means a higher speed at the bottom of the roller, which increases the shear force acting on the powder bed. This intensified shear force promotes a more uniform powder distribution, particularly over the central region of the building plate. On the other hand, As the roller's speed increases, the powder particles hit the right edge with more force, which lowers the packing density in that area. Supplementary Figure 6-16 clearly shows that larger roller radii make this effect even more noticeable, leading to a more significant drop in packing density near the right edge of the powder layer.

For the forward-rotating configuration, characterized by a spreading speed of 50 mm/s and a rotational speed of 40 rad/s, the roller operates in a super-rolling regime ($\omega > V_s/R_r$), leading to distinct spreading characteristics. Across approximately 90% of the building plate starting from the left edge, packing density remains unaffected by roller radius, as illustrated in Figure 3-10a. However, near the right edge, an increase in roller radius results in a notable decline in packing density, particularly when the roller radius reaches 17.5 times the desired layer thickness. This makes the layer more uneven and increases cavity formation in that area. As the roller radius grows, its speed increases, strengthening the backward dragging force on the powder. This backward pull causes the powder to pile up, making the layer thicker at specific locations than intended and disrupting uniform deposition, as shown in Figure 3-10b. At a roller radius of 22.5 times the desired layer thickness, the layer thickness at the right edge undergoes a sharp reduction, highlighting the instability introduced by excessive roller sizes. Regarding mass fraction distribution, for roller radii below 22.5 times the desired layer thickness, uniformity is maintained across approximately 80% of the building plate. However, beyond this threshold, fluctuations in mass fraction become more pronounced, as depicted in Figure 3-10c.

These variations indicate that while increasing roller radius may enhance specific spreading characteristics, excessive roller sizes can introduce undesirable nonuniformities, particularly in forward-rotating configurations.

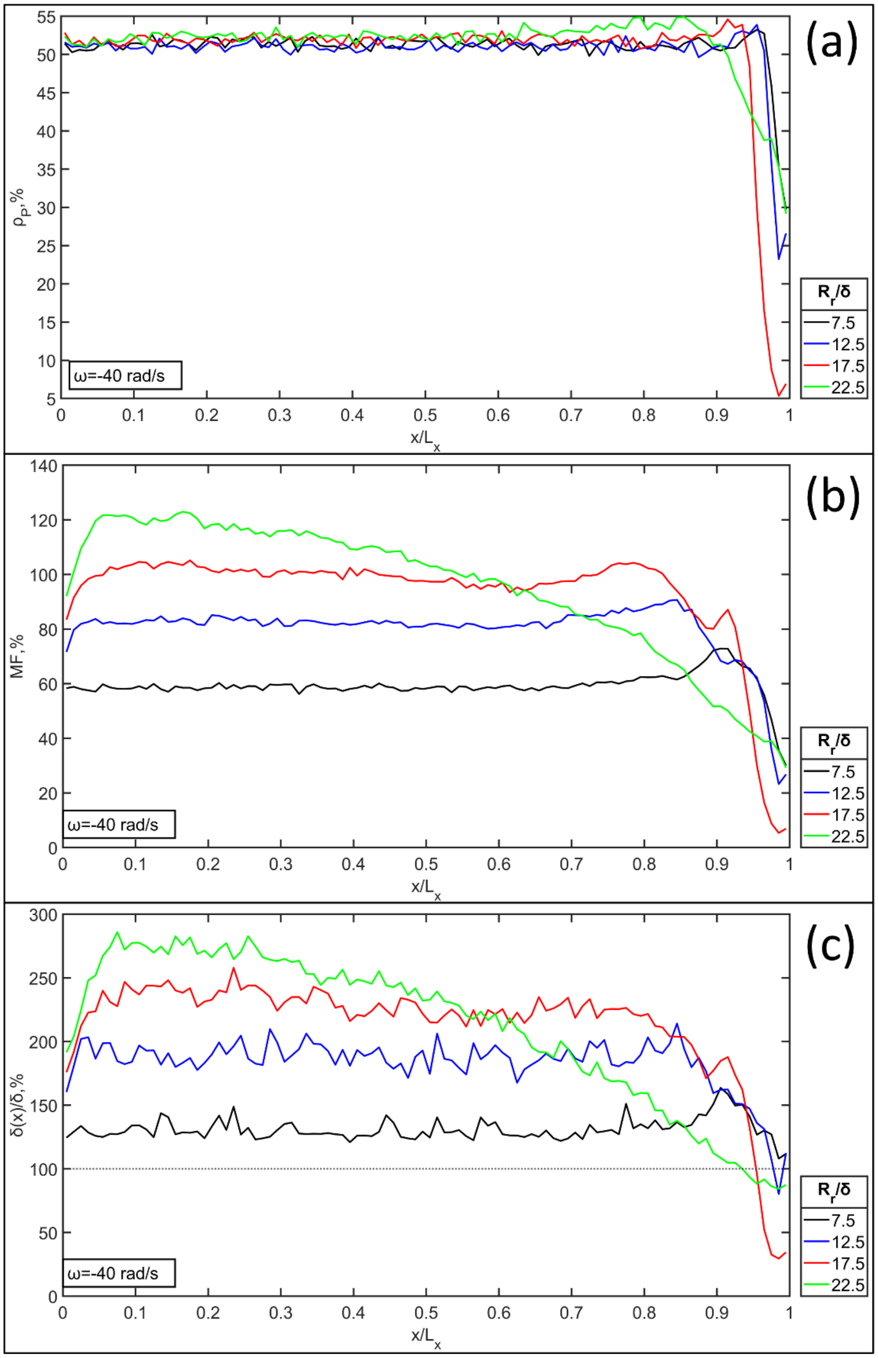

Figure 3-10. Characteristics of a powder layer with a normalized particle size of 0.25 spread using a forward-rotating roller at a spreading speed of 50 mm/s and rotational speed of 40 rad/s along the building plate length at different roller radius: (a) Packing density (ρ_p, %); (b) Normalized layer thickness (δ(x)/δ,%); (c) Mass fraction (MF,%).

3.4.2. Macroscopic analysis

This section takes a macroscopic look at how the roller's circumferential motion affects the powder bed by analyzing the average packing density($\rho_{P,avg}$), average mass fraction(MF_{avg}), and average layer thickness(δ_{act}) within the study area, as shown in Figure 3-1a. Located at the center of the building plate and spanning a width of 12δ, this area provides a representative section for evaluation. Furthermore, the uniformity of the powder distribution is assessed through the coefficient of variation of packing density ($\rho_{P,vc}$)and variation coefficient mass fraction (MF_{vc}), as well as surface roughness evaluation (Ra).

3.4.2.1. Effect of rotational speed on overall roller-spreading process performance

3.4.2.1.1. Non-rotating roller

Studying how a non-rotating roller spreads powder lays the foundation for understanding the impact of rotational speed—both in strength and direction. However, this brings up an important question: Does the analysis still hold if the powder size changes? A non-rotating roller of a normalized size of 12.5 is investigated to address this question, which spreads powders with normalized sizes ranging from 0.25 to 0.65 at a spreading speed of 50 mm/s. The results indicate a pronounced decline in average packing density with increasing normalized powder size. When the normalized powder size increased from 0.25 to 0.50, the average packing density decreased by 21.3%, while the increase from 0.25 to 0.65 led to a dramatic 63.9% reduction, as illustrated in Figure 3-11a. This significant drop in packing density highlights the inefficiency of larger powder particles in achieving a compact arrangement within the powder bed. The reduction in packing density is primarily attributed to gravity force, powder drag and the wall effect. The wall effect, encompassing static and dynamic interactions, affects powder spreading by restricting particle movement and hindering compaction. The static wall effect occurs when powder particles near fixed boundaries, such as the edges of the build plate or previously printed layers, experience limited mobility. As powder size increases, this effect becomes more pronounced, leading to more significant variations in local packing density. Meanwhile, the dynamic wall effect comes into play when powder near the roller's bottom edge gets disturbed, making the spreading process less uniform and lowering the overall packing density. When the layer is thin, the roller applies more direct compression, improving packing density. However, the roller's impact diminishes as the layer thickens, making powder arrangement less efficient. Both static and dynamic wall effects are influenced by powder size and layer thickness. However, their combined impact is best evaluated through the ratio of powder size to layer thickness (the normalized powder size). As this ratio increases, the wall effect becomes more significant, contributing to issues such as reduced packing density and uneven powder distribution.

Simultaneously, the variation coefficient of packing density exhibits a clear increasing trend with normalized powder size, indicating more significant nonuniformity in powder distribution. For example, as the normalized powder size increased from 0.25 to 0.5, the variation coefficient saw a modest rise of 3.8 %. However, the increase became much more pronounced when the normalized powder size exceeded 0.5, jumping to 12.6% at a normalized powder size of 0.65, as presented in Figure 3-11a. This notable rise suggests that larger powder particles increase heterogeneity, further complicating the powder spreading process. Larger particles get trapped near fixed boundaries while also being

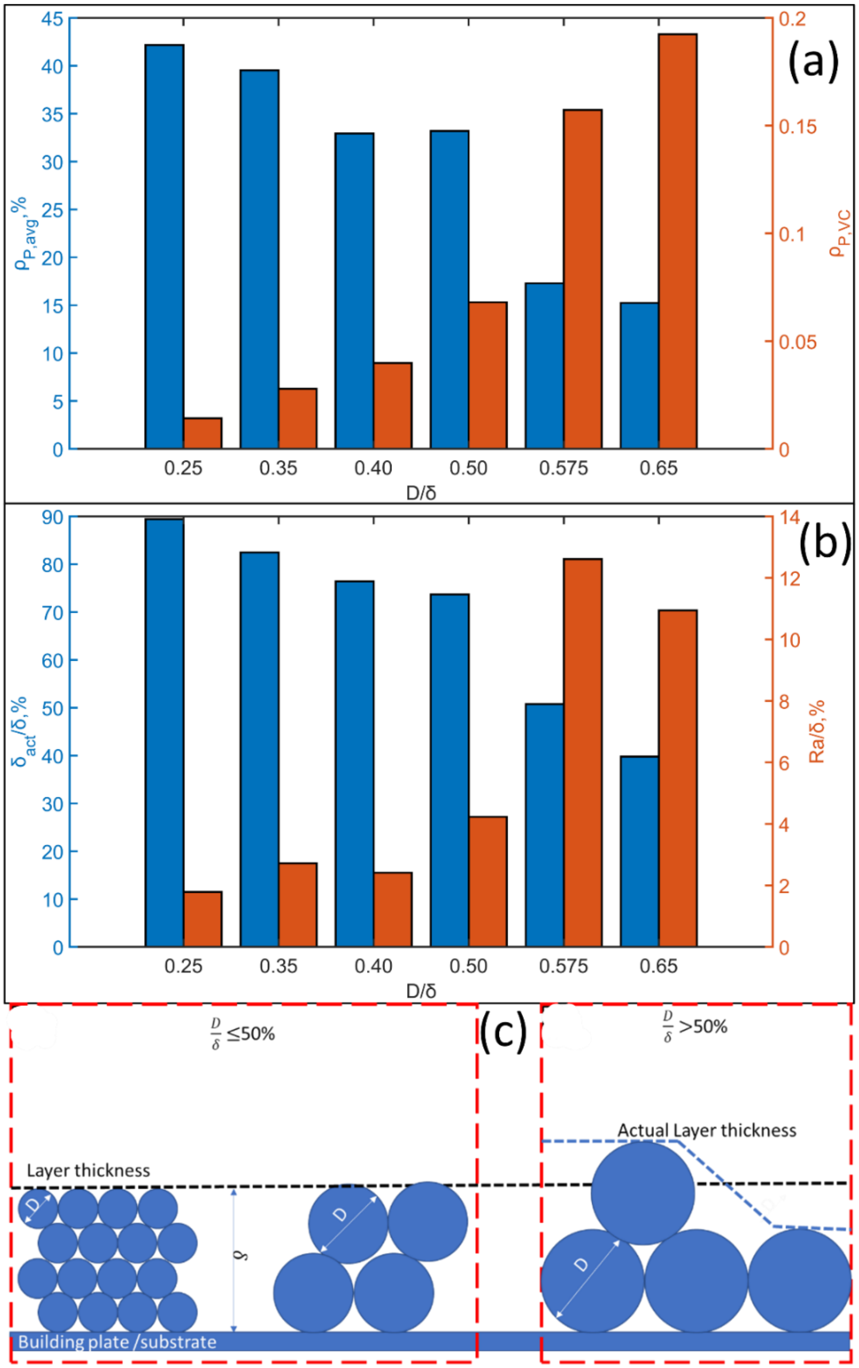

Figure 3-11.Packing density and layer thickness characteristics for a non-rotating roller as a function of normalized powder size within the study area. (a) Average packing density (right y-axis) and the coefficient of variation of packing density (left y-axis); (b) Normalized average layer thickness (right y-axis) and normalized surface roughness (left y-axis) ;(c) Presentation of powder particles over building plate in case of D/δ ≤50% and D/δ >50%.

disrupted more by the roller. This makes the packing density uneven, leading to noticeable inconsistencies across the powder bed. So, the static and dynamic wall effects behind this jump are in the variation coefficient for the packing density.

In terms of layer thickness, increasing the normalized powder size resulted in a significant reduction in the deposited layer thickness compared to the desired value. Specifically, the average layer thickness formed by the non-rotating roller remained below 90% of the intended thickness. As the normalized powder size increased from 0.25 to 0.65, the average layer thickness decreased by 55.5%, as shown in Figure 3-11b. This considerable reduction indicates that larger powder particles face greater difficulty filling the layer effectively, leading to increased void formation and reduced powder bed compaction, as presented in Figure 3-11c. The inability of coarse powders to form stable layers can be attributed to increased resistance to flow and a reduced capacity for interparticle rearrangement. Furthermore, as the ratio of powder size to layer thickness exceeds 50%, the static and dynamic wall effects become more pronounced, preventing efficient powder distribution and contributing to excessive variability in layer thickness.

Surface roughness also exhibited a strong correlation with normalized powder size. When the normalized powder size increased from 0.25 to 0.50, the normalized surface roughness rose from 1.79% to 4.23%. However, surface roughness increased dramatically beyond a normalized powder size of 0.5. At a normalized powder size of 0.65, the surface roughness escalated to 10.94%, as illustrated in Figure 3-11b. The sharp rise in surface roughness is mainly due to more substantial wall effects, which disrupt the even spread of particles and create more voids. These disturbances become even more pronounced with larger particles, leading to more significant surface irregularities and a less uniform powder bed. The influence of the wall effect on surface roughness is particularly evident at high normalized powder sizes, where limited particle rearrangement capabilities lead to pronounced undulations and inconsistencies across the powder layer.

In short, larger normalized powder sizes significantly impact powder bed quality due to more substantial wall effects. As the normalized powder size increases, packing density and layer thickness drop while density variations and surface roughness become pronounced.

3.4.2.1.2. Rotating roller

3.4.2.1.2.1. Packing density

The packing density of the powder layer during rolling-spreading is shaped by the roller's rotation, speed and direction, and the size of the powder particles. When employing a counter-rotating roller at a spreading speed of 50 mm/s, the impact on packing density varies based on the normalized powder size. For smaller powder sizes (normalized size ≤ 0.5), increasing the roller's counterclockwise rotational speed from 10 rad/s to 90 rad/s slightly reduces packing density due to the outward pushing force generated by the momentum exchange between the roller and the powder. This effect is comparable to an increase in spreading speed, leading to a decrease in packing density. For instance, at a normalized powder size of 0.35, increasing rotational speed up to 60 rad/s reduces packing density from 39.5% to 31.1%. However, when the normalized powder size exceeds 0.5, the rotation effect reverses slightly. As the rotational speed rises from 0 to 40 rad/s, the packing density rises from 15.2% to 22.9% at a normalized powder size of 0.65, as illustrated in

Figure 3-12a. Beyond this point, the packing density starts to decline gradually. This happens because larger powder particles, being heavier, do not respond as much to the roller's pushing force. In the end, the minimal effect of counterclockwise rotation on packing density suggests that the spreading speed has a more significant influence on powder compaction than the roller's rotational movement.

Conversely, a forward-rotating roller exhibits a different influence on packing density. The average packing density follows a distinct behaviour as the roller's clockwise rotational speed increases from 10 to 90 rad/s at a constant spreading speed of 50 mm/s. The packing density increases with clockwise rotational speed, reaching a maximum value before it decreases slightly. The rate of increase is closely tied to the normalized powder size, highlighting how rotational speed interacts with powder size to shape the final powder layer. Notably, the rotational speed at which maximum packing density occurs is close to the rolling rotational speed (ω_o = 20 rad/s). As the normalized powder size increases, the deviation from this rolling condition becomes more pronounced. For example, at normalized powder sizes of 0.25, 0.35, and 0.5, the corresponding rotational speeds at peak packing density are 20, 22, and 40 rad/s, respectively, as shown in Figure 3-12a. This pattern occurs due to the increased influence of backward acceleration of powder particles caused by the high circumferential speed at the bottom of the roller, which increases kinetic energy transfer and expands the powder volume on the building plate. However, increased turbulence due to powder burst phenomena causes a slight reduction in packing density at excessive rotational speeds.

Apart from average packing density, the variation coefficient of the packing density must also be considered to evaluate the uniformity of the powder bed. As the normalized powder size increases, the nonuniformity of packing density also rises due to intensified wall effects that cause uneven powder distribution along the building plate. This effect is especially pronounced at the boundaries of the building plate, where the interaction with the static walls is stronger. When the normalized powder size is ≤ 0.5, the variation coefficient remains below 0.1, indicating relatively uniform packing. However, the variation coefficient rises dramatically once the normalized powder size exceeds 0.5. For instance, at a normalized powder size of 0.65, the maximum variation coefficient reaches 0.2504, as presented in Figure 3-12b. Analyzing the effect of rotational direction on packing uniformity reveals a distinct trend. The variation coefficient generally increases as the rotational speed changes from -90 rad/s (forward-rotating) to 90 rad/s (counter-rotating). However, in the case of forward rotation and for normalized powder sizes greater than 0.5, increasing rotational speed significantly reduces nonuniformity. For example, at a normalized powder size of 0.65, increasing clockwise rotational speed from 20 rad/s (rolling case) to 90 rad/s decreases the variation coefficient from 0.25 to 0.06. This indicates that higher rotational speeds in the forward direction enhance powder compaction and uniformity. Moreover, for normalized powder sizes less than 0.5, the variation coefficient reaches its minimum at rotational speeds close to the rolling condition (ω_o). For instance, at normalized powder sizes of 0.25 and 0.35, the minimum variation coefficients are 0.00776 and 0.01511, occurring at rotational speeds of 20 and 28 rad/s, respectively. This minimum nonuniformity occurs when the momentum transfer due to rotational speed (backward direction) balances the momentum transfer due to spreading speed (forward direction).

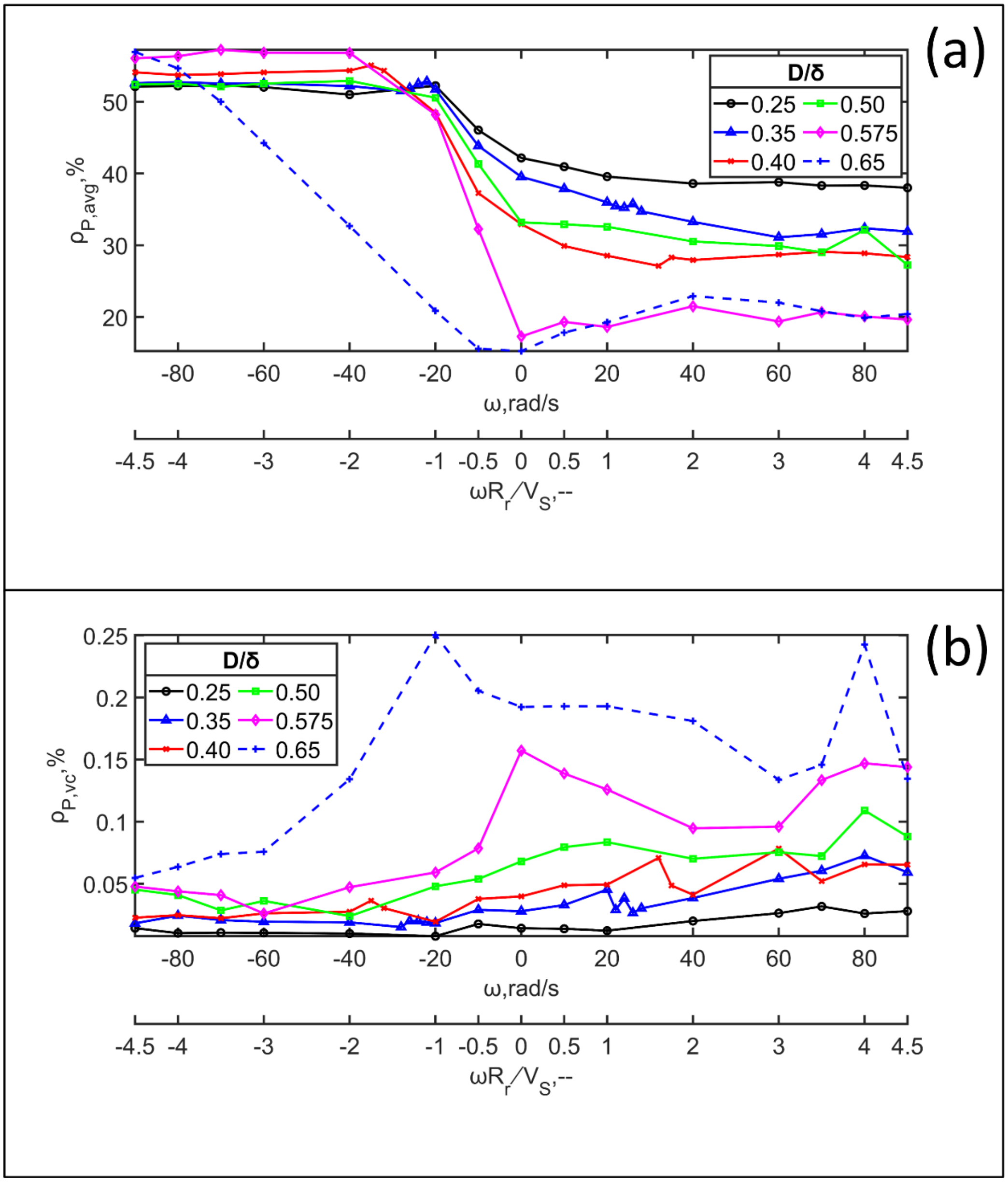

Figure 3-12. Effect of roller rotational speed on the powder layer's average packing density and variation coefficient for different normalized powder sizes at a spreading speed of 50 mm/s. (a) Average packing density and (b) variation coefficient of packing density as a function of rotational speed (ω) and normalized rotational speed ($\omega R_r/V_s$)

The Counterclockwise rotational speed has slightly affected the packing density and packing density uniformity; however, clockwise rotation speed significantly enhances packing density and packing density uniformity, especially at higher rotational speeds. Additionally, utilizing powder with a mean size smaller than 50% of the desired layer thickness promotes higher packing density and improved uniformity, with the most pronounced effect observed when the powder size is 25% of the desired layer thickness.

3.4.2.1.2.2. Layer thickness

Uniform and controlled layer thickness of the powder layer is a key factor in avoiding problems during printing, like excessive melting in the lower layer thickness or insufficient fusion in the larger layer thickness. This study systematically examines how counter-rotating (counterclockwise rotational speed) and forward-rotating (clockwise rotational speed) roller configurations interact with varying powder sizes at a spreading speed of 50 mm/s, shedding light on their effects on powder layer formation.

When employing a counter-rotating roller with rotational speeds ranging from 10 rad/s to 90 rad/s, the resulting layer thickness was consistently thinner than the desired layer thickness across all tested normalized powder sizes (0.25 to 0.65). The average layer thickness varied between 34.6% and 95% of the target thickness, with a clear trend showing that as the normalized powder size increased, the average layer thickness decreased, as illustrated in Figure 3-13a. This reduction is attributed to the wall effect, which becomes more pronounced with larger powder particles. For instance, at a clockwise rotational speed of 20 rad/s, increasing the normalized powder size from 0.25 to 0.65 resulted in a 52% reduction in average layer thickness. When using a counter-rotating roller with a normalized powder size of 0.5 or less, increasing the rotational speed from 0 to 90 rad/s causes a slight decrease in layer thickness. For example, the average layer thickness drops by 7% as the rotational speed increases from 0 to 90 rad/s with a normalized powder size of 0.25. This happens because the higher circumferential speed at the bottom, in the same direction as the spreading motion, leads to a greater pushing force of the powder away from the building plate. However, when the normalized powder size exceeded 0.5, layer thickness exhibited slight fluctuations with increasing rotational speed rather than a consistent trend.

On the other hand, As the clockwise rotational speed of the forward-rotating roller increased from 0 to 90 rad/s, the average layer thickness consistently increased across all normalized powder sizes. This increase can be attributed to the enhanced backward acceleration of powder particles induced by the high circumferential speed at the roller's base. This acceleration enhances kinetic energy transfer, causing the powder to expand on the building plate (i.e., a powder burst). At normalized powder sizes of 0.25 and 0.50, the average layer thickness increased by 157% and 182%, respectively, highlighting the strong correlation between rotational speed and the rate of layer thickness growth, as shown in Figure 3-13a. A critical observation is that at a clockwise rotational speed of 20 rad/s or higher (i.e., rolling speed), the average layer thickness exceeded the desired layer thickness. This characteristic can be leveraged to compensate for material loss due to shrinkage during layer solidification. Furthermore, for all forward-rotating configurations, increasing the normalized powder size led to a decrease in average layer thickness. For instance, as the normalized powder size increased from 0.25 to 0.5, the average layer thickness decreased by 3.14%, 3.16%, and 16.46% at clockwise rotational speeds of 10, 20, and 60 rad/s, respectively.

Surface roughness plays a vital role in powder layer quality and print consistency. The findings indicate that both powder size and roller speed have a significant impact on the roughness characteristics of the powder layer. For normalized powder sizes below 0.5, the maximum average surface roughness across the full range of rotational speeds (-90 rad/s to 90 rad/s) remained within 5% of the desired layer thickness, as shown in Figure 3-13b. However, for normalized powder sizes greater than 0.5, the maximum average surface roughness reached 10%, emphasizing the influence of larger powder particles on surface irregularities. Increasing the rotational speed for counter-rotating rollers with normalized powder sizes below 0.5 helped create a smoother surface by reducing surface roughness. This improvement results from the higher shear stress exerted by the roller, which redistributes the powder more evenly. On the other hand, As the clockwise rotational speed of the forward-rotating rollers increases, surface roughness increases due to the increases in the turbulent motion of the powder. However, when the normalized powder size exceeds 0.5, surface roughness becomes more erratic, showing significant fluctuations regardless of rotational speed. Additionally, random fluctuations in layer thickness and surface roughness at high normalized powder sizes (e.g., 0.65) can be attributed to the increased influence of gravity on larger powder particles and the wall effect.

Interestingly, the roughness of powder layers formed by forward-rotating rollers exhibited minimal variation with normalized powder size. However, the rate at which surface roughness increased with rotational speed became more pronounced as powder size increased. Comparing the two roller configurations, the average surface roughness of powder layers with normalized sizes ≤0.5, generated by a forward-rotating roller over a speed range of 10 to 90 rad/s, was approximately 6.7% of the desired layer thickness. For powder sizes greater than 0.5, surface roughness increased to 9.8%. In comparison, counter-rotating rollers resulted in a roughness of 5% for smaller powder sizes and 11% for larger ones, suggesting that they generally create smoother and more uniform layers.

In summary, the counter-rotating roller's performance is closely tied to powder size, whereas the forward-rotating roller is more affected by rotational speed. This highlights the fundamental difference between the two mechanisms. At the same time, counter-rotation relies on the powder's characteristics to achieve uniformity, and forward-rotation is driven by the impact of speed on powder dispersion.

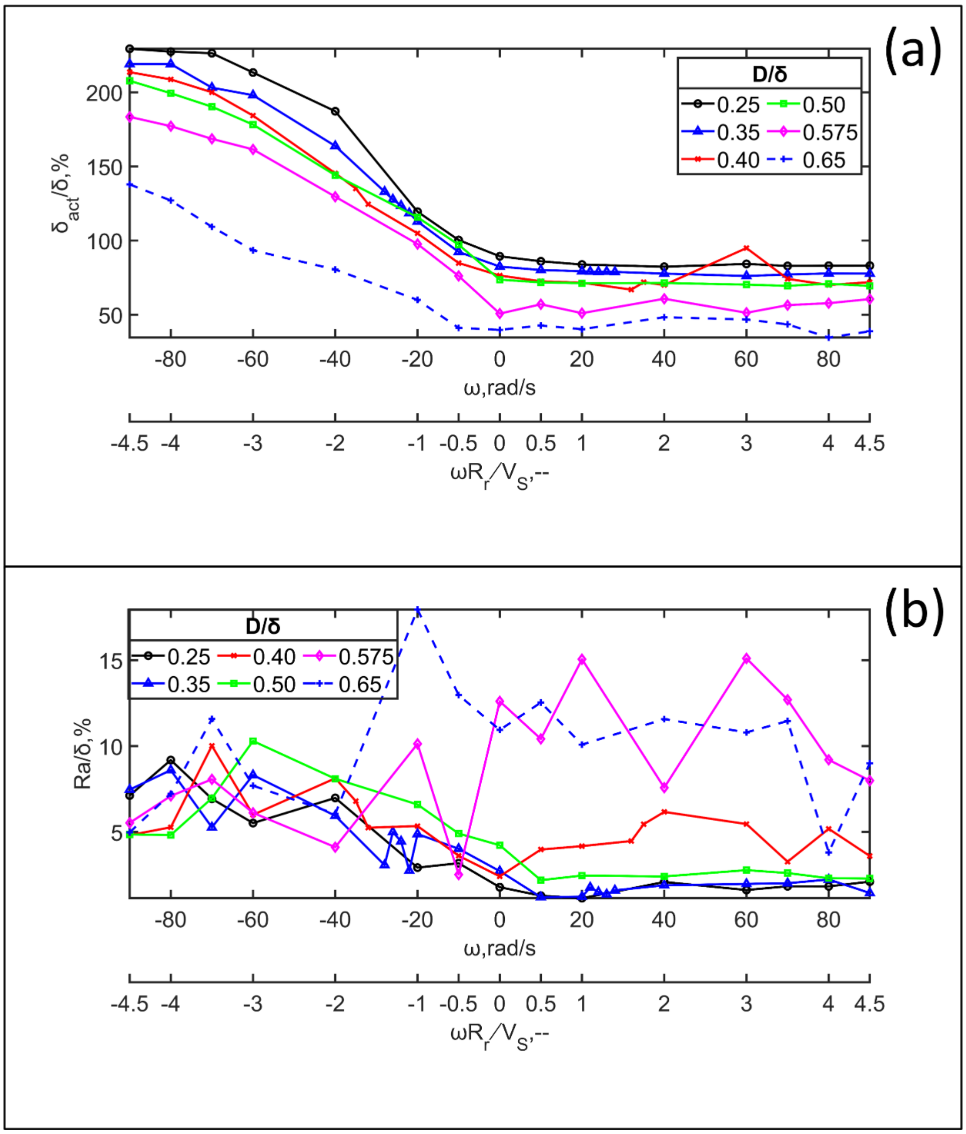

Figure 3-13.Effect of roller rotational speed on the powder layer's average layer thickness and surface roughness for different normalized powder sizes at a spreading speed of 50 mm/s. (a) normalized average layer thickness ;(b) normalized surface roughness as a function of rotational speed (ω) and normalized rotational speed ($\omega R_r/V_s$)

3.4.2.1.2.3. Mass fraction

The mass fraction of the powder layer, which quantifies the actual amount of powder deposited on the building plate, plays a crucial role in evaluating the performance of the spreading mechanism. Unlike packing density, which assesses the effectiveness of the spreading process, the mass fraction becomes particularly relevant in forward-rotating roller configurations, especially in super-rolling conditions where the deposited layer thickness exceeds the desired value. In such cases, the conventional metric of packing density fails to capture the actual effectiveness of the roller, making mass fraction the primary indicator of its performance.

A key observation in forward-rotating spreading is the consistent and significant increase in mass fraction with rotational speed, particularly under the super-rolling configuration. For instance, at a normalized powder size of 0.25, the mass fraction rises by 147% when rotational speed increases from zero to 90 rad/s, as illustrated in Figure 3-14a. This dramatic increase occurs due to the intensified powder accumulation on the building plate, a phenomenon driven by higher rotational speeds, which increases circumferential speed opposite the spreading direction at the roller bottom, leading to more force pushing powder in the backward direction, more powder accumulation, and, finally, increasing mass fraction. However, while increasing rotational speed boosts mass fractions, larger normalized powder sizes have the opposite effect, reducing the overall mass distribution.

As the normalized powder size increases from 0.25 to 0.5, mass fraction reductions of 10%, 2%, and 8% are observed at rotational speeds of 10 rad/s (sub-rolling), 20 rad/s (rolling), and 60 rad/s (super-rolling), respectively. This trend becomes even more pronounced when the normalized powder size extends to 0.65, leading to mass fraction reductions of 66%, 62%, and 53% at the same rotational speeds. The sharp decline in mass fraction at normalized powder sizes greater than 0.5 suggests a strong negative correlation between mass fraction and particle size. Larger powder particles are more affected by gravity and the wall effect, reducing their ability to disperse effectively and leading to a lower overall mass fraction.

In addition to mass fraction, its variation coefficient measures uniformity in powder distribution. For normalized powder sizes of 0.5 and above, the variation coefficient decreases as the rotational speed increases from 10 to 90 rad/s, suggesting an improvement in uniformity at higher speeds. The variation coefficient fluctuates but is low under 0.05 over speeds ranging from zero to 90 rad/s, leading to uniform powder distribution, as shown in Figure 3-14b. Furthermore, the variation coefficient increases significantly with normalized powder size due to the wall effect. Larger particles struggle to disperse evenly and compactly, resulting in more inconsistently distributed mass fractions than smaller powders.

For a more uniform powder distribution with minimal variation in mass fraction, any clockwise rotational speed within the rolling range works well for normalized powder sizes below 0.5. However, for larger powder sizes, using a higher clockwise rotational speed helps improve uniformity

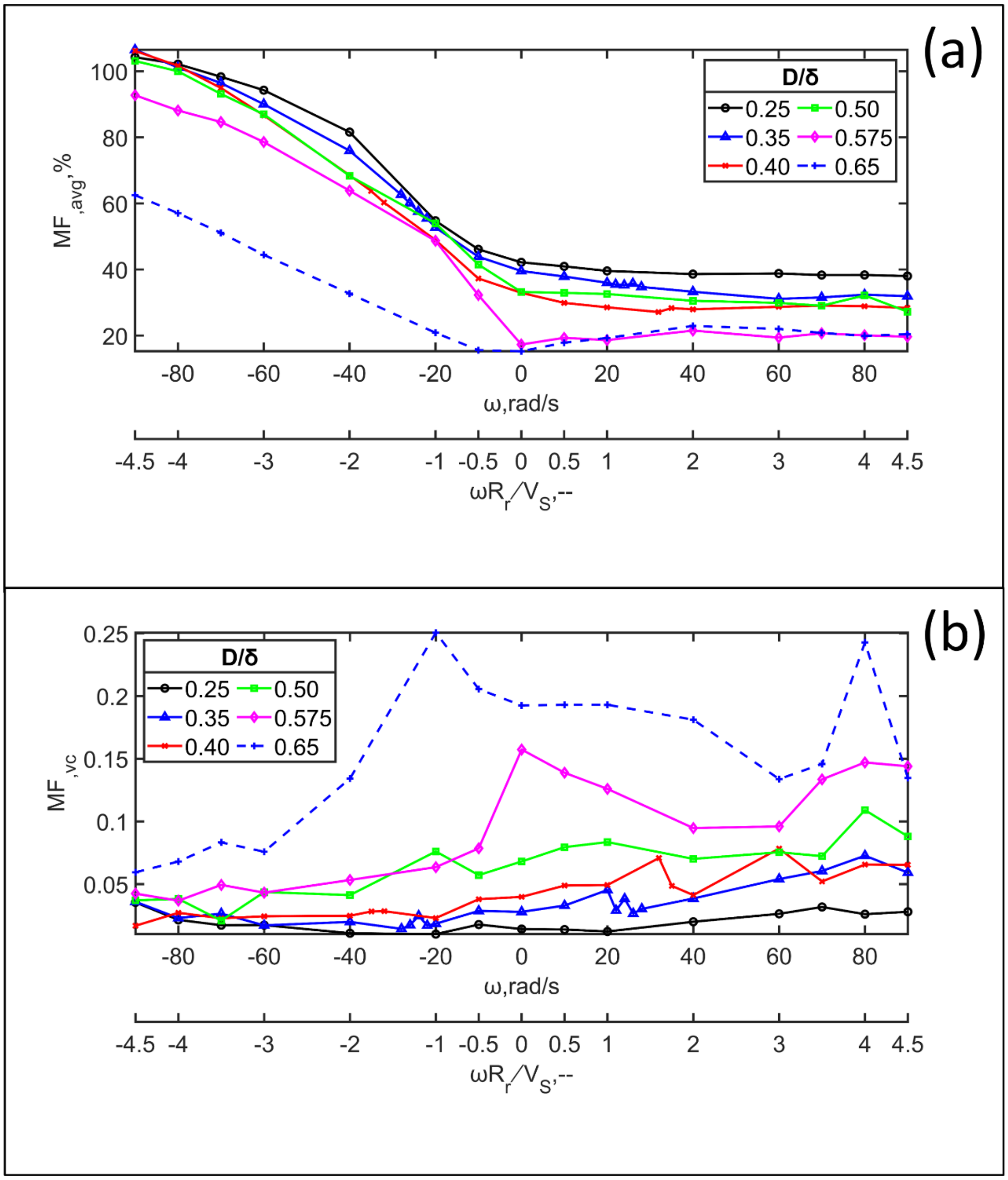

Figure 3-14. Effect of roller rotational speed on the powder layer's average mass fraction and variation coefficient for different normalized powder sizes at a spreading speed of 50 mm/s. (a) Average packing density and ;(b) variation coefficient of packing density as a function of rotational speed (ω) and normalized rotational speed ($\omega R_r/V_s$)

3.4.2.2. Effect of roller size on overall roller-spreading process performance

As the roller radius varies from 7.5 to 22.5 times the intended layer thickness, its effect on packing density, layer thickness, mass fraction, and surface roughness differ across the three spreading configurations: non-rotating, counter-rotating, and forward-rotating.

Since the roller is not spinning in the non-rotating setup, its size does not directly impact how the powder spreads. As a result, the packing density stays consistent at around 42.1±0.4%, with slight variation regardless of roller size. A similar trend is observed in the counter-rotating configuration at 40 rad/s, where packing density remains nearly constant at 38.9±0.3%, as shown in Figure 3-15a. However, in the forward-rotating setup with the

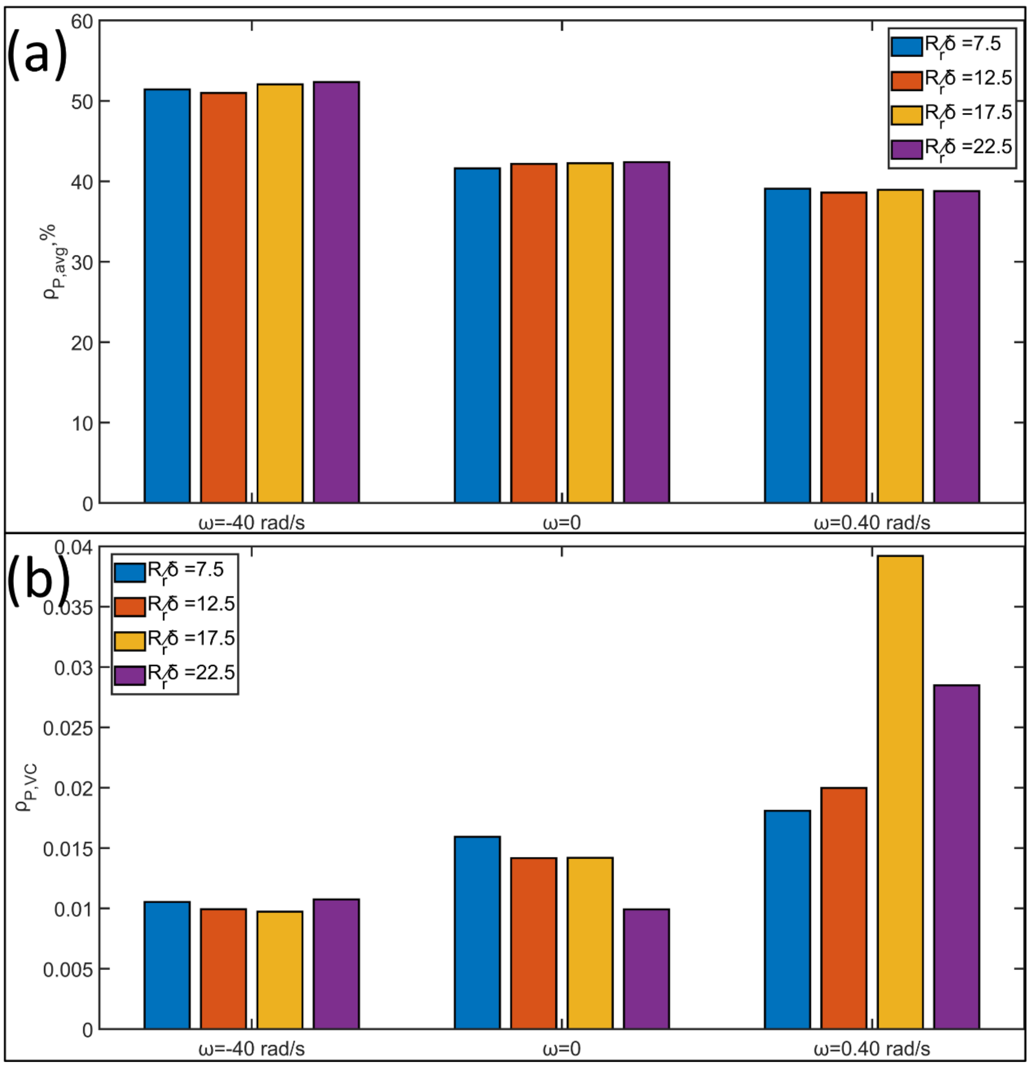

Figure 3-15. Effect of roller radius on the average packing density and variation coefficient of packing density at different configurations (forward-rotating (i.e., ω = -40 rad/s), non-rotating (i.e., ω = 0 rad/s), counter-rotating (i.e., ω = 40 rad/s)). (a) Average packing density and (b) variation coefficient of packing density for different normalized roller radii (R_r/δ= 7.5, 12.5, 17.5, and 22.5).

same rotational speed, a slight increase in packing density is noted as the roller radius grows, reaching 51.7±0.7%, representing a 1.8% increase. Larger roller sizes in the non-rotating setup help improve uniformity, leading to a 37.8% reduction in the variation coefficient, as illustrated in Figure 3-15b. However, a larger roller radius leads to a higher variation coefficient in the case of a counter-rotating roller (0.04 at roller radius equals 17.5 times the desired layer thickness) and indicates a reduction in packing uniformity. In the meantime, the forward-rotating configuration exhibits slight changes in the packing density variation coefficient.

A similar behaviour is observed in layer thickness, where both the non-rotating and counter-rotating configurations maintain nearly constant values of 178.4±1.7 μm and 165.6±0.8 μm, respectively, regardless of roller radius, as shown in Figure 3-16a. In the forward-rotating setup, layer thickness increases significantly by 81% as the roller radius expands. This growth is driven by the higher circumferential speed of larger rollers, which generates a stronger backward force, causing more powder to accumulate on the building plate and forming thicker layers. Surface roughness also fluctuates with roller radius, although these variations remain minor for non-rotating and counter-rotating rollers, as illustrated in Figure 3-16b. In contrast, forward-rotating rollers show more pronounced fluctuations, with smaller radii generally producing smoother powder layers.

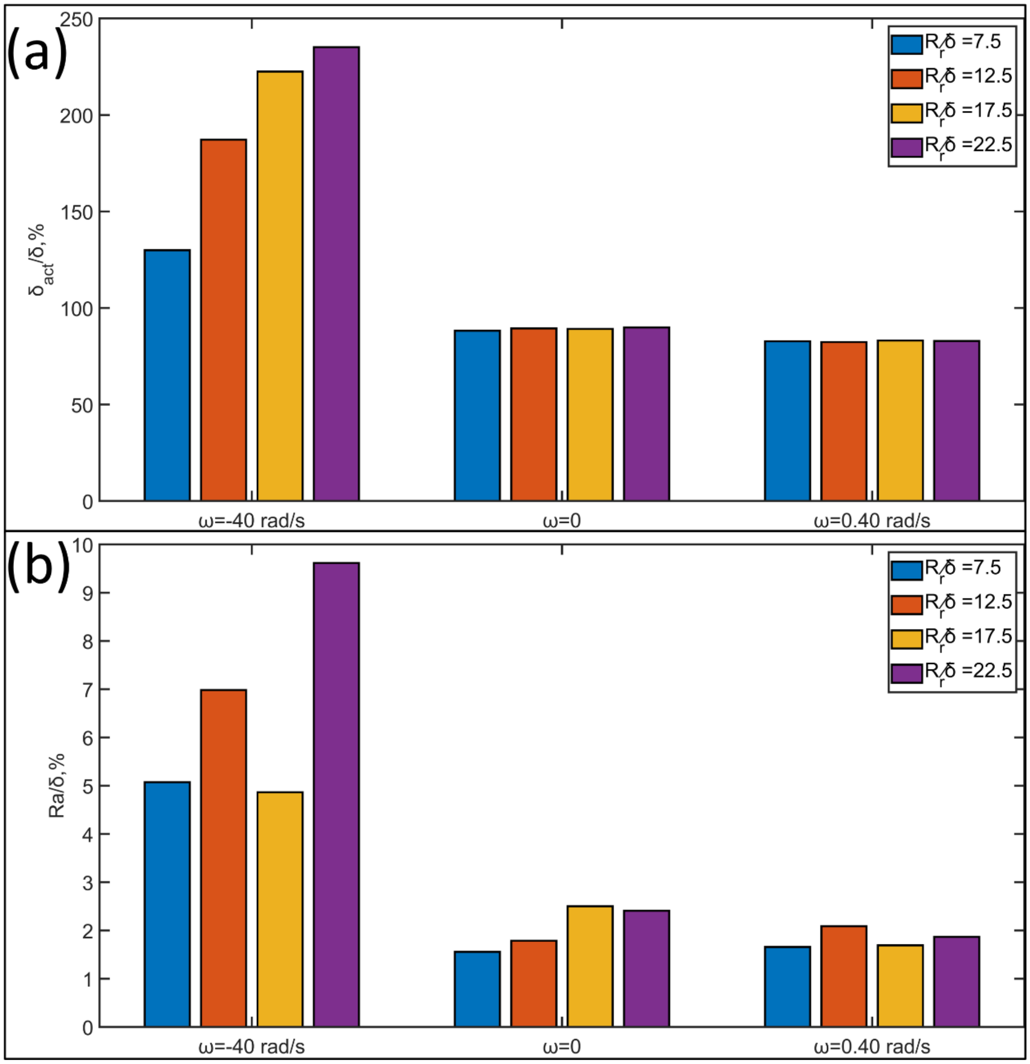

Figure 3-16.Effect of roller radius on the normalized average layer thickness and normalized surface roughness at different configurations (forward-rotating (i.e., ω = -40 rad/s), non-rotating (i.e., ω = 0 rad/s), counter-rotating (i.e., ω = 40 rad/s)). (a) Normalized average layer thickness and (b) Normalized surface roughness for different normalized roller radii (R_r/δ= 7.5, 12.5, 17.5, and 22.5).

In the non-rotating and counter-rotating setups, mass fraction remains relatively constant at 42.1±0.4% and 38.9±0.3%, respectively, highlighting its close relationship with packing density in these configurations, as illustrated in Figure 3-17a. However, in the forward-rotating setup, the mass fraction rises significantly by 78% as the roller radius increases due to powder accumulation due to backward circumferential speed. In a non-rotating setup, a larger roller radius maintains a more uniform distribution of powder. However, larger rollers maintain higher nonuniformity in powder distribution in the case of counter-rotating rollers. The effect is even more pronounced in the forward-rotating setup, where increasing the roller radius causes a sharp 250.8% rise in mass fraction variation, highlighting how crucial roller size is for maintaining an even powder layer, as shown in Figure 3-17b.

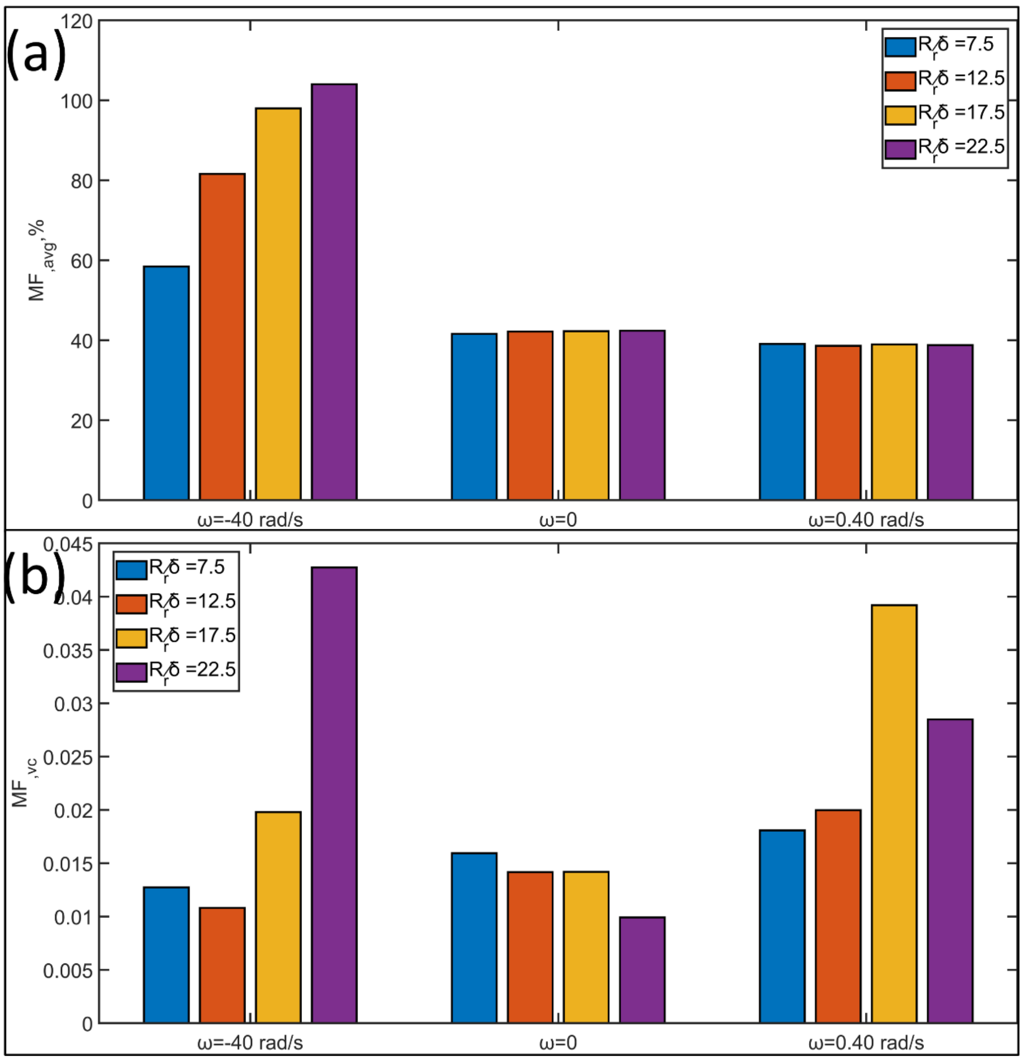

Figure 3-17. Effect of roller radius on the average mass fraction and variation coefficient of packing density at different configurations (forward-rotating (i.e., ω = -40 rad/s), non-rotating (i.e., ω = 0 rad/s), counter-rotating (i.e., ω = 40 rad/s)). (a) Average mass fraction and (b) variation coefficient of mass fraction for different normalized roller radii (R_r/δ= 7.5, 12.5, 17.5, and 22.5).

3.4.2.3. Consistency condition for different roller sizes at the same spreading speed

In a particular scenario where the spreading speed remains constant, it has been observed that the performance of rollers, including packing density, layer thickness, and surface roughness, tends to be similar. This is shown in Figure 3-18 when the circumferential speed remains constant, as indicated in the following equation.

$$\omega_1 R_{r,1} = \omega_2 R_{r,2} \ \ or \ \ \omega_1/\omega_2 = R_{r,2}/R_{r,1} \qquad 4$$

This proves that the roller's circumferential speed impacts the spreading process along with the spreading speed itself. Therefore, to ensure consistency in the spreading process, it is essential to maintain constant spreading and circumferential speeds. Moreover, the size of the roller does not significantly affect the spreading process. However, it becomes a significant spreading parameter once combined with the rotational (circumferential) speed. This finding suggests a correlation between the rotational speed and size of the rollers, indicating that a certain balance between these parameters can lead to comparable outcomes in terms of packing density, layer thickness, and surface roughness. It highlights the importance of considering the interplay between rotational speed and roller size in achieving consistent performance in roller-based operations.

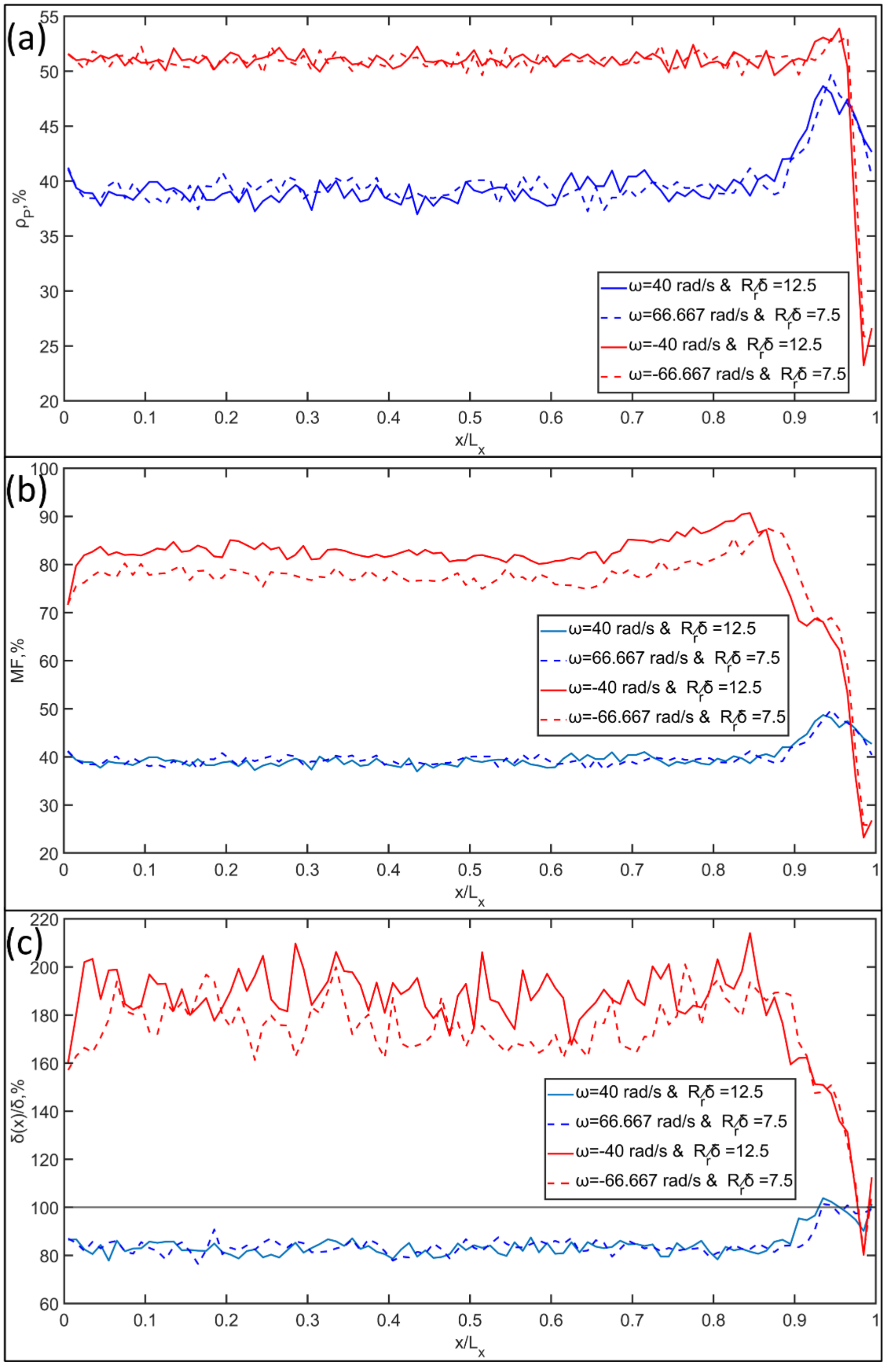

Figure 3-18. Distribution of (a) packing density, (b) mass fraction, and (c) normalized layer thickness along the normalized building plate length for different roller rotational speeds (ω = ±40 and ±66.667 rad/s) and normalized roller radii (R_n/δ = 7.5 and 12.5).

3.5. Conclusions

The current work investigated the impact of circumferential speed on the spreading process through a group of DEM simulations. It measured the influence of circumferential speed by applying a variation of rotational speed and roller size on the spreading process and observing the changes in packing density, layer thickness and mass fraction. The primary outcome of the work can be summarized as follows:

A. The non-rotating roller generates relatively uniform layers with lower packing density than rotating configurations. Forward-rotating rollers enhance powder compaction and improve distribution across the building plate; however, excessive circumferential speeds can induce powder bursts, leading to surface roughness, cavities forming at the right edge and reduced uniformity. In contrast, high-speed counter-rotating rollers exhibit significant powder scattering, decreasing uniformity and increasing porosity.

B. Maintaining a buffer zone between the building plate boundaries and the painting area ensures uniform packing density and layer thickness while minimizing cavities and uneven distribution caused by wall effects.

C. Larger normalized powder sizes ($D/\delta > 0.5$) lead to higher fluctuations in packing density across all configurations due to the wall effect, with the impact of circumferential speed diminishing in sub-rolling as powder size increases. While the rolling configuration stabilizes layer thickness and minimizes excessive powder displacement, super-rolling enhances uniformity but introduces cavity formation and thickness fluctuations at larger powder sizes due to powder accumulation.

D. Counter-rotating rollers generally reduce packing density due to outward powder displacement, with minimal impact on uniformity. In contrast, forward-rotating rollers significantly enhance packing density, with peak values occurring near the rolling speed ($\omega_o = V_s/R_r$), while higher speeds improve compaction and reduce nonuniformity, particularly for larger powder sizes. Additionally, normalized powder sizes smaller than 0.5 lead to denser, more uniform powder beds, with the most consistent results observed at 0.25.

E. Counter-rotating rollers consistently produce thinner layers than the desired thickness, with increasing rotational speed slightly reducing layer thickness for smaller powder sizes due to enhanced powder displacement. In contrast, forward-rotating rollers lead to thicker layers, often exceeding the target thickness at higher speeds, which can help compensate for material shrinkage during solidification. Counter-rotating rollers tend to create smoother surfaces, while forward-rotating rollers cause more roughness as rotational speed increases, especially with larger powder sizes.

F. Integrating packing density and mass fraction is essential to evaluate forward-rotating roller configurations. Higher rotational speeds significantly increase mass fraction, especially in super-rolling conditions, due to enhanced powder accumulation driven by backward-directed forces. Larger powder sizes lower the mass fraction due to gravitational effects and wall interactions, creating an inverse relationship between particle size and mass deposition. For a more even powder distribution, moderate rotational speeds work best for smaller powders, while higher speeds help improve uniformity for larger ones.

G. The findings show that packing density in roller spreading is mainly controlled by rotational and spreading speeds, with forward-rotating rollers being slightly influenced by roller size. Smaller rollers with forward rotation improve powder compaction, resulting in a denser, more uniform layer with better thickness and smoothness. Moreover, smaller rollers and forward rotation facilitate a more uniform mass fraction distribution, ensuring consistent powder deposition throughout the building process.

H. When the spreading speed remains constant, circumferential speed should be the same to have comparable outcomes in terms of packing density, layer thickness, and surface roughness, highlighting the importance of carefully controlling the interaction between rotational speed and roller size to achieve consistent performance in roller-based operations and improve quality and productivity.

Future research should focus on experimental validation of these numerical findings and developing adaptive control strategies to refine powder bed uniformity further and improve additive manufacturing outcomes.

References

[1] W. Zhang, A. De, A. Wilson-Heid, A.M. Beese, J.W. Elmer, J.S. Zuback, T. Mukherjee, J.O. Milewski, T. DebRoy, H.L. Wei, Additive manufacturing of metallic components – Process, structure and properties, Prog Mater Sci 92 (2017) 112–224. https://doi.org/10.1016/j.pmatsci.2017.10.001.

[2] M. Balbaa, A. Ghasemi, E. Fereiduni, K. Al-Rubaie, M. Elbestawi, Improvement of fatigue performance of laser powder bed fusion fabricated IN625 and IN718 superalloys via shot peening, J Mater Process Technol 304 (2022) 117571. https://doi.org/10.1016/j.jmatprotec.2022.117571.

[3] H.L. Wei, T. Mukherjee, W. Zhang, J.S. Zuback, G.L. Knapp, A. De, T. DebRoy, Mechanistic models for additive manufacturing of metallic components, Prog Mater Sci (2020). https://doi.org/10.1016/j.pmatsci.2020.100703.

[4] S.A. Khairallah, A.T. Anderson, A. Rubenchik, W.E. King, Laser powder-bed fusion additive manufacturing: Physics of complex melt flow and formation mechanisms of pores, spatter, and denudation zones, Acta Mater 108 (2016) 36–45. https://doi.org/10.1016/j.actamat.2016.02.014.

[5] M. Yakout, M.A. Elbestawi, S.C. Veldhuis, Density and mechanical properties in selective laser melting of Invar 36 and stainless steel 316L, J Mater Process Technol 266 (2019) 397–420. https://doi.org/10.1016/j.jmatprotec.2018.11.006.

[6] M. Yakout, M.A. Elbestawi, S.C. Veldhuis, A study of thermal expansion coefficients and microstructure during selective laser melting of Invar 36 and stainless steel 316L, Addit Manuf 24 (2018) 405–418. https://doi.org/10.1016/j.addma.2018.09.035.

[7] E. Fereiduni, A. Ghasemi, M. Elbestawi, Microstructural characterization and mechanical properties of nano-scale/sub-micron TiB-reinforced titanium matrix composites fabricated by laser powder bed fusion, J Alloys Compd 896 (2022) 163054. https://doi.org/10.1016/j.jallcom.2021.163054.

[8] W.J. Sames, F.A. List, S. Pannala, R.R. Dehoff, S.S. Babu, The metallurgy and processing science of metal additive manufacturing, International Materials Reviews 61 (2016) 315–360. https://doi.org/10.1080/09506608.2015.1116649.

[9] M.H. Sehhat, A. Mahdianikhotbesara, Powder spreading in laser-powder bed fusion process, Granul Matter 23 (2021) 1–18. https://doi.org/10.1007/s10035-021-01162-x.

[10] K.Q. Le, C. Tang, C.H. Wong, A study on the influence of powder packing density on the melt track in the selective laser melting process, Proceedings of the International Conference on Progress in Additive Manufacturing 2018-May (2018) 703–708. https://doi.org/10.25341/D4P301.

[11] S.S. Sih, J.W. Barlow, The prediction of the emissivity and thermal conductivity of powder beds, Particulate Science and Technology 22 (2004) 427–440. https://doi.org/10.1080/02726350490501682.

[12] H.C. Tran, Y.L. Lo, M.H. Huang, Analysis of Scattering and Absorption Characteristics of Metal Powder Layer for Selective Laser Sintering, IEEE/ASME Transactions on Mechatronics 22 (2017) 1807–1817. https://doi.org/10.1109/TMECH.2017.2705090.

[13] M. Bhuvanesh Kumar, P. Sathiya, Methods and materials for additive manufacturing: A critical review on advancements and challenges, Thin-Walled Structures 159 (2021) 107228. https://doi.org/10.1016/j.tws.2020.107228.

[14] S. Haeri, Y. Wang, O. Ghita, J. Sun, Discrete element simulation and experimental study of powder spreading process in additive manufacturing, Powder Technol 306 (2016) 45–54. https://doi.org/10.1016/j.powtec.2016.11.002.

[15] W. Nan, M. Pasha, M. Ghadiri, Numerical simulation of particle flow and segregation during roller spreading process in additive manufacturing, Powder Technol 364 (2020) 811–821. https://doi.org/10.1016/j.powtec.2019.12.023.

[16] J. Zhang, Y. Tan, T. Bao, Y. Xu, X. Xiao, S. Jiang, Discrete element simulation of the effect of roller-spreading parameters on powder-bed density in additive manufacturing, Materials 13 (2020). https://doi.org/10.3390/ma13102285.

[17] W. Nan, M. Ghadiri, Numerical simulation of powder flow during spreading in additive manufacturing, Powder Technol 342 (2019) 801–807. https://doi.org/10.1016/j.powtec.2018.10.056.

[18] S. Haeri, Optimisation of blade type spreaders for powder bed preparation in Additive Manufacturing using DEM simulations, Powder Technol 321 (2017) 94–104. https://doi.org/10.1016/j.powtec.2017.08.011.

[19] Y. Lee, A.K. Gurnon, D. Bodner, S. Simunovic, Effect of Particle Spreading Dynamics on Powder Bed Quality in Metal Additive Manufacturing, Integr Mater Manuf Innov 9 (2020) 410–422. https://doi.org/10.1007/s40192-020-00193-1.

[20] J. Zhang, Y. Tan, X. Xiao, S. Jiang, Comparison of roller-spreading and blade-spreading processes in powder-bed additive manufacturing by DEM simulations, Particuology 66 (2022) 48–58. https://doi.org/10.1016/j.partic.2021.07.005.

[21] M.A. Salim, S. Tullis, M. Elbestawi, Accelerating Laser Powder Bed Fusion: The Influence of Roller-Spreading Speed on Powder Spreading Performance, Metals (Basel) 14 (2024) 1137. https://doi.org/10.3390/met14101137.

[22] L. Meyer, A. Wegner, G. Witt, Influence of the Ratio between the Translation and Contra-Rotating Coating Mechanism on different Laser Sintering Materials and their Packing Density, n.d.

[23] K.J. Seluga, Three Dimensional Printing by Vector Printing of Fine Metal Powders, 2001.

[24] P.S. Desai, C. Fred Higgs, Spreading process maps for powder-bed additive manufacturing derived from physics model-based machine learning, Metals (Basel) 9 (2019). https://doi.org/10.3390/met9111176.

[25] W. Nan, M. Pasha, M. Ghadiri, Effect of gas-particle interaction on roller spreading process in additive manufacturing, Powder Technol 372 (2020) 466–476. https://doi.org/10.1016/j.powtec.2020.05.119.

[26] A. Budding, T.H.J. Vaneker, New strategies for powder compaction in powder-based rapid prototyping techniques, in: Procedia CIRP, Elsevier B.V., 2013: pp. 527–532. https://doi.org/10.1016/j.procir.2013.03.100.

[27] M. Ziaee, R. Hershman, A. Mahmood, N.B. Crane, Fabrication of demineralized bone matrix/polycaprolactone composites using large area projection sintering (LAPS), Journal of Manufacturing and Materials Processing 3 (2019). https://doi.org/10.3390/jmmp3020030.

[28] T. Niino, K. Sato, Effect of Powder Compaction in Plastic Laser Sintering Fabrication, n.d.

[29] M. Moghadasi, G. Miao, M. Li, Z. Pei, C. Ma, Combining Powder Bed Compaction and Nanopowders to Improve Density in Ceramic Binder Jetting Additive Manufacturing, 2021. https://www.sciencedirect.com/science/article/pii/S027288422102856X.

[30] M. Li, X. Wei, Z. Pei, C. Ma, Binder jetting additive manufacturing: observations of compaction-induced powder bed surface defects, Manuf Lett 28 (2021) 50–53. https://doi.org/10.1016/j.mfglet.2021.04.003.

[31] J.Q. Gan, A.B. Yu, Z.Y. Zhou, DEM simulation on the packing of fine ellipsoids, Chem Eng Sci 156 (2016) 64–76. https://doi.org/https://doi.org/10.1016/j.ces.2016.09.017.

[32] B.C. Burman, P.A. Cundall, O.D.L. Strack, A discrete numerical model for granular assemblies, Geotechnique 30 (1980) 331–336. https://doi.org/10.1680/geot.1980.30.3.331.

[33] R.D. Mindlin, H. Deresiewicz, Elastic Spheres in Contact Under Varying Oblique Forces, J Appl Mech 20 (2021) 327–344. https://doi.org/10.1115/1.4010702.

[34] K.L. Johnson, K. Kendall, A.D. Roberts, Surface energy and the contact of elastic solids, Proceedings of the Royal Society of London. A. Mathematical and Physical Sciences 324 (1971) 301–313. https://doi.org/10.1098/rspa.1971.0141.

[35] Altair EDEM 2021.1, (n.d.). https://www.altair.com/edem/.

[36] D. Yao, X. An, H. Fu, H. Zhang, X. Yang, Q. Zou, K. Dong, Dynamic investigation on the powder spreading during selective laser melting additive manufacturing, Addit Manuf 37 (2021). https://doi.org/10.1016/j.addma.2020.101707.

[37] H. Chen, Q. Wei, S. Wen, Z. Li, Y. Shi, Flow behavior of powder particles in layering process of selective laser melting: Numerical modeling and experimental verification based on discrete element method, Int J Mach Tools Manuf 123 (2017) 146–159. https://doi.org/10.1016/j.ijmachtools.2017.08.004.

[38] L. Wang, A. Yu, E. Li, H. Shen, Z. Zhou, Effects of spreader geometry on powder spreading process in powder bed additive manufacturing, Powder Technol 384 (2021) 211–222. https://doi.org/10.1016/j.powtec.2021.02.022.

4 Adaptive Rotational Speed Strategies for Reducing the Impact of high spreading Speed in laser powder bed fusion

Author Contributions:

- **Mohamed Awad Salim:** Conceptualization, methodology, software, validation, formal analysis, investigation, resources, data curation, writing—original draft preparation and visualization
- **Dr. M. A. Elbestawi:** Conceptualization, supervision, methodology, resources and writing—review and editing
- **Dr. Stephen Tullis:** Conceptualization, supervision, methodology, formal analysis, investigation, resources and writing—review and editing

4.1. Abstract

High-speed powder spreading in Laser Powder Bed Fusion (PBF-LP) introduces significant challenges in achieving uniformity, optimal packing density, and consistent layer quality, which are critical for additive manufacturing. This study leverages Discrete Element Method (DEM) simulations to systematically evaluate the effects of constant and variable rotational speed profiles on powder spreading performance at speeds of 0.15 m/s and 0.30 m/s. Constant rotational speed strategies were assessed, including non-rotating, counter-rotating, and clockwise configurations. While these approaches demonstrated varying degrees of success, they could not fully address critical issues such as cavity formation and non-uniform powder distribution. Variable rotational speed profiles (A–F) were developed and analyzed to overcome these limitations. Profile F emerged as the most effective strategy among these profiles, offering substantial improvements across multiple performance metrics. Characterized by a high initial clockwise rotational speed that gradually decreases to zero, Profile F achieved the highest packing density, minimal variation coefficient, and superior mass fraction. It demonstrated enhanced uniformity in layer thickness and significantly reduced surface roughness, even at high spreading speeds. This research underscores the importance of adaptive rotational speed strategies in optimizing powder layer quality. By balancing clockwise and counterclockwise rotational speeds, Profile F mitigates disturbances caused by high spreading speeds and boundary interactions. The findings provide valuable insights into improving the efficiency and reliability of PBF-LP processes, highlighting Profile F as a promising approach for industrial applications requiring precise and uniform powder deposition.

4.2. Introduction

Laser Powder Bed Fusion (PBF-LP) is considered a cutting-edge manufacturing technique in the fabrication of complicated parts. The process relies on spreading fine powder, which is subsequently fused and solidified through selective laser scanning[1–3]. A spreader distributes powder evenly across the building plate at a spreading speed during powder-spreading. Powder-spreading is critical because it directly influences the efficiency and quality of the subsequent layer-by-layer material deposition. The powder spreading mechanism plays a pivotal role in determining the initial conditions of the powder bed before laser sintering, with studies emphasizing the importance of optimizing this phase to minimize inconsistencies in the solid volume fraction and improve part quality [4]. While increasing the spreading speed can enhance temporal efficiency and shorten production cycles, it can also significantly affect cavity formation and lower packing density during the spreading process [5–9]. High spreading speeds often lead to non-uniform powder distribution, reduced packing density, and heightened surface roughness. These effects arise from insufficient time for powder particles to settle and reorganize, resulting in a turbulent flow and uneven layering [10–12]. So, High-speed powder spreading in Laser Powder Bed Fusion presents unique challenges in achieving uniformity and optimal packing density.

After spreading, cavities in the powder layer influence additive manufacturing parts' quality by affecting density variations, mechanical properties, dimensional accuracy, surface roughness, and thermal conductivity. Non-uniform packing density caused by cavities leads to uneven melting and density variations, weakening the structure and increasing susceptibility to cracks [13,14]. Cavities also contribute to porosity, weak interlayer bonding, and defects like keyholing and lack of fusion in metal additive manufacturing [15–18]. Mechanically, they reduce tensile strength and fatigue resistance by acting as stress concentrators [19]. Furthermore, the significant variations in layer thickness caused by cavity formation lead to dimensional inaccuracies and increased surface roughness, especially in precision applications [20,21]. Cavities cause residual stresses and warping by disrupting heat transfer. The printing process in laser powder bed fusion and the quality of printed parts are affected significantly by cavities formed during the phase of powder spreading. Poor powder flow leads to uneven distribution and density of the powder bed, creating surface roughness, voids, and ultimately weak bonding between layers, compromising the final product's mechanical properties and structural integrity[4,22].

Many strategies, like powder characteristics and spreading techniques, can be used to avoid cavity formation and its effects. Optimizing powder characteristics, such as ensuring a narrow particle size distribution and enhancing powder flowability, can significantly improve layer uniformity[23,24]. Integration vibration with spreader dynamics represents a good strategy for reducing cavity formation[25]. Roller-based systems, called roller-spreading [5,8,26], which employ a rotating roller to spread the powder instead of the blade, like in blade-spreading, can improve powder spreading uniformity.

The interplay between spreading speed and roller configuration significantly influences roller-based spreading systems' performance. Increasing the spreading speed generally decreases packing density and layer thickness due to higher momentum transfer, which drags powder particles off the build plate [6,10,27]. For non-rotating and counter-rotating rollers, the effects of spreading speed are pronounced, with the counter-rotating roller amplifying the reduction in packing density and layer thickness as its rotational speed adds to the momentum transfer[27,28]. In contrast, forward-rotating rollers exhibit a distinct behaviour. At low rotational speeds (sub-rolling configuration), they mirror the effects of non-rotating rollers. Still, at higher clockwise rotational speeds (super-rolling configuration), a balance between circumferential and spreading speeds is achieved[27]. This balance mitigates the adverse effects of high spreading speeds by inducing a "powder burst" phenomenon that compensates for particle dragging. So, balancing between the roller's translational and rotational motions is essential to prevent cavities and maximize powder bed quality, which will be the main focus of the current research.

Numerical methods like the discrete element method (DEM) have provided insights into how variations in input parameters, such as powder particle size, spreading dynamics and shape, affect flowability and packing density, highlighting the direct correlation between spreading efficiency and quality of the final parts [29,30].

The present work addresses the challenges of high-speed powder spreading in the PBF-LP process. This study uses discrete element method (DEM) simulations to examine two high-speed scenarios (0.15 and 0.30 m/s). The research begins by exploring the effects of constant rotational speeds on cavity formation and systematically analyzing powder layer uniformity. Building on these findings, a group of variable rotational speed profiles is proposed to maximize packing density and minimize nonuniformity. This comprehensive investigation provides valuable guidance for optimizing powder spreading at high spreading speeds in PBF-LP processes. This work Methodically investigates balancing between rotational speed and spreading speed during powder distribution to avoid cavities and enhance the quality of the powder bed, offering new strategies for achieving consistent layer deposition and minimizing imperfections.

4.3. Methodology

The roller-spreading system used in the Laser Powder Bed Fusion consists of three main components: powder delivery, spreading (i.e., Roller), and collection, as illustrated in Figure 4-1. During the spreading operation, the Roller, with a radius of 2.5 mm, advances across the building plate at a designated spreading velocity (V_s) while simultaneously rotating at a specified rotational speed (ω). This coordinated motion facilitates the uniform distribution of 112.32 mg of stainless steel 316 (SS316) powder, creating a powder layer with a thickness (δ) of 200 μm.

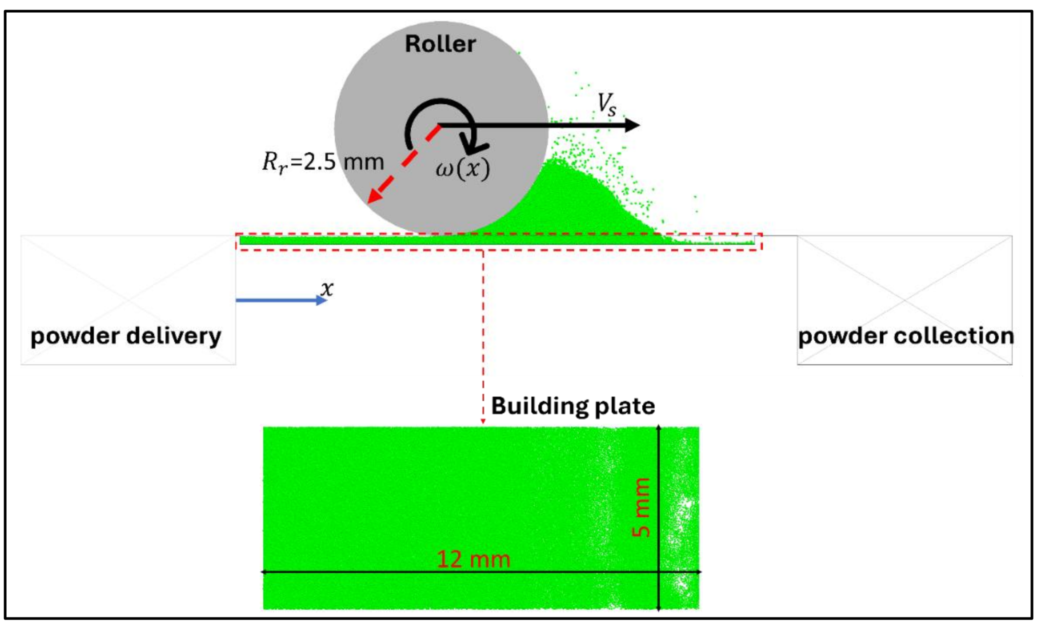

Figure 4-1. DEM model of roller-spreading technique used in PBF-LP

4.3.1. Mathematical and numerical model

The discrete element method (DEM) is used to effectively predict the distribution of powder particles during the spreading process. DEM operates by solving Newton's equations [31,32]of motion to evaluate particle dynamics, with translational motion governed by Equation (1) and rotational motion by Equation (2). These equations are integrated over time to determine the speed and position of each particle.

$$m_i \frac{dv_i}{dt} = m_i g + F_n + F_t \tag{1}$$

$$I_i \frac{d\omega_i}{dt} = \tau_s + \tau_r \tag{2}$$

where m_i, v_i, ω_i and I_i are the mass, velocity, angular velocity, and moment of inertia of particle i, respectively; F_n and F_t are the normal and tangential interaction forces on a particle i due to other particles j. τ_s and τ_r are the torques generated by tangential force and rolling friction. The kinematics of all particles are updated by the time integration of the previous equations [33]. The forces between particles include the impact of van der Waals interactions, modelled using the Hertz-Mindlin contact theory [34] with Johnson-Kendall-Roberts (JKR) cohesion[35].

As detailed in our previous work[27], the interactions between powder particles are modelled by incorporating contact, friction, and cohesion forces. Altair EDEM software (version 2021.1) is utilized for these simulations. [36]. Careful selection of the simulation time step is essential to maintain numerical stability and ensure convergence. A time step of $1.62949 \times 10^{-7} s$, representing 20% of the Rayleigh time, is adopted. This value balances accurately capturing dynamic behaviour and high-frequency phenomena while avoiding instability and computational inaccuracies. The computational grid is configured with a mesh size three times the radius of the smallest particle, ensuring precise particle contact detection. Consequently, the simulation domain comprises 4018008 cells.

This research utilized mono-sized stainless steel 316 powder (SS316), which was selected deliberately to reduce complexities associated with variations in particle size distribution. This simplification enables a more focused investigation of roller dynamics' effects. The physical and material properties of SS316, essential for the discrete element method (DEM) simulations, are listed comprehensively in Table 4-1. The surface energy of SS316 was established through detailed material characterization involving static and dynamic angle of repose measurements, as outlined in prior studies [27].

Table 4-1. Process parameters and properties used in the simulations

Parameter	Value	ref
Poisson's ratio,ν	0.3	[6,37]
bulk density, ρ	7800 kg/m^3	
Young's modulus, E	2.2e+8 pa	
Coefficient of restitution, e	0.64	
Coefficient of sliding friction,μ_s	0.6	
Coefficient of rolling friction, μ_r	0.085	
Surface energy, γ	0.001 J/m^2	[27]

A mono-sized stainless steel 316 (SS316) powder with a particle diameter of 50 µm was chosen, ensuring a particle size-to-layer thickness ratio of 0.25. This specific selection streamlined the modelling process and supported numerical stability. This deliberate choice allows for isolating the effects of roller dynamics while minimizing the impact of size variability. By employing a controlled environment with mono-sized particles, the analysis focuses on the influence of roller dynamics without the added challenges of polydisperse powders. The 0.25 ratio represents realistic powder dimensions [38], promotes effective packing, reduces wall-induced disturbances, and ensures a clear and focused investigation of the powder spreading dynamics. This setup simplifies the study while maintaining fidelity to practical scenarios.

4.3.2. Parameters of powder layer evaluation

The evaluation of powder layer quality relies on two primary parameters: packing density and layer thickness. The **packing density** (ρ_P) is defined as the ratio of the particle-occupied volume to the total volume of the specified spatial configuration. The cuboid volume, representing the spatial configuration, is derived based on the target layer thickness. The building plate is segmented along the x-axis, and local densities are calculated within each segment to investigate variations in packing density. The uniformity of the bed structure is assessed through the normalized variance of packing density ($\rho_{P,VC}$) across the entire bed.

The **local powder layer thickness** ($\delta(x)$) is computed as the average of the maximum particle elevations in each x-direction segment of the building plate. The global or **actual layer thickness** (δ_{act}) is the overall average of these local thickness values. To characterize the surface texture of the powder bed, the **surface roughness** (Ra) is used and can be determined using the centerline average method, capturing the surface profile's deviation along the building plate's length. Based on these parameters, the comprehensive analysis of the results ensures an accurate assessment of the powder layer's structural and surface properties, which are critical for achieving high-quality manufacturing processes.

4.3.3. Simulation setup

The simulation setup examines the rotational speed variation in the roller-spreading process in PBF-LP to eliminate cavities associated with high spreading speeds. Two spreading velocities, 0.15 m/s and 0.3 m/s, were selected to represent a high spreading speed scenario while utilizing a Roller with a radius of 2.5 mm. The study is conducted in two phases, with the initial phase investigating the effects of constant rotational speeds. Three roller configurations are explored: counterclockwise rotation, non-rotating translation, and clockwise rotation. The clockwise case is further subdivided into three categories based on the rotational speed to rolling rotational speed (ω_o) ratio with , where $\omega_o = V_s/R_r$. These categories include sub-rolling ($\omega < \omega_o$), rolling ($\omega = \omega_o$), and super-rolling ($\omega > \omega_o$). This phase aims to analyze the influence of each configuration on cavity formation during spreading and to identify the most favourable conditions for achieving uniform powder distribution. Following the insights gained from the constant speed analysis, the second phase explores six profiles (will be described in 4.4.2) of variable rotational speed. These profiles are designed to maximize packing density and minimize nonuniformity in the powder layer.

4.4. Results

The results section explores the impact of roller rotational speed variations on powder layer quality in PBF-LP under high spreading speeds. In the first phase, we analyze the effects of constant rotational speeds across different roller configurations on cavity formation and powder distribution. The second phase introduces variable speed profiles based on insights gained from the first phase and examines them to enhance packing density and uniformity. Key metrics such as cavity formation, packing density, and layer uniformity guide the identification of optimal spreading conditions, offering valuable insights for efficient powder spreading at high speeds.

4.4.1. Assessment of constant rotational speed's integration speed with high spreading speed

To establish a foundational understanding, we begin with the non-rotating roller configuration. In this base case, the roller moves at a set spreading speed without any rotational motion, providing a clear benchmark for evaluating the effect of rotational speed. DEM simulations of two high spreading speeds of non-rotating rollers, which are 0.15 m/s and 0.3 m/s, are conducted to address how high spreading speeds affect the quality of powder layers in the case of roller-spreading. The roller imparts significant momentum to the powder particles, causing them to shift away from the left edge of the building plate. This movement results in decreased packing density at the starting edge while packing density gradually increases and fluctuates around an average value as the roller moves along the plate, as shown in Figure 4-2 and Figure 4-3. At the higher spreading speed of 0.3 m/s, the roller exerts even more force on the powder, leading to a continuous and large cavity on the left side of the building plate, as illustrated in Figure 4-4a. As the roller transitions to the right side, it drives the powder against the solid edge at high speed, which creates an impact that reflects the powder flow direction to the backward direction. This reflection causes a localized powder accumulation, resulting in high packing density near the right edge and a sharp decline shortly after. This behaviour is also reflected in the layer thickness: it remains low on the left side, gradually increases to an average level (though still below the desired thickness), fluctuates around this mean, peaks near the right edge, and then experiences an abrupt drop. These observations underscore the challenges of uneven layer distribution at high spreading speeds.

Building on the insights from the non-rotating roller, we introduce the effect of counterclockwise rotational speed with the roller (i.e., counter-rotating roller). In this configuration, the roller rotates counterclockwise with rolling rotational speed (ω_o), where the roller moves forward along the x-axis. As a result of the combined effects of forward translation and rotational motion ($V_{roller\ bottom} = V_s + \omega_o R_r$) The roller exerts a more forward force on the powder particles directly beneath the roller, driving them toward its spreading direction. The roller applies a more pronounced forward force on the powder particles directly beneath it. This force propels the particles toward the roller's motion, enhancing their alignment and distribution along the intended spreading path. This forward momentum transfer helps to spread the powder more evenly along the x-axis, filling gaps efficiently and potentially enhancing packing density distribution. However, the average packing density remains slightly lower than in the non-rotating case, as shown in Figure 4-2 and Figure 4-3. As the roller rotates counterclockwise while advancing along the positive x-axis, its motion induces a force component in the y-direction. On the left side of the roller (facing the -y direction), particles are pushed downward and slightly backward; on the right side (facing the +y direction), particles are moved upward and slightly forward. This lateral redistribution of forces helps evenly spread the powder, minimizing the formation of large cavities and creating small, uniformly distributed voids across the building plate. This behaviour contrasts sharply with the non-rotating roller, which typically results in a single large cavity on the left side of the plate due to the lack of rotational redistribution.

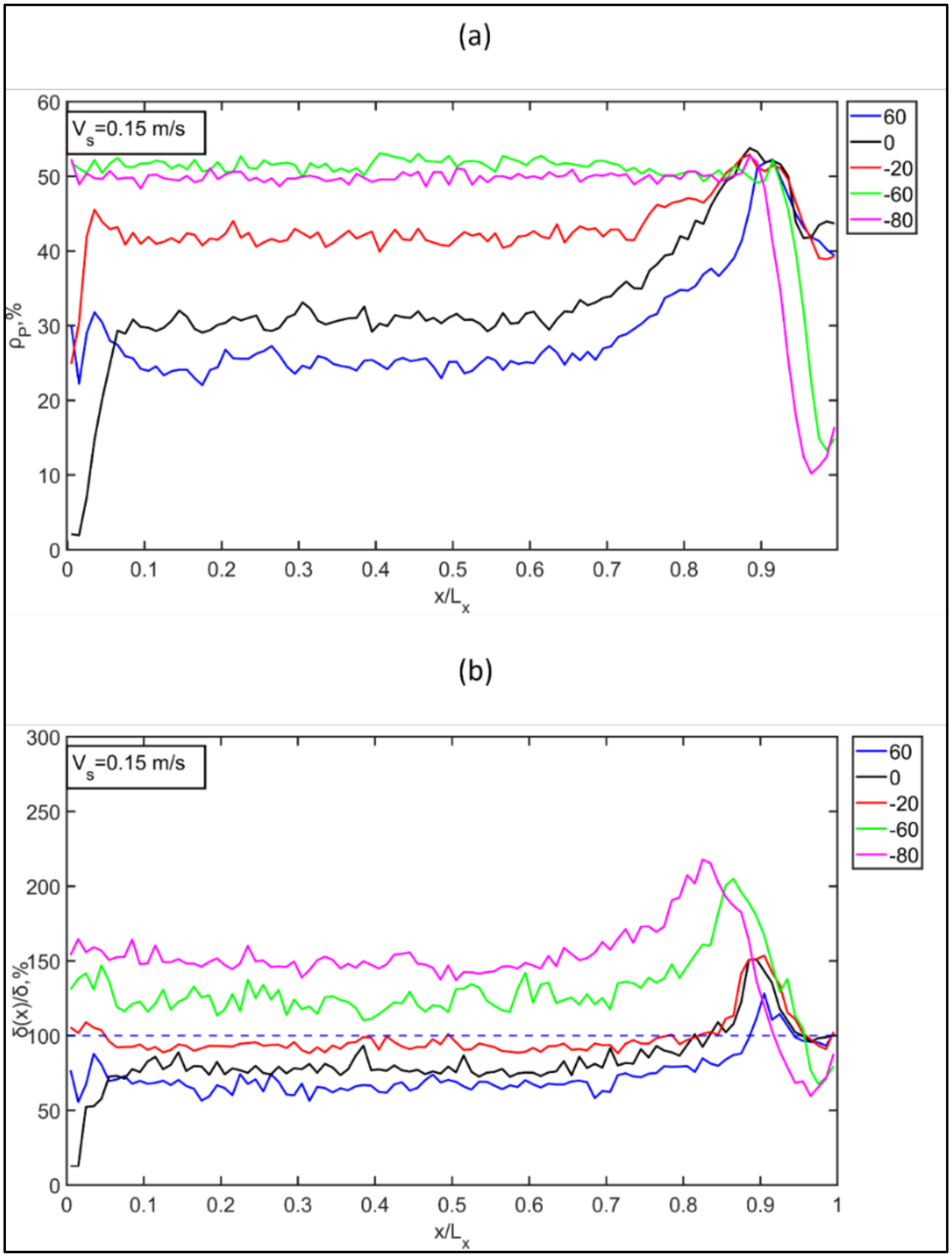

Figure 4-2. Characteristics of the powder layer developed by roller moves at 0.15 m/s versus the building plate length at different constant rotational speeds: (a) packing density and (b) layer thickness.

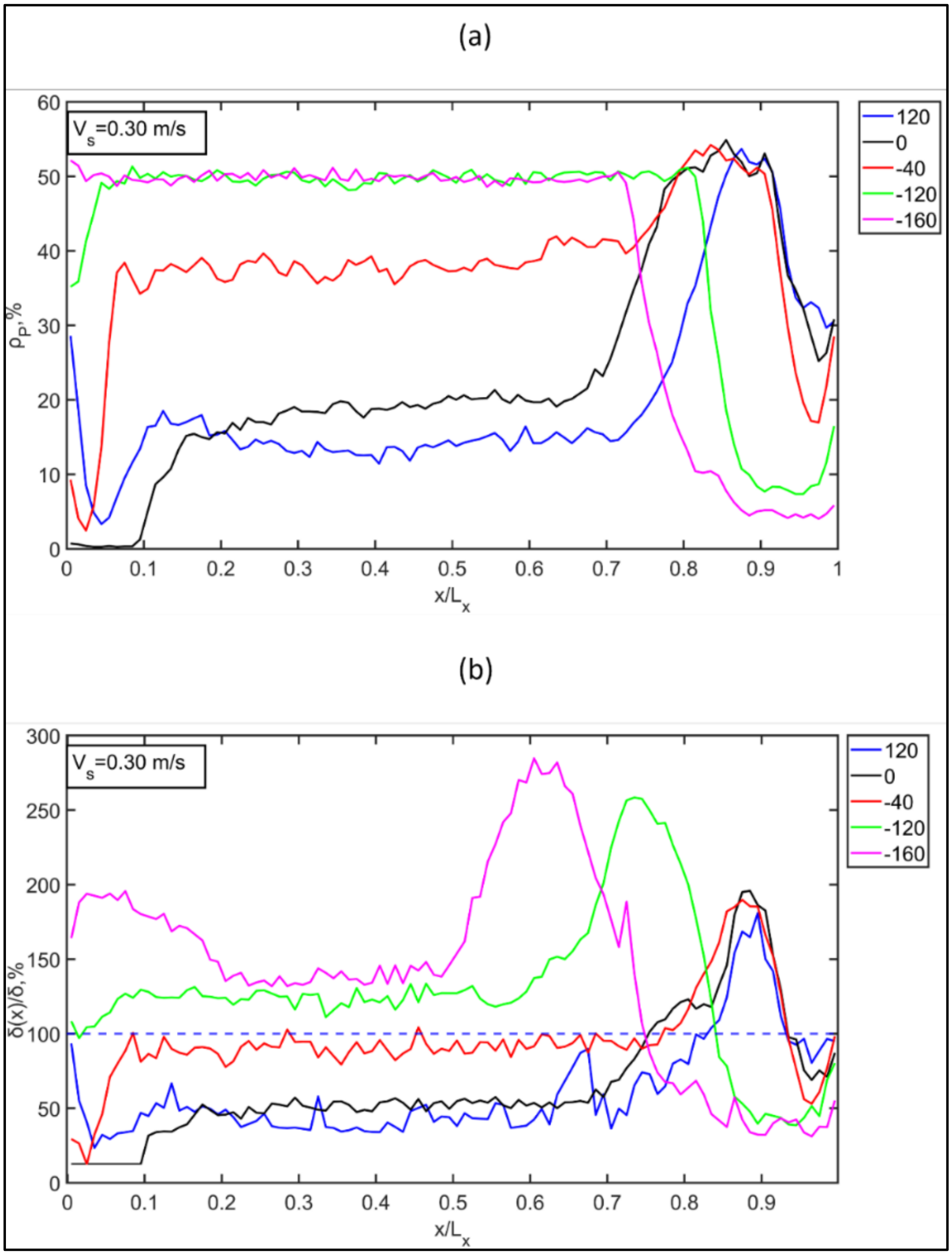

Figure 4-3. Characteristics of the powder layer developed by roller moves at 0.30 m/s versus the building plate length at different constant rotational speeds: (a) packing density and (b) layer thickness.

The decreased packing density with the counter-rotating roller is due to these small void formations. At the same time, the increase in uniformity results from enhanced shear forces applied by the roller's bottom surface. However, at a high spreading speed (e.g., 0.3 m/s), the impact of the spreading speed becomes more dominant than the rotational speed. As a result, a large, continuous cavity forms on the left side, as shown in Figure 4-4b, slightly improving overall uniformity.

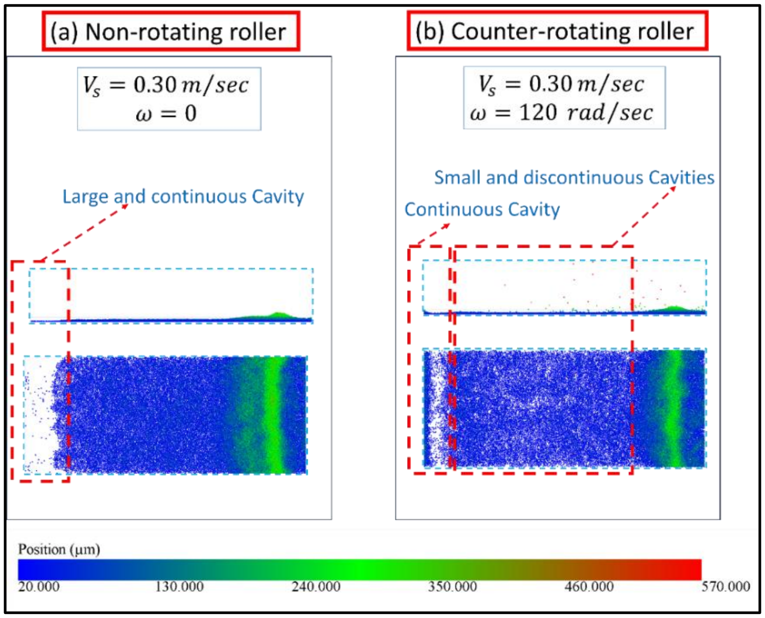

Figure 4-4. The powder bed's top and front views are coloured by the powder position in the Z-direction (i.e., layer thickness) after spreading at a speed of 0.30 m/s; (a) non-rotating roller (i.e., $\omega = 0$);(b) counter-rotating roller (i.e. $\omega = 120 = V_s/R_r$)

Moving beyond the counter-rotation configuration, we examine the forward-rotating roller setup, in which the roller rotates clockwise while moving forward along the x-axis. In this configuration, the speed of the roller's bottom surface is determined by the difference between the spreading speed and the roller's circumferential speed ($V_{roller\ bottom} = V_s - \omega R_r$). This speed can be positive (i.e., sub-rolling), zero (i.e., rolling), or negative (i.e., super-rolling), depending on the rotational speed of the roller. In the "sub-rolling" configuration, the roller rotates at a speed lower than the rolling speed (i.e., $\omega < \omega_o$). In this case, the speed of the bottom surface aligns with the spreading direction but at a reduced rate. This decrease in speed influences the powder distribution pattern.

Specifically, the continuous cavity observed on the left side of the building plate, which is prominent in the non-rotating roller scenario, diminishes and becomes smaller as the clockwise rotational speed combines with the spreading motion, as shown in Figure 4-5a. This cavity reduction occurs because the circumferential speed component in the negative x-direction counteracts the forward force applied by the spreading motion, slightly pushing the powder backward to fill the cavity partially.

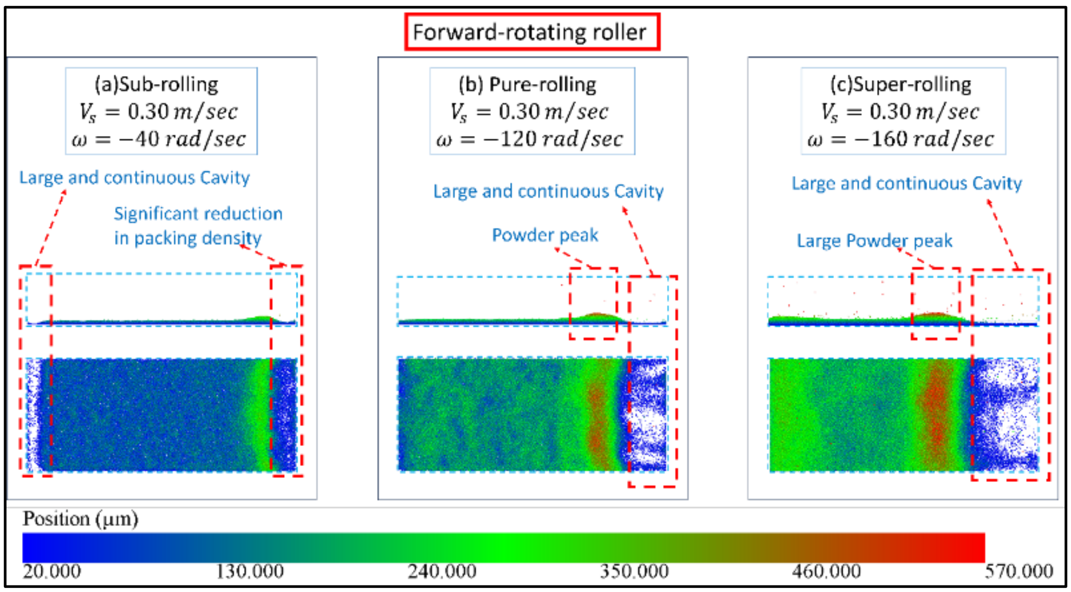

Figure 4-5. The powder bed's top and front views are coloured by the powder position in the Z-direction (i.e., layer thickness) after spreading at a speed of 0.30 m/s; (a) sub-rolling (i.e., ω=-40 rad/s);(b) rolling (i.e., ω=-120 rad/s);(c) super-rolling (i.e., ω=-160 rad/s)

Continuing along the spectrum, we examine the rolling configuration, where the roller's rotational speed is fully synchronized with its forward movement (i.e., $\omega = \omega_o$). The cavity at the left side formed by a non-rotating roller and a sub-rolling roller is filled with powder, achieving higher and uniform packing density due to increases in clockwise rotational speed, which increases the force that pulls powder in the backward direction. Due to the interaction between the powder particles and the roller's right edge, combined with the high clockwise rotational speed that pulls the powder backward, a significant peak of powder forms on the right half of the building plate. This accumulation is followed by discontinuous cavities concentrated along the right edge, as shown in Figure 4-5b. These effects collectively lead to an increase in packing density and nonuniformity across the powder layer, impacting the overall quality of the spread.

To complete the analysis, we examine the super-rolling configuration, in which the roller rotates at a speed that exceeds the rolling one (i.e., $\omega > \omega_o$). At this elevated rotational speed, the speed of the roller's bottom surface reverses direction to negative x-direction. This reversal creates a pronounced backward pull on the powder particles, leading to a significant powder accumulation along the building plate. The dominance of the clockwise rotational speed over the forward spreading velocity enhances this effect, causing substantial amounts of powder to shift backward. As a result, a large, continuous cavity forms along the right edge of the building plate, as illustrated in Figure 4-5c, disrupting the uniformity and compactness of the powder layer.

Throughout the configurations tested from non-rotating to super-rolling rollers, each rotational speed improves packing density and layer uniformity but leads to cavity formation in specific areas of the building plate. For instance, the non-rotating, counter-rotating, and sub-rolling rollers create cavities on the left side of the building plate, while the rolling and super-rolling rollers produce cavities on the right side. Furthermore, at high spreading speeds, all roller configurations tend to generate a powder peak just before reaching the building plate's right edge due to the impact of the powder on the right edge. These findings suggest that a constant rotational speed, regardless of its direction or intensity, still needs to fully resolve the challenges associated with high spreading speed.

Therefore, we propose a variable rotational speed strategy adjusted based on constant rotational speed analysis, enabling greater control over powder flow and deposition. This strategy provides a level of control previously unattainable, instilling confidence in its potential to address the challenges of high spreading speed.

4.4.2. Assessment of variable rotational speed with high spreading speed

An adaptive approach of variable rotational speed is used to restore the reduction in packing density due to high spreading speed and address the issue of cavity formation. The proposed profiles were designed to begin with a clockwise rotational speed, reducing the likelihood of cavities forming on the left side of the building plate. The rotational speed then transitions towards zero or a counterclockwise direction as the roller reaches the right side, helping to prevent cavity formation in that area. This systematic variation in rotational direction and intensity across the roller's path is intended to create a more uniform powder distribution and enhance layer consistency.

In Figure 4-6, six profiles illustrate various approaches to implementing the adaptive rotational speed strategy, each offering a unique level of control over the roller's speed along its path. Profile A features a single-step transition, starting with a clockwise rotational speed at ω_o during the first half of the path. This is followed by a switch to a counterclockwise speed at ω_o for the second half. This basic configuration effectively addresses cavity formation on both sides of the building plate. Next, profile B introduces two intermediate steps, transitioning from a clockwise speed at ω_o to zero to a counterclockwise speed at ω_o in three segments. This segmentation facilitates a smoother transition, allowing for more gradual control over powder spreading. Subsequent refinements in Profiles C, D, E, and F introduce a more sophisticated approach by employing multiple smaller rotational speed increments. Profile C transitions progressively from a clockwise rotational speed equal to ω_o to a counterclockwise rotational speed of ω_o. In contrast, Profile D modifies the final step by replacing it with a zero rotational speed, eliminating any counterclockwise rotation. Profile E adopts a more gradual transition, starting with a clockwise rotational speed of less than ω_o and smoothly reducing it to zero. Finally, Profile F begins with a clockwise rotational speed greater than ω_o and systematically decreases to zero, representing the most dynamic configuration among the profiles. These additional steps provide finer control and allow for more continuous rotational adjustments. Through these increasing levels of segmentation, each profile demonstrates a more refined strategy for adjusting rotational speed to enhance powder flow and deposition quality, effectively addressing the associated with high-speed powder spreading.

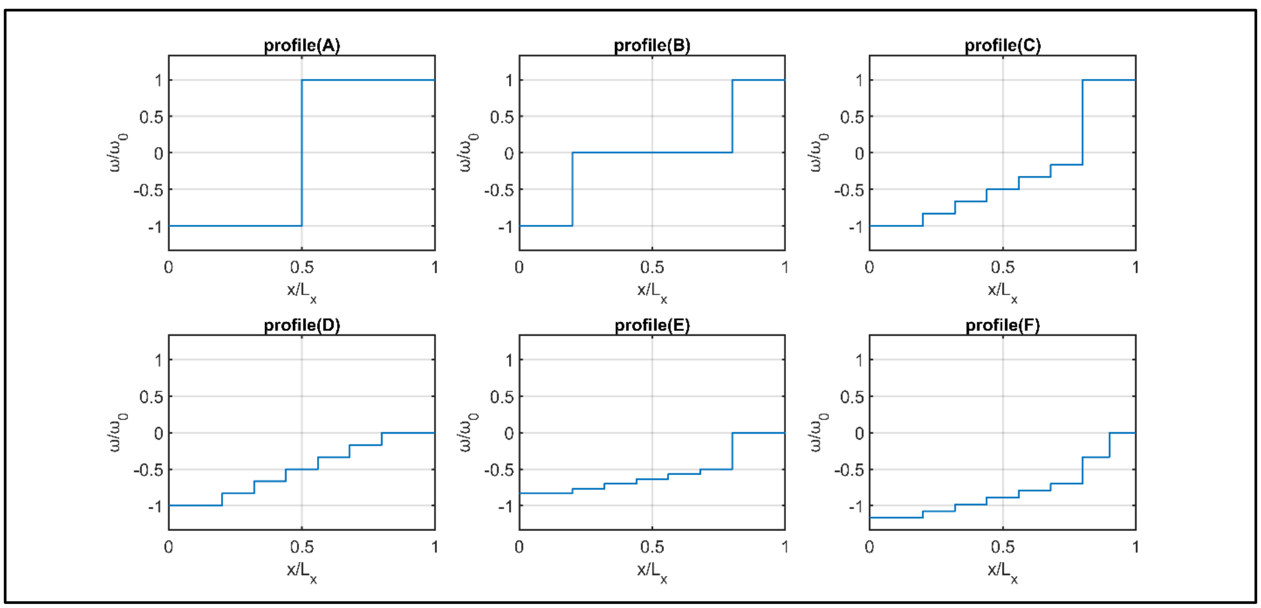

Figure 4-6.Representation of six Rotational Speed Profiles (A - F) Used in the Current Work

4.4.2.1. Profile (A)

Profile A's rotational speed configuration strategy employs a single-step transition, with the roller initially rotating clockwise at rotational speed ω_o before switching to counterclockwise rotation at ω_o along the right half of the building plate. Profile A presents an opportunity to explore the intricate relationship between rotational motion direction and powder dynamics, particularly under high spreading speeds of 0.15 m/s and 0.3 m/s. This rotational strategy provides a foundation for understanding how variations in rotational speed influence powder distribution during high spreading speed and can be considered a baseline approach.

Figure 4-7a demonstrates distinct patterns of packing density of the powder layer at spreading speeds of 0.15 m/s and 0.3 m/s along the length of the building plate. In the initial region, spanning from the left edge to $x/L_x = 0.1$, The packing density shows a progressive increase, reaching a stable value. This is followed by a stable region extending from $x/L_x = 0.1$ to $x/L_x = 0.45$, where the packing density stabilizes at a relatively high and consistent value. Notably, at a spreading speed of 0.30 m/s, the packing density within this stable region reaches approximately 50%. This stability can be attributed to the clockwise rotational speed, which facilitates powder accumulation by inducing a backward motion of the powder. This backward motion effectively compensates for the reduction in powder availability caused by the high spreading speed. As the roller advances from $x/L_x = 0.5$ to 0.75, a sharp decline in packing density is observed, followed by a stabilization region. This decrease is particularly pronounced at the higher spreading speed of 0.30 m/s, where the packing density drops to approximately 8%. Notably, this spreading speed forms small, discontinuous voids near the center that extend toward the right side, as depicted in Figure 4-7c&d. This behaviour is primarily attributed to the roller's switch from a rotational direction to counterclockwise, which generates a forward force on the powder. The increased speed of the roller's bottom surface is approximately equal to $V_s + \omega_o R_r$, amplifies this forward motion, pushing excess powder out of the building plate. Consequently, the combination of high spreading speed and counterclockwise rotation depletes powder in these regions, leading to the observed cavities and reduced uniformity. The heightened velocity of powder near the right edge (starting from $x/L_x = 0.8$) causes particles to strike the solid edge with significant force, altering their trajectories and leading to rebound effects. As a result, a substantial accumulation of powder occurs in this region, increasing the packing density to 52% at a spreading speed of 0.3 m/s. Beyond this localized accumulation, the density sharply drops to 28%, creating an uneven distribution. Additionally, the impact disperses powder backward, contributing further to the irregularity along the edge.

The variation in layer thickness along the building plate length mirrors the trends in packing density, as shown in Figure 4-7b. On the left half of the building plate, the layer thickness increases and stabilizes, fluctuating around 127% of the intended value at a spreading speed of 0.3 m/s. This results in a relatively consistent yet overfilled condition in this region. As the roller transitions to counterclockwise rotation, the layer thickness experiences a sharp decline, stabilizing around 36% of the desired value at a spreading speed of 0.3 m/s. Near the right edge, the layer thickness trends mirror the packing density behaviour, initially increasing before dropping sharply. This drop is caused by the high-speed impact of powder particles against the solid boundary, disrupting the uniform distribution.

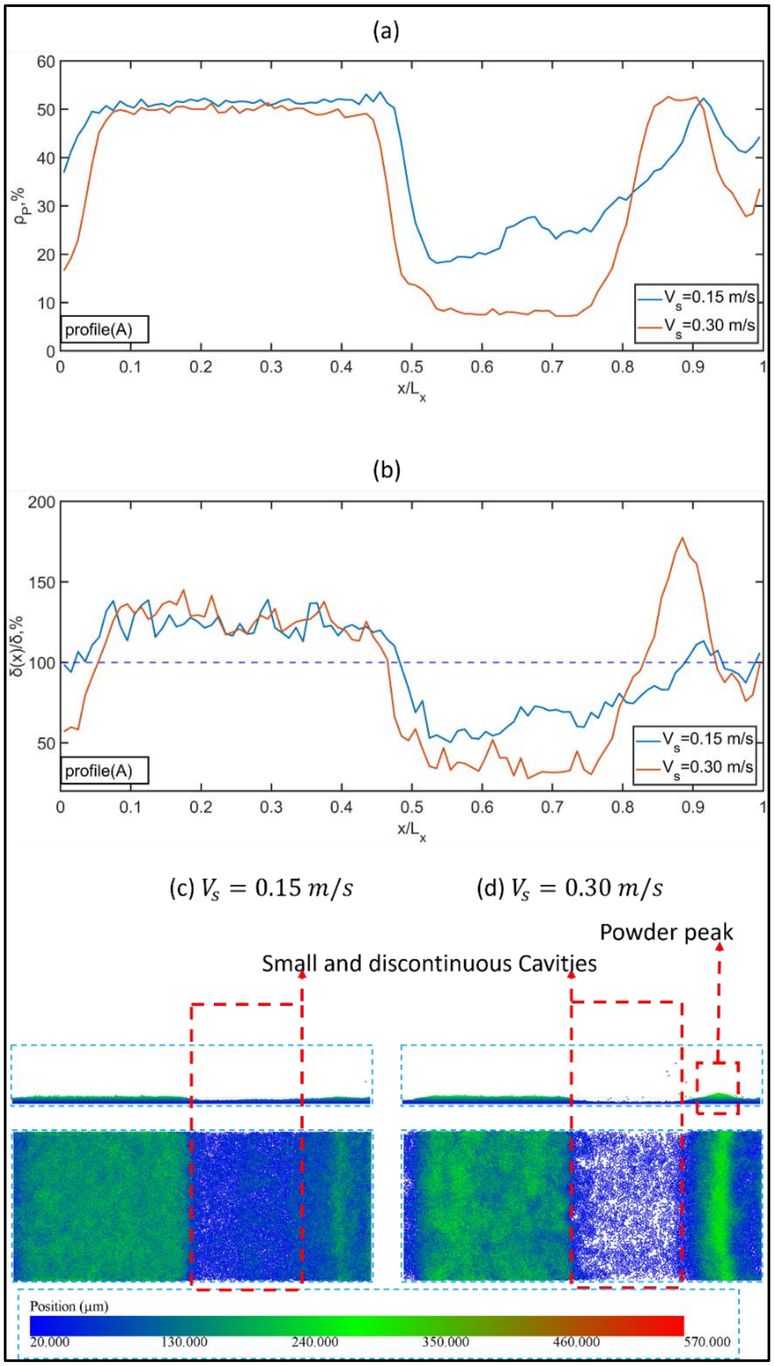

Figure 4-7.Powder layer characteristics of roller-spreading rotating under **profile A** and moving forward with 0.15 and 0.30 m/s versus the building plate length. (a) Packing density, (b) layer thickness, and (c) top view and front view of the powder bed after spreading with the speed of 0.15 m/s. (d) The top and front views of the powder bed after spreading at a speed of 0.30 m/s; coloured by the powder position in the Z-direction (i.e., layer thickness).

In summary, Profile A demonstrates that clockwise rotational speed effectively achieves high and stable packing density and layer thickness in the first half of the building plate.

However, the single-step transition to counterclockwise rotation fails to maintain similar control on the right side. This underscores the need for more sophisticated rotational strategies to address the limitations of Profile A, particularly in regions influenced by counterclockwise rotation.

4.4.2.2. Profile (B)

Building on the findings from Profile A, Profile B introduces a more segmented rotational speed configuration to refine powder distribution. Under rotational speed profile B, the packing density along the building plate exhibits a distinct trend, as illustrated in Figure 4-7a. From the left edge to $x/L_x = 0.05$, the packing density increases and reaches 48% at a spreading speed of 0.3 m/s. Beyond this point, the density stabilizes with minor fluctuations between $x/L_x = 0.05$ and $x/L_x = 0.15$. The roller's clockwise rotation at ω_o drives this progression and stability, which induces a backward flow of powder. This mechanism counteracts the high spreading speed by ensuring adequate powder accumulation, thereby maintaining a dense and consistent layer along the region between $x/L_x = 0.05$ and $x/L_x = 0.15$. As the roller transitions to a non-rotating state in the middle section, the packing density drops and stabilizes at 17.2% at a spreading speed of 0.3 m/s from $x/L_x = 0.2$ to $x/L_x = 0.7$. In this region, high spreading speeds and the absence of roller rotation contribute to the formation of tiny voids, particularly under high spreading speeds. This reduction is less pronounced than in Profile A, as the absence of counterclockwise rotation minimizes the forward displacement of powder. As a result, more material remains within the building plate, reducing significant cavity formation and contributing to a more uniform distribution in this region. It is observed that switching the rotational speed from clockwise to zero and subsequently to counterclockwise creates powder peaks near the boundaries, as presented in Figure 4-7c&d. In the final segment, extending from $x/L_x = 0.7$ to the right edge, the packing density shows significant fluctuations. This variability is attributed to the introduction of counterclockwise roller rotation, which increases the velocity of the powder. The high-speed impact with the right edge alters the motion of the powder, causing localized accumulation and sharp changes in packing density. This abrupt powder motion near the right edge exacerbates the fluctuations, driven by the interaction of rotational and translational forces at high speeds.

The variation in layer thickness along the building plate, as illustrated in Figure 4-7b, closely parallels the observed trends in packing density. In the initial region, extending from the left edge to $x/L_x = 0.2$, the layer thickness progressively increases, peaking at 136% of the desired thickness at a spreading speed of 0.3 m/s. This overfilled condition arises due to powder accumulation facilitated by the backward motion of powder induced by the roller's clockwise rotation. Following this peak, the layer thickness gradually decreases as the roller transitions from a clockwise rotation to a non-rotating state. It stabilizes at 46% of the desired thickness between $x/L_x = 0.2$ and $x/L_x = 0.7$. this reduction reflects the high spreading speed's role in limiting powder retention without rotational motion, emphasizing the direct influence of spreading velocity on layer thickness. In the final region, significant fluctuations in layer thickness emerge as counterclockwise roller rotation is introduced. This shift amplifies the effects of spreading speed, causing powder particles to impact the solid edge with increased velocity. The resulting change in particle direction contributes to localized over-accumulation, reaching 158% of the desired layer thickness, accompanied by pronounced variability.

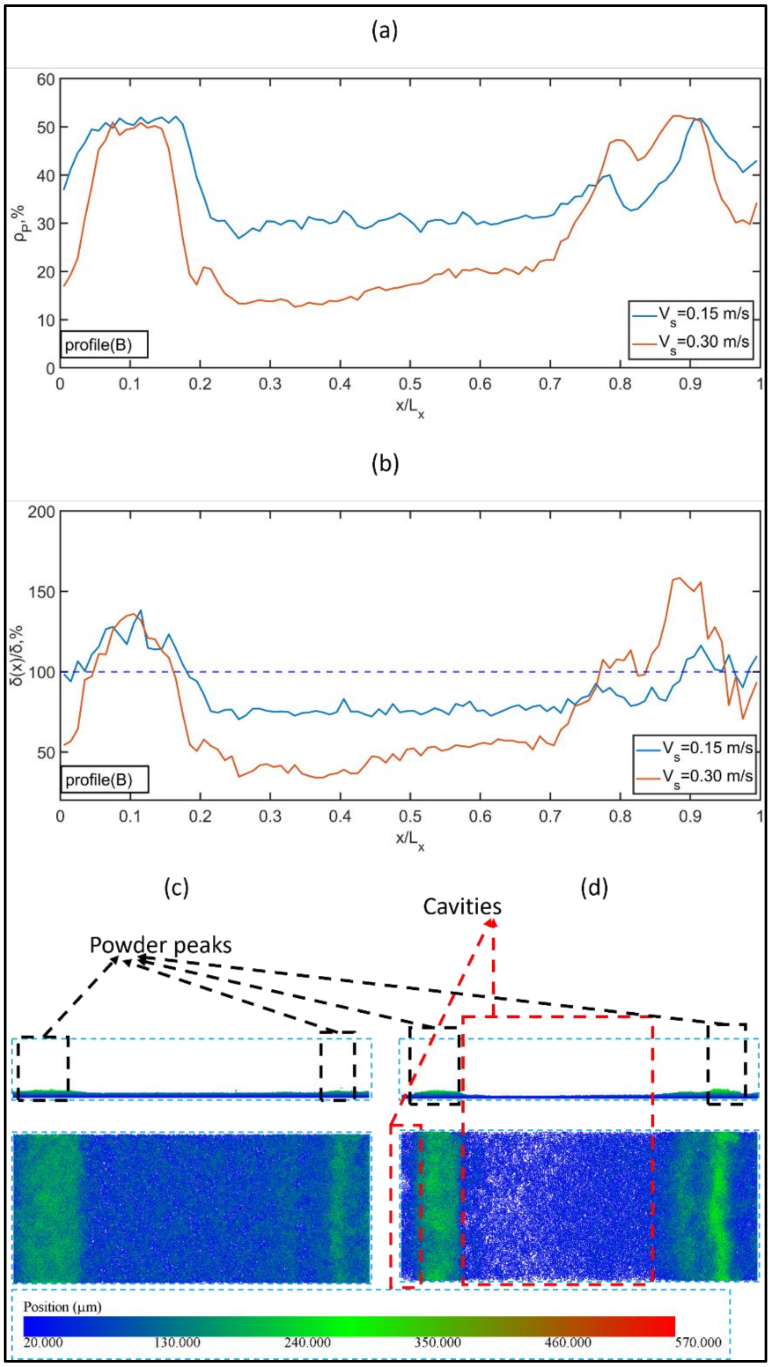

Figure 4-8.Powder layer characteristics of roller-spreading rotating under **profile B** and moving forward with 0.15 and 0.30 m/s versus the building plate length. (a) Packing density, (b) layer thickness, and (c) top view and front view of the powder bed after spreading with the speed of 0.15 m/s. (d) The top and front views of the powder bed after spreading at a speed of 0.30 m/s; coloured by the powder position in the Z-direction (i.e., layer thickness).

In summary, Profile B demonstrates a significant improvement in powder distribution and layer thickness uniformity across the region between $x/L_x = 0.2$ and $x/L_x = 0.7$, when compared to Profile A. However, Profile B exhibits lower layer thickness and packing density than Profile A. Additionally, challenges remain in achieving consistent uniformity near the solid edges of the plate.

4.4.2.3. Profile (C)

Profile C enhances system adaptability by implementing finer increments within the rotational speed configuration. The roller undergoes a gradual transition, commencing with a clockwise rotation at ω_o, which progressively decreases in magnitude to $1/6\,\omega_o$ at $x/L_x = 0.8$. Beyond this point, the rotation reverses to counterclockwise at ω_o. These refined adjustments enable smoother and more precise control of the system, significantly enhancing the uniformity of packing density across most of the building plate.

Figure 4-9a demonstrates the variation in packing density across the building plate under Profile C, revealing four distinct regions: the initial, stable, transition, and impact regions. In the initial region, spanning from the left edge to $x/L_x = 0.1$, the packing density steadily increases to approximately 50% at a spreading speed of 0.30 m/s. This indicates effective powder accumulation at the beginning of the spreading process. However, small and discontinuous cavities are observed near the left boundary, especially at the higher spreading speed of 0.30 m/s, as shown in Figure 4-9c &d. These cavities result from the insufficient backward force generated by the clockwise roller motion, which is too slow to compensate for cavity formation fully. In the stable region (from $x/L_x = 0.1$ to $x/L_x = 0.75$), the packing density slightly stabilizes around 42%, despite fluctuations.

This stability suggests consistent powder distribution during this phase. The slight decrease in packing density within this region is attributed to the gradual reduction in the roller's clockwise rotational speed, which diminishes the backward force acting on the powder and reduces powder accumulation behind the roller. The transition region, beginning at $x/L_x = 0.8$, is characterized by a notable 26% reduction in packing density at a spreading speed of 0.30 m/s. This reduction arises from reversing the roller's rotational direction counterclockwise, eliminating the backward force and increasing the forward force, pushing the powder away. Finally, in the impact region, significant fluctuations in packing density are observed, ranging from 23% to 52%. These considerable variations are attributed to boundary effects, where high-speed impacts between the powder and the solid edge induce localized powder reorganization. This behaviour aligns with trends observed in Profiles A and B, highlighting the influence of boundary dynamics on packing density in this region.

Figure 4-9b illustrates the layer thickness variation across the building plate under Profile C, exhibiting trends similar to the packing density distribution. In the initial region, from the left edge to $x/L_x = 0.1$, the layer thickness increases significantly, reaching 133% of the desired layer thickness at a spreading speed of 0.30 m/s. This increase indicates substantial powder accumulation at the start of the spreading process due to the high clockwise rotational speed. In the stable region spanning $x/L_x = 0.1$ to $x/L_x = 0.75$, the layer thickness stabilizes around 99% of the desired value, with minor fluctuations. This stabilization suggests sufficient and consistent powder packing facilitated by the clockwise rotational speed of the roller, which effectively distributes the powder across the building plate.

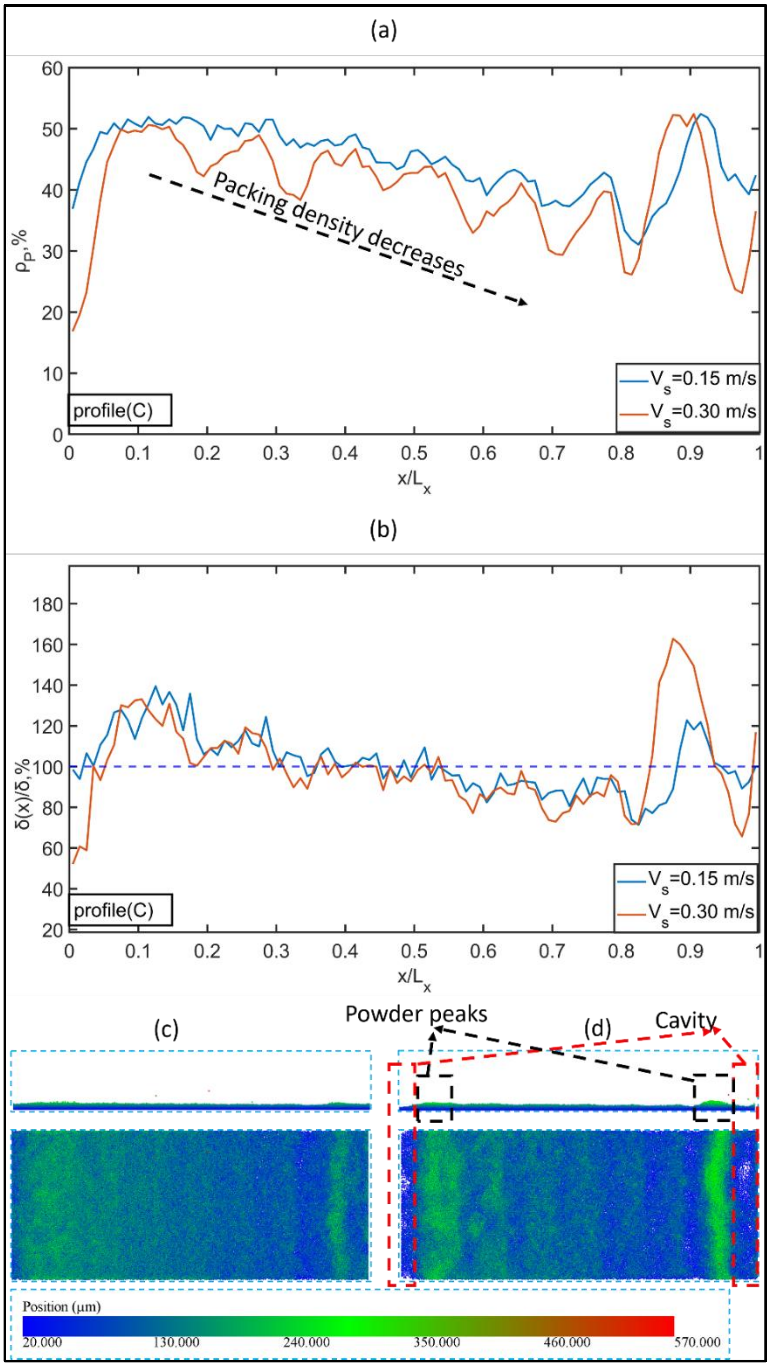

Figure 4-9. Powder layer characteristics of roller-spreading rotating under **profile C** and moving forward with 0.15 and 0.30 m/s versus the building plate length. (a) Packing density, (b) layer thickness, and (c) top view and front view of the powder bed after spreading with the speed of 0.15 m/s. (d) The top and front views of the powder bed after spreading at a speed of 0.30 m/s; coloured by the powder position in the Z-direction (i.e., layer thickness).

At $x/L_x = 0.8$, marking the transition region, the layer thickness decreases to 72% of the desired value at a spreading speed of 0.30 m/s. This reduction is attributed to the change in the roller's rotational direction to counterclockwise, eliminating the backward force and increasing the forward force, pushing the powder away and reducing the deposited layer thickness. In the impact region, pronounced variations in layer thickness are observed, ranging from 66% to 163% of the desired value. These fluctuations result from the high-speed impact of powder with the right edge of the building plate and the sudden change in powder motion direction, which facilitates localized powder reorganization.

Profile C improves how the system adapts and controls powder by making smooth, gradual adjustments to the rotating speed. It starts with a gentle decrease in clockwise motion before switching to counterclockwise. This approach makes a noticeable difference in packing density and helps keep layer thickness consistent across most of the building plate. However, there are still some issues to work through. For example, we see a higher level of nonuniformity near the edges and a slight decline in the stable region over time. Addressing these problems is crucial for maintaining a consistent layer thickness and maximizing the uniform packing density.

4.4.2.4. Profile (D)

Significant packing density fluctuations near the powder layer's right edge are observed under Profile C. These fluctuations are attributed to the high-speed impact of powder with the right boundary, leading to localized disturbances. Reducing the powder speed near the right edge is expected to mitigate these fluctuations and provide a stabilizing effect. Profile D is introduced to test this hypothesis, retaining the same rotational speed configuration as Profile C but eliminating the counterclockwise rotation in the final 20% of the building plate. Instead, Profile D maintains a zero rotational speed in this region, aiming to dampen fluctuations and enhance powder layer uniformity.

The behaviour of Profile D closely resembles that of Profile C across most of the building plate, as illustrated in Figure 4-10a&b, with packing density and layer thickness distributions following similar trends. However, significant differences arise in the final 20% of the plate, as shown in Figure 4-11. While Profile C exhibits significant fluctuations and small discontinuous cavities near the right edge, Profile D effectively eliminates these defects, as shown in Figure 4-10c&d. This results in improved packing density uniformity, with reductions of 17.8% at a spreading speed of 0.15 m/s and 9.4% at 0.30 m/s. The observed improvement stems from Profile D’s use of zero rotational speed in the final section of the plate, replacing the counterclockwise rotation employed in Profile C. By reducing the powder velocity before impact with the right edge, Profile D dampens the forward momentum of the powder, minimizing its disruptive effects and preventing the cavity formation seen in Profile C. Additionally, Figure 4-11a highlights the reduced packing density fluctuations under Profile D in the last 20% of the plate, demonstrating the stabilizing effect of halting rotational motion.

On the other hand, despite the improvement in packing density uniformity near the boundary, Profile D does not significantly alter the fluctuations in layer thickness distribution, as shown in Figure 4-11b. Both profiles exhibit similar layer thickness behaviour near the right edge, leading to comparable surface roughness. This suggests that eliminating rotational motion near the right edge improves packing density consistency but does not significantly affect the powder’s vertical distribution near the boundary. Consequently, Profile D successfully addresses packing density defects without compromising layer thickness performance, offering a more uniform and stable powder layer near the plate's edge than Profile C.

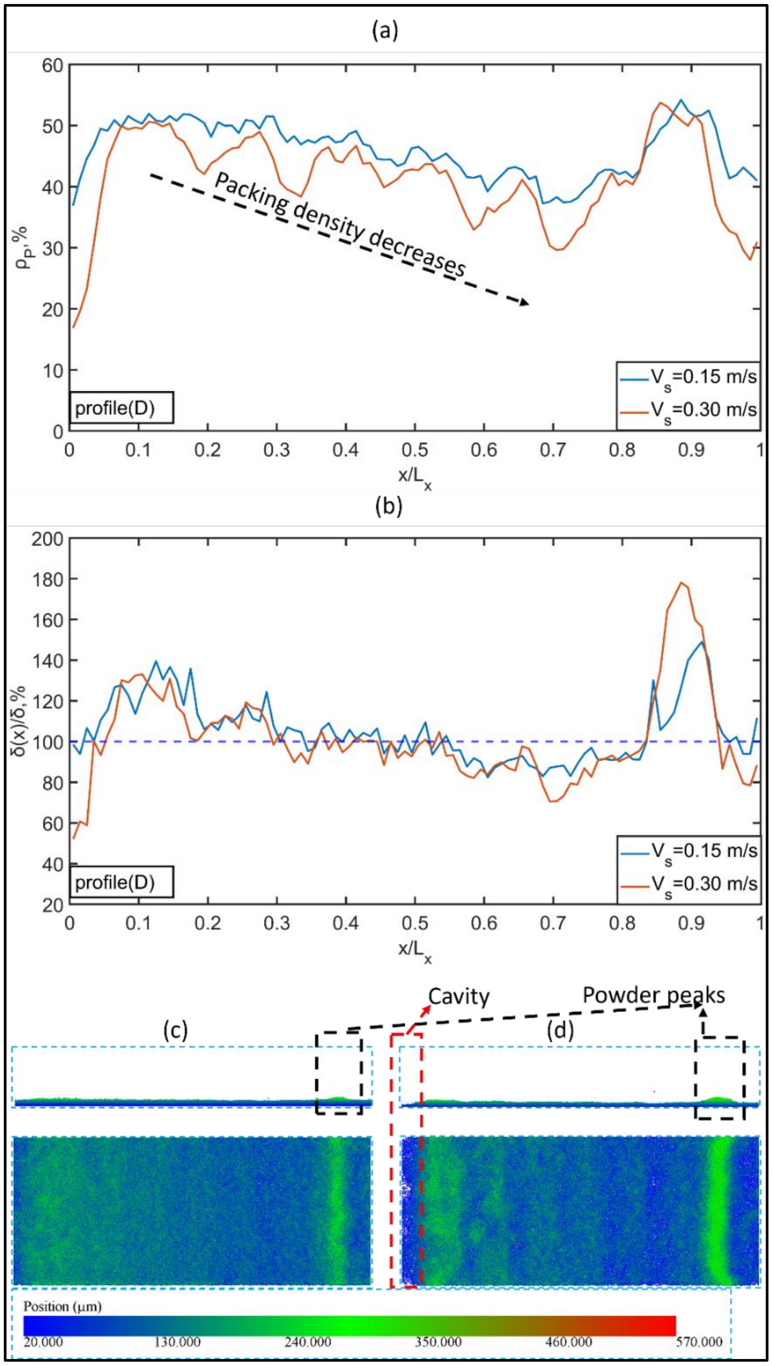

Figure 4-10.Powder layer characteristics of roller-spreading rotating under **profile D** and moving forward with 0.15 and 0.30 m/s versus the building plate length. (a) Packing density, (b) layer thickness, and (c) top view and front view of the powder bed after spreading with the speed of 0.15 m/s. (d) The top and front

views of the powder bed after spreading at a speed of 0.30 m/s; coloured by the powder position in the Z-direction (i.e., layer thickness).

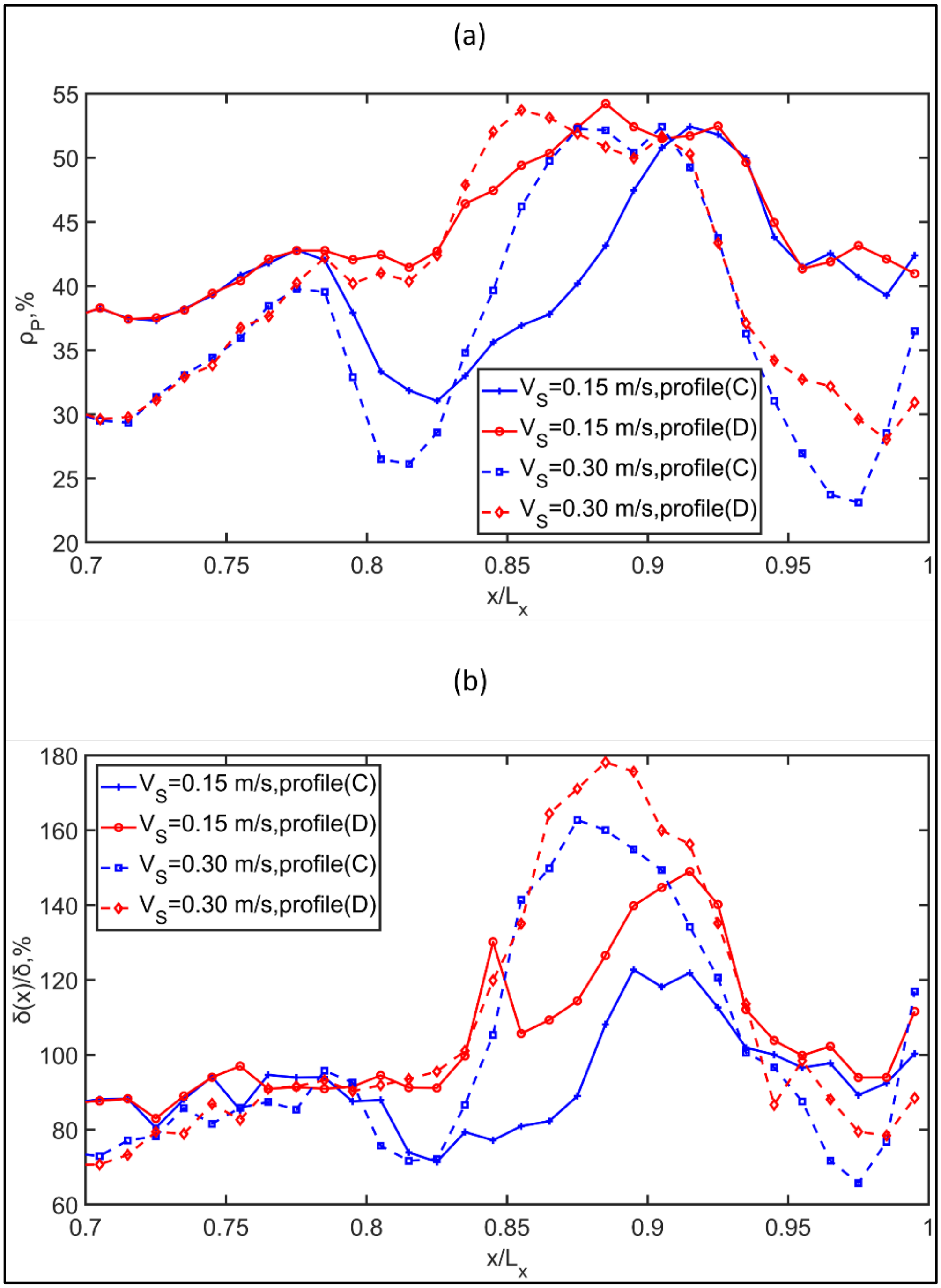

Figure 4-11. Powder layer characteristics of roller-spreading rotating under profiles C and D and moving forward with 0.30 m/s versus the building plate length. (a) Packing density, (b) layer thickness.

Profile D introduces zero rotational speed in the last 20% of the building plate to address large packing density fluctuations and small cavities observed under Profile C. However, the layer thickness fluctuations and surface roughness remain similar for both profiles, indicating that Profile D effectively enhances powder layer uniformity without altering overall layer thickness behaviour.

4.4.2.5. Profile (E)

In profile E, The roller gradually transitions from a clockwise rotation at $5/6\,\omega_o\ to\ 1/2\,\omega_o$, eventually shifting to without rotation. This configuration incorporates precisely managed transitions, alternating between clockwise and counterclockwise rotations at varying intensities. These refined adjustments are expected to enhance continuity in system control, significantly improving the capability to address challenges related to powder redistribution.

The distribution of packing density along the building plate, as shown in Figure 4-12a, offers a detailed perspective on the powder spreading process at speeds of 0.15 m/s and 0.3 m/s, utilizing the rotational speed profile E. In the initial region (from the left solid boundary to $x/L_x = 0.1$), the packing density begins at 4.7% and 23.23% for spreading speeds of 0.30 m/s and 0.15 m/s, respectively. It then increases sharply, reaching 47.5% and 50% as the spreader moves forward. This rise reflects the initial accumulation of powder, forming a base layer. However, the formation of a cavity near the left boundary is attributed to the high spreading speed and insufficient backward-directed powder movement due to the clockwise rotational motion, as shown in Figure 4-12c&d. In the stable region **(**$x/L_x = 0.1$ to $x/L_x = 0.78$**),** the packing density stabilizes at approximately 48% for a spreading speed of 0.15 m/s and 46.2% for 0.30 m/s. This consistent distribution is attributed to the fine gradual reduction in clockwise rotational speed, transitioning from $5/6\,\omega_o$ to $1/2\,\omega_o$. The stability observed in this region reflects a balance of high spreading speed effect and backward-directed powder movement. In the transitional region**,** A significant reduction in packing density occurs at $x/L_x = 0.8$, dropping to 41.9% and 38.4% in the case of a spreading speed of 0.15 m/s and 0.3m/s, respectively, with the effect being more pronounced at the higher spreading speed of 0.3 m/s. This localized inconsistency is attributed to the transition in rotational speed, changing from clockwise to zero. This shift amplifies the forward force on the powder, pushing it excessively forward and leading to a reduction in the material at this location, causing a dip in density. Beyond this region lies the impact zone, characterized by significant fluctuations in packing density. For a spreading speed of 0.15 m/s, the packing density varies between 22.2% and 53.4%, whereas a spreading speed of 0.3 m/s ranges from 39.8% to 53.7%, as illustrated in Figure 4-12a. These fluctuations in packing density are attributed to the high-speed impact of the powder against the solid boundary. This high-speed impact results from the change in the roller's bottom speed, transitioning from $V_s - 1/2\,\omega_o$ to V_s, which significantly accelerates the powder towards the solid boundary.

Figure 4-12b presents the layer thickness distribution across the building plate at spreading speeds of 0.15 m/s and 0.3 m/s under rotational speed Profile E. In the initial region, spanning from the left edge to $x/L_x = 0.1$, the layer thickness exhibits a sharp increase. It rises from 76.7% to 121.7% of the desired value at a spreading speed of 0.15 m/s. Similarly, for a spreading speed of 0.30 m/s, the thickness increases from 43.2% to 113.2% of the desired value. This steep rise is attributed to the powder accumulation facilitated by the clockwise rotation of the roller, which effectively pulls and compacts the powder. In the stable region ($x/L_x = 0.1$ to $x/L_x = 0.8$), the layer thickness remains consistent with minor fluctuations, averaging approximately 105.1% and 104.2% of the desired value for spreading speeds of 0.15 m/s and 0.30 m/s, respectively. This consistency reflects efficient and uniform spreading due to the gradual decrease in the roller's rotational speed, balancing the spreading speed and backward powder movement. However, at $x/L_x = 0.8$, where the roller ceases rotation, the layer thickness decreases to 88.1% and 91.4% of the desired value for spreading speeds of 0.15 m/s and 0.30 m/s, respectively. This reduction is likely attributed to diminished powder accumulation as the backward force weakens. In the impact region (extending from $x/L_x = 0.8$ to the right edge), substantial fluctuations in layer thickness are observed. For a spreading speed of 0.15 m/s, the thickness ranges from 88.1% to 151.7% of the desired value, while for a spreading speed of 0.30 m/s, it varies between 66.9% and 183.9% of the desired value. These variations can be attributed to the high-speed impact of powder with the right solid edge, causing changes in powder flow direction and localized accumulation.

Overall, Profile E offers an advanced, adaptive method for controlling powder spreading, effectively addressing redistribution challenges through precise adjustments to the rotational speed. The packing density and layer thickness distributions along the building plate remain stable across the majority of the plate but exhibit areas of nonuniformity, including a sharp increase in the initial region, a significant reduction during the transition in the rotational direction, and high nonuniformity near the right edge. To improve overall performance, Profile E should be modified to address and minimize these sources of nonuniformity.

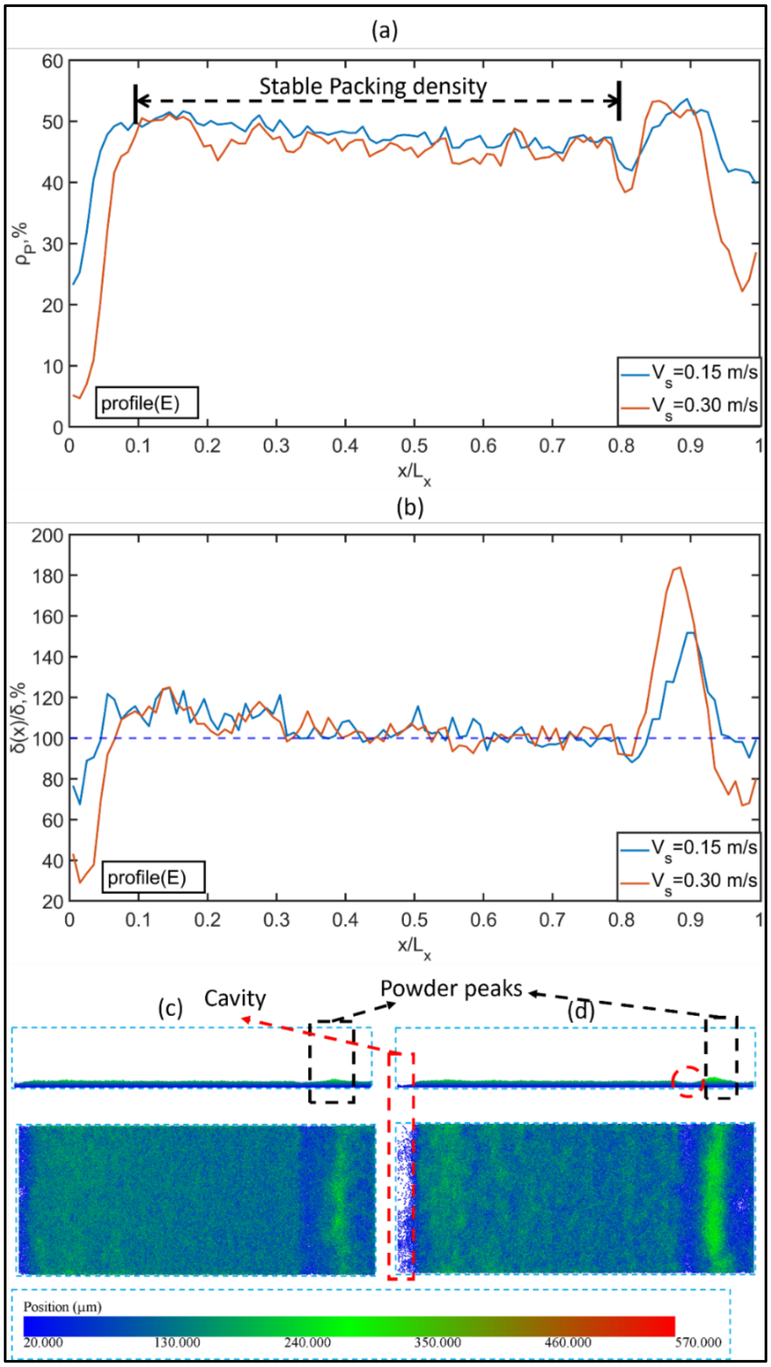

Figure 4-12. Powder layer characteristics of roller-spreading rotating under profile E and moving forward with 0.15 and 0.30 m/s versus the building plate length. (a) Packing density, (b) layer thickness, and (c) top view and front view of the powder bed after spreading with the speed of 0.15 m/s. (d) The top and front views of the powder bed after spreading at a speed of 0.30 m/s; coloured by the powder position in the Z-direction (i.e., layer thickness).

4.4.2.6. *Profile (F)*

Profile E was refined to develop Profile F to mitigate cavity formation near the left edge at higher spreading speeds. The modification involved increasing the clockwise rotational speed beyond ω_o during the first 20% of the building plate, with a subsequent gradual decrease following the same slope as Profile E. Furthermore, in the final 20% of the plate, a clockwise rotational speed of $\omega_o/3$ is introduced. Beyond this point, the roller rotation ceases entirely, eliminating rotation over the remaining distance to the right edge of the plate.

The packing density distribution along the building plate produced by the roller operating under Profile F closely resembles that of Profile E, with notable differences near the left boundary, as shown in Figure 4-13a & Figure 4-14a. Under Profile E, the packing density initially exhibits low values, starting at 23.23% for a spreading speed of 0.15 m/s and approximately 4.7% at 0.3 m/s. It then gradually stabilizes at around 48% and 46.25% for spreading speeds of 0.15 m/s and 0.3 m/s, respectively. In contrast, Profile F demonstrates a significantly higher initial packing density, commencing near its stable value. For a spreading speed of 0.15 m/s, the packing density increases from 48.48% to a stable value of 50.8%, while at 0.3 m/s, it rises from 41.45% to a stable value of 47.6%. This improvement is attributed to the increased clockwise rotational speed at the start of spreading in Profile F, which enhances the backward powder movement, compensating for the powder reduction caused by the roller's high spreading speed. Consequently, cavities near the left solid boundary are effectively eliminated, as presented in Figure 4-13c&d, leading to an overall improvement in the uniformity of packing density. Under Profile F, the spreading domain begins with a stable packing density of 50.8% and 47.6% at spreading speeds of 0.15 m/s and 0.30 m/s, respectively, which extends with minor fluctuations over approximately 80% of the building plate length. Between $x/L_x = 0.75$ to $x/L_x = 0.81$, the packing density experiences a sharp decline to 37.3% at a spreading speed of 0.3 m/s, similar to the behaviour observed in Profile E. This reduction is attributed to a significant 33.33% decrease in the clockwise rotational speed, which diminishes the backward force responsible for redistributing powder in the reverse direction. Consequently, the powder accumulation is insufficient, leading to a pronounced drop in packing density. In the subsequent impact region, the packing density demonstrates considerable fluctuations, ranging from 41.5% to 54.4% at a spreading speed of 0.15 m/s and from 17.5% to 53.8% at 0.30 m/s. These variations can be primarily attributed to the high-speed impact of the powder against the solid boundary. This impact is driven by changes in the roller's bottom speed, transitioning from $V_s - 1/2\ \omega_o$ to $V_s - 1/3\ \omega_o$ and then to zero, which substantially accelerates the powder as it approaches the boundary.

Under Profile F, the roller maintains a stable layer thickness with minimal fluctuations across the first 80% of the building plate, as shown in Figure 4-13b. At a spreading speed of 0.15 m/s, the layer thickness initially increases from 114.6% to a stable value of 118.4% of the desired thickness. At a spreading speed of 0.30 m/s, the thickness rises from 105% to a stable value of 113.9% of the desired thickness. This stability is due to the high initial clockwise rotational speed, which gradually decreases, effectively balancing the forward motion of the powder with its backward redistribution, ensuring uniform spreading. The impact of the high initial clockwise rotational speed is particularly evident when comparing Profiles E and F, as illustrated in Figure 4-14b. However, when the clockwise rotational speed reduces to $1/3\ \omega_o$ at $x/L_x = 0.8$, the layer thickness decreases to 94.1% and 95.2% of the desired thickness for spreading speeds of 0.15 m/s and 0.30 m/s, respectively.

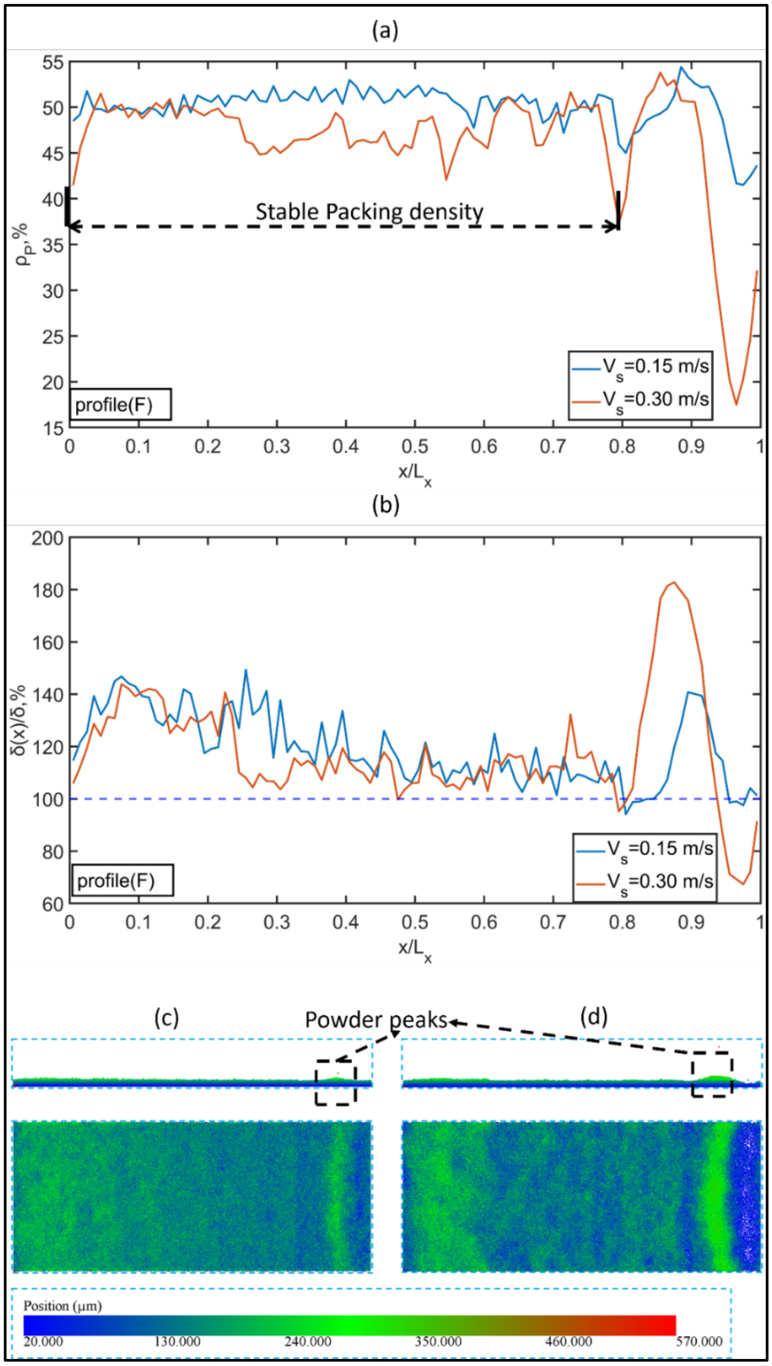

Figure 4-13. Powder layer characteristics of roller-spreading rotating under **profile F** and moving forward with 0.15 and 0.30 m/s versus the building plate length. (a) Packing density, (b) layer thickness, and (c) top view and front view of the powder bed after spreading with the speed of 0.15 m/s. (d) The top and front

views of the powder bed after spreading at a speed of 0.30 m/s; coloured by the powder position in the Z-direction (i.e., layer thickness).

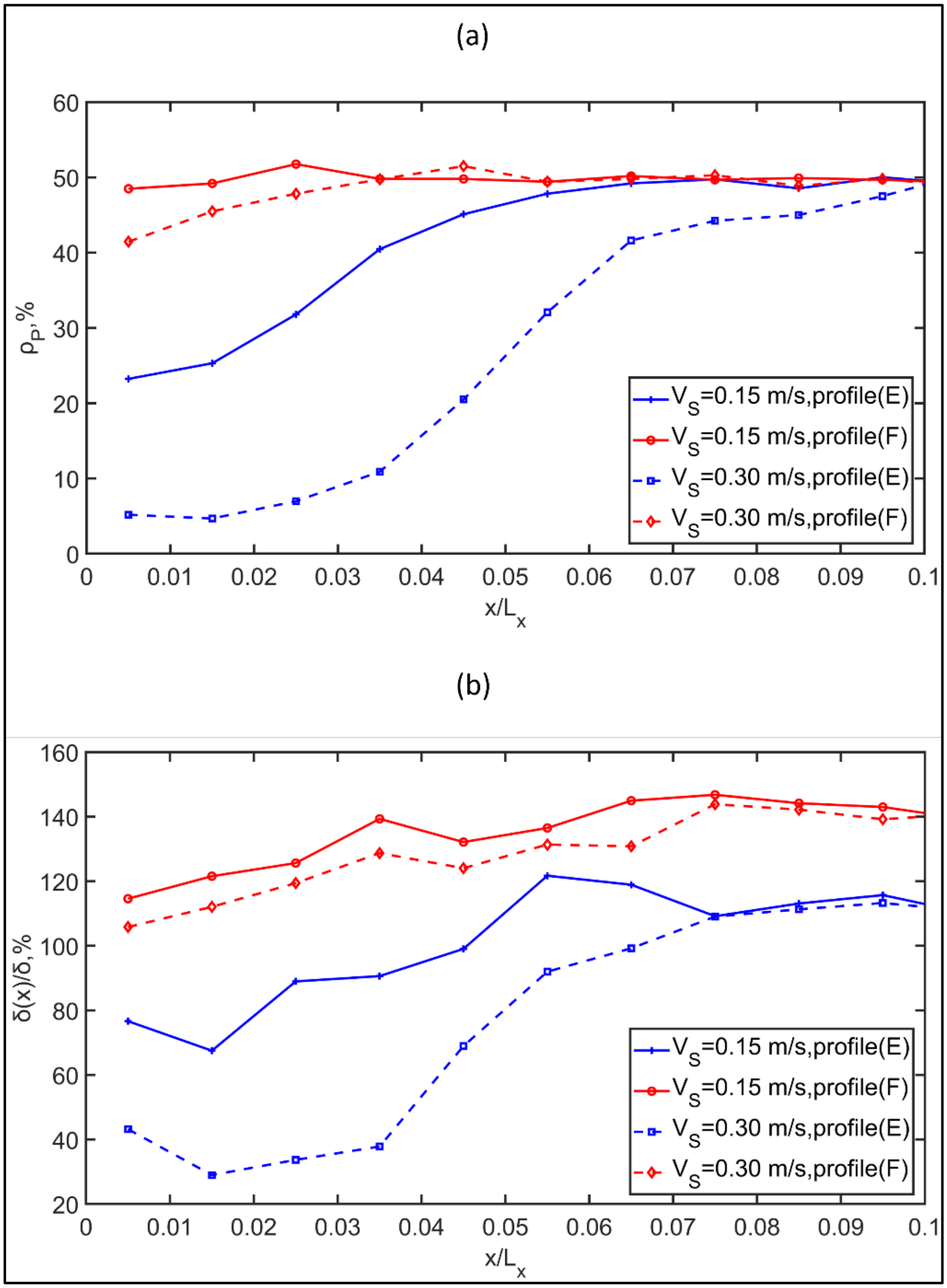

Figure 4-14. Powder layer characteristics of roller-spreading rotating under profiles E and F and moving forward with 0.15 and 0.30 m/s versus the building plate length. (a) Packing density, (b) layer thickness.

Beyond this point, the powder impacts the right boundary, causing a redirection of its motion backward. This interaction leads to significant fluctuations in layer thickness, ranging from 94.1% to 140.8% of the desired thickness at 0.15 m/s and from 67.3% to 182.8% at 0.30 m/s. These fluctuations reflect the instability caused by the high-speed powder interacting with the boundary.

To sum up, Profile F demonstrates improved uniformity in packing density compared to Profile E, mainly by eliminating cavities near the left boundary and expanding the high and stable packing density area. While Profile F demonstrated better uniformity than Profile E, it failed to fully address the non-uniformities at the impact zone, particularly at high spreading speeds.

4.4.3. Macroscopic analysis

The following section explores the impact of rotational speed profiles on the macroscopic properties of the powder layer, focusing on packing density and layer thickness. This analysis evaluates these properties' average values and variations across the entire building plate. Across both spreading speeds, clockwise rotational speeds and profiles such as C, D, E, and F exhibit higher packing densities. This is primarily due to the clockwise rotational speed, which generates a backward force that compensates for powder loss caused by high spreading speeds, effectively balancing spreading and circumferential speeds. Profile F stands out among these profiles, achieving the maximum packing density, as shown in Figure 4-15a and Figure 4-16a . This is attributed to its unique rotational speed strategy, which starts at a high speed greater than ω_o and gradually decreases to stabilize and enhance packing density while minimizing fluctuations. Furthermore, Profile F consistently demonstrates the lowest variation coefficient of the packing density, indicating superior uniformity in the powder bed. The exceptional performance is attributed to the profile's expanded high and stable packing density region, which extends from the left edge to 80% of the building plate.

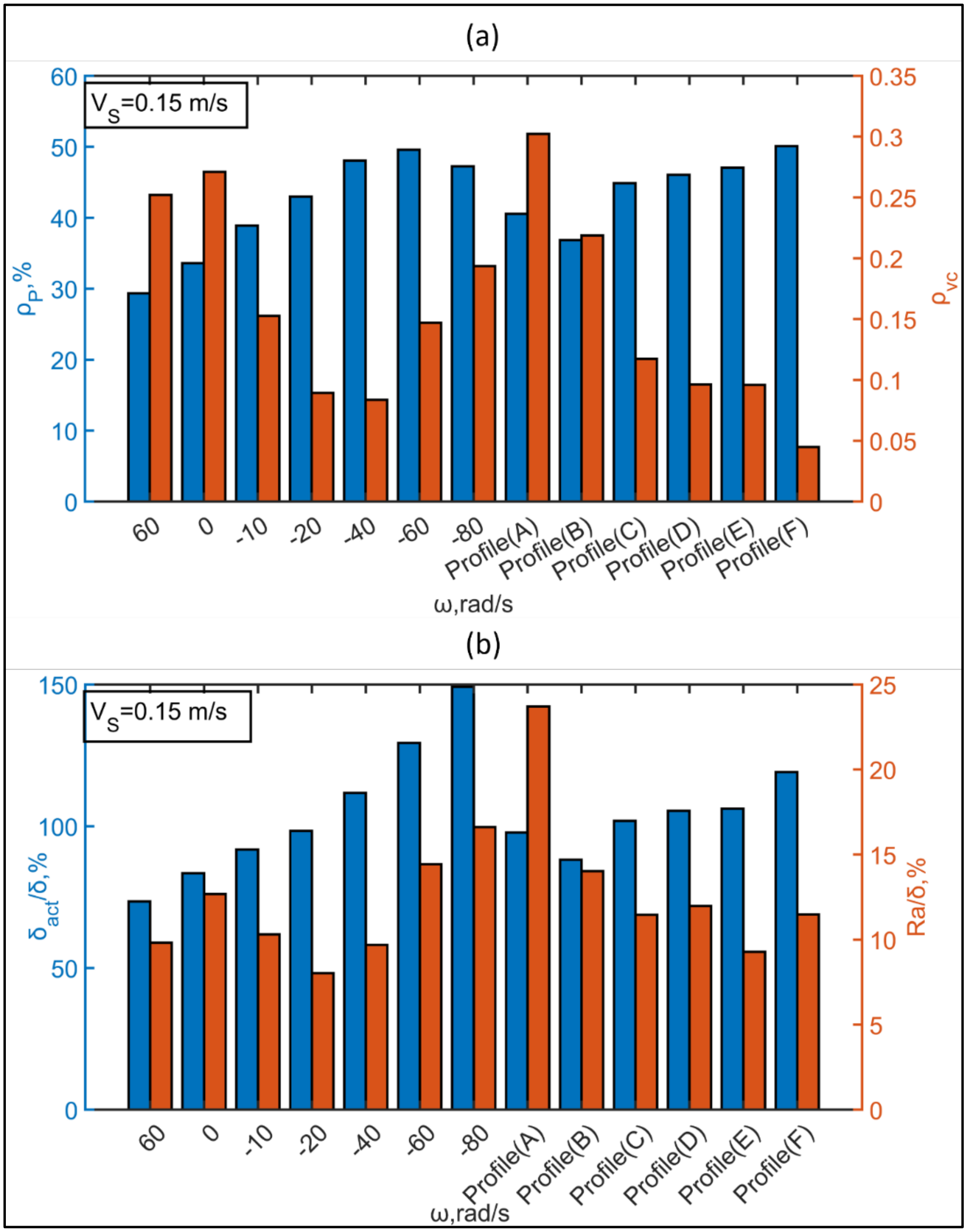

Figure 4-15.Powder layer characteristics of roller-spreading at a spreading speed of 0.15 m/s for various rotational speed profiles. (a)Average packing density (left y-axis) and its variation coefficient (right y-axis), (b)normalized average layer thickness (left y-axis) and surface roughness (right y-axis).

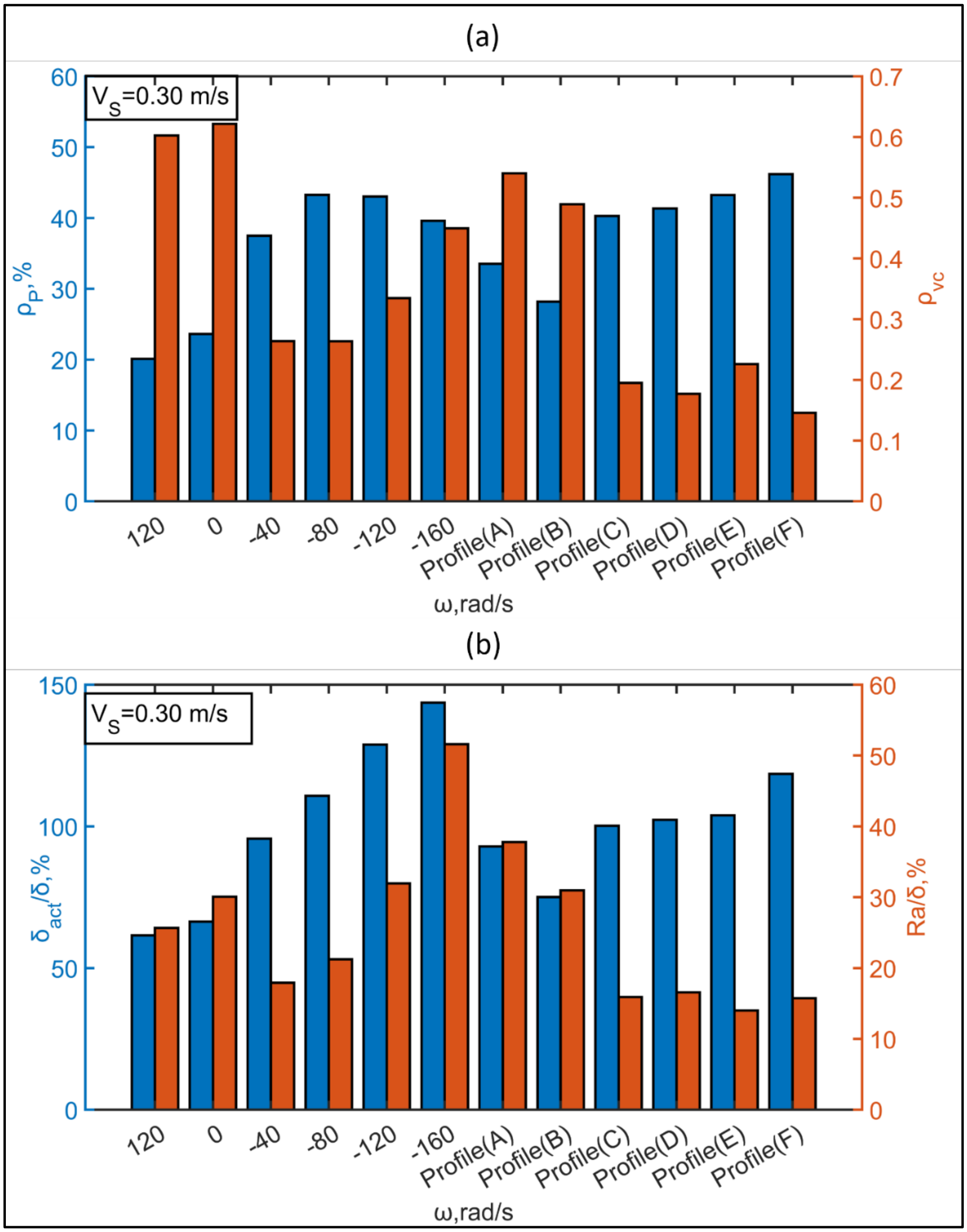

Figure 4-16. Powder layer characteristics of roller-spreading at a spreading speed of 0.3 m/s for various rotational speed profiles. (a)Average packing density (left y-axis) and its variation coefficient (right y-axis), (b)normalized average layer thickness (left y-axis) and surface roughness (right y-axis).

Layer thickness and surface roughness are equally critical in evaluating powder spreading performance. Profiles with clockwise rotational speed generally produce higher layer thicknesses due to backward powder accumulation. However, despite its high packing density, profile F achieves an average layer thickness exceeding the desired thickness by 18.5%, as illustrated in Figure 4-15b and Figure 4-16b. This deviation highlights the challenges in balancing packing density with precise layer thickness. Surface roughness, on the other hand, tends to increase with spreading speed. Nevertheless, Profiles D, E, and F demonstrate smoother surfaces due to effectively balancing spreading and rotational speeds. Profile F, in particular, strikes an optimal balance, yielding a high packing density and a relatively smooth surface, even under high spreading speed conditions. These characteristics emphasize its robustness and adaptability to varying operational conditions.

Packing density and layer thickness are essential metrics, but they are insufficient to comprehensively evaluate the rotational speed strategies' effectiveness. These parameters provide valuable insights into the structural attributes of the powder bed with the desired layer thickness but fail to capture the overall efficiency of spreading process consistency, especially the nonuniformity of the powder surface after spreading, so the mass fraction parameter can address this gap. Defined as the ratio of the mass of powder particles deposited on the building plate to the total mass required to achieve the desired layer thickness, it provides insights into both the efficiency of the spreader and the uniformity of powder deposition. Mass fraction serves as a comprehensive metric for assessing the quality of the powder layer and the spreader's performance. Quantifying the amount of powder effectively deposited by the roller evaluates spreading efficiency, while its variation coefficient provides a reliable measure of overall surface uniformity.

Profiles employing high clockwise rotational speeds, particularly in super-rolling configurations, tend to achieve the maximum mass fraction. At a spreading speed of 0.15

m/s, the highest average mass fraction of 65.6% is observed under a constant clockwise rotational speed of 80 rad/s (super-rolling). However, this comes with a high variation coefficient of 0.2557, indicating significant nonuniformity, as illustrated in Figure 4-17a. Similarly, at a spreading speed of 0.30 m/s, the maximum average mass fraction of 60.3% is achieved at a clockwise rotational speed of 160 rad/s (super-rolling), again accompanied by a high variation coefficient of 0.5786, reflecting pronounced variability in powder distribution, as shown in Figure 4-17b. In contrast, Profile F demonstrates a more balanced performance by combining relatively high mass fraction values with significantly lower variation coefficients. At a spreading speed of 0.15 m/s, Profile F achieves an average mass fraction of 53.2%, with a variation coefficient of 0.088, the minimum within all cases, indicating much-improved uniformity compared to super-rolling cases. Similarly, at a spreading speed of 0.30 m/s, Profile F achieves an average mass fraction of 50.1%, with a variation coefficient of 0.2168, reflecting its ability to maintain consistent powder distribution even at higher speeds. While super-rolling cases achieve the highest mass fraction values, their elevated variation coefficients suggest poor uniformity, compromising the powder layer's overall quality. On the other hand, Profile F strikes an optimal balance by delivering mass fraction values close to the maximum while maintaining significantly better uniformity.

This consistency across both spreading speeds is attributed to Profile F's optimized rotational strategy, which balances clockwise and counterclockwise motions to reduce disturbances and ensure effective powder redistribution. By achieving the highest packing density, superior mass fraction, and minimal variation coefficients, Profile F emerges as the most effective strategy for achieving a high-quality powder layer under challenging conditions like high spreading speeds.

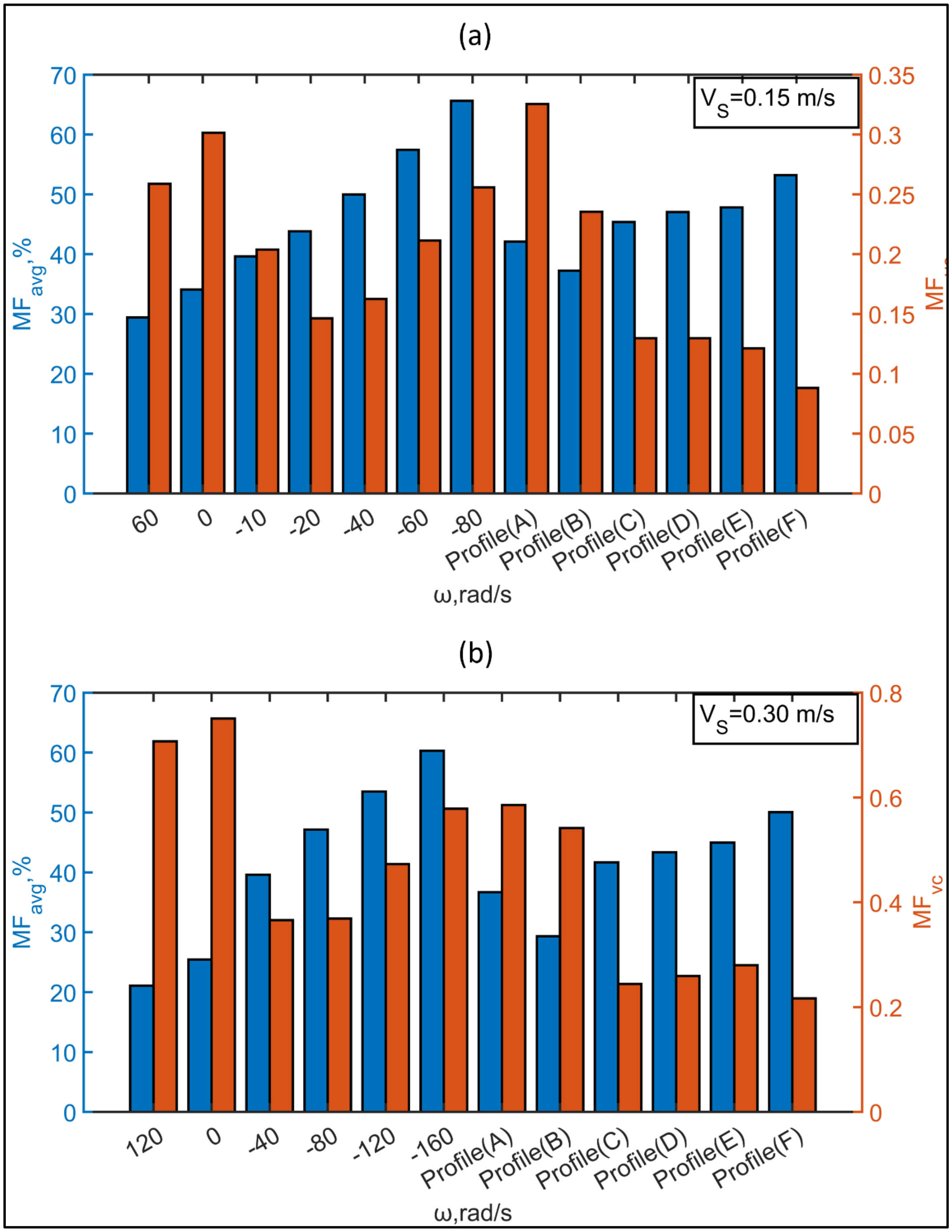

Figure 4-17.Powder layer characteristics of roller-spreading at a spreading speed of 0.3 m/s for various rotational speed profiles. (a)at a spreading speed of 0.15 m/s (b) at a spreading speed of 0.30 m/s

4.5. Conclusions

This study investigated the use of adaptive rotational speed, a novel approach that involves adjusting the rotational speed of the roller during the spreading process to mitigate the adverse effects of high spreading speed in laser powder bed fusion. This study used discrete Element Method (DEM) simulations to examine six adaptive rotational speed profiles under high spreading speeds of 0.15 m/s and 0.30 m/s. These profiles were selected based on the performance of constant rotational speed, which was also evaluated in the study.

Constant rotational speed strategies, including non-rotating, counter-rotating, sub-rolling, rolling, and super-rolling—each impact packing density and layer uniformity in unique ways, yet consistently lead to cavity formation on the left or right side of the building plate at high spreading speeds. Constant rotational speed failed to maintain high-quality powder quality due to an unbalancing between the spreading and circumferential speeds.

Variable rotational speed profiles (A–F) were introduced to mitigate these challenges, incorporating adaptive transitions in rotational speed to improve powder distribution. Among these, Profile F emerged as the optimal strategy, outperforming all other configurations across both spreading speeds. Its unique approach begins with a high clockwise rotational speed exceeding ω_o. It gradually decreases to zero, achieving the highest packing density, minimal variation coefficients for packing density and mass fraction, and improved surface roughness. Furthermore, Profile F demonstrated average layer thickness, exceeding the desired value by 18.5%, while maintaining low surface roughness.

Despite the impressive performance of Profile F, it has its challenges. The high-speed impact of the powder against the solid right boundary still led to packing density and layer thickness fluctuations, particularly at 0.30 m/s. As a result, nonuniformity on the right side remained a challenge. These hurdles underscore the necessity for further strategies to address disturbances caused by the right boundary. This call for additional research should motivate the field to optimize the process and explore the integration of advanced control systems for real-time adjustment of spreading process parameters based on powder flow dynamics.

Ultimately, this work underscores the pivotal role of adaptive rotational speed strategies in elevating powder spreading quality in PBF-LP under high spreading speed. The findings reveal that Profile F presents a promising avenue for achieving uniform and high-quality powder layers despite the challenges posed by high spreading speed, instilling a sense of optimism in the field.

References

[1] M. Yakout, M.A. Elbestawi, S.C. Veldhuis, On the characterization of stainless steel 316L parts produced by selective laser melting, International Journal of Advanced Manufacturing Technology 95 (2018) 1953–1974. https://doi.org/10.1007/s00170-017-1303-0.

[2] M. Yakout, A. Cadamuro, M.A. Elbestawi, S.C. Veldhuis, The selection of process parameters in additive manufacturing for aerospace alloys, International Journal of Advanced Manufacturing Technology 92 (2017) 2081–2098. https://doi.org/10.1007/s00170-017-0280-7.

[3] E. Fereiduni, A. Ghasemi, M. Elbestawi, Unique opportunities for microstructure engineering via trace B4C addition to Ti-6Al-4V through laser powder bed fusion process: As-built and heat-treated scenarios, Addit Manuf 50 (2022) 102557. https://doi.org/10.1016/j.addma.2021.102557.

[4] V. Lampitella, M. Trofa, A. Astarita, G. D'Avino, Discrete Element Method Analysis of the Spreading Mechanism and Its Influence on Powder Bed Characteristics in Additive Manufacturing, Micromachines (Basel) 12 (2021) 392. https://doi.org/10.3390/mi12040392.

[5] J. Zhang, Y. Tan, T. Bao, Y. Xu, X. Xiao, S. Jiang, Discrete element simulation of the effect of roller-spreading parameters on powder-bed density in additive manufacturing, Materials 13 (2020). https://doi.org/10.3390/ma13102285.

[6] D. Yao, X. An, H. Fu, H. Zhang, X. Yang, Q. Zou, K. Dong, Dynamic investigation on the powder spreading during selective laser melting additive manufacturing, Addit Manuf 37 (2021). https://doi.org/10.1016/j.addma.2020.101707.

[7] L. Wang, Z. Zhou, E. Li, H. Shen, A. Yu, Powder deposition mechanism during powder spreading with different spreader geometries in powder bed fusion additive manufacturing, Powder Technol 395 (2022) 802–810. https://doi.org/10.1016/j.powtec.2021.10.017.

[8] S. Haeri, Y. Wang, O. Ghita, J. Sun, Discrete element simulation and experimental study of powder spreading process in additive manufacturing, Powder Technol 306 (2016) 45–54. https://doi.org/10.1016/j.powtec.2016.11.002.

[9] Z. Xiang, M. Zhang, R. Yan, Q. Yin, K. Zhang, Powder-spreading dynamics and packing quality improvement for laser powder bed fusion additive manufacturing, Powder Technol 389 (2021) 278–291. https://doi.org/10.1016/j.powtec.2021.05.036.

[10] Y.M. Fouda, A.E. Bayly, A DEM study of powder spreading in additive layer manufacturing, Granul Matter 22 (2020) 1–18. https://doi.org/10.1007/s10035-019-0971-x.

[11] C. Meier, R. Weissbach, J. Weinberg, W.A. Wall, A. John Hart, Modeling and characterization of cohesion in fine metal powders with a focus on additive manufacturing process simulations, Powder Technol 343 (2019) 855–866. https://doi.org/10.1016/j.powtec.2018.11.072.

[12] S. Wu, Z. Lei, M. Jiang, J. Liang, B. Li, Y. Chen, Experimental investigation and discrete element modeling for particle-scale powder spreading dynamics in powder-bed-fusion-based additive manufacturing, Powder Technol 403 (2022) 117390. https://doi.org/10.1016/j.powtec.2022.117390.

[13] E.J.R. Parteli, J. Schmidt, C. Blümel, K.E. Wirth, W. Peukert, T. Pöschel, Attractive particle interaction forces and packing density of fine glass powders, Sci Rep 4 (2014). https://doi.org/10.1038/srep06227.

[14] P.K. Gokuldoss, S. Kolla, J. Eckert, Additive manufacturing processes: Selective laser melting, electron beam melting and binder jetting-selection guidelines, Materials 10 (2017). https://doi.org/10.3390/ma10060672.

[15] H. Gong, K. Rafi, H. Gu, G.D. Janaki Ram, T. Starr, B. Stucker, Influence of defects on mechanical properties of Ti-6Al-4V components produced by selective laser melting and electron beam melting, Mater Des 86 (2015) 545–554. https://doi.org/10.1016/j.matdes.2015.07.147.

[16] G. Yang, Y. Xie, S. Zhao, L. Qin, X. Wang, B. Wu, Quality Control: Internal Defects Formation Mechanism of Selective Laser Melting Based on Laser-powder-melt Pool Interaction: A Review, Chinese Journal of Mechanical Engineering: Additive Manufacturing Frontiers 1 (2022) 100037. https://doi.org/10.1016/j.cjmeam.2022.100037.

[17] Y.S. Lee, W. Zhang, Mesoscopic Simulation of Heat Transfer and Fluid Flow in Laser Powder Bed Additive Manufacturing, International Solid Free Form Fabrication Symposium, Austin (2015) 1154–1165. http://sffsymposium.engr.utexas.edu/sites/default/files/2015/2015-94-Lee.pdf.

[18] L. Thijs, F. Verhaeghe, T. Craeghs, J. Van Humbeeck, J.P. Kruth, A study of the microstructural evolution during selective laser melting of Ti-6Al-4V, Acta Mater 58 (2010) 3303–3312. https://doi.org/10.1016/j.actamat.2010.02.004.

[19] J. Zielinski, S. Vervoort, H.-W. Mindt, M. Megahed, Influence of Powder Bed Characteristics on Material Quality in Additive Manufacturing, BHM Berg- Und Hüttenmännische Monatshefte 162 (2017) 192–198. https://doi.org/10.1007/s00501-017-0592-9.

[20] L. Parry, I.A. Ashcroft, R.D. Wildman, Understanding the effect of laser scan strategy on residual stress in selective laser melting through thermo-mechanical simulation, Addit Manuf 12 (2016) 1–15. https://doi.org/10.1016/j.addma.2016.05.014.

[21] J.C. Snyder, K.A. Thole, Understanding laser powder bed fusion surface roughness, Journal of Manufacturing Science and Engineering, Transactions of the ASME 142 (2020). https://doi.org/10.1115/1.4046504.

[22] W. Nan, M. Ghadiri, Numerical simulation of powder flow during spreading in additive manufacturing, Powder Technol 342 (2019) 801–807. https://doi.org/10.1016/j.powtec.2018.10.056.

[23] L. Haferkamp, M.S. Rwth, Effect of the Particle Size Distribution and Morphology on Powder Processability in Laser Powder Bed Fusion, n.d.

[24] L. Haferkamp, L. Haudenschild, A. Spierings, K. Wegener, K. Riener, S. Ziegelmeier, G.J. Leichtfried, The influence of particle shape, powder flowability, and powder layer density on part density in laser powder bed fusion, Metals (Basel) 11 (2021) 1–15. https://doi.org/10.3390/met11030418.

[25] R. Rothfelder, L. Lanzl, J. Selzam, D. Drummer, M. Schmidt, Vibrational Microfeeding of Polymer and Metal Powders for Locally Graded Properties in Powder-Based Additive Manufacturing, J Mater Eng Perform 30 (2021) 8798–8809. https://doi.org/10.1007/s11665-021-06271-5.

[26] W. Nan, M. Pasha, M. Ghadiri, Numerical simulation of particle flow and segregation during roller spreading process in additive manufacturing, Powder Technol 364 (2020) 811–821. https://doi.org/10.1016/j.powtec.2019.12.023.

[27] M.A. Salim, S. Tullis, M. Elbestawi, Accelerating Laser Powder Bed Fusion: The Influence of Roller-Spreading Speed on Powder Spreading Performance, Metals (Basel) 14 (2024) 1137. https://doi.org/10.3390/met14101137.

[28] H. Chen, Y. Chen, Y. Liu, Q. Wei, Y. Shi, W. Yan, Packing quality of powder layer during counter-rolling-type powder spreading process in additive manufacturing, Int J Mach Tools Manuf 153 (2020) 103553. https://doi.org/10.1016/j.ijmachtools.2020.103553.

[29] U. Habiba, R.J. Hebert, Powder Spreading Mechanism in Laser Powder Bed Fusion Additive Manufacturing: Experiments and Computational Approach Using Discrete Element Method, Materials 16 (2023). https://doi.org/10.3390/ma16072824.

[30] A.K. Sood, A. Equbal, Z.A. Khan, I.A. Badruddin, M. Hussien, FEM-Based Simulative Study for Multi-Response Optimization of Powder Bed Fusion Process, Mathematics 10 (2022). https://doi.org/10.3390/math10142505.

[31] J.Q. Gan, A.B. Yu, Z.Y. Zhou, DEM simulation on the packing of fine ellipsoids, Chem Eng Sci 156 (2016) 64–76. https://doi.org/https://doi.org/10.1016/j.ces.2016.09.017.

[32] H.P. Zhu, Z.Y. Zhou, R.Y. Yang, A.B. Yu, Discrete particle simulation of particulate systems: A review of major applications and findings, Chem Eng Sci 63 (2008) 5728–5770. https://doi.org/https://doi.org/10.1016/j.ces.2008.08.006.

[33] B.C. Burman, P.A. Cundall, O.D.L. Strack, A discrete numerical model for granular assemblies, Geotechnique 30 (1980) 331–336. https://doi.org/10.1680/geot.1980.30.3.331.

[34] R.D. Mindlin, H. Deresiewicz, Elastic Spheres in Contact Under Varying Oblique Forces, J Appl Mech 20 (2021) 327–344. https://doi.org/10.1115/1.4010702.

[35] K.L. Johnson, K. Kendall, A.D. Roberts, Surface energy and the contact of elastic solids, Proceedings of the Royal Society of London. A. Mathematical and Physical Sciences 324 (1971) 301–313. https://doi.org/10.1098/rspa.1971.0141.

[36] Altair EDEM 2021.1, (n.d.). https://www.altair.com/edem/.

[37] H. Chen, Q. Wei, S. Wen, Z. Li, Y. Shi, Flow behavior of powder particles in layering process of selective laser melting: Numerical modeling and experimental verification based on discrete element method, Int J Mach Tools Manuf 123 (2017) 146–159. https://doi.org/10.1016/j.ijmachtools.2017.08.004.

[38] D. Gu, M. Xia, D. Dai, On the role of powder flow behavior in fluid thermodynamics and laser processability of Ni-based composites by selective laser melting, Int J Mach Tools Manuf 137 (2019) 67–78. https://doi.org/10.1016/j.ijmachtools.2018.10.006.

5 Conclusions

5.1.Summary and conclusions

The research presented in this thesis has systematically advanced the understanding of powder spreading dynamics in laser powder bed fusion (PBF-LB), focusing on the impact of roller configurations, spreading speed, rotational speeds, Roller radius, and mean powder size on roller-spreading performance. Furthermore, this work investigated using adaptive control strategies to achieve uniform and high-quality powder layers in the case of high-spreading speed. This study explores the dynamic interaction between spreading speed and circumferential speed through a detailed series of discrete element method (DEM) simulations, offering practical insights to enhance the efficiency and consistency of laser powder bed fusion processes.

The findings collectively demonstrate that the quality of powder spreading is highly sensitive to operational parameters and that careful optimization of these parameters can significantly improve powder bed characteristics, such as packing density, layer thickness, and surface roughness. This chapter synthesizes the key conclusions drawn from the research and outlines their implications for the field of additive manufacturing while also proposing directions for future work to address remaining challenges.

This research highlights the crucial role of roller configuration and rotational speed in shaping powder bed quality. While non-rotating and counter-rotating rollers establish a baseline performance, they tend to reduce packing density and layer thickness at higher spreading speeds due to momentum transfer effects. A higher spreading speed is a key factor in reducing the processing time of laser powder bed fusion, contributing to a more efficient and streamlined manufacturing process. In contrast, forward-rotating rollers offer a more efficient solution, especially in a super-rolling setup where the circumferential speed matches or exceeds the spreading speed. Balancing forward and backward momentum creates a powder burst effect that helps counteract material loss while improving packing density and uniformity. For instance, a forward-rotating roller operating at a spreading speed of 0.15 m/s with a gradually increasing rotational speed improved packing density by 69.4%, increased layer thickness by 62%, and reduced the variation coefficient by 46%. Hence, the super-rolling configuration should be optimized to achieve a more consistent and high-quality powder layer and avoid the drawbacks of higher spreading speed.

Forward-rotating rollers enhanced packing density and layer uniformity, particularly in super-rolling configurations. However, these benefits come with trade-offs, as higher rotational speeds contribute to increased surface roughness. So, the balance between roller dynamics parameters is required to balance high powder compaction and carefully against potential surface quality degradation. Furthermore, the findings emphasize the importance of maintaining a buffer zone between the powder deposition area and the boundaries of the building plate to mitigate wall effects and achieve uniform powder distribution.

The study also highlights the critical role of powder and roller size in controlling powder bed characteristics. Smaller normalized powder sizes ($D/\delta < 0.5$) consistently produced denser and more uniform powder beds, with the most stable results observed at a normalized size of 0.25. In contrast, larger powder sizes caused noticeable fluctuations in packing density and layer thickness because of gravitational forces and wall effects. On the other hand, smaller rollers with forward rotation helped improve powder compaction and uniformity, resulting in denser and more consistent layers. Hence, powder size, layer thickness, and roller geometry should be selected carefully to optimize powder spreading and enhance the overall efficiency of the process.

Mass fraction should be considered alongside packing density when evaluating forward-rotating rollers, particularly in super-rolling configurations. While forward-rotating rollers promote higher mass deposition through backward-directed forces, larger powder sizes reduce mass fraction due to gravitational effects and particle-wall interactions. The results indicate that moderate rotational speeds are optimal for smaller powders, whereas higher speeds can enhance uniformity for larger ones. When the spreading speed remains constant, the circumferential speed should be kept consistent to achieve consistent performance in roller-based spreading.

Another key contribution of this research is developing and evaluating adaptive rotational speed strategies to address the challenges of high-spreading speeds. Traditional constant rotational speed strategies, including non-rotating, counter-rotating, and forward-rotating configurations, were insufficient in maintaining high-quality powder layers at high spreading speeds (i.e., 0.30 m/s). These strategies often result in cavity formation and nonuniformity on the left or right side of the building plate due to an imbalance between spreading and circumferential speeds. Six adaptive rotational speed profiles were introduced to overcome these limitations, with Profile F emerging as the most effective. This profile, which begins with a high clockwise rotational speed(i.e., greater than V_s/R_r) and gradually decreases to zero, achieved the highest packing density, minimal variation coefficients, and improved surface roughness. Despite its success, Profile F faced challenges related to nonuniformity on the right side of the building plate, particularly at higher spreading speeds. These findings highlight the potential of adaptive rotational speed strategies to improve powder spreading quality, underscoring the need for further research to address boundary effects and optimize real-time control systems.

5.2.Future Work

Although this thesis has comprehensively investigated the impact of roller-spreading dynamics on the performance of the spreading process, there are still many exciting opportunities for future research. First, Experimental validation of the DEM simulation results is essential to confirm the practical applicability of the proposed strategies, especially for adaptive rotational speed. This could involve imaging techniques like X-rays to analyze powder bed characteristics in real-time. Second, integrating machine learning design algorithms with real-time measurements and control systems into laser powder bed fusion could allow the printer to adjust spreading parameters in real-time. This adaptive approach could further enhance powder bed uniformity and reduce defects in the final product. Third, the effects of material properties like shape, size distribution, and cohesion should be investigated to understand the spreading process comprehensively. Fourth, developing novel roller designs, including textured or segmented rollers, could provide additional control over powder distribution and compaction. Finally, further research could expand into novel spreading methods, particularly for multi-material applications.

In conclusion, this thesis has provided meaningful insights into how roller-spreading dynamics influence powder distribution. The findings highlight the crucial balance between translational and rotational motion in achieving uniform, high-quality powder layers while pointing to areas requiring further exploration. Beyond advancing the scientific understanding of powder spreading mechanics, this work offers practical solutions that can be readily applied to enhance the quality and efficiency of additive manufacturing processes.

6 Appendix 1:

Supplementary Material for Optimizing Roller-Spreading Performance in Laser Powder Bed Fusion: Numerical Study of the Circumferential Speed's Effect

6.1. Introduction

This supplementary material provides additional data and visualizations supporting the study "Optimizing Roller-Spreading Performance in Laser Powder Bed Fusion: Numerical Study of the Circumferential Speed's Effect." The figures included illustrate the impact of roller rotation on powder distribution, with a particular focus on the effect of different rotational speeds and normalized powder sizes. The dataset includes results for counter-rotating and forward-rotating rollers, highlighting variations in packing density, layer thickness, and mass fraction along the building plate length. These insights contribute to a comprehensive understanding of powder behaviour in laser powder bed fusion (LPBF) processes, improving the predictability and optimization of spreading performance.

6.2. Description of Figures

- **Figure 6-1** and **Figure 6-2**: Top and front views of the powder bed after spreading with a counter-rotating roller (radius = 2.5 mm, spreading speed = 50 mm/s). The figures depict powder position in the Z-direction, representing layer thickness variations at different rotational speeds and normalized powder sizes.

- **Figure 6-3 to Figure 6-7**: Characteristics of powder layers with different normalized particle sizes (0.35, 0.40, 0.50, 0.575, and 0.65) using a counter-rotating roller. Each figure presents (a) packing density, (b) normalized layer thickness, and (c) mass fraction along the building plate length.
- **Figure 6-8 and Figure 6-9**: Top and front views of the powder bed after spreading with a forward-rotating roller under varying rotational speeds and normalized powder sizes. The roller exhibits sub-rolling, rolling, and super-rolling configurations.
- **Figure 6-10 to Figure 6-14:** Characteristics of powder layers with different normalized particle sizes using a forward-rotating roller. Similar to the counter-rotating roller figures, each figure details (a) packing density, (b) normalized layer thickness, and (c) mass fraction along the building plate length.
- **Figure 6-15 and Figure 6-16:** Characteristics of a powder layer with a normalized particle size of 0.25 spread using a non-rotating roller and counter-rotating roller (40 rad/s) at a spreading speed of 50 mm/s along the building plate length at different roller radius figures, each figure details (a) packing density, (b) normalized layer thickness, and (c) mass fraction along the building plate length.

These supplementary figures provide additional context to the main paper, demonstrating the effect of roller configurations and rotational speeds on powder spreading efficiency and uniformity.

6.3. Impact of Rotational Speed on Powder Distribution

6.3.1. Non-rotating and counter-rotating rollers

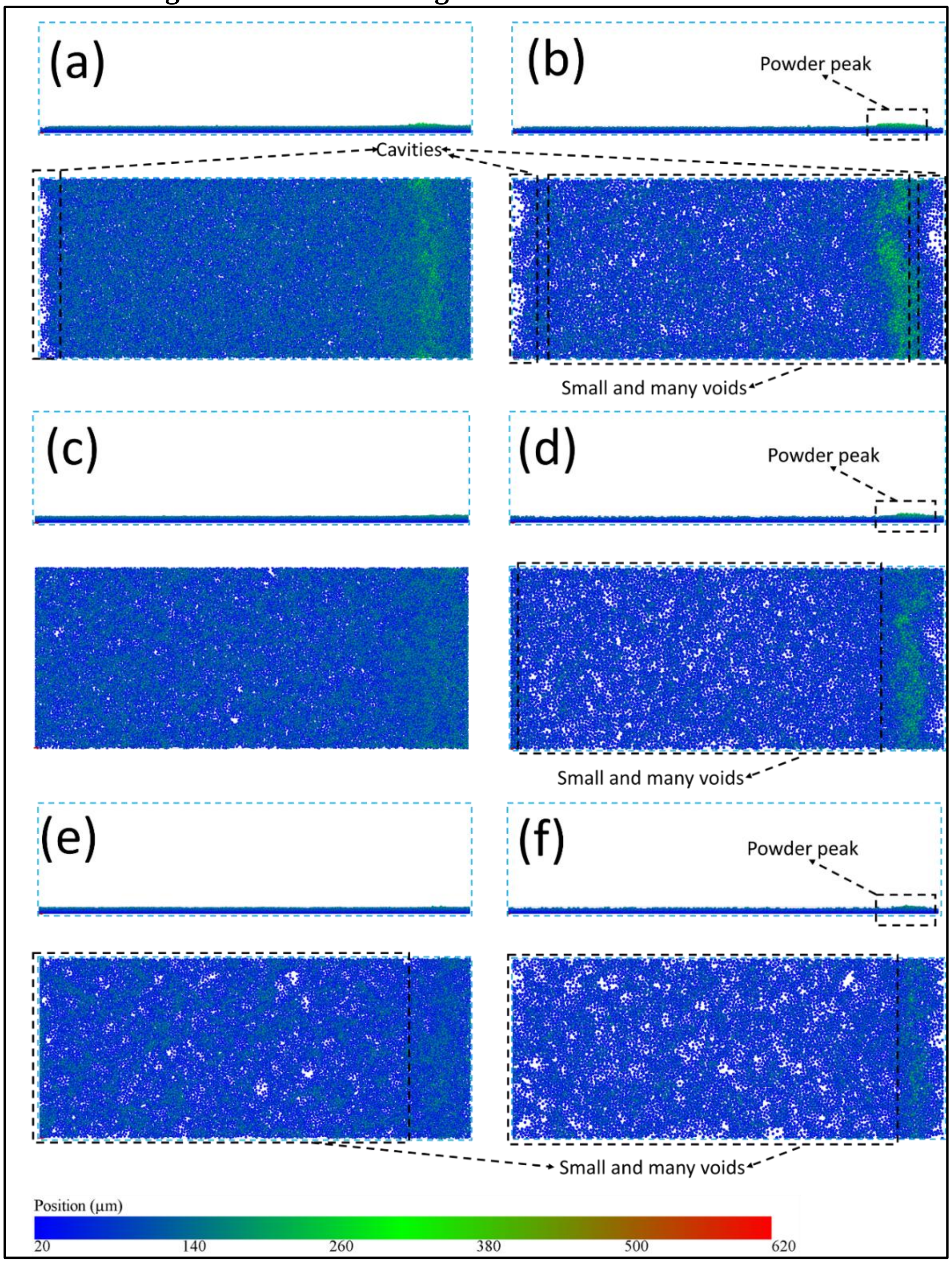

Figure 6-1. Top view and front view of the powder bed after spreading by roller (radius = 2.5 mm) with a spreading speed of 50 mm/s, coloured by powder position in Z-direction (i.e., layer thickness) at different rotational speeds and normalized powder sizes. (a)$\omega = 0\,rad/s\,\&\,D/\delta = 0.35$;(b)$\omega = 0\,rad/s\,\&\,D/\delta = 0.40$;(c)$\omega = 20\,rad/s\,\&\,D/\delta = 0.35$;(d)$\omega = 20\,rad/s\,\&\,D/\delta = 0.40$;(e)$\omega = 90\,rad/s\,\&\,D/\delta = 0.35$;and(f)$\omega = 90\,rad/s\,\&\,D/\delta = 0.40$.

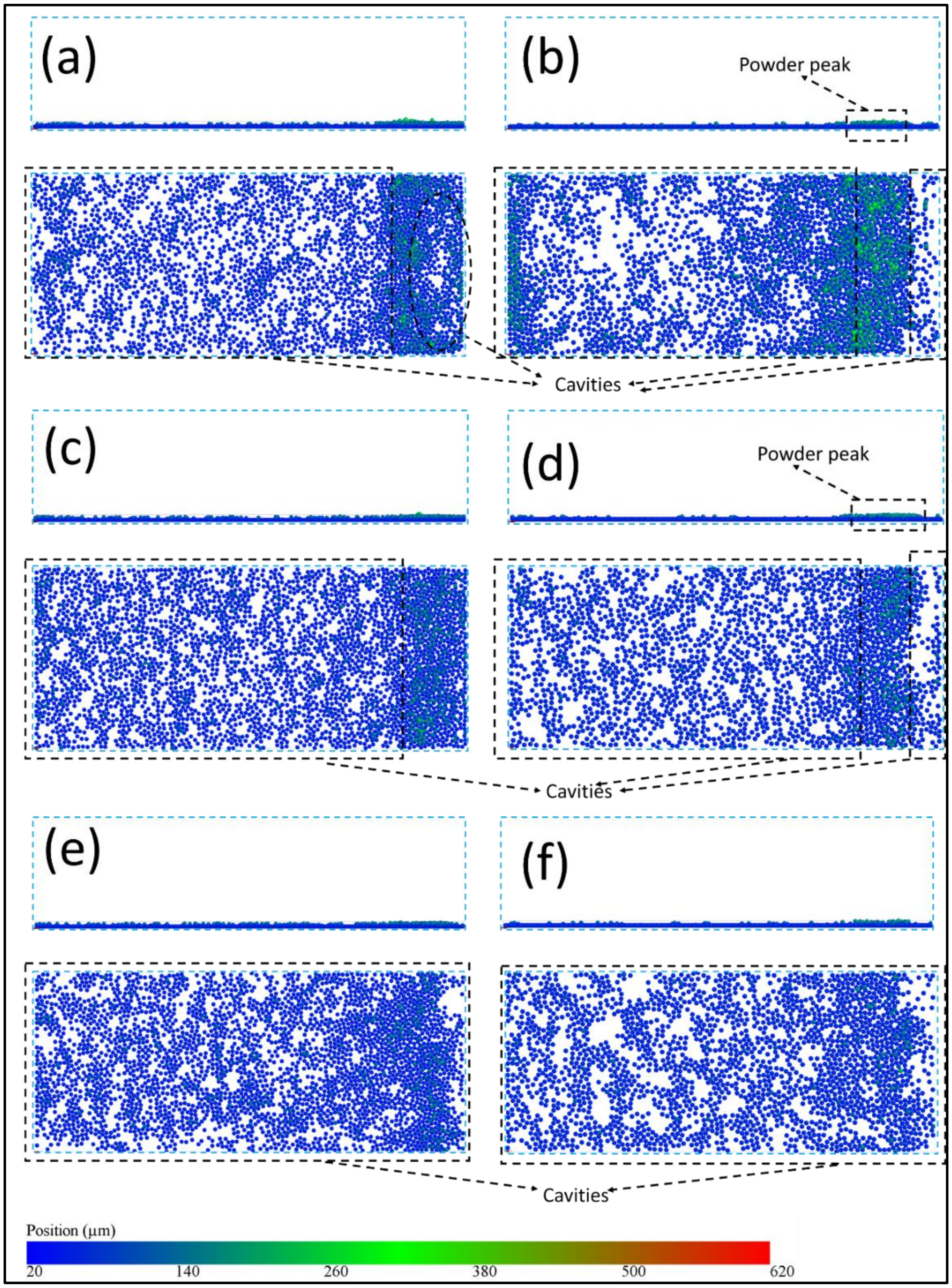

Figure 6-2. Top view and front view of the powder bed after spreading by roller (radius = 2.5 mm) with a spreading speed of 50 mm/s, coloured by powder position in Z-direction (i.e., layer thickness) at different rotational speeds and normalized powder sizes. (a)$\omega = 0\,rad/s\,\&\,D/\delta = 0.575$;(b)$\omega = 0\,rad/s\,\&\,D/\delta = 0.65$;(c)$\omega = 20\,rad/s\,\&\,D/\delta = 0.575$;(d)$\omega = 20\,rad/s\,\&\,D/\delta = 0.65$;(e)$\omega = 90\,rad/s\,\&\,D/\delta = 0.575$;and(f)$\omega = 90\,rad/s\,\&\,D/\delta = 0.65$.

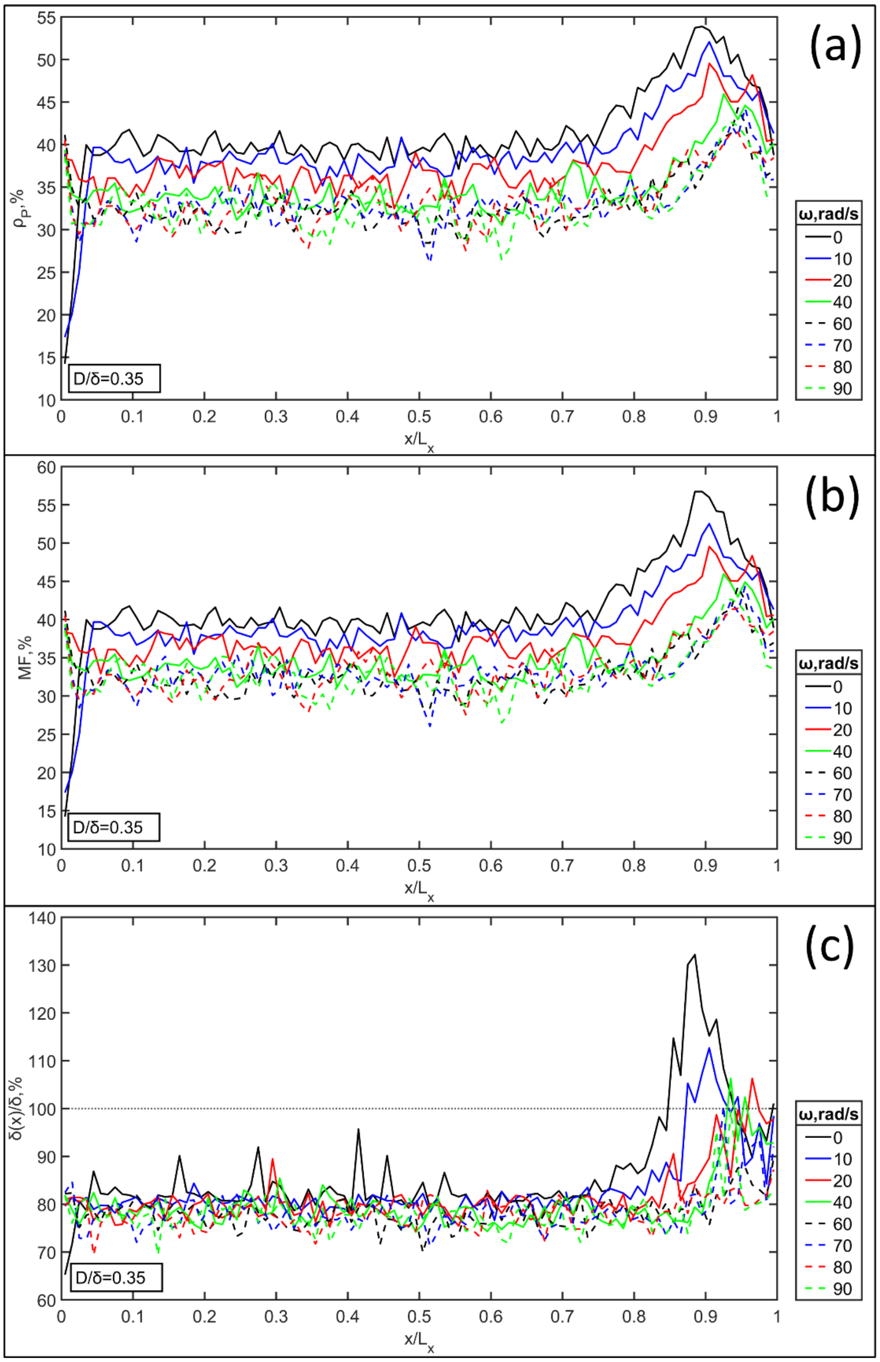

Figure 6-3. Characteristics of a powder layer with a normalized particle size of 0.35 spread using a counter-rotating roller (R_r = 2.5 mm) at a spreading speed of 50 mm/s along the building plate length: (a) Packing density (ρ_p, %); (b) Normalized layer thickness (δ(x)/δ,%); (c) Mass fraction (MF,%).

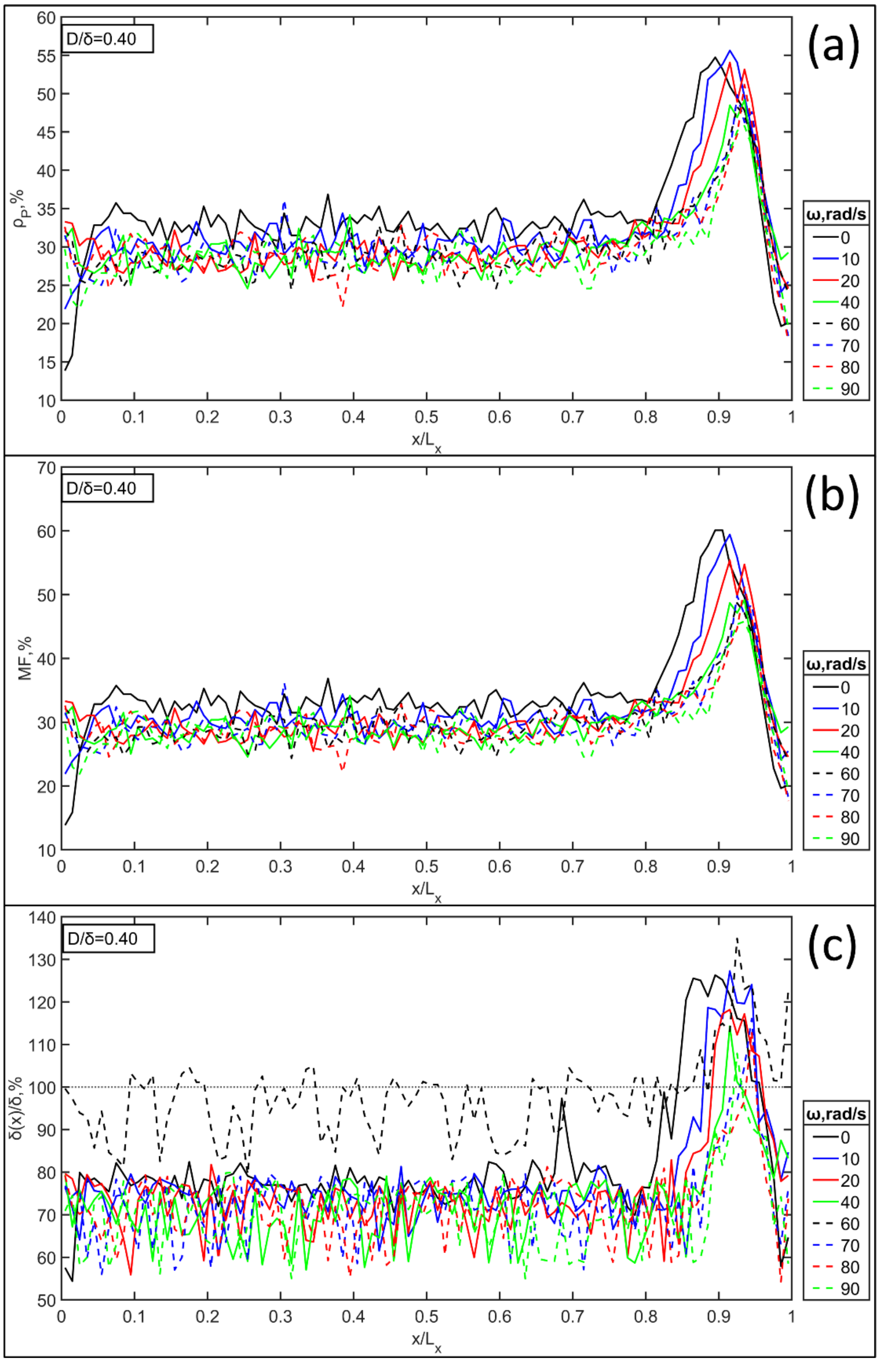

Figure 6-4. Characteristics of a powder layer with a normalized particle size of 0.40 spread using a counter-rotating roller (R_r = 2.5 mm) at a spreading speed of 50 mm/s along the building plate length: (a) Packing density (ρ_p,%); (b) Normalized layer thickness(δ(x)/δ,%); (c) Mass fraction (MF,%).

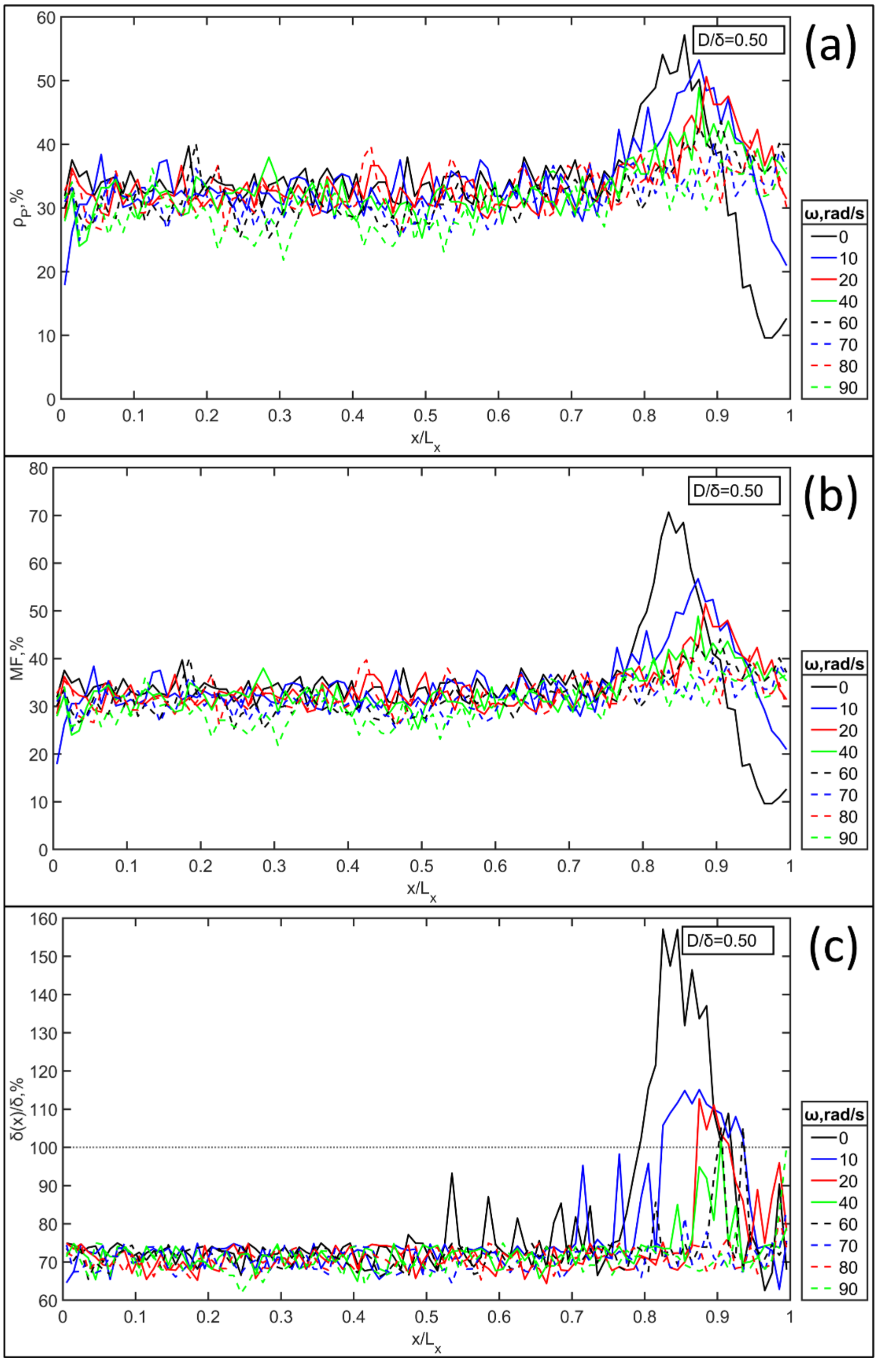

Figure 6-5. Characteristics of a powder layer with a normalized particle size of 0.50 spread using a counter-rotating roller (R_r = 2.5 mm) at a spreading speed of 50 mm/s along the building plate length: (a) Packing density (ρ_p,%); (b) Normalized layer thickness(δ(x)/δ,%); (c) Mass fraction (MF,%).

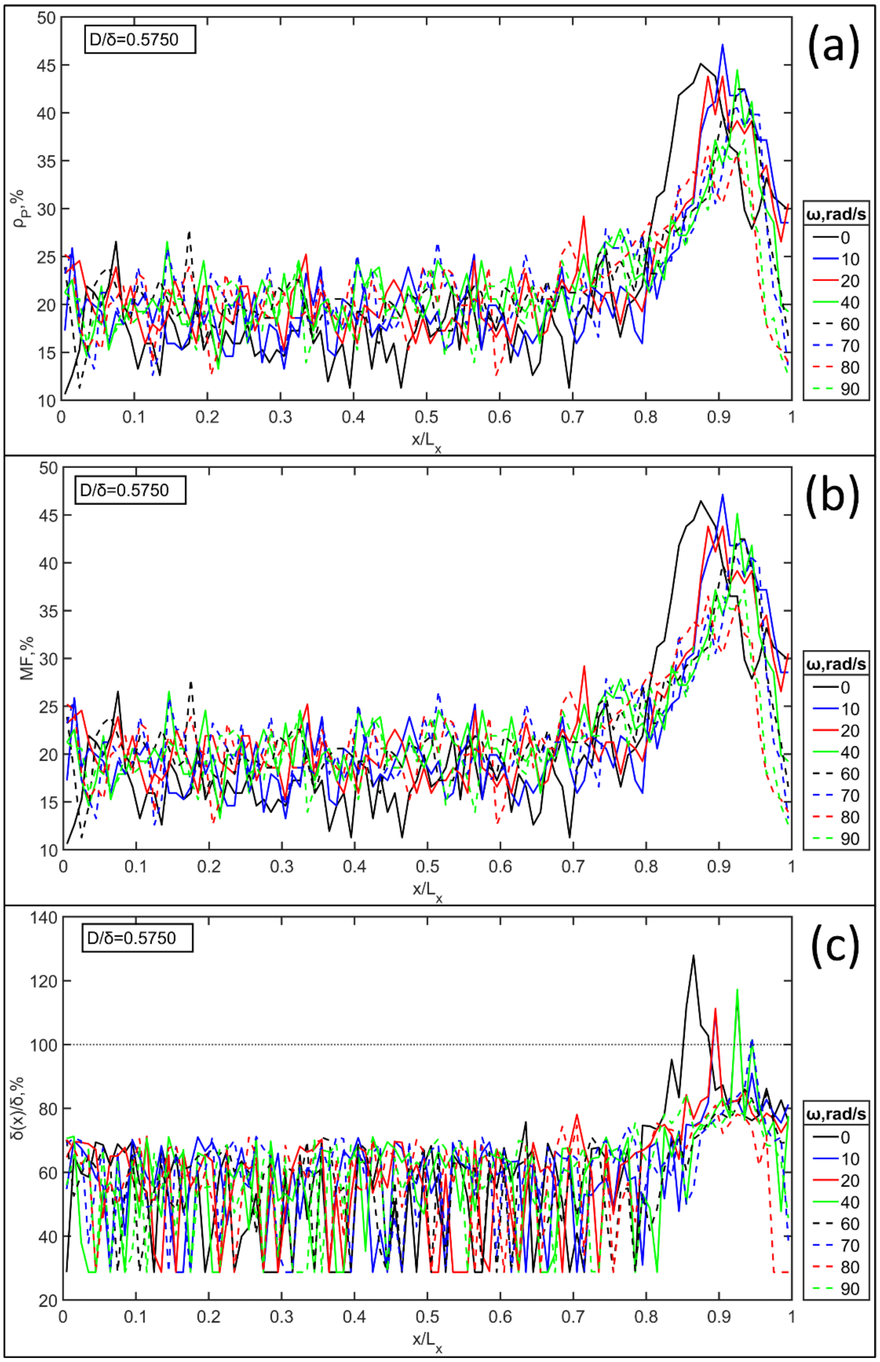

Figure 6-6. Characteristics of a powder layer with a normalized particle size of 0.575 spread using a counter-rotating roller (R_r = 2.5 mm) at a spreading speed of 50 mm/s along the building plate length: (a) Packing density (ρ_p,%); (b) Normalized layer thickness(δ(x)/δ,%); (c) Mass fraction (MF,%).

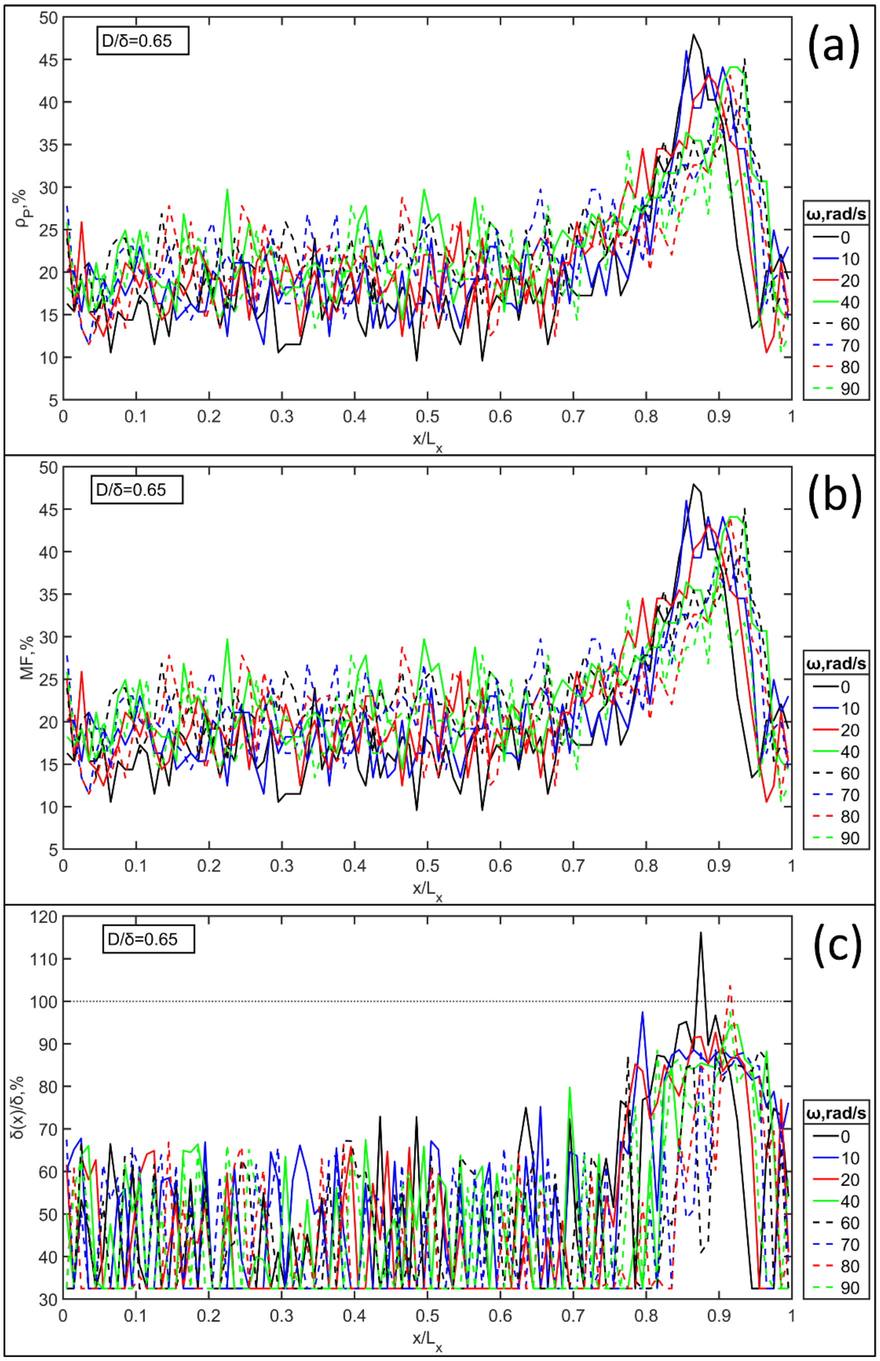

Figure 6-7. Characteristics of a powder layer with a normalized particle size of 0.65 spread using a counter-rotating roller (R_r = 2.5 mm) at a spreading speed of 50 mm/s along the building plate length: (a) Packing density (ρ_p,%); (b) Normalized layer thickness(δ(x)/δ,%); (c) Mass fraction (MF,%).

6.3.2. Forward-rotating rollers

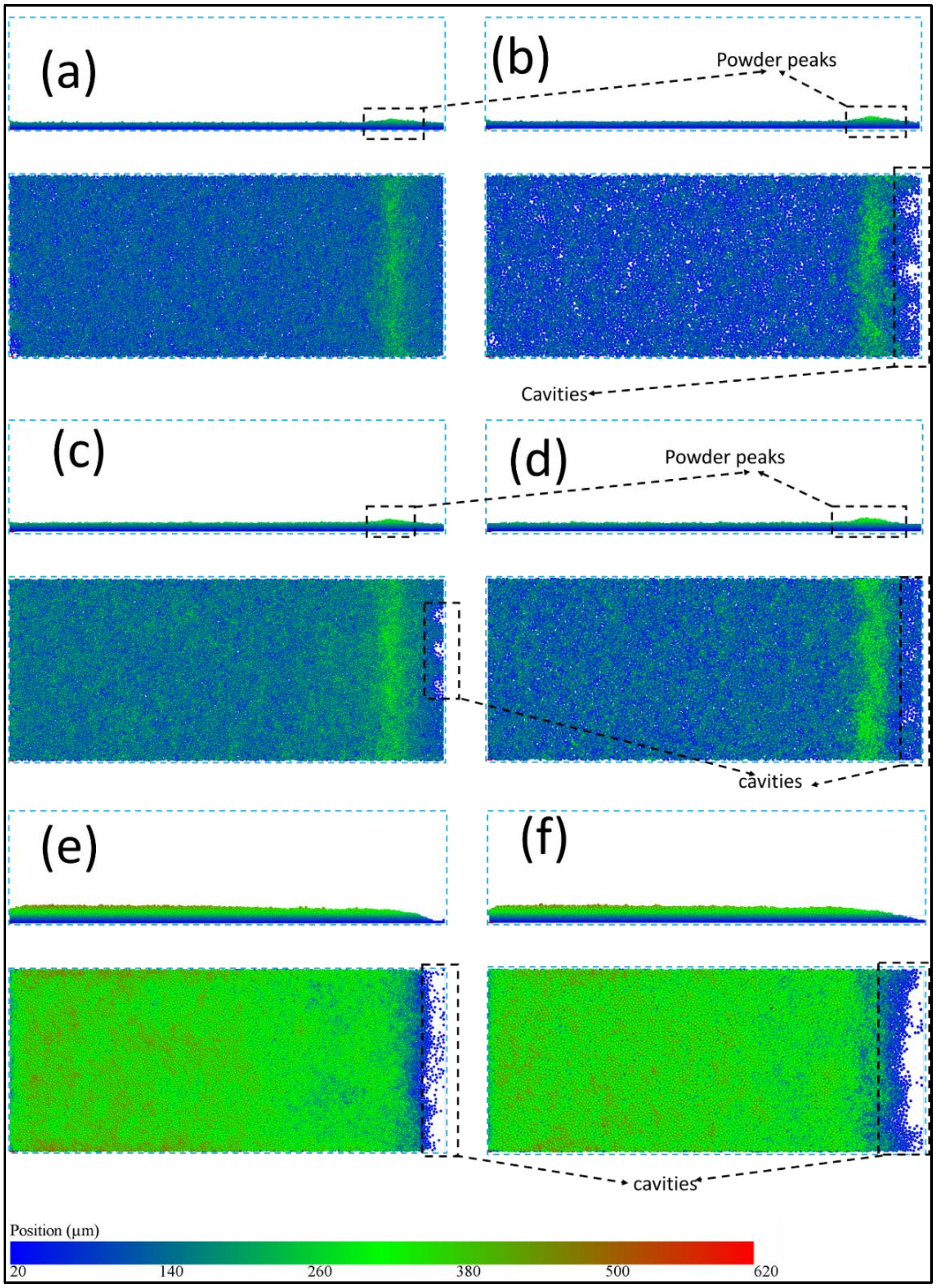

Figure 6-8. Top view and front view of the powder bed after spreading by forward-rotating roller (R_r = 2.5 mm) with a spreading speed of 50 mm/s, coloured by powder position in Z-direction (i.e., layer thickness) at different rotational speeds and normalized powder sizes ; (a)sub-rolling;$\omega = -10\, rad/s\, \&\, D/\delta = 0.35$;(b)sub-rolling ;$\omega = -10\, rad/s\, \&\, D/\delta = 0.40$;(c)Rolling ; $\omega = -20\, rad/s\, \&\, D/\delta = 0.35$;(d)rolling ; $\omega = -20\, rad/s\, \&\, D/\delta = 0.40$;(e)super-rolling; $\omega = -90\, rad/s\, \&\, D/\delta = 0.35$;and(f)super-rolling; $\omega = -90\, rad/s\, \&\, D/\delta = 0.40$.

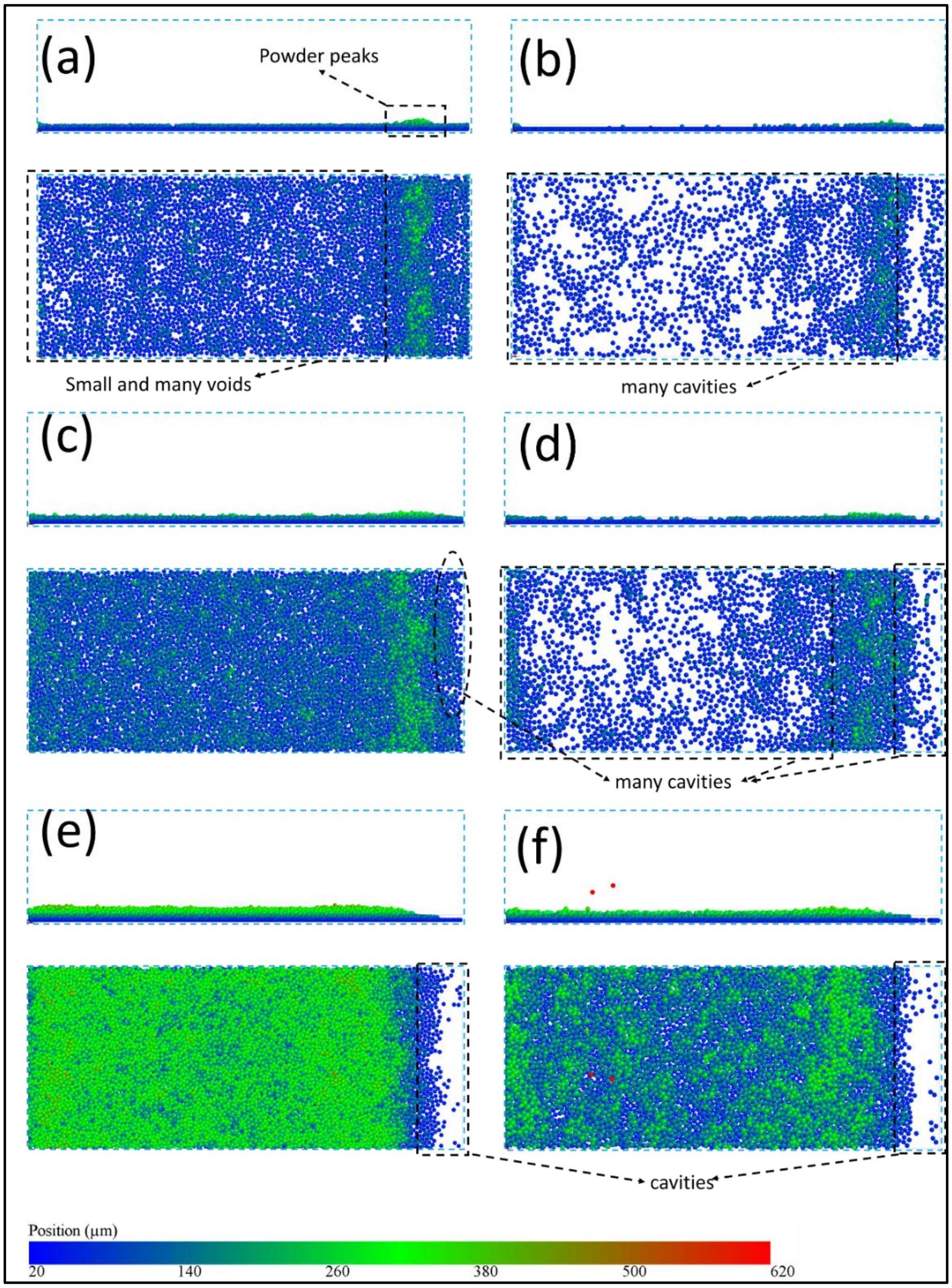

Figure 6-9. Top view and front view of the powder bed after spreading by forward-rotating roller (R_r = 2.5 mm) with a spreading speed of 50 mm/s, coloured by powder position in Z-direction (i.e., layer thickness) at different rotational speeds and normalized powder sizes ; (a)sub-rolling;$\omega = -10\, rad/s$ & $D/\delta = 0.575$;(b)sub-rolling ;$\omega = -10\, rad/s$ & $D/\delta = 0.65$;(c)Rolling ; $\omega = -20\, rad/s$ & $D/\delta = 0.575$;(d)rolling ; $\omega = -20\, rad/s$ & $D/\delta = 0.65$;(e)super-rolling; $\omega = -90\, rad/s$ & $D/\delta = 0.575$;and(f)super-rolling; $\omega = -90\, rad/s$ & $D/\delta = 0.65$

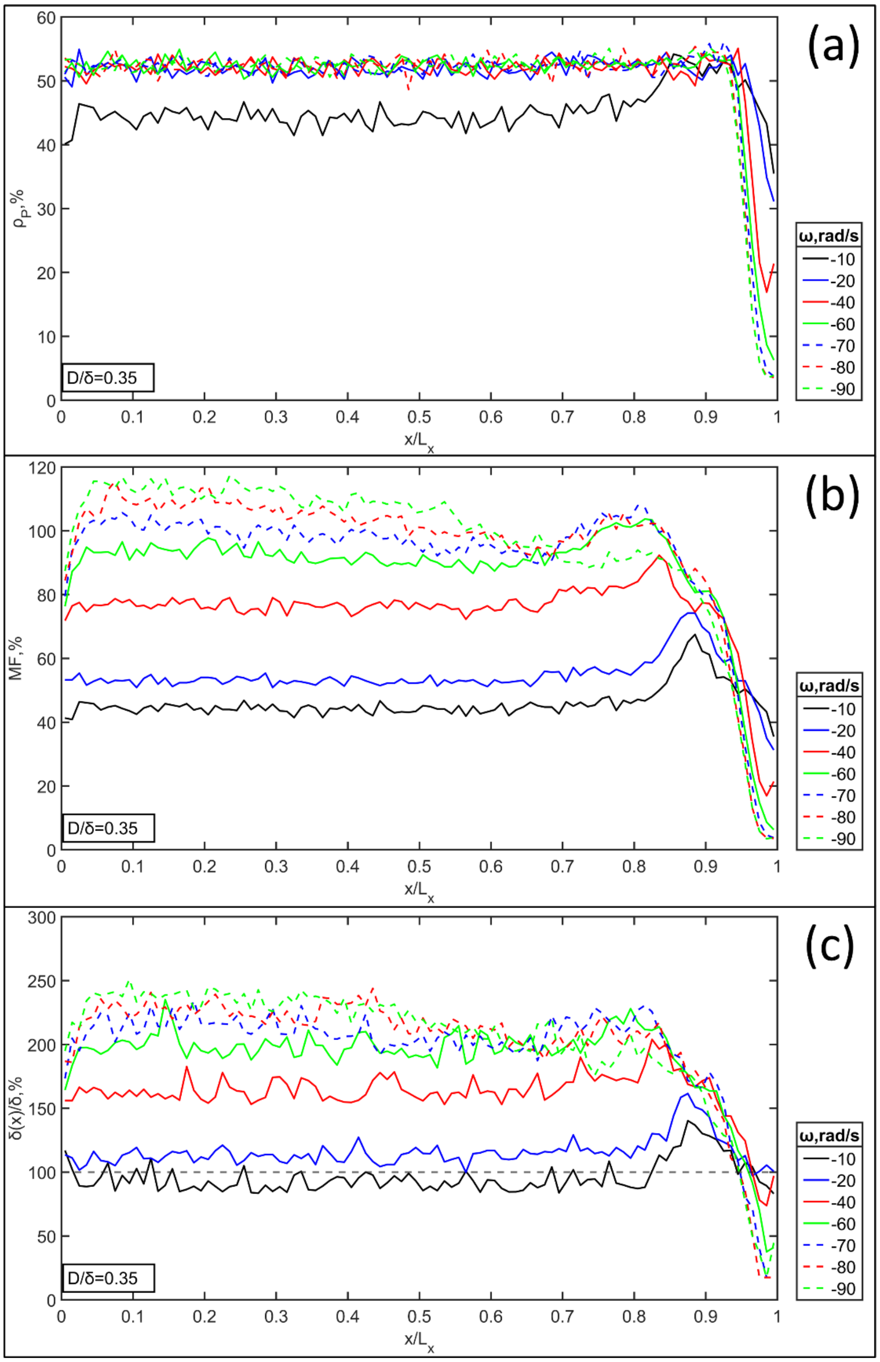

Figure 6-10. Characteristics of a powder layer with a normalized particle size of 0.35 spread using a forward-rotating roller (R_r = 2.5 mm) at a spreading speed of 50 mm/s along the building plate length: (a) Packing density (ρ_p, %); (b) Normalized layer thickness (δ(x)/δ,%); (c) Mass fraction (MF,%).

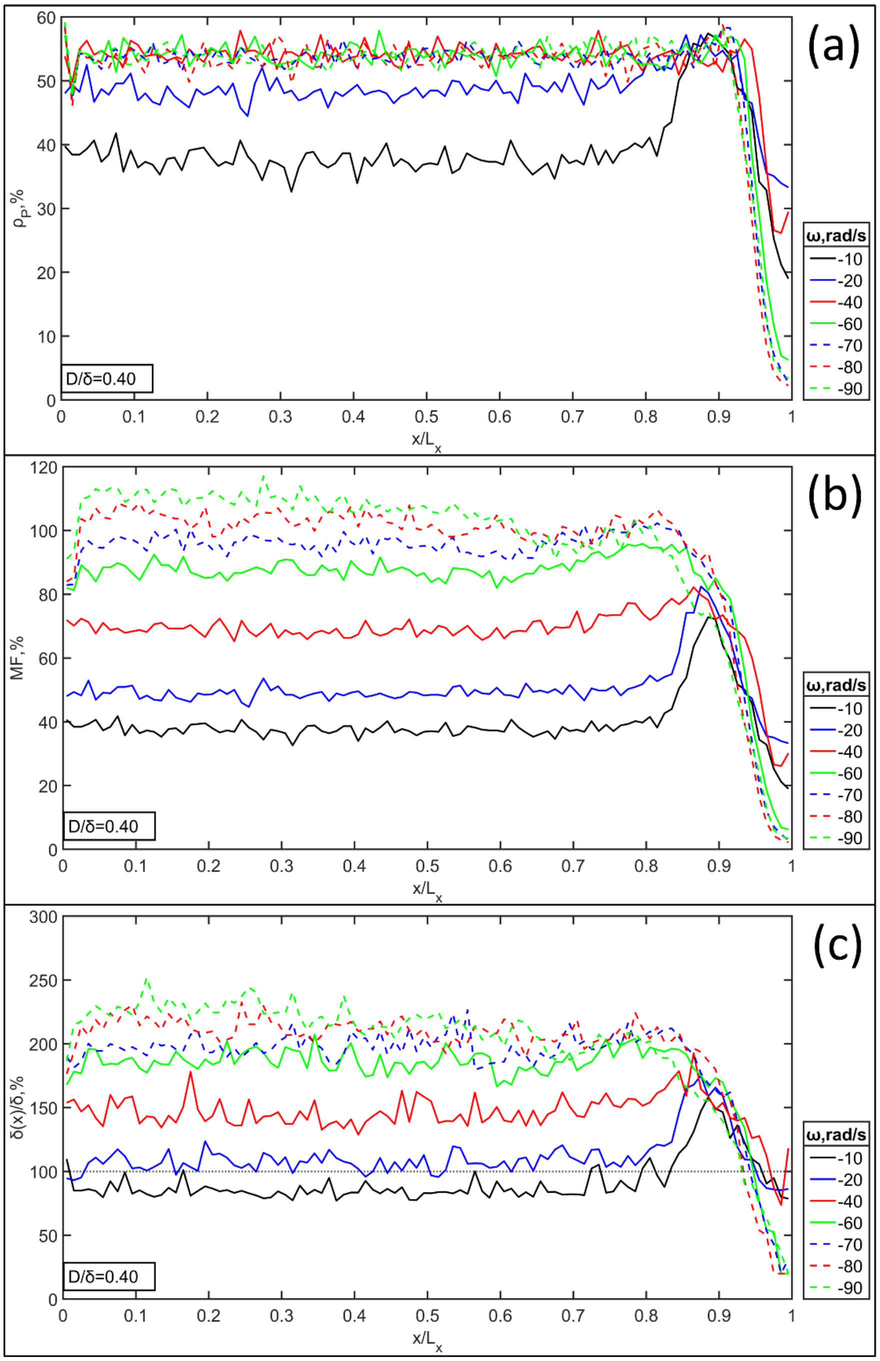

Figure 6-11. Characteristics of a powder layer with a normalized particle size of 0.40 spread using a forward-rotating roller (R_r = 2.5 mm) at a spreading speed of 50 mm/s along the building plate length: (a) Packing density (ρ_p, %); (b) Normalized layer thickness (δ(x)/δ,%); (c) Mass fraction (MF,%).

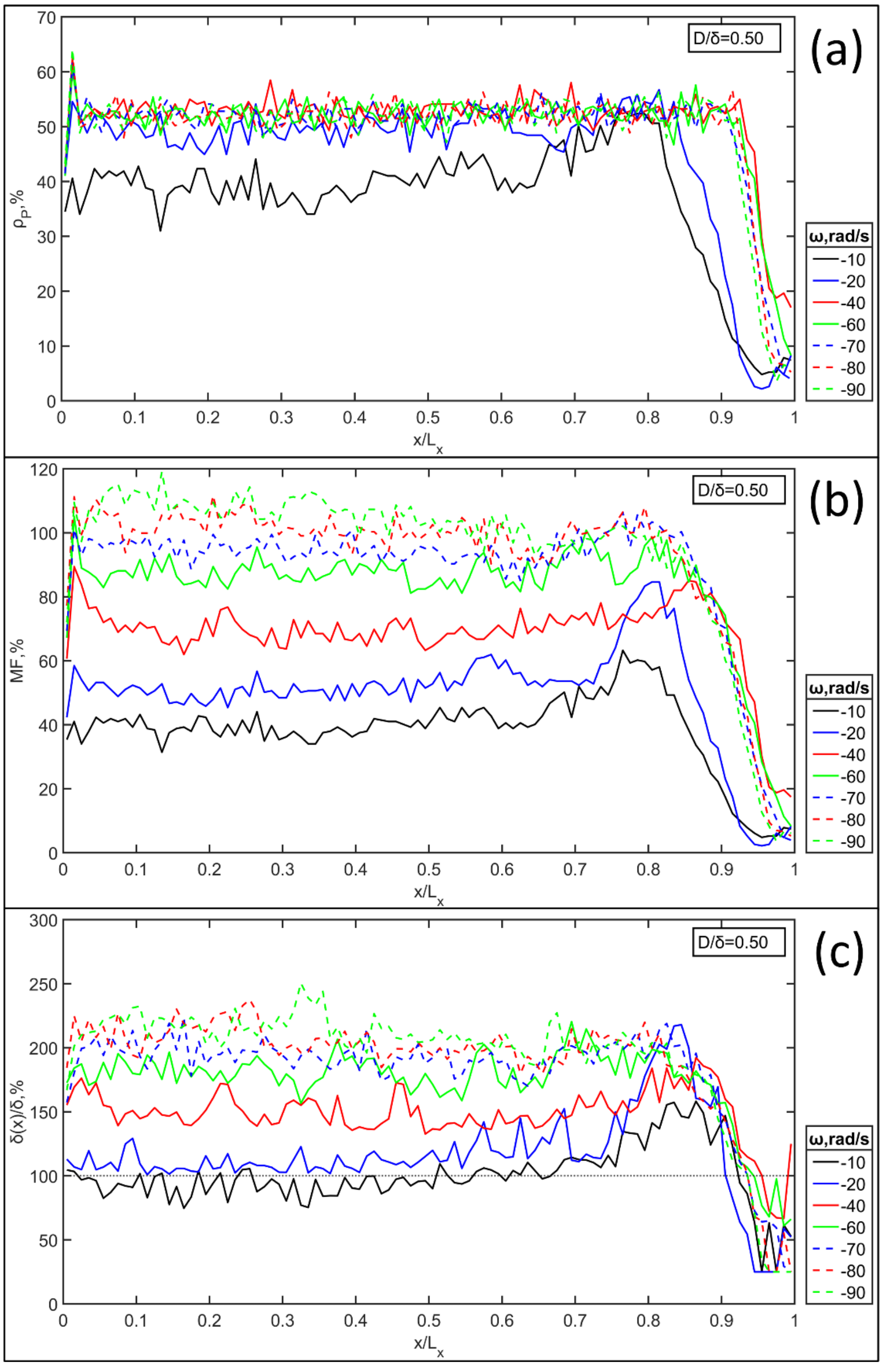

Figure 6-12. Characteristics of a powder layer with a normalized particle size of 0.50 spread using a forward-rotating roller (R_r = 2.5 mm) at a spreading speed of 50 mm/s along the building plate length: (a) Packing density (ρ_p, %); (b) Normalized layer thickness (δ(x)/δ,%); (c) Mass fraction (MF,%).

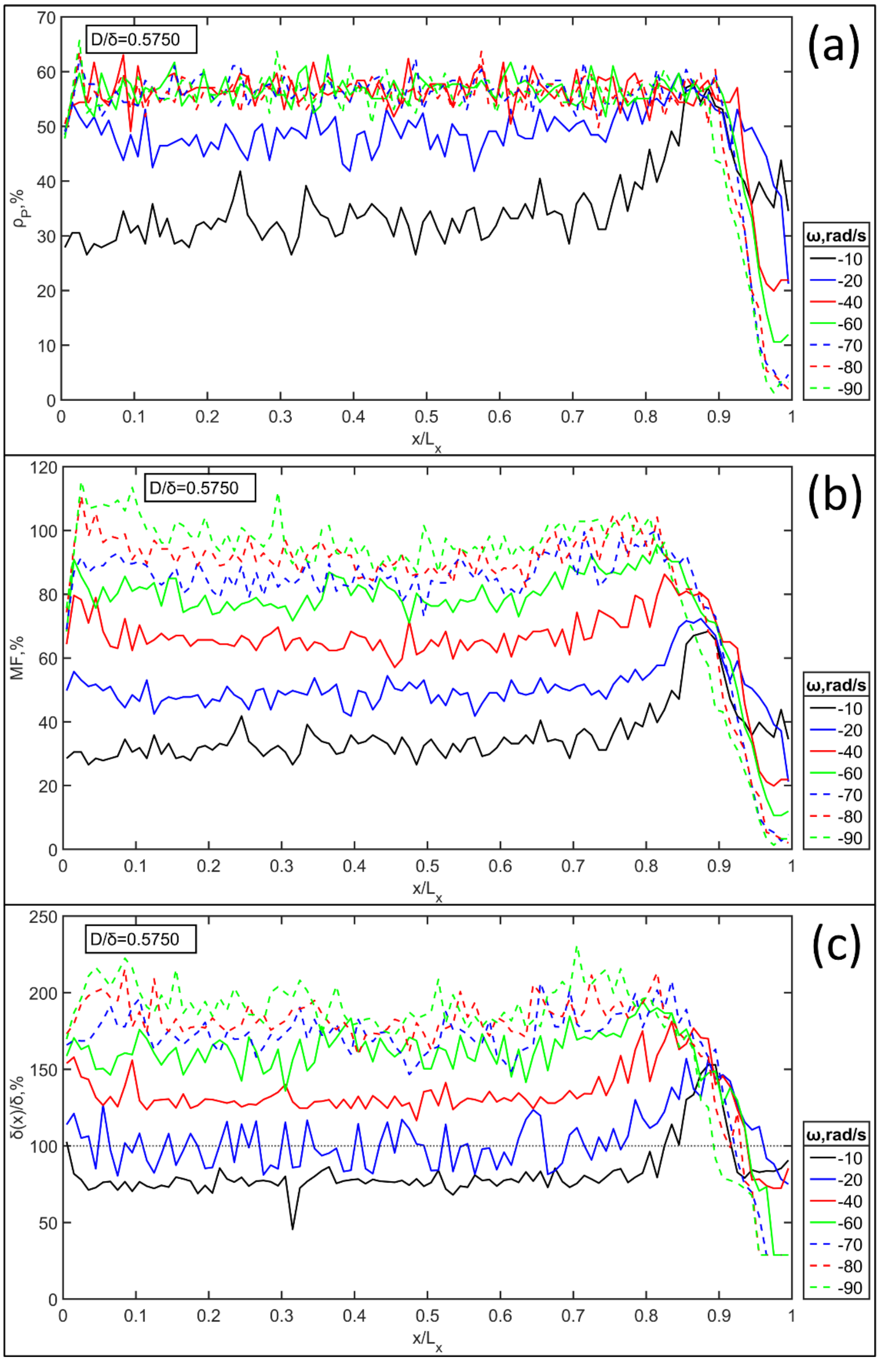

Figure 6-13. Characteristics of a powder layer with a normalized particle size of 0.575 spread using a forward-rotating roller (R_r = 2.5 mm) at a spreading speed of 50 mm/s along the building plate length: (a) Packing density (ρ_p, %); (b) Normalized layer thickness (δ(x)/δ,%); (c) Mass fraction (MF,%).

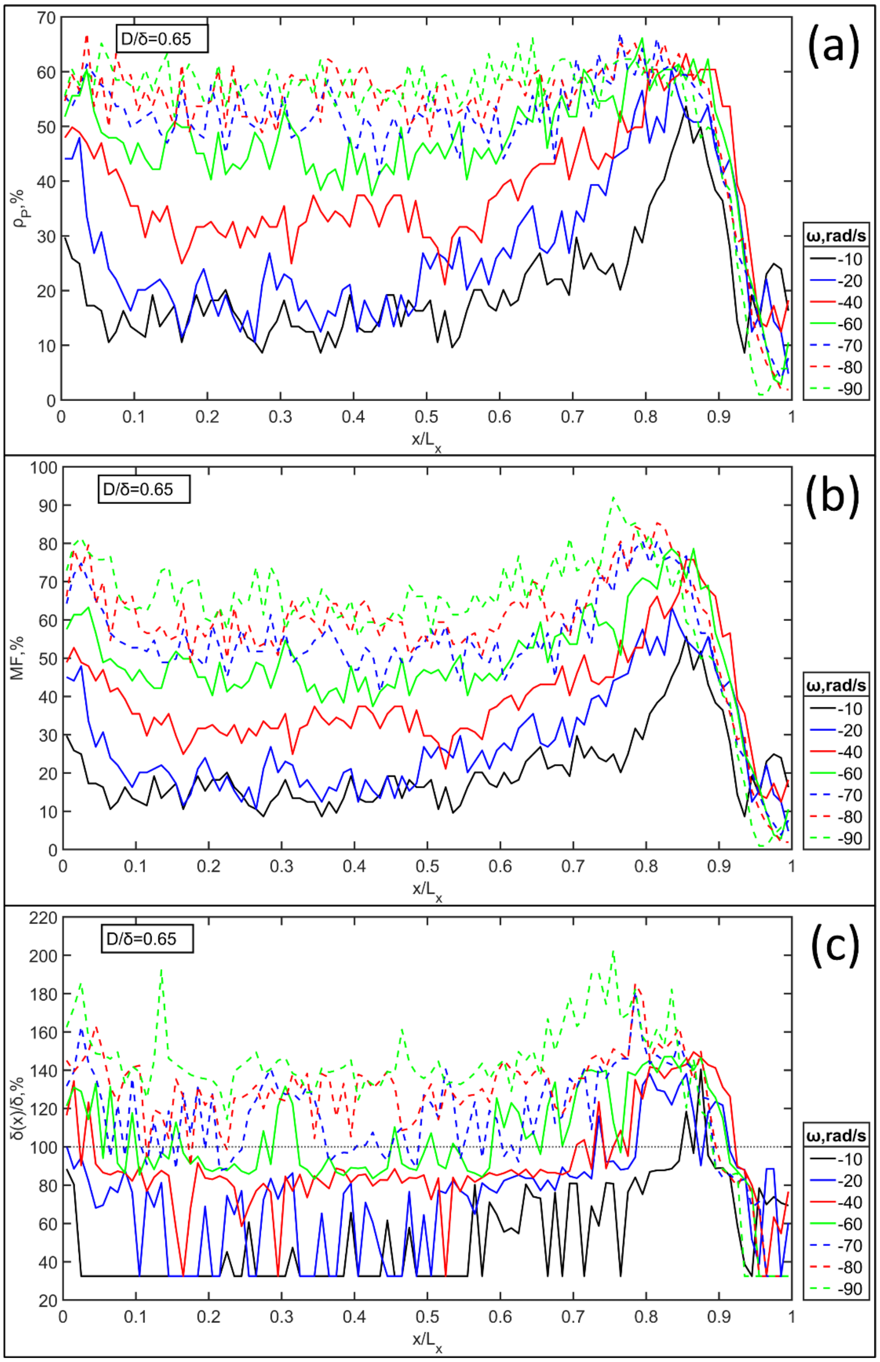

Figure 6-14. Characteristics of a powder layer with a normalized particle size of 0.65 spread using a forward-rotating roller (R_r = 2.5 mm) at a spreading speed of 50 mm/s along the building plate length: (a) Packing density (ρ_p, %); (b) Normalized layer thickness (δ(x)/δ,%); (c) Mass fraction (MF,%).

6.4. Impact of Roller Radius on Powder Distribution

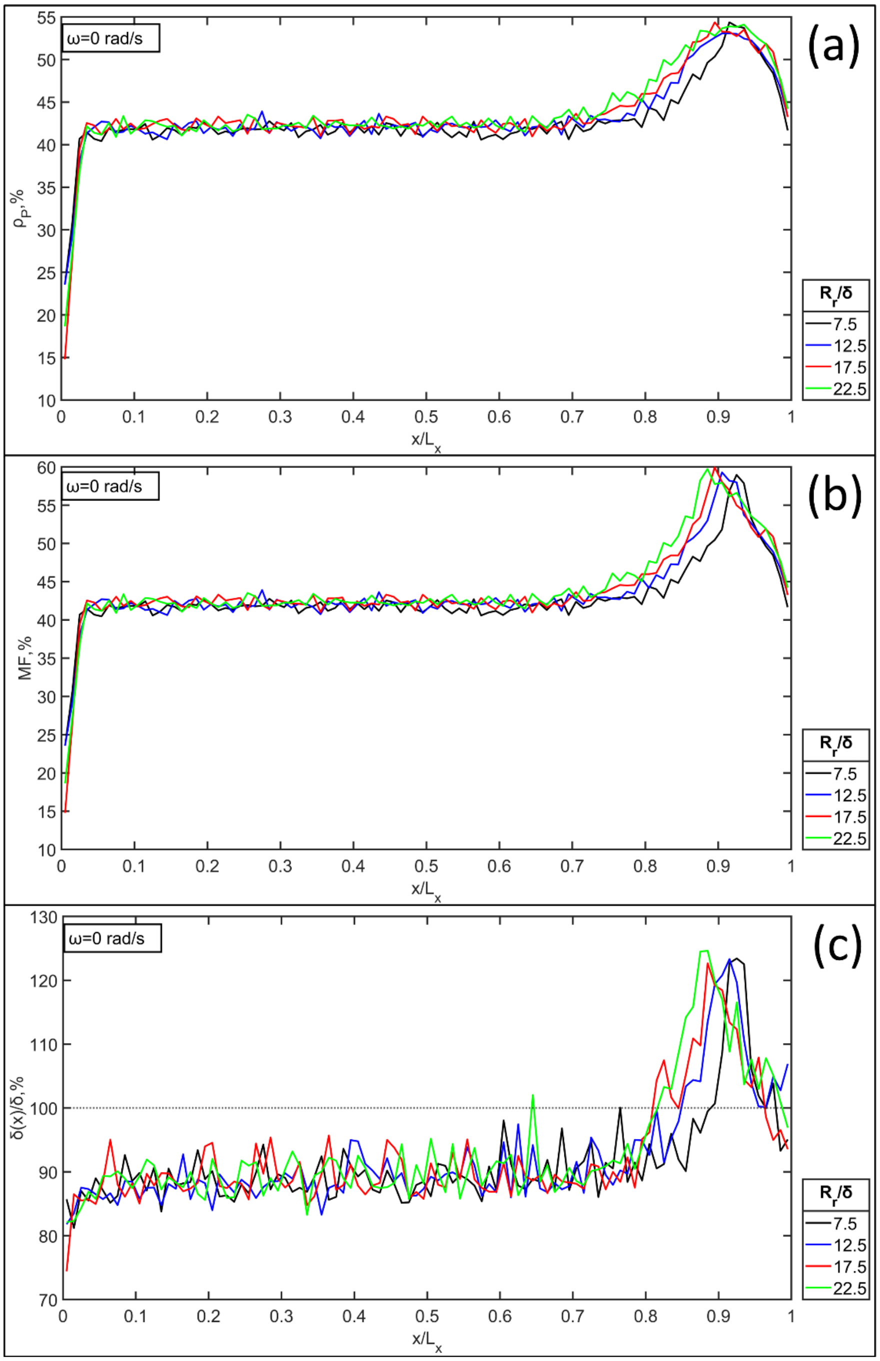

Figure 6-15. Characteristics of a powder layer with a normalized particle size of 0.25 spread using a non-rotating roller at a spreading speed of 50 mm/s along the building plate length at different roller radius: (a) Packing density (ρ_p,%); (b) Normalized layer thickness (δ(x)/δ,%); (c) Mass fraction (MF,%).

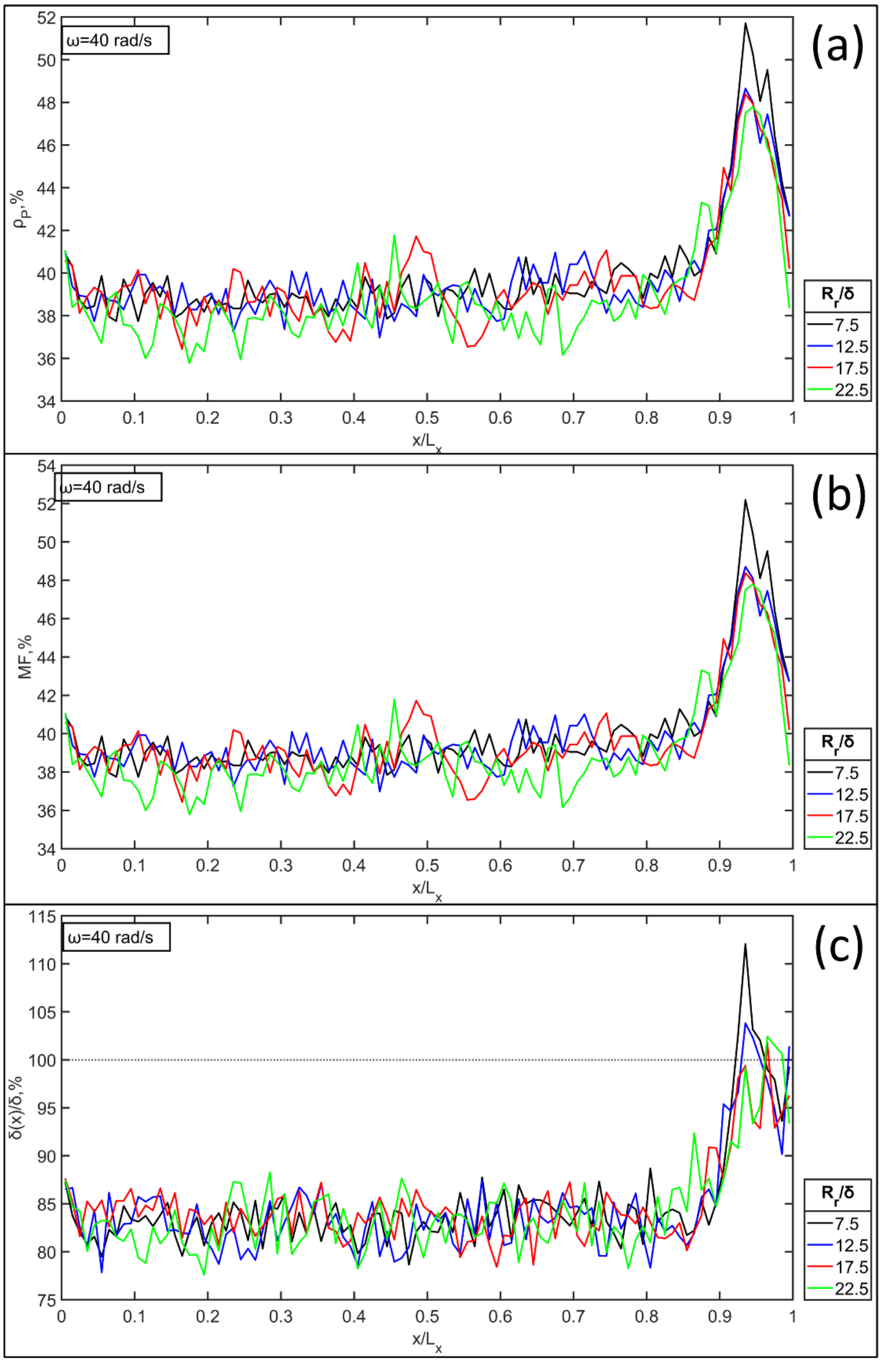

Figure 6-16. Characteristics of a powder layer with a normalized particle size of 0.25 spread using a counter-rotating roller at a spreading speed of 50 mm/s and rotational speed of 40 rad/s along the building plate length at different roller radius: (a) Packing density (ρ_p, %); (b) Normalized layer thickness ($\delta(x)/\delta$,%); (c) Mass fraction (MF,%).